Journal of Membrane Science 540 (2017) 261–276

Contents lists available at ScienceDirect

Journal of Membrane Science

journal homepage: www.elsevier.com/locate/memsci

Using the Maxwell-Stefan formulation for highlighting the influence of interspecies (1 − 2) friction on binary mixture permeation across microporous and polymeric membranes

Rajamani Krishna

Van 't Hoff Institute for Molecular Sciences, University of Amsterdam, Science Park 904, 1098 XH Amsterdam, The Netherlands

ARTICLE INFO

Keywords:
Langmuir adsorption
Membrane permeation
Maxwell Stefan diffusion
Thermodynamic correction factors
Flory Huggins thermodynamics

ABSTRACT

The Maxwell-Stefan (M-S) "frictional" formulation has been used to develop a unified description of mixture permeation across membranes consisting of thin layers of zeolites, metal-organic frameworks or polymers. Explicit analytic expressions are derived for determining the fluxes for steady-state permeation of binary mixtures of species 1 and 2 across a membrane (m), clearly delineating the relative influences of the 1-m, 2-m and interspecies (1 − 2) frictional contributions. Simplified expressions are derived for two limiting scenarios: negligible 1–2 friction and dominant 1–2 friction; these scenarios help to determine the upper and lower bounds of permeation fluxes and selectivities. The developed model is used to analyze a wide variety of published experimental data on mixture permeation across zeolite and polymer membranes. In each case, the influence of 1–2 friction is analyzed. In cases such as pervaporation across polymer membranes, the 1–2 frictional contribution is found to be extremely significant.

1. Introduction

Membrane technologies find applications in a variety of separation applications such as gas separations, water/alcohol pervaporation, dialysis, electrodialysis, and desalination [1,2]. The membrane layer could consist of porous materials, polymeric chains, or hybrid "mixed matrix" materials. The design and development of membrane separation technologies requires accurate and robust models for description of mixture permeation.

In the majority of cases of industrial interest, the mixture permeation characteristics cannot be predicted solely on the basis of data on *unary* permeation of individual species in the mixture. As illustration, Fig. 1a compares the experimental data on permeances of CO_2 and H_2 determined for unary and binary mixture permeation across an MFI membrane [3]. The CO_2 and H_2 mixture permeances are both lower than the corresponding values for unary systems. For H_2, the lowering is by about one order of magnitude, while the CO_2 permeance is lowered by a factor of about two. This implies that mixture permeation is CO_2-selective, whereas the data based on unary permeation demonstrates H_2-selective performance. What causes the lowering of the component permeances in the mixture, and why is the extent of lowering significantly higher for H_2?

For CO_2/H_2 mixture permeation across SAPO-34 membrane, a different result is reported [4,5]; see Fig. 1b. In this case there is no lowering of CO_2 permeance in the mixture from the corresponding unary values. What is the explanation for the contrasting observations in Figs. 1a, and 1b?

Fig. 2a shows experimental data [6] on the pervaporation fluxes of water(1)/ethanol(2) mixtures across an hydrophilic polyimide membrane (m) as a function of the mass fraction of water in the upstream liquid feed mixture, ω_1^L. Increasing ω_1^L results in a monotonous increase in the water permeation flux, as is to be expected. However, the corresponding ethanol flux does not decrease monotonously, but displays a maximum at $\omega_1^L \approx 0.2$. As reassurance that these data are not an aberration, it is noteworthy that a similar maximum has been reported for water/ethanol pervaporation across an hydrophilic poly (vinyl alcohol) /poly (acrylonitrile) (PVA/PAN) composite membrane [7], but at the feed composition $\omega_1^L \approx 0.7$; see Fig. 2b. The observed maximum in the ethanol flux cannot be easily rationalized by a simple permeation model that assumes each penetrant to transfer independently of the partner penetrants within the polymer membrane. Is the maximum in the ethanol flux caused by non-idealities in phase equilibrium thermodynamics? Are diffusional "coupling" effects also in play here?

Clearly, a quantitative description of the variety of observations in Figs. 1 and 2 requires the use of modelling framework that (a) takes proper account of non-ideal phase equilibrium thermodynamics, and (b) mutual diffusional "interactions" between penetrants, and not just the interaction between each penetrant and the membrane.

E-mail address: r.krishna@contact.uva.nl.

http://dx.doi.org/10.1016/j.memsci.2017.06.062
Received 4 April 2017; Received in revised form 20 June 2017; Accepted 24 June 2017
Available online 28 June 2017
0376-7388/

Nomenclature

a_i	activity of species i, dimensionless
b_i	parameter in the pure component Langmuir adsorption isotherm, Pa^{-1}
c_i	molar concentration of species i, mol m^{-3}
c_t	total molar concentration in mixture, mol m^{-3}
$Đ_i$	M-S diffusivity of component i for molecule-pore interactions, $m^2 s^{-1}$
$Đ_i(0)$	M-S diffusivity at zero-loading, $m^2 s^{-1}$
$Đ_{ij}^V$	modified M-S diffusivity for binary penetrant pair i-j, $m^2 s^{-1}$
$Đ_{im}^V$	modified M-S diffusivity for penetrant i in polymer m, $m^2 s^{-1}$
$Đ_{ij}$	M-S exchange coefficient, $m^2 s^{-1}$
$Đ_{12}$	M-S exchange coefficient for binary mixture, $m^2 s^{-1}$
f_i	partial fugacity of species i, Pa
$[I]$	Identity matrix with elements δ_{ij}, dimensionless
n	number of penetrants, dimensionless
n_i	number of molecules of species i in simulation box, dimensionless
N_i	molar flux of species i defined in terms of the membrane area, mol $m^{-2} s^{-1}$
N_i^V	volumetric flux of species i, $m^3 m^{-2} s^{-1}$
p_i	partial pressure of species i, Pa
p_t	total system pressure, Pa
q_i	molar loading of species i, mol kg^{-1}
$q_{i,sat}$	molar loading of species i at saturation, mol kg^{-1}
q_t	total molar loading of mixture, mol kg^{-1}
$\mathbf{r}_{l,i}(t)$	position vector for molecule l of species i at any time t, m
R	gas constant, 8.314 J $mol^{-1} K^{-1}$
T	absolute temperature, K
u_i	velocity of motion of i, m s^{-1}
$\overline{V_i}$	partial molar volume of species i, $m^3 mol^{-1}$
$\overline{V}$	molar volume of mixture, $m^3 mol^{-1}$
V_p	pore volume, $m^3 kg^{-1}$
x_i	mole fraction of species i in adsorbed phase, dimensionless
z	distance coordinate, m

Greek letters

Γ_{ij}	thermodynamic factors, dimensionless
$[\Gamma]$	matrix of thermodynamic factors, dimensionless
δ	thickness of membrane, m
δ_{ij}	Kronecker delta, dimensionless
ζ	Bearman friction coefficient
η	dimensionless distance, dimensionless
θ_i	fractional occupancy of component i, dimensionless
θ_t	fractional occupancy of adsorbed mixture, dimensionless
θ_V	fractional vacancy, dimensionless
$[\Lambda]$	matrix of Maxwell-Stefan diffusivities, $m^2 s^{-1}$
μ_i	molar chemical potential, J mol^{-1}
Π_i	permeability of species i for polymer membrane, mol m $m^{-2} s^{-1} Pa^{-1}$
Π_i	permeance of species i for zeolite membrane, mol $m^{-2} s^{-1}$ Pa^{-1}
ρ	framework density, kg m^{-3}
ρ_i	mass density of component i, kg m^{-3}
ω_i	mass fraction of component i, dimensionless
ω_i^L	mass fraction of component i in liquid phase feed mixture, dimensionless

Subscripts

0	upstream face of membrane
1	referring to species 1
2	referring to species 2
i,j	components in mixture
m	refers to membrane, dimensionless
t	referring to total mixture
s	referring to surface at position $\xi = 1$.
sat	referring to saturation conditions
V	vacancy
δ	downstream face of membrane
η	position along membrane

Vector and matrix notation

( )	component vector
[ ]	square matrix

The Maxwell-Stefan (M-S) formulation, that is firmly rooted in the theory of irreversible thermodynamics, affords a rigorous platform to develop the necessary expressions for the permeation fluxes [5,8–17]. In essence, the M-S equations represent a balance between the force exerted per mole of species i with the drag, or friction, experienced with each of the partner species j in the mixture. We may expect that the frictional drag to be proportional to differences in the velocities of the diffusing species $(u_i - u_j)$, where u_i is the velocity of motion of the "guest" species i. For permeation of a mixture containing a total of n penetrants through a membrane matrix, denoted by the suffix m, we write

$$-\frac{d\mu_i}{dz} = \sum_{j=1,j\neq i}^{n} \frac{RT}{Đ_{ij}} X_j (u_i - u_j) + \frac{RT}{Đ_{im}} X_m (u_i - u_m); \quad i = 1.2..n \tag{1}$$

The left member of Eq. (1) is the negative of the gradient of the chemical potential, with the units N mol^{-1}; it represents the driving force acting per mole of species i. For transport of ionic species, the left members are replaced by the electrochemical potential gradients [2,18,19]. Eq. (1) defines two types of M-S diffusivities: $Đ_{im}$, quantifying i-m interactions, and $Đ_{ij}$ for describing i-j interactions. The term $RT/Đ_{im}$ is interpreted as the drag or friction coefficient between the penetrant i and the membrane. The membrane phase is usually stationary, i.e. $u_m = 0$. The term $RT/Đ_{ij}$ is to be interpreted as the friction coefficient for the i-j pair of penetrants. At the molecular level, the $Đ_{ij}$ reflect how the facility for transport of species i *correlates* with that of species j; they are also termed *exchange coefficients* [11,20].

The multiplier X_j in each of the right members represents any measure of the composition of component j in the mixture because we expect the friction to be dependent on the number of molecules of j relative to that of component i. A wide variety of composition measures X_i may be employed, including mole fractions, x_i; molar concentrations, c_i; mass fractions, ω_i; mass densities, ρ_i; volume fractions, ϕ_i [12,13,15,16,21,22]. For example, the formally equivalent Bearman friction formulation [23]

$$-\frac{d\mu_i}{dz} = \sum_{\substack{j=1 \\ j\neq i}}^{n} c_j \varsigma_{ij} (u_i - u_j) + c_m \varsigma_{im} (u_i - u_m) \tag{2}$$

where ς_{ij}, ς_{im} are the Bearman friction coefficients, is often used to describe diffusion in polymers [21,22].

The M-S diffusivities $Đ_{im}$ are determinable from unary permeation experiments; the values thus obtained provide a convenient platform

for characterizing the permeation of the same species *i* in the presence of other penetrants in the membrane. The exchange coefficients $Đ_{ij}$, on the other hand, cannot be determined explicitly from experiments. In some simple cases, use of Molecular Dynamics (MD) simulations [11,20,24–29] allow some insights to be gained on the characteristics of $Đ_{ij}$; invariably the MD simulated values are not accurate enough for direct use in membrane process design and development. For *meso*-porous materials with pores in the 20–500 Å size range the values of the binary exchange coefficient $Đ_{12}$ are the nearly the same as the binary *fluid phase* M-S diffusivity, $Đ_{12,fl}$, over the entire range of pore concentrations [20,24,30,31]. For micro-porous materials and polymers, the exchange coefficient $Đ_{12}$ cannot be directly identified with the corresponding fluid phase diffusivity $Đ_{12,fl}$ because the molecule-molecule interactions are also significantly influenced by molecule-membrane interactions. For binary mixtures of simple non-polar molecules, the values of the exchange coefficient $Đ_{12}$ often lie between the M-S diffusivities $Đ_1$, and $Đ_2$, and the logarithmic Vignes interpolation formula provides reasonable estimates [32,33]. However, for water/alcohol mixtures, hydrogen bonding between the water and alcohol molecules causes mutual-slowing down of both species in the mixtures, and the logarithmic interpolation formula to estimate $Đ_{12}$ fails to a significant extent [34–36].

The primary objective of this article is to gain deeper insights into the characteristics and influence of the *i-j* frictional terms on permeation fluxes. Using the M-S formulation, we derive simple explicit analytic expressions that describe the upper and lower bounds for the influence of 1–2 friction. The limiting scenarios are invaluable in determining the maximum extent to which the first right member of Eq.

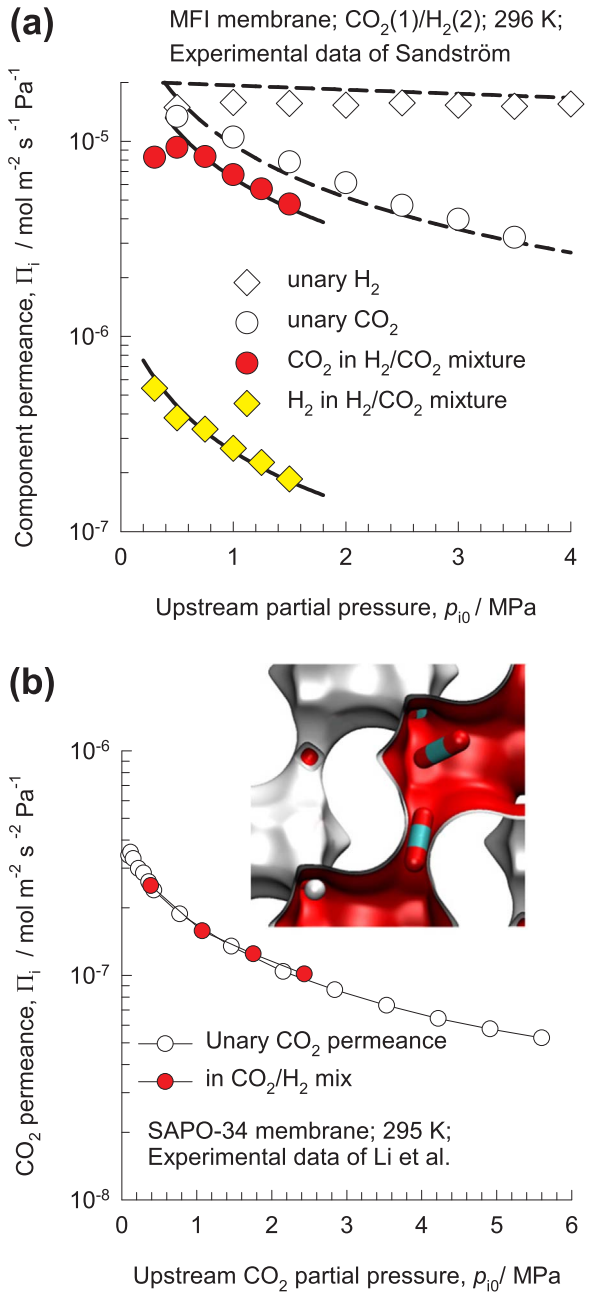

Fig. 1. (a) Experimental data [3] for the permeances of CO_2(1) and H_2(2) determined for unary and binary equimolar mixture permeation across MFI membrane at 296 K. The data are plotted as a function of the partial pressure of CO_2 (= H_2) in the upstream feed mixture. (b) Comparison of CO_2 permeance data [4,5] for CO_2/H_2 mixtures across SAPO-34 membrane, with data on unary permeation.

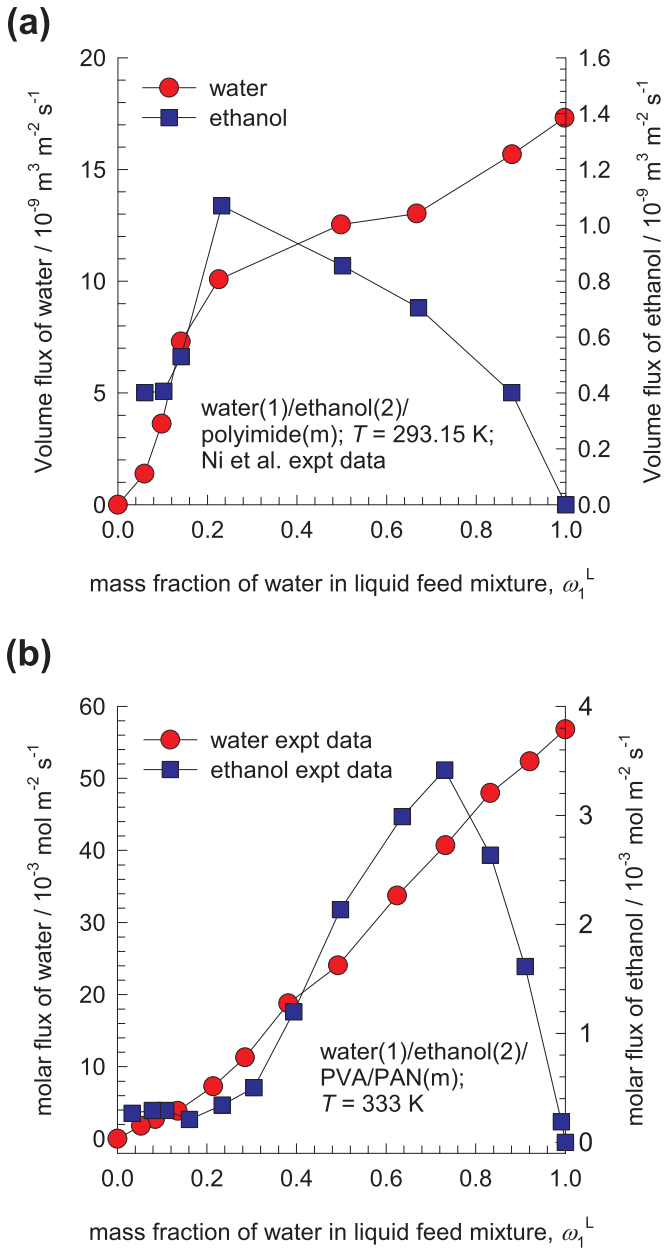

Fig. 2. (a) Experimental data [6] for volumetric pervaporation fluxes of water(1)/ethanol (2) mixtures across polyimide (m) membrane at 293.15 K. (b) Experimental data [7] for the molar permeation fluxes for pervaporation of water(1)/ethanol(2) mixtures across a poly (vinyl alcohol) /poly (acrylonitrile) (PVA/PAN) composite membrane (m) at 333 K. The *x*-axis is the mass fraction of water in the liquid mixture in the upstream compartment.

(1) may influence the mixture permeation characteristics. We aim to demonstrate that these limiting scenarios could contribute to the choice of the "ideal" membrane framework structure to maximize the permeation selectivity.

To fulfil the stated objectives, we undertook detailed analyses of a diverse variety of published experimental data on unary and binary mixture permeation experiments, such as those shown in Figs. 1 and 2, with two different classes of membrane materials: zeolites and polymers.

The Supplementary material accompanying this publication provides: (1) structural details of the zeolite and polymeric membranes investigated, (2) unary isotherm data for adsorption of guest species in the zeolites, along with estimation methods for mixture adsorption equilibrium, (4) Flory-Huggins parameters for fluid-polymer equilibria, (5) detailed derivations of analytic expressions for calculation of steady-state fluxes and permeances, (6) input data on M-S diffusivities for simulations of membrane permeation, and (7) detailed results of simulations and comparisons with published experimental data. The information provided in the Supplementary material is sufficiently detailed to enable interested researchers and practitioners to reproduce all of the calculations presented in this article.

We begin our discussions by considering binary mixture permeation across zeolite membranes.

2. Maxwell-Stefan analysis of zeolite membrane permeation

Within microporous crystalline materials, such as zeolites, metal-organic frameworks (MOFs), zeolitic imidazolate frameworks (ZIFs), and carbon molecular sieves, the guest molecules exist in the adsorbed phase; the phenomenological descriptions of transport in all microporous crystalline materials are formally identical [24]. It is convenient to use as composition measures the mole fractions of the components in the adsorbed phase, $x_i = q_i/q_t$ where q_i is the molar loading of adsorbate, and q_t is the total mixture loading $q_t = \sum_{i=1}^{2} q_i$. The composition "fraction" of the membrane, X_m, is undefined; the membrane does not form part of the mixture, and we redefine the M-S diffusivity for interaction of the penetrant i with the membrane as $Đ_i \equiv Đ_{im}/X_m$.

In terms of mole fractions, Eq. (1) are re-written for binary mixtures, consisting of species 1 and 2, as

$$-\frac{d\mu_i}{dz} = \sum_{j=1,j\neq i}^{2} \frac{RT}{Đ_{ij}} x_j(u_i - u_j) + \frac{RT}{Đ_i}(u_i); \quad i = 1.2 \tag{3}$$

The Onsager Reciprocal Relations imply that the M-S exchange diffusivities are symmetric

$$Đ_{12} = Đ_{21} \tag{4}$$

We define N_i as the number of moles of species i transported per m^2 of crystalline material per second

$$N_i \equiv \rho q_i u_i \tag{5}$$

where ρ is the zeolite framework density with units of kg m^{-3}. Multiplying both sides of Eq. (3) by ρq_i, the M-S equations take the form [10,11,31]

$$\begin{aligned} -\rho\frac{q_1}{RT}\frac{d\mu_1}{dz} &= \frac{x_2N_1 - x_1N_2}{Đ_{12}} + \frac{N_1}{Đ_1} \\ -\rho\frac{q_2}{RT}\frac{d\mu_2}{\partial z} &= \frac{x_1N_2 - x_2N_1}{Đ_{12}} + \frac{N_2}{Đ_2} \end{aligned} \tag{6}$$

At thermodynamic equilibrium, the chemical potential of component i in the bulk gas mixture equals the chemical potential of that component in the adsorbed phase within the membrane at both upstream and downstream faces. For the bulk gas phase mixture we have

$$\frac{1}{RT}\frac{d\mu_i}{dz} = \frac{d\ln p_i}{dz} = \frac{1}{p_i}\frac{dp_i}{dz}; \quad i = 1.2 \tag{7}$$

The chemical potential gradients $d\mu_i/dz$ can be related to the gradients of the molar loadings, q_i, by defining thermodynamic correction factors Γ_{ij}

$$\frac{q_i}{RT}\frac{d\mu_i}{dz} = \sum_{j=1}^{2} \Gamma_{ij}\frac{dq_j}{dz}; \quad \Gamma_{ij} = \frac{q_i}{p_i}\frac{\partial p_i}{\partial q_j}; \quad i,j = 1.2 \tag{8}$$

The thermodynamic correction factors Γ_{ij} can be calculated by differentiation of the model describing mixture adsorption equilibrium. Generally speaking, the Ideal Adsorbed Solution Theory (IAST) of Myers and Prausnitz [37] is the preferred method for estimation of mixture adsorption equilibrium. In some special cases, the mixed-gas Langmuir model

$$\theta_i = \frac{q_i}{q_{i,sat}} = \frac{b_ip_i}{1 + b_1p_1 + b_2p_2}; \quad i = 1.2 \tag{9}$$

may be of adequate accuracy. Analytic differentiation of Eq. (9) yields [38]

$$\begin{bmatrix} \Gamma_{11} & \Gamma_{12} \\ \Gamma_{21} & \Gamma_{22} \end{bmatrix} = \frac{1}{\theta_V}\begin{bmatrix} 1-\theta_2 & \frac{q_{1,sat}}{q_{2,sat}}\theta_1 \\ \frac{q_{2,sat}}{q_{1,sat}}\theta_2 & 1-\theta_1 \end{bmatrix} \tag{10}$$

where the fractional vacancy θ_V is defined as

$$\theta_V = 1 - \theta_1 - \theta_2 \tag{11}$$

In proceeding further, it is convenient to define a 2 × 2 dimensional square matrix $[\Lambda]$:

$$\begin{aligned} [\Lambda] &= \begin{bmatrix} \frac{1}{Đ_1} + \frac{x_2}{Đ_{12}} & -\frac{x_1}{Đ_{12}} \\ -\frac{x_2}{Đ_{12}} & \frac{1}{Đ_2} + \frac{x_1}{Đ_{12}} \end{bmatrix}^{-1} \\ &= \frac{1}{1 + \frac{x_1Đ_2}{Đ_{12}} + \frac{x_2Đ_1}{Đ_{12}}}\begin{bmatrix} Đ_1\left(1 + \frac{x_1Đ_2}{Đ_{12}}\right) & \frac{x_1Đ_1Đ_2}{Đ_{12}} \\ \frac{x_2Đ_1Đ_2}{Đ_{12}} & Đ_2\left(1 + \frac{x_2Đ_1}{Đ_{12}}\right) \end{bmatrix} \end{aligned} \tag{12}$$

The elements of $[\Lambda]$ cannot be determined from experimental measurements. However, Λ_{ij} are directly accessible from MD simulations [24,30,39,40] by monitoring the individual molecular displacements

$$\Lambda_{ij} = \frac{1}{2}\lim_{\Delta t\to\infty}\frac{1}{n_j}\frac{1}{\Delta t}\left\langle\left(\sum_{l=1}^{n_i}(\mathbf{r}_{l,i}(t+\Delta t) - \mathbf{r}_{l,i}(t))\right)\cdot\left(\sum_{k=1}^{n_j}(\mathbf{r}_{k,j}(t+\Delta t) - \mathbf{r}_{k,j}(t))\right)\right\rangle \tag{13}$$

Combining Eqs. (6), (8), and (12) we write using 2-dimensional matrix notation

$$(N) = -\rho[\Lambda][\Gamma]\frac{d(q)}{dz} \tag{14}$$

For steady-state transfer across a membrane, the permeation fluxes N_i are obtained by solving the set of two coupled ordinary differential equations (ODEs) (14) for the following set of boundary conditions (see schematic in Fig. 3)

$$\text{upstream face:} \quad z = 0; \quad p_i = p_{i0}; \quad q_i = q_{i0}; \quad \theta_i = \theta_{i0}; \quad \theta_V = \theta_{V0} \tag{15}$$

$$\text{downstream face:} \quad z = \delta; \quad p_i = p_{i\delta}; \quad q_i = q_{i\delta}; \quad \theta_i = \theta_{i\delta}; \quad \theta_V = \theta_{V\delta} \tag{16}$$

Exact analytic solutions to Eqs. (14), (15) and (16), allowing explicit calculations of the permeation fluxes, can be derived for the mixed-gas Langmuir description of adsorption equilibrium [38]; details are provided in the Supplementary material. There are many instances in which mixture adsorption equilibrium cannot be adequately described by the mixed-gas Langmuir model given by Eq. (9); this situation arises

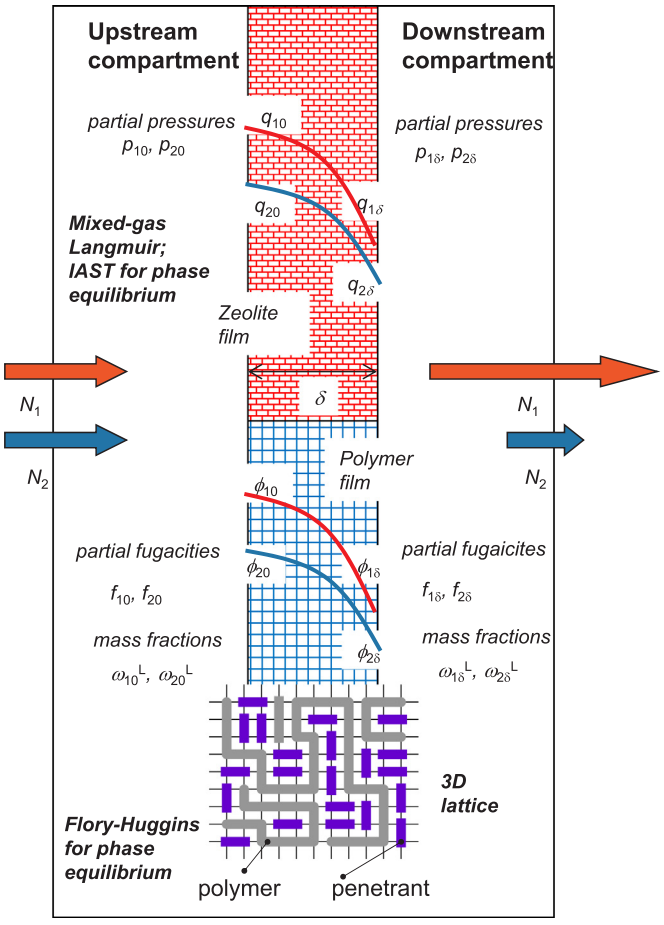

Fig. 3. Schematic showing mixture permeation across zeolite or polymeric membrane.

for permeation of linear and branched alkanes across MFI membranes for which the dual-site Langmuir model need to be used to take account of isotherm inflections [10,11]. Exact analytic solutions for steady-state fluxes cannot be derived in such cases; numerical solutions of the set of coupled ODEs are required [38]. An alternative, practical, approach is to determine the two matrices $[\Lambda]$, and $[\Gamma]$ at the averaged adsorbed phase loadings, mole fractions, and occupancies within the membrane: $q_{i,av} = \frac{q_{i0}+q_{i\delta}}{2}$; $x_{i,av} = \frac{x_{i0}+x_{i\delta}}{2}$; $\theta_{i,av} = \frac{\theta_{i0}+\theta_{i\delta}}{2}$.

In this *linearized* model, the fluxes are calculated explicitly as follows

$$\begin{pmatrix} N_1 \\ N_2 \end{pmatrix} = \frac{\rho}{\delta}\,[\Lambda]\,[\Gamma]\begin{pmatrix} q_{10}-q_{1\delta} \\ q_{20}-q_{2\delta} \end{pmatrix} \tag{17}$$

The component permeances can be determined using the definitions

$$\Pi_i \equiv \frac{N_i}{p_{i0}-p_{i\delta}} \tag{18}$$

The linearized model essentially assumes that the component loading profiles within the membrane layer are linear. The accuracy of the linearized model for flux calculations has been established by comparisons with exact solutions; see Fig. S33 of Supplementary material.

3. M-S diffusivities, and limiting scenarios for correlation effects

To get a feel for the relative magnitudes of the M-S diffusivities, consider the diffusion of a mixture of CO_2(1) and H_2(2) in MFI zeolite, that consists of a set of intersecting channels of 5.5 Å dimension (see computational snapshot in Fig. 4a). MD data on the three M-S diffusivities, Đ$_1$, Đ$_2$, and Đ$_{12}$ are plotted in Fig. 4b as a function of the total

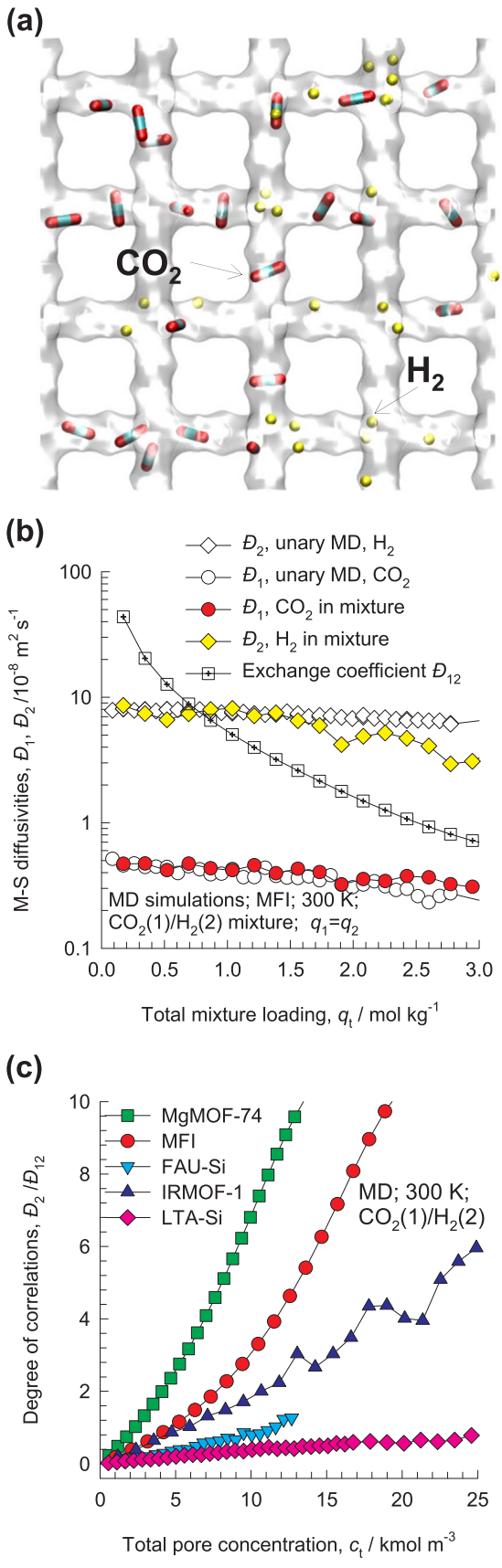

(caption on next page)

Fig. 4. (a) Snapshot showing the location of $CO_2(1)$ and $H_2(2)$ adsorbates within the intersecting channel structures of MFI. (b) MD simulation data [26] on the M-S diffusivities, $Đ_1$, and $Đ_2$, of CO_2, and H_2 as a function of the adsorbate loading; both for unary and for equimolar binary $CO_2(1)/H_2(2)$ mixtures. (c) MD simulation data [26] for the degree of correlations, MD simulation data for the degree of correlations, $Đ_1/Đ_{12}$, for diffusion of equimolar CO_2/H_2 mixtures at 300 K in a variety of host materials, as a function of the total pore concentration, $c_t = (q_1 + q_2)/V_p$.

loading of the adsorbed phase, q_t. The M-S diffusivities $Đ_1$, $Đ_2$ for unary diffusion are practically the same as those in the mixture; this suggests that unary permeation measurements allow estimations of the diffusivity data inputs for mixture permeation. Furthermore, we note that both diffusivities decrease with increased loading; accurate modelling of mixture permeation requires appropriate description of the loading dependence. A simple model to describe the loading dependence is

$$Đ_i = Đ_i(0)\theta_V \tag{19}$$

where θ_V is the fractional vacancy. Eq. (19) is essentially based on a simple hopping model in which a molecule can jump from one adsorption site to an adjacent one, provided it is not already occupied; the jump frequency is proportional to the fractional vacancy [20,27].

Fig. 4b shows that for mixture loadings, q_t, exceeding 1 mol kg^{-1}, the exchange coefficient $Đ_{12}$ is significantly smaller than $Đ_2$; this implies that the 1–2 frictional term has a significant impact on the H_2 flux. This rationalizes, albeit qualitatively at this stage, the lowering of H_2 permeance in the mixture that was observed in Fig. 1a.

It is convenient to define the ratios $\frac{Đ_1}{Đ_{12}}$, and $\frac{Đ_2}{Đ_{12}}$ to quantify the *degree of correlations*, using the terminology that is commonly used for zeolites; these ratios may also be viewed as quantifying the significance of 1–2 friction in relation to the 1-m and 2-m frictional contributions. These ratios may also be interpreted as signifying the importance of 1–2 friction in relation to 1-m, and 2-m frictional contributions. For $CO_2(1)/H_2(2)$ mixtures, Fig. 4c presents MD data on $Đ_2/Đ_{12}$ in five different micro-porous host materials, as a function of the total pore concentration, $c_t = (q_1 + q_2)/V_p$, where V_p is the accessible pore volume of the host. Generally speaking, correlation effects get stronger with increased loading; consequently, such effects are stronger for operations at elevated pressures. The observed hierarchy of correlation effects is: MgMOF-74 (hexagonal channels of 11 Å) > MFI (intersecting channels of 5.5 Å) > IRMOF-1 (two alternating, inter-connected, cavities of 10.9 Å and 14.3 Å with window size of 8 Å) > FAU (11.4 Å size cages separated by 7.4 Å size windows) > LTA (11.2 Å size cages separated by 4.1 Å size windows). Broadly speaking, correlation effects are stronger in larger "open" frameworks and for structures consisting of intersecting channels. Strong correlation effects cause slowing-down of more-mobile-less-strongly-adsorbed H_2 molecules by tardier-more-strongly-adsorbed-partner CO_2. Correlation effects are less significant, practically negligible, in hosts such as LTA, ZIF-8, CHA, DDR, ERI that consist of cages separated by narrow windows in the 3.2–4.2 Å size range [20,24,26,41]. Molecules jump one-at-a-time across the narrow windows, leading to un-correlated inter-cage hopping of guest species.

CO_2/H_2 separations will be H_2-selective in ZIF-7 and ZIF-8 membranes in which correlation effects are negligible [42,43], while MFI-membrane will result in CO_2-selective separations, as witnessed in the experiments of Sandström et al.[3] (cf. Fig. 1a).

For the scenario in which correlations effects are of negligible importance, we derive

$$\frac{Đ_1}{Đ_{12}} \to 0; \quad \frac{Đ_2}{Đ_{12}} \to 0; \quad \begin{bmatrix} Λ_{11} & Λ_{12} \\ Λ_{21} & Λ_{22} \end{bmatrix} \to \begin{bmatrix} Đ_1 & 0 \\ 0 & Đ_2 \end{bmatrix} \tag{20}$$

As validation of Eq. (20), Fig. 5a presents MD simulations of the elements of the matrix $Λ_{11}$, $Λ_{12}$, $Λ_{22}$ for equimolar Ne(1)/Ar(2) mixtures in CHA. We note that the values of the off-diagonal elements $Λ_{12} = Λ_{21}$ are about 1 – 3 orders of magnitude lower than the corresponding values of the diagonal elements $Λ_{11}$, $Λ_{22}$. The diagonal elements are practically the same as the unary M-S diffusivities $Đ_1$, and $Đ_2$; this is consistent with Eq. (20). Analogous results are obtained for Ne(1)/Ar(2) and $CO_2(1)/H_2(2)$ mixture diffusion in LTA zeolite; see Figs. 5b, and 5c.

When correlation effects are negligible, the diffusional coupling effects are solely traceable to mixture adsorption thermodynamics, embodied in the matrix $[Γ]$.

The other limiting scenario is the one in which the correlation effects are dominant (detailed derivations are provided in the Supplementary material):

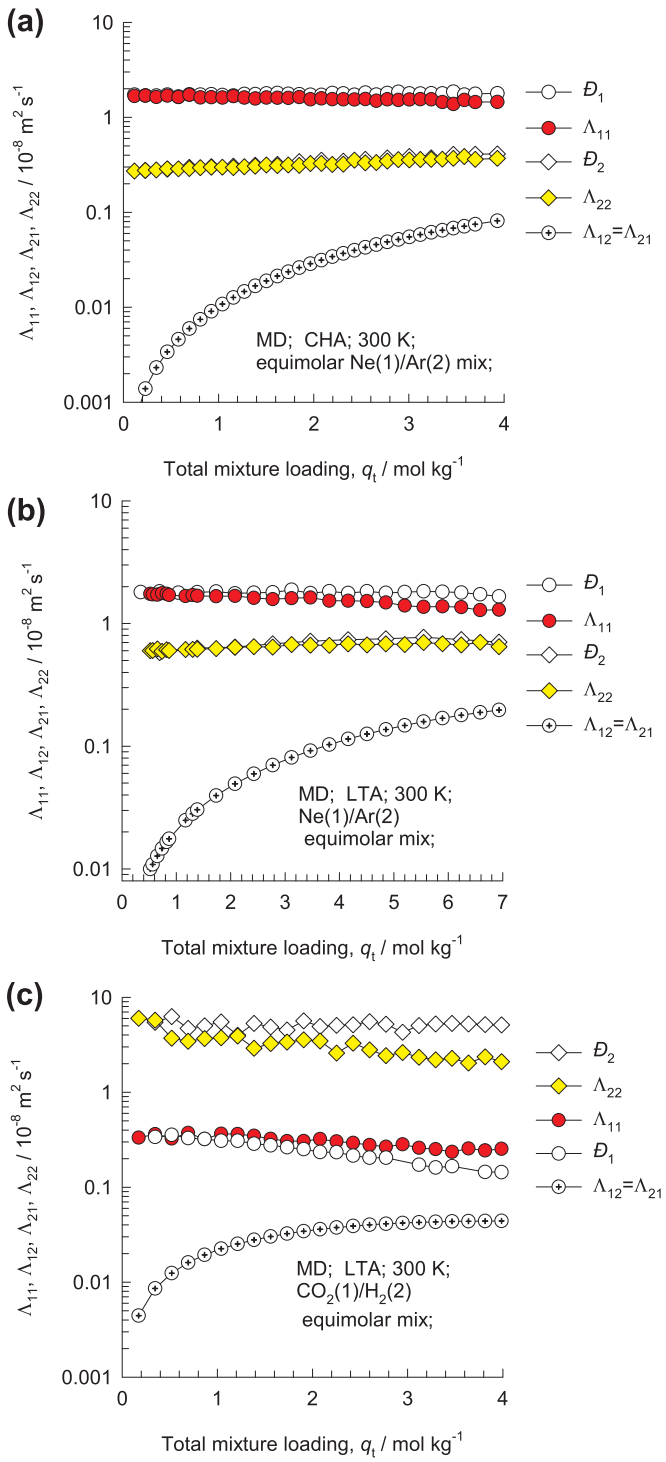

Fig. 5. MD simulation data [30,39,40] on the elements of the matrix $Λ_{11}$, $Λ_{12}$, $Λ_{22}$ for equimolar (a) Ne(1)/Ar(2) mixtures in CHA, (b) Ne(1)/Ar(2) mixtures in LTA, and (b) $CO_2(1)/H_2(2)$ mixtures in LTA at 300 K. The data are plotted as a function of the total mixture loading, q_t. Also shown the MD simulations of unary M-S diffusivities $Đ_1$, and $Đ_2$.

$$\frac{Đ_1}{Đ_{12}} >> 1; \quad \frac{Đ_2}{Đ_{12}} >> 1; \quad [\Lambda] = \frac{1}{\frac{x_1}{Đ_1} + \frac{x_2}{Đ_2}} \begin{bmatrix} x_1 & x_1 \\ x_2 & x_2 \end{bmatrix} \tag{21}$$

Remarkably, in this scenario, $\Lambda_{11} = \Lambda_{12}$, and $\Lambda_{21} = \Lambda_{22}$. For equimolar mixtures, $x_1 = x_2$, all the four elements of $[\Lambda]$ are equal to one another.

The dominant correlations scenario is a good approximation under pore saturation conditions [40]. As illustration, Fig. 6a,b,c present MD simulation data of the elements of the matrix Λ_{11}, Λ_{12}, Λ_{22} for equimolar (a) $CH_4(1)/C_3H_8(2)$ mixtures in BEA, (b) $C_2H_6(1)/C_3H_8(2)$ mixtures in MFI, and (b) $CH_4(1)/C_2H_6(2)$ mixtures in ISV. All three zeolites have intersecting channel topologies, and in all three cases we note that the elements Λ_{11}, Λ_{12}, Λ_{22} converge to the same diffusivity value at increasing mixture loadings; the continuous solid lines are the calculations of Λ_{11}, Λ_{12}, Λ_{22} using Eq. (21). In this scenario, there is only one characteristic diffusivity in the mixture when the zeolite pores are saturated.

Eqs. (20) and (21) provide lower and upper bounds for the influence of 1–2 friction on binary mixture diffusion in micro-porous materials. With this theoretical background, we investigate some published experimental data on mixture permeation across zeolite membranes.

4. Kr/Xe mixture permeation across SAPO-34 membrane

Experimental data for Kr/Xe permeation across SAPO-34 membranes are reported by Kwon et al. [44] at various temperatures, T. SAPO-34 has the same structural topology of CHA zeolite, consisting of 8.4 Å size cages separated by 3.8 Å × 4.2 Å size windows; see pore landscapes in Fig. 7a. In view of the data presented in Fig. 5a, for Ne/Ar/CHA, we anticipate the inter-cage hopping of Kr and Xe across the narrow windows to be un-correlated [41]. Eq. (20), used in conjunction with Eqs. (17) and (18), allows backing-out of the M-S diffusivities $Đ_1$ and $Đ_2$ directly from the data on unary and 10/90 Kr/Xe mixture permeances at various T. The two different sets of backed-out diffusivity values correspond closely to each other (see Fig. 7b), confirming the applicability of the negligible correlations scenario. Furthermore, the T-dependence of $Đ_i$ has an Arrhenius character; this suggests the existence of a free-energy barrier for inter-cage hopping [41].

The backed-out diffusivity values from 90/10, and 9/91 Kr/Xe mixture permeance data of Feng et al.[45] demonstrate that $Đ_1$ and $Đ_2$ do not depend on mixture composition (see Fig. 7c); this conclusion is also a direct consequence of the negligible correlations scenario described by Eq. (20).

The detailed Maxwell-Stefan analysis presented by Li et al. [4,5] on permeation of CO_2/CH_4, CO_2/N_2, N_2/CH_4 H_2/CH_4, H_2/N_2, H_2/CO, and $CO_2/CH_4/N_2$ mixtures across SAPO-34 membrane also validates the negligible correlations scenario, and rationalizes the data plotted in Fig. 1b showing that the CO_2 permeance in CO_2/H_2 mixtures is the same as the unary values.

The negligible correlations scenario does not, however, lead to the conclusion that the flux Eq. (17) are uncoupled. Fig. 8a plots the ratios of the elements of thermodynamic correction factors, $\frac{\Gamma_{12}}{\Gamma_{11}}$, $\frac{\Gamma_{21}}{\Gamma_{22}}$ as function of the mole fraction of Kr(1) in the bulk gas phase for Kr(1)/Xe(2) mixture adsorption in SAPO-34 at 298 K for total pressure $p_1 + p_2 = p_t = 0.2$ MPa. The off-diagonal elements are significant fractions of the corresponding diagonal elements, signaling strong thermodynamic coupling.

An important consequence of the coupling induced by the thermodynamic correction factors, is that during transient approach to steady-state the more mobile species often exhibits transient flux overshoots. As illustration, Fig. 8b shows the transient fluxes for permeation fluxes of 10/90 Kr/Xe across SAPO-34 membrane. During the initial transience, the Kr/Xe selectivity exceeds the steady-state value by about three orders of magnitude. The Kr flux overshoot, that is indicative of uphill diffusion [9,10], disappears if the matrix of thermodynamic

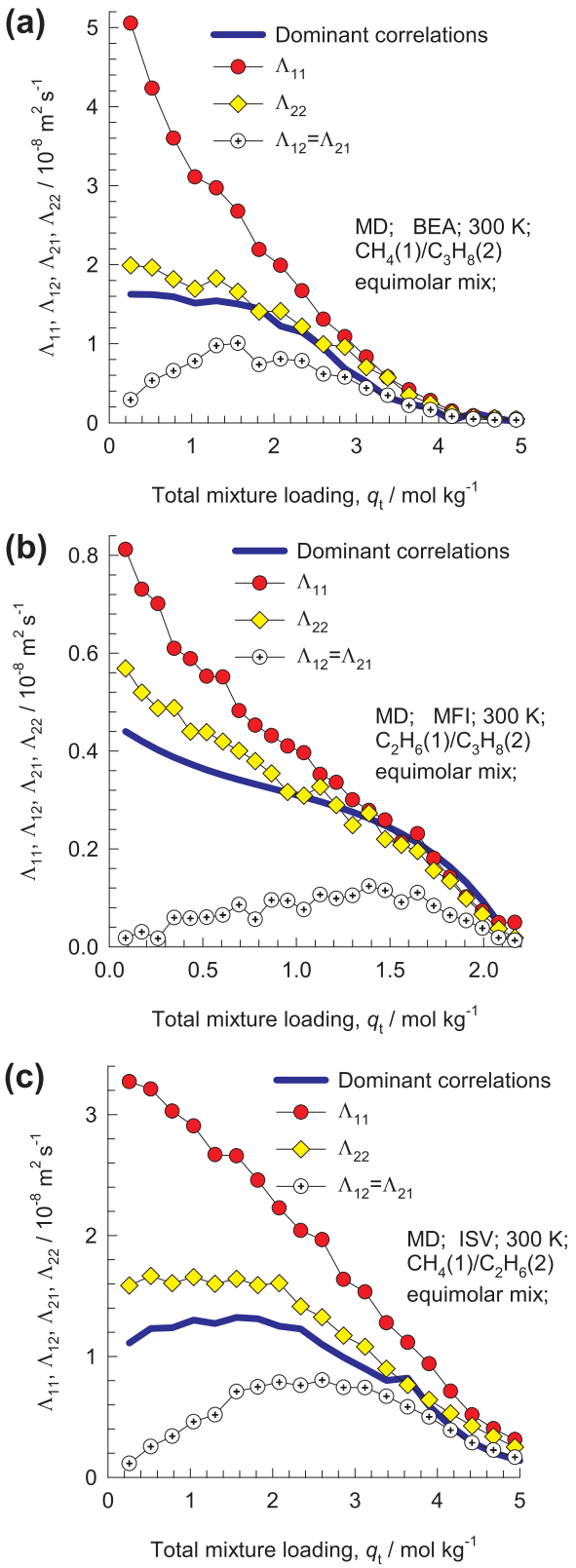

Fig. 6. MD simulation data [40] of the elements of the matrix Λ_{11}, Λ_{12}, Λ_{22} for equimolar (a) $CH_4(1)/C_3H_8(2)$ mixtures in BEA, (b) $C_2H_6(1)/C_3H_8(2)$ mixtures in MFI, and (b) $CH_4(1)/C_2H_6(2)$ mixtures in ISV at 300 K. The data are plotted as a function of the total mixture loading, q_t. The continuous solid lines are the calculations of Λ_{11}, Λ_{12}, Λ_{22} using Eq. (21).

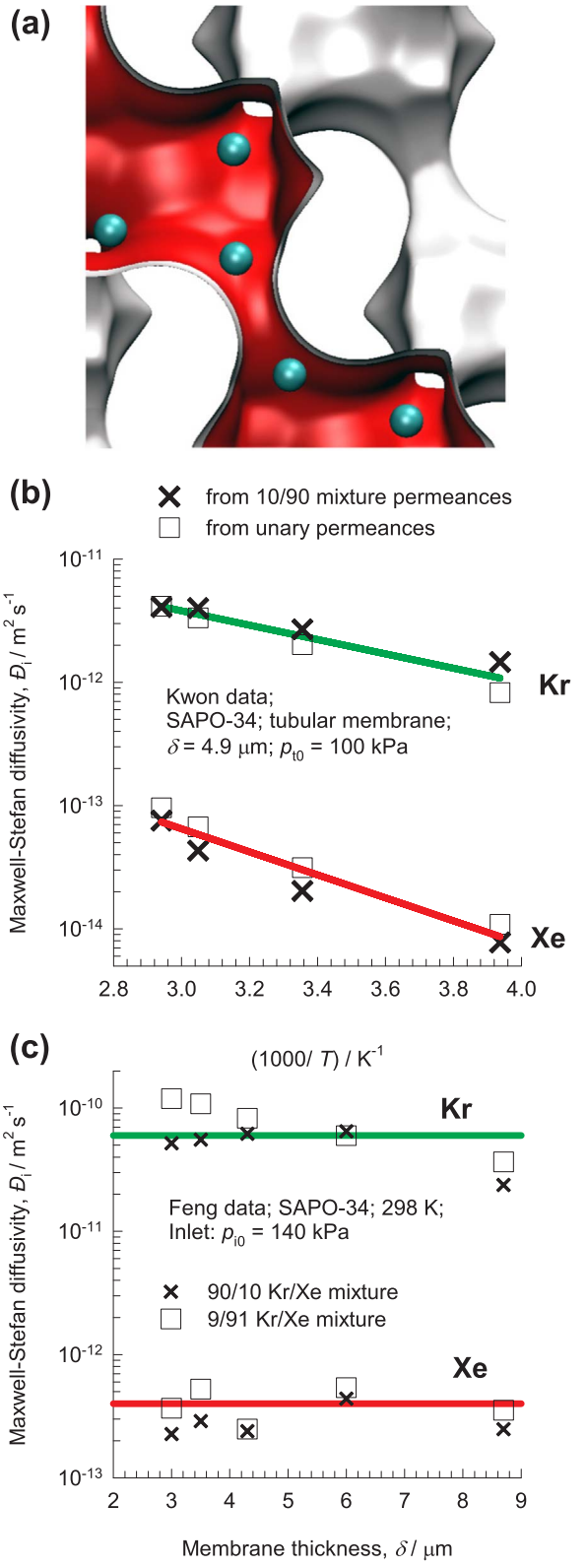

Fig. 7. (a) Pore landscape of CHA zeolite. (b) M-S diffusivities, $Đ_i$, of Kr (1) and Xe (2) for SAPO-34 tubular membrane of thickness δ = 4.9 μm thickness, backed out from experimental data [44] on unary and binary 10/90 Kr/Xe mixture permeances at various T. (c) M-S diffusivities, $Đ_i$, of Kr (1) and Xe (2) for SAPO-34 membranes of varying thicknesses, δ, backed out from experimental data [45] on 90/10, and 9/91 Kr/Xe mixture permeances. Further calculation details are provided in the Supplementary material.

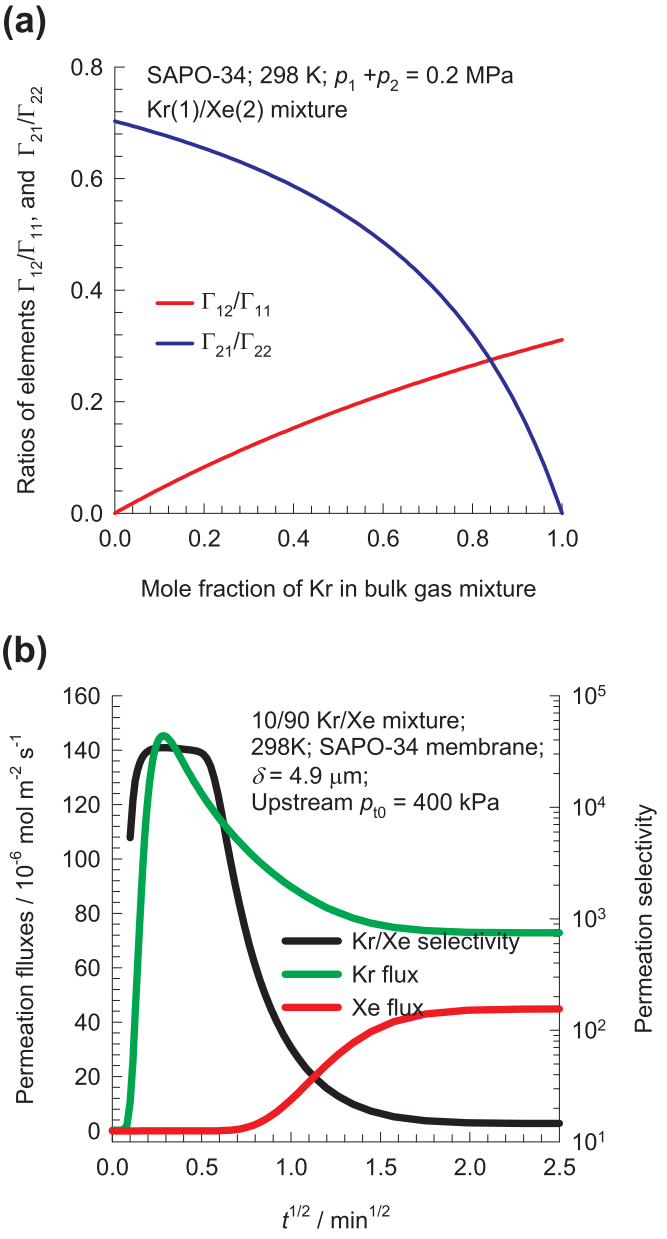

Fig. 8. (a) Ratios of the elements of thermodynamic correction factors, $\frac{\Gamma_{12}}{\Gamma_{11}}$, $\frac{\Gamma_{21}}{\Gamma_{22}}$ as function of the mole fraction of Kr(1) in the bulk gas phase for Kr(1)/Xe(2) mixture adsorption in SAPO-34 at 298 K for total pressure $p_1 + p_2 = p_t$ = 0.2 MPa. (b) Transient permeation of 10/90 Kr (1)/Xe (2) across SAPO-34 membrane of thickness δ = 4.9 μm at upstream total pressure of 400 kPa, and T = 298 K. Further calculation details are provided in the Supplementary material.

correction factors $[\Gamma]$ is assumed to equal the identity matrix $[I]$, with elements $\Gamma_{ij} = \delta_{ij}$, the Kronecker delta [9,10]. The exploitation of transient overshoot phenomena to attain enhanced selectivities, albeit for short time durations, is a fertile area for further investigations.

Geus et al.[46] report experimental data on transient 50/50 CH_4/nC_4H_{10} mixture permeation across an MFI membrane; the flux of the more mobile CH_4 exhibits a pronounced overshoot during the approach to steady state; the origin of this overshoot has also been traced to the influence of thermodynamic coupling [9,10].

5. CO_2/H_2 mixture permeation across MFI membrane

We now analyze the experimental data of Sandström [3] presented in Fig. 1a. Using Eq. (19) to describe the loading dependences of the M-S diffusivities, the experimental data on unary pearmances are used to

determine the transport coefficients at zero-loading, $\rho Đ_1(0)/\delta = 3.2$, and $\rho Đ_2(0)/\delta = 100$ kg m^{-2} s^{-1}. For the prediction of the component permeances in binary mixtures, we need additional data inputs on the degrees of correlation; for this purpose we use the MD data in Fig. 4c as guidelines. In the Sandström [3] experiments, the values of the total mixture loadings, q_t, are in the range 1–3 mol kg^{-1}, and MD simulated $Đ_2/Đ_{12}$ values for MFI lie in the range of 2–10 for this range of mixture loadings. An excellent match with the experimental permeances can be achieved using the linearized model solution (Eqs. (17) and (18)), with the choice $Đ_2/Đ_{12} = 8$; see the continuous solid lines in Fig. 9a. Generally speaking, correlation effects have a strong *retarding* influence of the permeation of more-mobile-less-strongly-adsorbed molecules. Conversely, correlation effects are of lesser importance for tardier-more-strongly-adsorbed species. The choice of the precise value of the degree of correlations does not have a significant influence on the CO_2 permeance, but the value of H_2 permeance is severely affected. In order to demonstrate this, Fig. 9b compares the experimental data on permeances of H_2 with the estimations based on increasing degrees of correlations, $Đ_2/Đ_{12} = 2$, 8, 20, and 40. Also shown in Fig. 9b are the estimates of the permeances, using the limiting scenarios of negligible correlations (Eq. (20)), and dominant correlations (Eq. (21)). The experimental data on H_2 permeance lies about midway between the values of the two limiting scenarios for degrees of correlations. The results in Fig. 9 highlight the importance of using proper estimates of correlation effects to predict the permeances of H_2.

Fig. 10a shows the experimental data of Sjöberg et al.[47] on the permeation fluxes of CO_2 and H_2 as a function of the upstream total pressure, p_{t0}; these data were measured at a slightly lower temperature of 273 K. The continuous solid lines in Fig. 10a are the flux estimations using Eq. (17), along with the same input data: $\rho Đ_1(0)/\delta = 3.2$, and $\rho Đ_2(0)/\delta = 100$ kg m^{-2} s^{-1} and $Đ_2/Đ_{12} = 8$, as used to model the Sandström experiments. The estimations are in excellent agreement with the experimental data. The strong influence of the choice of the degree of correlations $Đ_2/Đ_{12}$ is highlighted in the calculations in Fig. 10b. For H_2, invoking the negligible correlations scenario, leads to larger fluxes than observed experimentally. For CO_2/H_2 separations, this implies that neglecting correlations leads to the most pessimistic estimates of permeation selectivities. The dominant correlations scenario indicates the maximum attainable CO_2/H_2 selectivities.

An important message to emerge from the foregoing analysis is that accurate estimates of the exchange coefficient $Đ_{12}$ are of vital importance in predicting mixture permeation characteristics. A further conclusion to be drawn in that CO_2/H_2 permeation selectivities can be improved by appropriate choice of membrane materials that lead to increased degree if correlations. The MD data in Fig. 4c indicates that MgMOF-74 has significantly higher degree of correlations than MFI; the potential of this MOF for selective CO_2 permeation from a variety of gaseous mixtures has been underscored in earlier work [48].

6. Maxwell-Stefan analysis of mixture permeation across polymer membranes

The sorption thermodynamics of penetrants and polymer is most commonly described by the Flory-Huggins (F-H) relations [2,49,50]; the F-H model is based on the idea that the chain elements of the polymer arrange themselves randomly (but with the molecules remaining connected) on a three-dimensional lattice (see schematic in Fig. 3). The F-H model expresses the component activities, a_i, in the polymer phase as function of the component volume fractions, $\phi_i = c_i \overline{V_i} = x_i c_t \overline{V_i} = x_i \frac{\overline{V_i}}{\overline{V}}$ where $\overline{V_i}$ is the partial molar volume, and $\overline{V} = \frac{1}{c_t} = \sum_{k=1}^{m} x_k \overline{V_k}$ is the mean molar volume of the mixture. The polymer chains are considered to form part of the mixture and are treated as the $(n+1)th$ component. For compatibility with the F-H relations, it is most convenient to re-write the M-S Eq. (1) using volume fractions as composition measures

$$-\frac{1}{RT}\frac{d\mu_i}{dz} = \sum_{j=1,j\neq i}^{n} \frac{\phi_j(u_i - u_j)}{Đ_{ij}^V} + \frac{\phi_m(u_i - u_m)}{Đ_{im}^V}; \quad i = 1.2, ,n \tag{22}$$

The modified M-S diffusivities obey the symmetry constraint $\frac{Đ_{12}^V}{V_2} = \frac{Đ_{21}^V}{V_1}$ that is imposed by the Onsager Reciprocal Relations. Eq. (22) apply generally to polymeric *solutions*; for permeation across polymeric membranes, we impose the additional constraint $u_m = 0$, implying the stagnancy of the membrane material.

Let us define the *volumetric* flux of component i, expressed as m^3 m^{-2} s^{-1} as $N_i^V = \phi_i u_i$. The molar flux of component i, expressed as mol m^{-2} s^{-1} is $N_i = c_i u_i = \frac{\phi_i}{V_i} u_i = \frac{N_i^V}{V_i}$. For the specific case of binary mixtures there is a total of three species in the mixture: 1, 2 and m. In terms of the volumetric fluxes of components, Eq. (22) can be transformed to

$$-\frac{\phi_i}{RT}\frac{d\mu_i}{dz} = \sum_{j=1,j\neq i}^{2} \frac{(\phi_j N_i^V - \phi_i N_j^V)}{Đ_{ij}^V} + \frac{(\phi_m N_i^V)}{Đ_{im}^V}; \quad i = 1.2 \tag{23}$$

The chemical potential gradients are relatable to the gradients in volume fraction by defining thermodynamic correction factors [Γ]

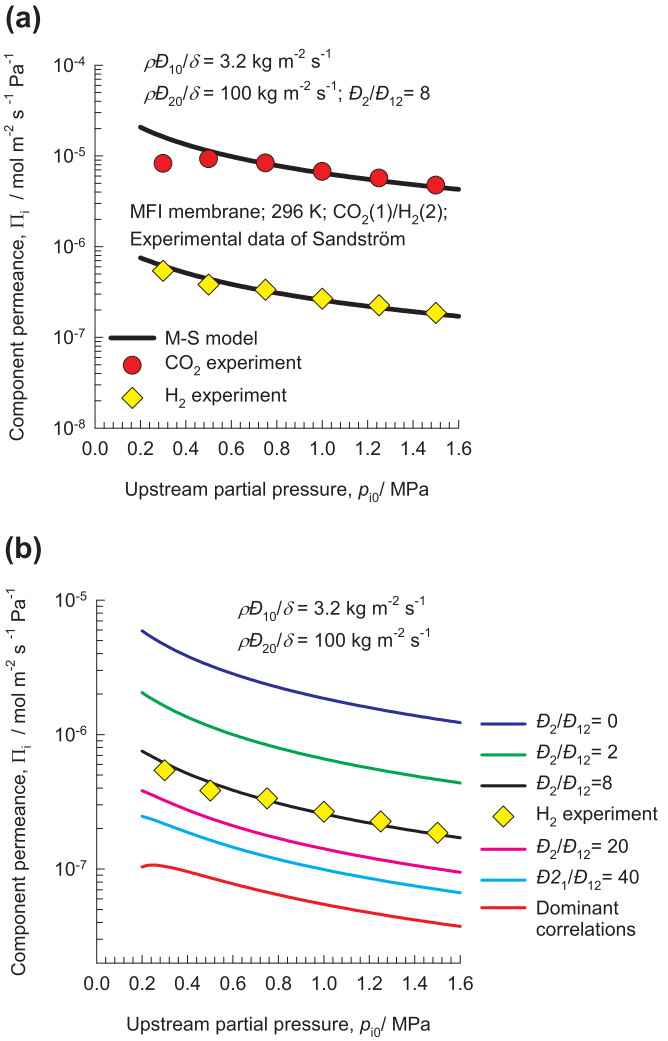

Fig. 9. (a) Experimental data [3] on permeances of $CO_2(1)$ and $H_2(2)$ across MFI membrane at 296 K compared with the estimations using Eqs. (17) and (18), along with the values of $\rho Đ_1(0)/\delta = 3.2$, and $\rho Đ_2(0)/\delta = 100$ kg m^{-2} s^{-1}, and $Đ_2/Đ_{12} = 8$. (b) Experimental data on permeances of H_2 and compared with the estimations based on varying degrees of correlations, $Đ_2/Đ_{12}$. Further calculation details are provided in the Supplementary material.

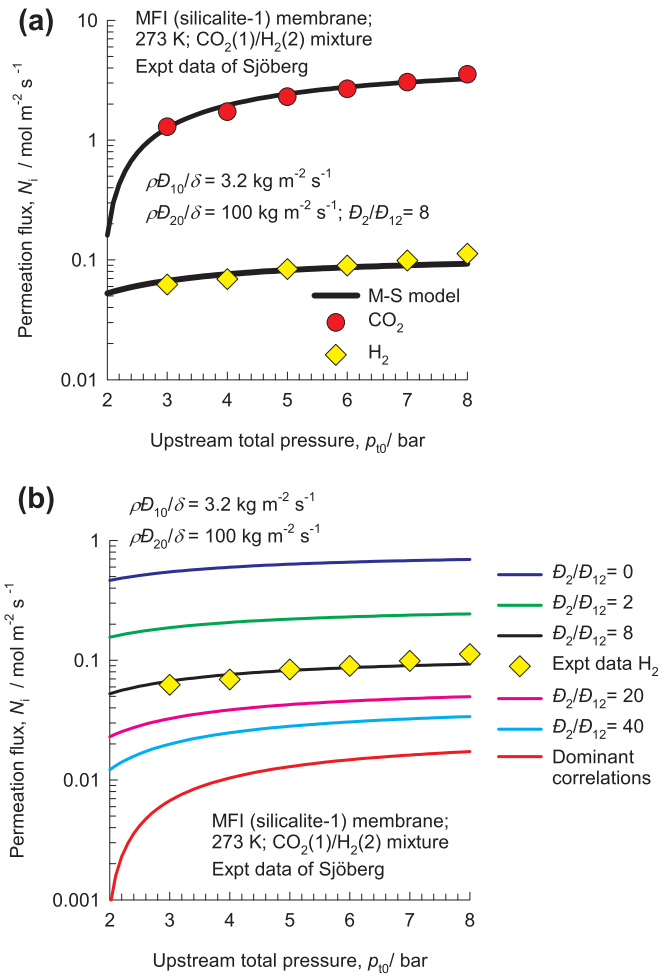

Fig. 10. (a) Experimental data [47] on permeation fluxes of CO_2(1) and H_2(2) across MFI membrane at 273 K compared with the estimations using Eq. (17), along with the values of $\rho Đ_1(0)/\delta = 3.2$, and $\rho Đ_2(0)/\delta = 100$ kg m^{-2} s^{-1}, and $Đ_2/Đ_{12} = 8$. (b) Experimental data on permeances of H_2 and compared with the estimations based on varying degrees of correlations, $Đ_2/Đ_{12}$. Further calculation details are provided in the Supplementary material.

$$\frac{\phi_i}{RT}\frac{d\mu_i}{dz} = \phi_i\frac{d\ln a_i}{dz} = \sum_{j=1}^{j=n}\Gamma_{ij}\frac{d\phi_j}{dz}; \qquad \Gamma_{ij} = \frac{\phi_i}{\phi_j}\frac{\partial \ln a_i}{\partial \ln \phi_j}; \qquad i,j = 1, ...n \tag{24}$$

The elements Γ_{ij} can be obtained by analytic differentiation of the F-H equations.

For steady-state permeation of binary mixtures across a polymer membrane of thickness, δ, we can derive explicit expressions for the volumetric fluxes N_i^V by assuming linear variations of volume fractions within the polymer film:

$$(N^V) = \frac{[\Lambda]}{\delta}[\Gamma](\phi_0 - \phi_\delta) \tag{25}$$

The elements of the matrix $[\Lambda]$ are determined explicitly

$$\begin{bmatrix}\Lambda_{11} & \Lambda_{12}\\ \Lambda_{21} & \Lambda_{22}\end{bmatrix} = \frac{1}{\phi_m\left(\frac{\phi_1 Đ_{2m}^V}{Đ_{21}^V} + \frac{\phi_2 Đ_{1m}^V}{Đ_{12}^V} + \phi_m\right)}\begin{bmatrix} Đ_{1m}^V\left(\phi_m + \frac{\phi_1 Đ_{2m}^V}{Đ_{21}^V}\right) & Đ_{1m}^V\frac{\phi_1 Đ_{2m}^V}{Đ_{21}^V}\\ Đ_{2m}^V\frac{\phi_2 Đ_{1m}^V}{Đ_{12}^V} & Đ_{2m}^V\left(\phi_m + \frac{\phi_2 Đ_{1m}^V}{Đ_{12}^V}\right)\end{bmatrix} \tag{26}$$

It is noteworthy that an important difference between the expression for $[\Lambda]$ in zeolites (Eq. (12)), and polymers (Eq. (26)) is the appearance of ϕ_m in the denominator of the right member of Eq. (26); this is because the polymer membrane is considered to be part of the *ternary* (1, 2, m) mixture.

The permeabilities of components in the polymer membrane can be calculated using

$$\Pi_i = \frac{N_i^V/\overline{V_i}}{(f_{i0} - f_{i\delta})/\delta} \tag{27}$$

Readers will note that the same symbol Π_i has been used earlier for zeolite membrane *permeances*. The SI units for the permeability is mo m m^{-2} s^{-1} Pa^{-1}. The more commonly used engineering unit for permeability is the Barrer expressed in cm^3 (STP) cm cm^{-2} s^{-1} (cm Hg)$^{-1}$. To convert to the commonly used engineering units of Barrers we divide the value in mol m m^{-2} s^{-1} Pa^{-1} by 3.348 × 10^{-16}.

In the limiting scenario in which 1–2 friction is considered to be of negligible importance: $\frac{\phi_1 Đ_{2m}^V}{Đ_{21}^V} \to 0$; $\frac{\phi_2 Đ_{1m}^V}{Đ_{12}^V} \to 0$. For this scenario, the matrix $[\Lambda]$ simplifies to yield

$$\begin{bmatrix}\Lambda_{11} & \Lambda_{12}\\ \Lambda_{21} & \Lambda_{22}\end{bmatrix} = \frac{1}{\phi_m}\begin{bmatrix} Đ_{1m}^V & 0\\ 0 & Đ_{2m}^V\end{bmatrix} \tag{28}$$

Broadly speaking, we should expect the negligible 1–2 friction scenario to hold when the volume fractions of both penetrants in the membrane are negligibly small.

We consider 1–2 friction to dominate if $\frac{\phi_2 Đ_{1m}^V}{\phi_m Đ_{12}^V} >> 1$; $\frac{\phi_1 Đ_{2m}^V}{\phi_m Đ_{21}^V} >> 1$. In this scenario, we get the simple expression, analogous to Eq. (21) for zeolites:

$$\begin{bmatrix}\Lambda_{11} & \Lambda_{12}\\ \Lambda_{21} & \Lambda_{22}\end{bmatrix} = \frac{1}{\phi_m\left(\frac{\phi_1}{V_1 Đ_{1m}^V} + \frac{\phi_2}{V_2 Đ_{2m}^V}\right)}\begin{bmatrix}\frac{\phi_1}{V_1} & \frac{\phi_1}{V_1}\\ \frac{\phi_2}{V_2} & \frac{\phi_2}{V_2}\end{bmatrix} \tag{29}$$

7. Water/ethanol pervaporation across polymer membranes

In applying the linearized Eq. (25), the elements of $[\Gamma]$ and $[\Lambda]$ are evaluated at the arithmetic averaged volume fractions $\phi_{i,av} = \frac{(\phi_{i0} + \phi_{i\delta})}{2}$. For validating the accuracy of the linearized solution, comparisons are made with numerical solutions of the set of coupled ODEs for water/ethanol pervaporation across cellulose acetate [51,52], and polyimide [6] membranes. Fig. 11a shows the volume fractions within cellulose acetate (CA) membrane layer for a liquid phase water(1)/ethanol(2) feed mixture with mass fraction $\omega_1^L = 0.40563$. From the F-H phase equilibrium relations, the volume fractions at the upstream face are $\phi_1 = 0.16187$ $\phi_2 = 0.26327$. The continuous solid lines are the profiles obtained from an exact numerical solution to the set of two coupled ODEs, resulting in the fluxes $N_1^V = 2.4 \times 10^{-7}$, and $N_2^V = 2.2 \times 10^{-7}$ m^3 m^{-2} s^{-1}. The dashed lines are the linear profiles resulting from the linearized model, using Eq. (25), that results in the permeation flux values of $N_1^V = 2.33 \times 10^{-7}$, and $N_2^V = 1.98 \times 10^{-7}$ m^3 m^{-2} s^{-1}.

Fig. 11b shows calculations of the volume fractions within the polyimide membrane layer for a liquid phase water(1)/ethanol(2) feed mixture with mass fraction $\omega_1^L = 0.7473$. From the F-H phase equilibrium relations, the volume fractions at the upstream face are $\phi_1 = 0.1424$; $\phi_2 = 0.0226$. The volumetric fluxes calculated using Eq. (25), are $N_1^V = 15.78 \times 10^{-9}$, and $N_2^V = 0.448 \times 10^{-9}$ m^3 m^{-2} s^{-1}. The corresponding volume fraction profiles within the membrane layer are linear. An exact numerical solution to the set of two coupled ODEs, results in the flux values $N_1^V = 15.5 \times 10^{-9}$, and $N_2^V = 0.487 \times 10^{-9}$ m^3 m^{-2} s^{-1}.

In both examples, the linearized model estimates the pervaporation fluxes to within about 5% of the exact numerical solutions.

Having established the accuracy of the linearized model, we now attempt to rationalize the maximum in the ethanol flux observed in the water/ethanol/polyimide pervaporation experiments [6] shown in

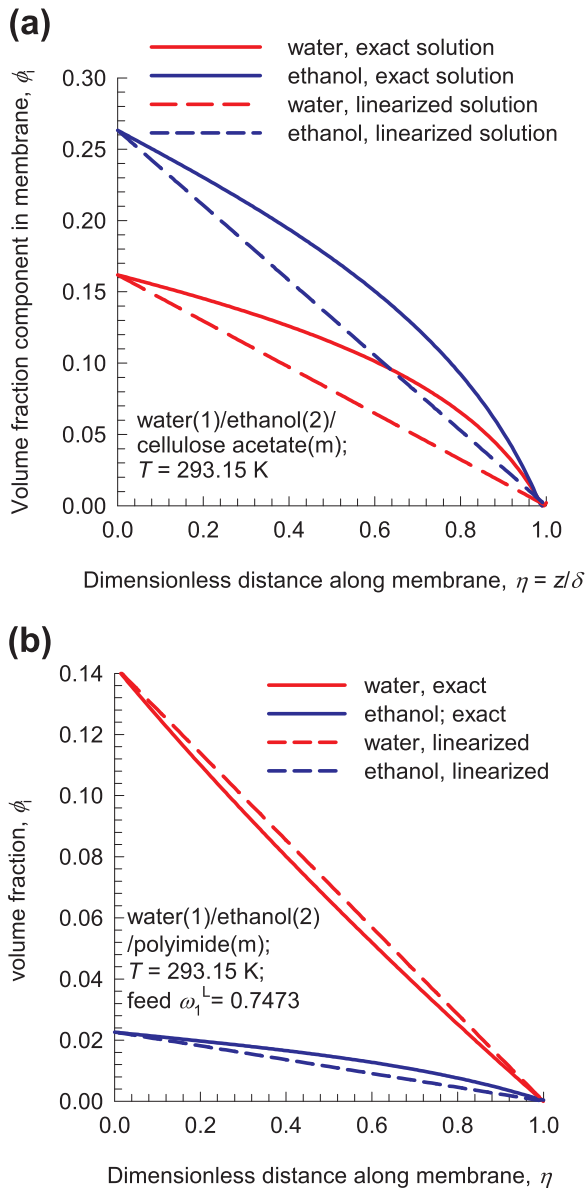

Fig. 11. Volume fractions of penetrants water (1) and ethanol (2) within (a) cellulose acetate (CA), and (b) polyimide membranes. The continuous solid lines are the profiles obtained from an exact numerical solution to the set of two coupled ODEs for steady-state permeation. The dashed lines are the linear profiles resulting from the linearized model. Further calculation details are provided in the Supplementary material.

Fig. 2a. The most likely explanation for the observed maximum in the ethanol flux is the coupling with the flux of water. There are two possible origins of coupling between the fluxes of water and ethanol; these are traceable to the off-diagonal elements of the two matrices $[\Gamma]$, and $[\Lambda]$. Thermodynamic coupling effects are of significant importance as demonstrated by the ratios of the elements of thermodynamic correction factors, $-\frac{\Gamma_{12}}{\Gamma_{11}}$, $-\frac{\Gamma_{21}}{\Gamma_{22}}$, plotted as function of the mass fraction of water in the liquid feed mixture in the upstream compartment, ω_1^L in Fig. 12a. The off-diagonal elements are significant in magnitude in comparison with the diagonal elements. Particularly noteworthy is the maximum in the value of $-\frac{\Gamma_{21}}{\Gamma_{22}}$. Comparisons of the experimental data with flux estimations using Eq. (25) are shown in Fig. 12b,c for three different scenarios for 1–2 friction. The experimentally observed maximum in the ethanol flux, observed at a feed mixture mass fraction $\omega_1^L \approx 0.2$, can only be captured if the chosen value of $\frac{Đ_{2m}^V}{Đ_{21}^V}$ exceeds 2. An increase of 1–2 friction has the effect of slowing down the more mobile water molecules, while speeding up the tardier ethanol; i.e. the permeation

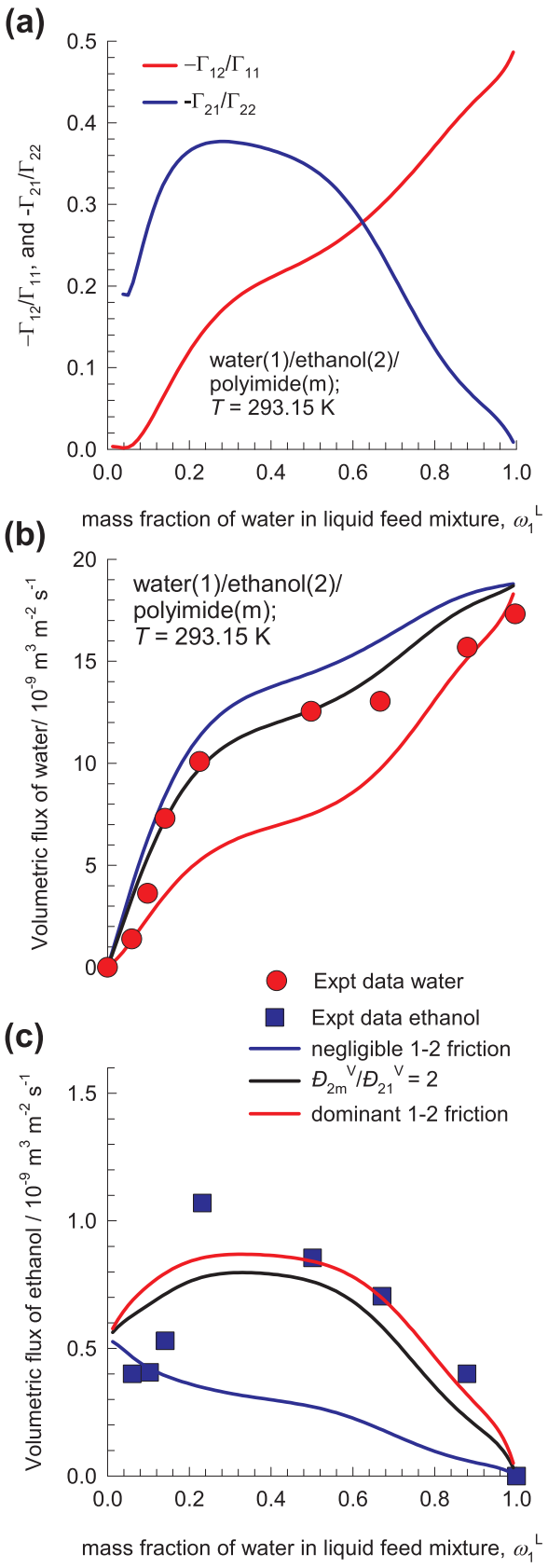

Fig. 12. (a) Ratios of the elements of thermodynamic correction factors, $-\frac{\Gamma_{12}}{\Gamma_{11}}$, $-\frac{\Gamma_{21}}{\Gamma_{22}}$ for water(1)/ethanol/(2)/polyimide as function of the mass fraction of water(1) in the liquid feed mixture in the upstream compartment ω_1^L. (b, c) Comparison of experimental data [6] on volumetric fluxes of water, and ethanol with model estimations for three different 1–2 friction scenarios. Further calculation details are provided in the Supplementary material.

selectivity diminishes with increased $\frac{Đ^V_{2m}}{Đ^V_{21}}$.

The rationalization of the water(1)/ethanol(2)/PVA/PAN experiments [7] proceeds along precisely analogous lines. The off-diagonal elements are significant in magnitude in comparison with the corresponding diagonal elements (cf. Fig. 13a); clearly, thermodynamic coupling has a significant influence on the permeation fluxes. The experimental fluxes of both water and ethanol can be matched reasonably well if the 1–2 friction is quantified using $\frac{Đ^V_{2m}}{Đ^V_{21}} = 4$. Values of $\frac{Đ^V_{2m}}{Đ^V_{21}}$ lower than 4 results in underestimation of the ethanol flux, whilst overestimating the water flux. Conversely, choosing $\frac{Đ^V_{2m}}{Đ^V_{21}}$ larger than 4 tends to reduce the flux of the more mobile water, thereby reducing the permeation selectivity. If the 1–2 frictional contribution is considered to be negligible, there is no maximum in the ethanol flux but causes a maximum in the water flux, that is not experimentally detected.

8. Analysis of CO_2/C_2H_6 permeation across XLPEO membrane

The permeabilities for unary permeation of CO_2 and C_2H_6 across a cross-linked polyethylene oxide (XLPEO) membrane at 263.15 K, and 298.15 are reported Ribeiro et al. [53]. Fig. 14a,b show the backed-out, averaged, M-S diffusivities $Đ^V_{im}$ for CO_2 and C_2H_6 at the two temperatures. The backed-out diffusivities demonstrate the validity of the exponential model $Đ^V_{im} = Đ^V_{im,0}\exp[A_i\phi_i]$, commonly used to describe the composition dependence of M-S diffusivities in polymers.

Ribeiro et al.[53] have published extensive data on CO_2/C_2H_6 mixture permeation across XLPEO membrane, measured at temperatures of 263.15 K, and 298.15 K at varying upstream compositions and partial fugacities. In the absence of guidelines from MD simulation data on significance of 1–2 friction contributions, we first attempt an analysis neglecting 1–2 friction and using the simplified model described by Eq. (28), allowing the backing-out of the M-S diffusivities $Đ^V_{im}$ directly from mixture permeabilities. In Figs. 14c, and d, the data on $Đ^V_{im}$ are plotted as function of the averaged volume fraction of penetrants, $\phi_{1,av} + \phi_{2av}$. At both temperatures, there is qualitative agreement between the M-S diffusivity in the mixture with the corresponding composition dependence of unary diffusivities. For the more mobile CO_2, the diffusivity in the mixture is somewhat lower than the corresponding unary diffusivity values, when compared at the same total, average, volume fraction in the membrane $\phi_{1,av} + \phi_{2av}$. Conversely, for the tardier C_2H_6, the diffusivity in the mixture is slightly higher than the corresponding unary diffusivity values. For both penetrants, the deviations are higher at the lower temperature; this is to be expected because of the higher volume fractions occupied by the penetrants within the membrane. The lack of perfect match between the data on M-S diffusivities backed out from unary and mixture permeation experiments indicates that the assumption of negligible 1–2 friction does not hold perfectly.

For a quantitative analysis of the Ribeiro experiments, we need to include the 1–2 friction contributions. Good match between the experimental data is obtained with the choice $\frac{Đ^V_{2m}}{Đ^V_{21}} = 4$, at either temperature; see comparisons in Fig. 15. The *x*-axis represents the partial fugacity of the permeants in the bulk gas phase in the upstream compartment; five different mixture compositions are considered. We note that the permeability of C_2H_6 is strongly influenced (increased) by increasing proportion of CO_2 in the bulk gas phase mixture in the upstream compartment. On the other hand, the permeability of the more strongly sorbed CO_2 is influenced to a much reduced extent by the feed mixture composition. The permeability estimations using Eqs. (25), (26), and (27), shown by the continuous solid lines, quantitatively capture all the essential features of the composition dependence of the permeabilities of CO_2 and C_2H_6, for all feed mixture compositions and partial fugacities.

In order to gain further insights into the influence of 1–2 friction on the component permeabilities, the parity plots in Fig. 16 compare the

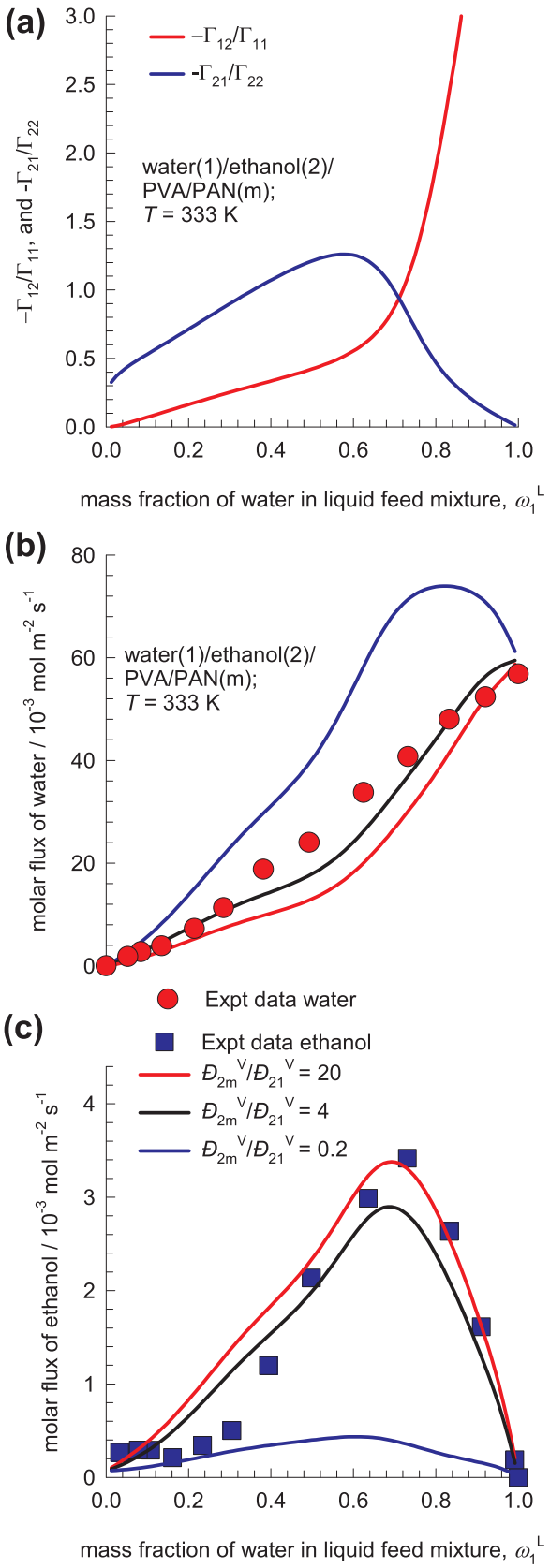

Fig. 13. (a) Ratios of the elements of thermodynamic correction factors, $-\frac{\Gamma_{12}}{\Gamma_{11}}$, $-\frac{\Gamma_{21}}{\Gamma_{22}}$ for water(1)/ethanol(2)/PVA/PAN as function of the mass fraction of water(1) in the liquid feed mixture in the upstream compartment ω_1^L. (b, c) Comparison of experimental data [7] on molar fluxes of water, and ethanol with model estimations for three different 1–2 friction scenarios. Further calculation details are provided in the Supplementary material.

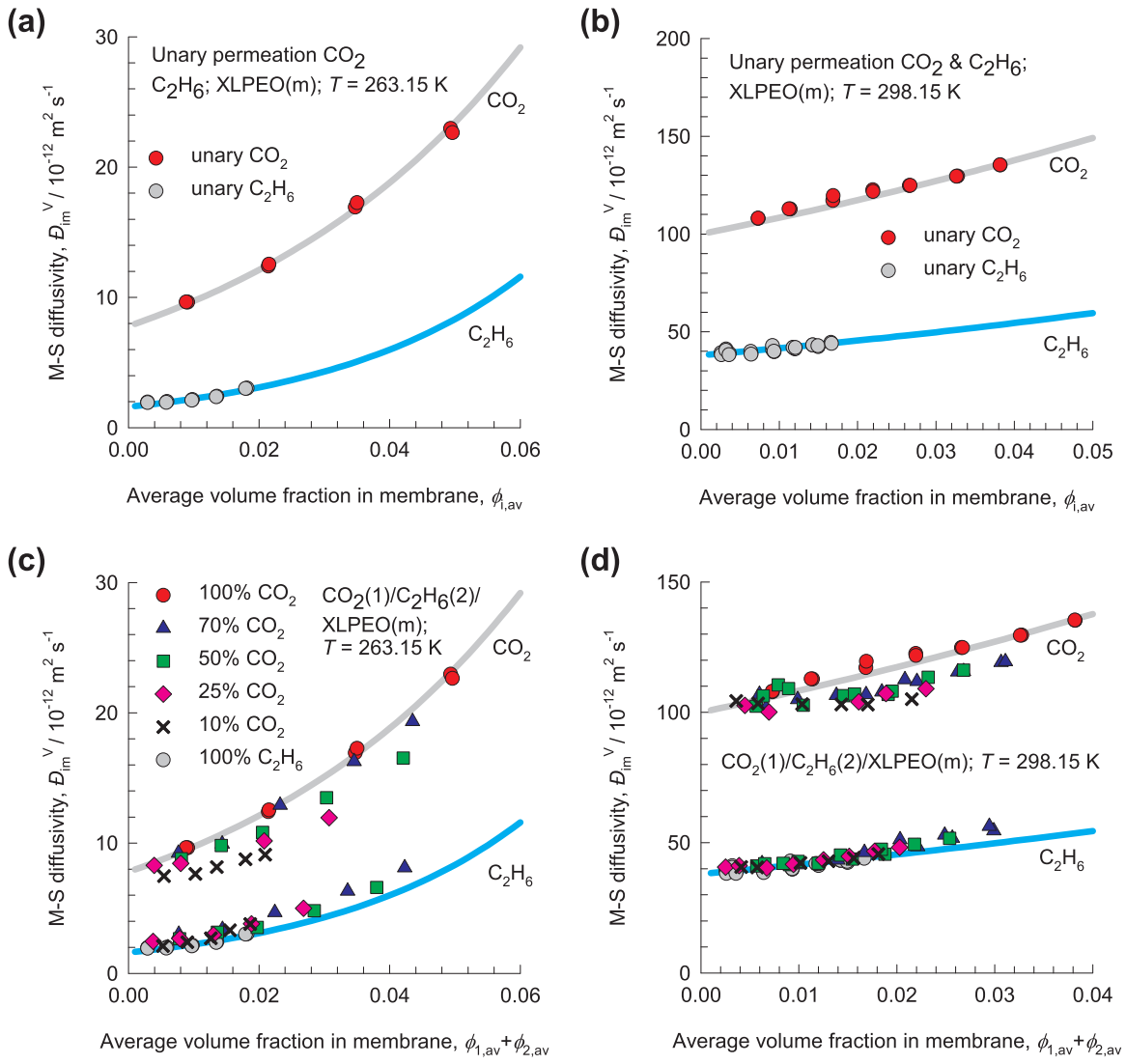

Fig. 14. Averaged values of the Maxwell-Stefan diffusivities for CO_2(1) and C_2H_6(2) in cross-linked polyethylene oxide (XLPEO) membrane at (a, c) 263.15 K, and (b, d) 298.15 K. The *x*-axis represents the average volume fraction in the membrane, calculated from $\phi_{i,av} = \frac{(\phi_{i0}+\phi_{i\delta})}{2}$, assuming $\phi_{i\delta} \approx 0$. The diffusivities are backed out from experimental data [53] on the (a, b) unary permeabilities, and (c, d) mixture permeabilities. The continuous solid lines are the exponential fits of the *unary* diffusivities alone. Further calculation details are provided in the Supplementary material.

model predictions with experiments for the limiting scenarios of negligible and dominant friction, along with the "fitted' value $\frac{Đ^V_{2m}}{Đ^V_{21}} = 4$. Neglecting 1–2 friction leads to over-prediction of the CO_2 permeability, while under-predicting that of the tardier C_2H_6. In the other extreme, adoption of the dominant friction scenario has the effect of slowing-down the more mobile CO_2 while speeding-up the transport of C_2H_6; this influence is precisely the same as seen earlier for pervaporation processes. The Maxwell-Stefan formulation serves to provide insights into how 1–2 friction affects the separation selectivity, and whether improvements can be obtained by perhaps altering the degree of polymer cross-linking to adjust the 1–2 friction to the optimum level.

The approach that is adopted here is distinctly different from that used by Ribeiro et al. [15] to model their own experiments; their approach involves numerical solution of the set of coupled ODEs, using values of $Đ^V_{1m}$, $Đ^V_{2m}$, and $Đ^V_{21} = \frac{Đ^V_{12}}{\overline{V_2}}\overline{V_1}$ that are fitted to experimental CO_2/C_2H_6/XLPEO *mixture* permeation data at the two temperatures. In our approach, the input values of the M-S diffusivities $Đ^V_{im}$ are determined from *unary* permeation experiments; the only other "fitting" parameter employed is the value of $\frac{Đ^V_{2m}}{Đ^V_{21}} = 4$ for both temperatures.

It is noteworthy that the foregoing analyses of experimental data on CO_2/C_2H_6/XLPEO, water/ethanol/polyimide, and water/ethanol/PVA/PAN all show that the 1–2 frictional contribution is best described by values of $\frac{Đ^V_{2m}}{Đ^V_{21}}$ in the range of 2 – 4, and the hierarchy of magnitudes $Đ^V_{1m} > Đ^V_{2m} > Đ^V_{21} = \frac{Đ^V_{12}}{\overline{V_2}}\overline{V_1}$; this hierarchy implies that $Đ^V_{21} = \frac{Đ^V_{12}}{\overline{V_2}}\overline{V_1}$ cannot be estimated using the Vignes interpolation formula commonly used for zeolites [32,33].

9. Conclusions

The Maxwell-Stefan "frictional" formulation has been used to develop a unified description of mixture permeation across zeolite and polymer membranes. The following major conclusions emerge from the analysis of published experimental data, along with MD simulations.

(1) For membrane permeation of binary mixtures of species 1 and 2 across membrane (m), the M-S formulation for permeation fluxes clearly delineates the 1-m, 2-m, and interspecies (1 − 2) frictional contributions. Generally speaking, the influence of 1–2 friction is to slow down the more mobile species in the mixture.
(2) Two limiting scenarios for the 1–2 friction are identified and

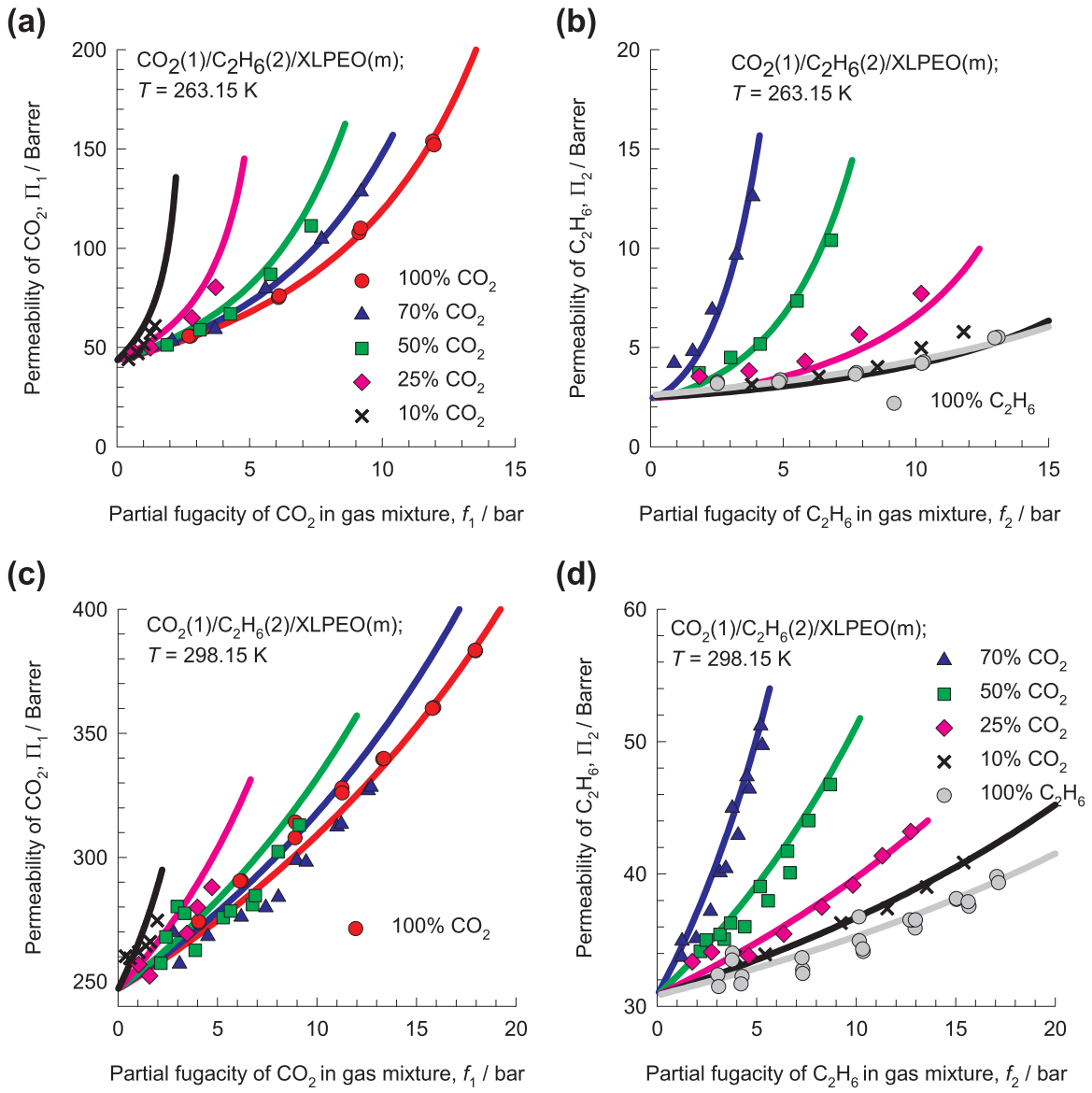

Fig. 15. Membrane permeabilities, expressed in Barrers, of (a, c) CO_2(1), and (b, d) C_2H_6(2) for binary CO_2/C_2H_6 mixture permeation across a cross-linked polyethylene oxide (XLPEO) membrane at (a, b) 263.15 K, (c, d) 298.15 K. The *x*-axis represents the partial fugacity of (a, c) CO_2, and (b,d) C_2H_6 in the bulk gas phase in the upstream compartment. The experimental data [53] are shown by the symbols. The continuous solid lines are the calculations using the linearized Eqs. (25), (26), and (27). Further calculation details are provided in the Supplementary material.

characterized: negligible 1–2 friction and dominant 1–2 friction. The two limiting scenarios determine the upper and lower bounds of permeation selectivities, suggesting which type of material to choose for the purposes of improving separation performance.

(3) For zeolites, the scenario of negligible 1–2 friction, also termed as the scenario for negligible correlation effects, is realized in structures such as LTA, CHA, DDR, ZIF-8, and ERI that consists of cages, separated by narrow windows in the 3 Å – 4.2 Å range. For polymer membranes, the assumption of negligible 1–2 friction only holds when the volume fractions of the penetrants in the membrane phase are vanishingly small.

(4) Even if 1–2 friction is of negligible importance, the fluxes are coupled because of phase equilibrium thermodynamics. For transient permeation, thermodynamic coupling often results in transient overshoots and the occurrence of uphill diffusion, as illustrated for SAPO-34 membrane in Fig. 8b.

(5) The contribution of 1–2 friction is particularly significant, often dominant, for water/alcohols pervaporation processes across polymeric membranes. There is need for further research on developing reliable procedures for estimating 1–2 frictional contributions for both zeolites and polymer membranes.

(6) The linearized solutions to M-S equations for steady-state permeation, Eqs. (17) and (25), afford simple, and robust, procedure for explicit determination of fluxes.

The linearized solution to the M-S equations can also be gainfully employed for modelling of the immersion precipitation process for membrane preparation; see Figs. S53 and S54. Uphill diffusion is routinely encountered is routinely encountered in such processes, impacting on the membrane structure created [54,55].

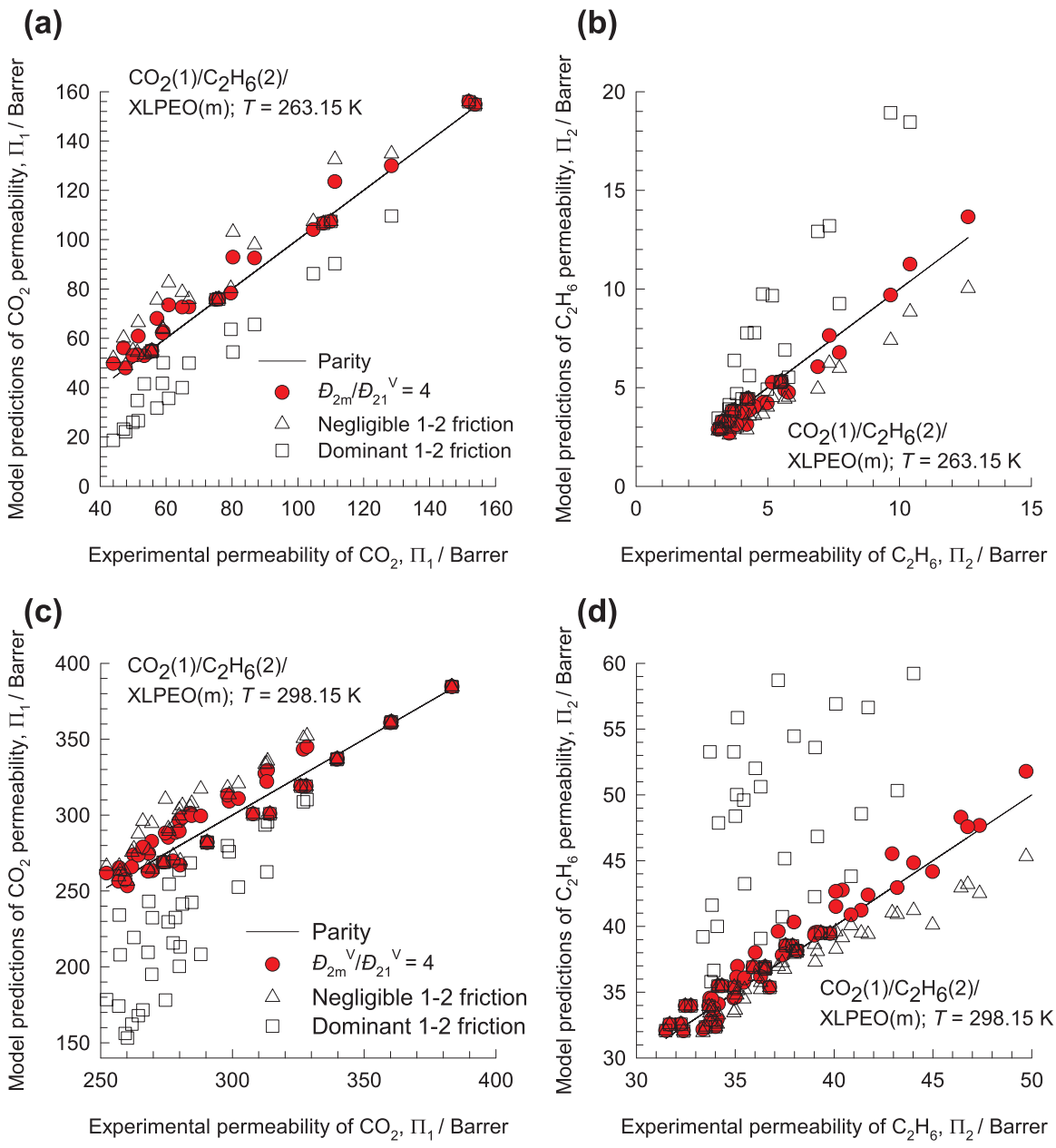

Fig. 16. Comparison of the experimental data [53] on membrane permeabilities of (a, c) CO_2(1), and (b, d) C_2H_6(2) for binary CO_2/C_2H_6 mixture permeation across a cross-linked polyethylene oxide (XLPEO) membrane at (a, b) 263.15 K, (c, d) 298.15 K with the model predictions using the linearized model using three different scenarios for estimation of 1–2 friction. Further calculation details are provided in the Supplementary material.

Appendix A. Supporting information

Supplementary data associated with this article can be found in the online version at http://dx.doi.org/10.1016/j.memsci.2017.06.062.

References

[1] K.K. Sirkar, Separation of Molecules, Macromolecules and Particles. Principles, Phenomena and Processes, Cambridge University Press, Cambridge, 2014.
[2] J.A. Wesselingh, R. Krishna, Mass Transfer in Multicomponent Mixtures, VSSD, Delft, 2000.
[3] L. Sandström, E. Sjöberg, J. Hedlund, Very high flux MFI membrane for CO_2 separation, J. Membr. Sci. 380 (2011) 232–240.
[4] R. Krishna, S. Li, J.M. van Baten, J.L. Falconer, R.D. Noble, Investigation of slowing-down and speeding-up effects in binary mixture permeation across SAPO-34 and MFI membranes, Sep. Purif. Technol. 60 (2008) 230–236.
[5] S. Li, J.L. Falconer, R.D. Noble, R. Krishna, Interpreting unary, binary and ternary mixture permeation across a SAPO-34 membrane with loading-dependent Maxwell-Stefan diffusivities, J. Phys. Chem. C 111 (2007) 5075–5082.
[6] X. Ni, X. Sun, D. Ceng, Coupled diffusion of water and ethanol in a polyimide membrane, Polym. Eng. Sci. 41 (2001) 1440–1447.
[7] A. Heintz, W. Stephan, A generalized solution-diffusion model of the pervaporation process through composite membranes Part II. Concentration polarization, coupled diffusion and the influence of the porous support layer, J. Membr. Sci. 89 (1994) 153–169.
[8] G.L. Standart, R. Taylor, R. Krishna, The Maxwell-Stefan formulation of irreversible thermodynamics for simultaneous heat and mass transfer, Chem. Eng. Commun. 3 (1979) 277–289.
[9] R. Krishna, Uphill diffusion in multicomponent mixtures, Chem. Soc. Rev. 44 (2015) 2812–2836.
[10] R. Krishna, Tracing the origins of transient overshoots for binary mixture diffusion in microporous crystalline materials, Phys. Chem. Chem. Phys. 18 (2016) 15482–15495.
[11] R. Krishna, The Maxwell-Stefan description of mixture diffusion in nanoporous crystalline materials, Microporous Mesoporous Mater. 185 (2014) 30–50.
[12] R. Krishna, Describing mixture permeation across polymeric membranes by a combination of Maxwell-Stefan and Flory-Huggins models, Polymer 103 (2016) 124–131.
[13] F. Fornasiero, J.M. Prausnitz, C.J. Radke, Multicomponent diffusion in highly asymmetric systems. An extended Maxwell-Stefan model for starkly different-sized, segment-accessible chain molecules, Macromolecules 38 (2005) 1364–1370.
[14] F. Fornasiero, F. Krull, J.M. Prausnitz, C.J. Radke, Steady-state diffusion of water

through soft-contact-lens materials, Biomaterials 26 (2005) 5704–5716.
[15] C.P. Ribeiro, B.D. Freeman, D.R. Paul, Modeling of multicomponent mass transfer across polymer films using a thermodynamically consistent formulation of the Maxwell-Stefan equations in terms of volume fractions, Polymer 52 (2011) 3970–3983.
[16] A. Heintz, W. Stephan, A generalized solution-diffusion model of the pervaporation process through composite membranes Part I. Prediction of mixture solubilities in the dense active layer using the UNIQUAC model, J. Membr. Sci. 89 (1994) 143–151.
[17] M. Yu, J.L. Falconer, R.D. Noble, R. Krishna, Modeling transient permeation of polar organic mixtures through a MFI zeolite membrane using the Maxwell-Stefan equations, J. Membr. Sci. 293 (2007) 167–173.
[18] J. Newman, K.E. Thomas-Alyea, Electrochemical Systems, 3rd ed., John Wiley & Sons, Inc, Hoboken, New Jersey, 2004.
[19] R. Krishna, Highlighting coupling effects in ionic diffusion, Chem. Eng. Res. Des. 114 (2016) 1–12.
[20] R. Krishna, Diffusion in porous crystalline materials, Chem. Soc. Rev. 41 (2012) 3099–3118.
[21] J.S. Vrentas, J.L. Duda, Molecular diffusion in polymer solutions, AIChEJ 25 (1979) 1–24.
[22] P.E. Price, I.H. Romdhane, Multicomponent diffusion theory and its applications to polymer-solvent systems, AIChEJ 49 (2003) 309–322.
[23] R.J. Bearman, On the molecular basis of some current theories of diffusion, J. Phys. Chem. 65 (1961) 1961–1968.
[24] R. Krishna, Describing the diffusion of guest molecules inside porous structures, J. Phys. Chem. C 113 (2009) 19756–19781.
[25] R. Krishna, J.M. van Baten, Investigating the relative influences of molecular dimensions and binding energies on diffusivities of guest species inside nanoporous crystalline materials, J. Phys. Chem. C 116 (2012) 23556–23568.
[26] R. Krishna, J.M. van Baten, Investigating the influence of diffusional coupling on mixture permeation across porous membranes, J. Membr. Sci. 430 (2013) 113–128.
[27] R. Krishna, J.M. van Baten, Influence of adsorption thermodynamics on guest diffusivities in nanoporous crystalline materials, Phys. Chem. Chem. Phys. 15 (2013) 7994–8016.
[28] R. Krishna, J.M. van Baten, Insights into diffusion of gases in zeolites gained from molecular dynamics simulations, Microporous Mesoporous Mater. 109 (2008) 91–108.
[29] R. Krishna, J.M. van Baten, Diffusion of alkane mixtures in MFI zeolite, Microporous Mesoporous Mater. 107 (2008) 296–298.
[30] R. Krishna, J.M. van Baten, Unified Maxwell-Stefan description of binary mixture diffusion in micro- and meso- porous materials, Chem. Eng. Sci. 64 (2009) 3159–3178.
[31] R. Krishna, J.M. van Baten, Maxwell-Stefan modeling of slowing-down effects in mixed gas permeation across porous membranes, J. Membr. Sci. 383 (2011) 289–300.
[32] A.I. Skoulidas, D.S. Sholl, R. Krishna, Correlation effects in diffusion of CH_4/CF_4 mixtures in MFI zeolite. A study linking MD simulations with the Maxwell-Stefan formulation, Langmuir 19 (2003) 7977–7988.
[33] F. Kapteijn, J.A. Moulijn, R. Krishna, The generalized Maxwell-Stefan model for diffusion in zeolites: sorbate molecules with different saturation loadings, Chem. Eng. Sci. 55 (2000) 2923–2930.
[34] R. Krishna, J.M. van Baten, Highlighting pitfalls in the maxwell-stefan modeling of water-alcohol mixture permeation across pervaporation membranes, J. Membr. Sci. 360 (2010) 476–482.
[35] R. Krishna, J.M. van Baten, Hydrogen bonding effects in adsorption of water-alcohol mixtures in zeolites and the consequences for the characteristics of the Maxwell-Stefan diffusivities, Langmuir 26 (2010) 10854–10867.
[36] R. Krishna, J.M. van Baten, Mutual slowing-down effects in mixture diffusion in zeolites, J. Phys. Chem. C 114 (2010) 13154–13156.
[37] A.L. Myers, J.M. Prausnitz, Thermodynamics of mixed gas adsorption, AIChEJ 11 (1965) 121–130.
[38] R. Krishna, R. Baur, Modelling issues in zeolite based separation processes, Sep. Purif. Technol. 33 (2003) 213–254.
[39] R. Krishna, J.M. van Baten, Onsager coefficients for binary mixture diffusion in nanopores, Chem. Eng. Sci. 63 (2008) 3120–3140.
[40] R. Krishna, J.M. van Baten, Describing mixture diffusion in microporous materials under conditions of pore saturation, J. Phys. Chem. C 114 (2010) 11557–11563.
[41] R. Krishna, J.M. van Baten, A molecular dynamics investigation of the diffusion characteristics of cavity-type zeolites with 8-ring windows, Microporous Mesoporous Mater. 137 (2011) 83–91.
[42] Y. Li, F. Liang, H. Bux, W. Yang, J. Caro, Zeolitic imidazolate framework ZIF-7 based molecular sieve membrane for hydrogen separation, J. Membr. Sci. 354 (2010) 48–54.
[43] R. Krishna, J.M. van Baten, In silico screening of zeolite membranes for CO_2 capture, J. Membr. Sci. 360 (2010) 323–333.
[44] Y.H. Kwon, C. Kiang, E. Benjamin, Pr Crawford, S. Nair, R. Bhave, Krypton-xenon separation properties of SAPO-34 zeolite materials and membranes, AIChEJ 63 (2017) 761–769.
[45] X. Feng, Z. Zong, S. Elsaidi, J.B. Jasinski, R. Krishna, P.K. Thallapally, M.A. Carreon, Kr/Xe separation over a chabazite zeolite membrane, J. Am. Chem. Soc. 138 (2016) 9791–9794.
[46] E.R. Geus, H. van Bekkum, W.J.W. Bakker, J.A. Moulijn, High-temperature stainless steel supported zeolite (MFI) membranes: preparation, module construction, and permeation experiments, Microporous Mater. 1 (1993) 131–147.
[47] E. Sjöberg, S. Barnes, D. Korelskiy, J. Hedlund, MFI membranes for separation of carbon dioxide from synthesis gas at high pressures, J. Membr. Sci. 486 (2015) 132–137.
[48] R. Krishna, J.M. van Baten, Investigating the potential of MgMOF-74 membranes for CO_2 capture, J. Membr. Sci. 377 (2011) 249–260.
[49] C.P. Ribeiro, B.D. Freeman, Sorption, dilation, and partial molar volumes of carbon dioxide and ethane in cross-linked poly(ethylene oxide), Macromolecules 41 (2008) 9458–9468.
[50] C.P. Ribeiro, B.D. Freeman, Solubility and partial molar volume of carbon dioxide and ethane in crosslinked poly(ethylene oxide) copolymer, J. Polym. Sci.: Part B: Polym. Phys. 41 (2010) 9458–9468.
[51] M.H.V. Mulder, C.A. Smolders, On the mechanism of separation of ethanol/water mixtures by pervaporation. I. Calculation of concentration profiles, J. Membr. Sci. 17 (1984) 289–307.
[52] M.H.V. Mulder, A.C.M. Franken, C.A. Smolders, On the mechanism of separation of ethanol/water mixtures by pervaporation. II. Experimental concentration profiles, J. Membr. Sci. 22 (1985) 41–58.
[53] C.P. Ribeiro, B.D. Freeman, D.R. Paul, Pure- and mixed-gas carbon dioxide/ethane permeability and diffusivity in a cross-linked poly(ethylene oxide) copolymer, J. Membr. Sci. 377 (2011) 110–123.
[54] G.B. van den Berg, C.A. Smolders, Diffusional phenomena in membrane separation processes, J. Membr. Sci. 73 (1992) 103–118.
[55] A.J. Reuvers, C.A. Smolders, Formation of membranes by means of immersion precipitation Part II. The mechanism of formation of membranes prepared from the system cellulose acetate - acetone - water, J. Membr. Sci. 34 (1987) 67–86.

Supplementary Material to accompany

Using the Maxwell-Stefan formulation for Highlighting the Influence of Interspecies (1-2) Friction on Binary Mixture Permeation across Microporous and Polymeric Membranes

Rajamani Krishna

Van 't Hoff Institute for Molecular Sciences, University of Amsterdam, Science Park 904,

1098 XH Amsterdam, The Netherlands

*Tel +31 20 6270990; Fax: + 31 20 5255604;

email: r.krishna@contact.uva.nl

Table of Contents

1. Preamble

This Supplementary material accompanying the article *Using the Maxwell-Stefan formulation for Highlighting the Influence of Interspecies (1-2) Friction on Binary Mixture Permeation across Microporous and Polymeric Membranes* provides: (1) structural details of the zeolite and polymeric membranes investigated, (2) unary isotherm data for adsorption of guest species in the zeolites, along with estimation methods for mixture adsorption equilibrium, (4) Flory-Huggins parameters for fluid-polymer equilibria, (5) detailed derivations of analytic expressions for calculation of steady-state fluxes and permeances, (6) input data on M-S diffusivities for simulations of membrane permeation, and (7) detailed results of simulations and comparisons with published experimental data.

The information provided in this supplementary document is sufficiently detailed to enable interested researchers and practitioners to reproduce all of the calculations presented in this article.

For ease of reading, this Supplementary material is written as a stand-alone document; as a consequence, there is some overlap of material with the main manuscript.

2. Structural topology and connectivity of some common zeolites

A number of different channel topologies and connectivities are encountered in zeolite structures; these can be divided into five broad classes:

A number of different channel topologies and connectivities are encountered in zeolite structures; these can be divided into five broad classes:

1. One-dimensional (1D) channels (e.g. LTL, TON, LTL).

2. 1D channels with side pockets (e.g. MOR, FER).
3. Intersecting channels (e.g. MFI, BEA, ISV)
4. Cages separated by narrow windows (e.g. LTA, CHA)
5. Cavities with large windows (e.g. FAU).

The crystallographic data are available on the zeolite atlas website of the International Zeolite Association (IZA).[1, 2] The pore topology and structural details of some common zeolites are provided are provided in the accompanying Figures as indicated below:

BEA (Figures 1, 2); CHA (see Figures 3, 4); ERI (Figures.7, 8); DDR (see Figures 5, 6); ISV (Figures 11, 12); FAU (see Figures 9, 10); LTA (see Figures 13, 14); MFI (see Figures 15, 16)

SAPO-34 has the same structural topology of CHA zeolite, as shown in Figures 3, and 4. This consists of 8.4 Å size cages separate by 3.8 Å × 4.2 Å size windows. The crystal framework density of CHA is 1444.1 kg m^{-3}. Readers should note that the SAPO-34 permeation model calculations presented by Kwon et al.[3] use the wrong value of the framework density of 1800 kg m^{-3}, as indicated in Page S6 of the Supporting Information accompanying their publication. Consequently, the numerical values of the Maxwell-Stefan diffusivities they have reported are in error; we return to this point later in this document.

Besides zeolites, the following MOFs and ZIFs are also discussed in the article: IRMOF-1 (Figures 17, 18);,MgMOF-74 (Figures 19, 20),ZIF-8 (Figures 21, 22).

Further details on the structure, landscape, pore dimensions of a very wide variety of micro-porous materials are available in our earlier publications.[4-11]

3. The Maxwell-Stefan description of *n*-component mixture permeation across microporous membranes

Within microporous crystalline materials, such as zeolites, metal-organic frameworks (MOFs), and zeolitic imidazolate frameworks (ZIFs), the guest molecules, or, "penetrants", exist in the adsorbed phase. The phenomenological description of transport of penetrants inside all microporous crystalline materials are formally identically, and for convenience, we use the term "zeolites" as a common terminology. The Maxwell-Stefan (M-S) equations represent a balance between the force exerted per mole of species *i* with the drag, or friction, experienced with each of the partner species in the mixture. We may expect that the frictional drag to be proportional to differences in the velocities of the diffusing species $\left(u_i - u_j\right)$, where u_i is the velocity of motion of the adsorbate. For a mixture containing a total of *n* penetrants, 1, 2, 3,..*n* we write

$$
\begin{aligned}
-\frac{d\mu_1}{dz} &= \frac{RT}{Đ_{12}} X_2\left(u_1 - u_2\right) + \frac{RT}{Đ_{13}} X_3\left(u_1 - u_3\right) + \ldots + \frac{RT}{Đ_{1m}} X_m\left(u_1 - u_m\right) \\
-\frac{d\mu_2}{dz} &= \frac{RT}{Đ_{21}} X_1\left(u_2 - u_1\right) + \frac{RT}{Đ_{23}} X_3\left(u_2 - u_3\right) + \ldots + \frac{RT}{Đ_{2m}} X_m\left(u_2 - u_m\right) \\
&\cdots\cdots \\
-\frac{d\mu_n}{dz} &= \frac{RT}{Đ_{n1}} X_1\left(u_n - u_1\right) + \frac{RT}{Đ_{n2}} X_2\left(u_n - u_3\right) + \ldots + \frac{RT}{Đ_{nm}} X_m\left(u_n - u_m\right)
\end{aligned}
\qquad (1)
$$

The left members of equation (1) are the negative of the gradients of the chemical potentials, with the units N mol^{-1}; it represents the driving force acting per mole of species 1, 2, 3,..*n*. The subscript m refers to the membrane, that is regarded as the (*n*+1) th component in the mixture; the membrane is considered to be stationary, i.e., $u_m = 0$. The term $RT/Đ_{im}$ is interpreted as the drag or friction coefficient between the penetrant *i* and the membrane wall. The term $RT/Đ_{ij}$ is interpreted as the friction coefficient for the *i-j* pair of penetrants. The multiplier X_j in each of the right members represents a measure of the composition of component *j* in the mixture because

we expect the friction to be dependent on the number of molecules of *j* relative to that of component *i*. Since the composition fraction X_m of the zeolite membrane is undefined, we redefine the M-S diffusivity for interaction of the penetrant *i* with the membrane as $Đ_i \equiv Đ_{im} / X_m$. An important, persuasive, argument for the use of the M-S formulation for mixture diffusion is that the M-S diffusivity $Đ_i$ in mixtures can be estimated using information on the loading dependence of the corresponding unary diffusivity values. Put another way, the M-S diffusivity $Đ_i$ can be estimated from experimental data on *unary* permeation across zeolite membranes; we return to this point later.

The M-S diffusivity $Đ_{ij}$ has the units $m^2\ s^{-1}$ and the physical significance of an *inverse* drag coefficient. The magnitudes of the M-S diffusivities $Đ_{ij}$ do not depend on the choice of the mixture reference velocity because equation (1) is set up in terms of velocity differences. At the molecular level, the $Đ_{ij}$ reflect how the facility for transport of species *i correlates* with that of species *j*; they are also termed *exchange coefficients*. For mesoporous materials with pores in the 20 Å to 100 Å size range the values of the exchange coefficient $Đ_{12}$ are the nearly the same as the binary *fluid phase* M-S diffusivity, $Đ_{12,fl}$, over the entire range of pore concentrations.[4, 6, 12, 13] For micro-porous materials, the exchange coefficient $Đ_{12}$ cannot be directly identified with the corresponding fluid phase diffusivity $Đ_{12,fl}$ because the molecule-molecule interactions are also significantly influenced by molecule-wall interactions.

For zeolite, MOF and ZIF membranes, it is convenient to use as composition measures the mole fractions of the components in the adsorbed phase, x_i, $x_i = q_i / q_t$ where q_i is the molar loading of adsorbate, and q_t is the *total* mixture loading $q_t = \sum_{i=1}^{2} q_i$. In terms of mole fractions, equations (1) are modified as follows

$$
\begin{aligned}
-\frac{d\mu_1}{dz} &= \frac{RT}{Đ_{12}} x_2(u_1 - u_2) + \frac{RT}{Đ_{13}} x_3(u_1 - u_3) + ... + \frac{RT}{Đ_1}(u_1) \\
-\frac{d\mu_2}{dz} &= \frac{RT}{Đ_{21}} x_1(u_2 - u_1) + \frac{RT}{Đ_{23}} x_3(u_2 - u_3) + ... + \frac{RT}{Đ_2}(u_2) \\
&\cdots\cdots \\
-\frac{d\mu_n}{dz} &= \frac{RT}{Đ_{n1}} x_1(u_n - u_1) + \frac{RT}{Đ_{n2}} x_2(u_n - u_3) + ... + \frac{RT}{Đ_n}(u_n)
\end{aligned}
\tag{2}
$$

The Maxwell-Stefan diffusion formulation (2) is consistent with the theory of irreversible thermodynamics. The Onsager Reciprocal Relations imply that the M-S pair diffusivities are symmetric

$$Đ_{ij} = Đ_{ji} \tag{3}$$

We define N_i as the number of moles of species *i* transported per m^2 of crystalline material per second

$$N_i \equiv \rho q_i u_i \tag{4}$$

where ρ is the framework density with units of kg m^{-3}. Multiplying both sides of equation (2) by ρq_i, the M-S equations for *n*-component diffusion in zeolites, MOFs, and ZIFs take the form[5, 13, 14]

$$-\rho \frac{q_i}{RT}\frac{d\mu_i}{dz} = \sum_{\substack{j=1 \\ j\neq i}}^{n} \frac{x_j N_i - x_i N_j}{Đ_{ij}} + \frac{N_i}{Đ_i}; \quad i = 1,2,..n \tag{5}$$

Earlier publications[10, 15-17] on *n*-component mixture diffusion in microporous crystalline materials have been developed the M-S formulation in a different manner, using the fractional occupancies, θ_i, of species *i* in relation to the saturation capacities, $q_{i,sat}$, for adsorption of each species

$$\theta_i = \frac{q_i}{q_{i,sat}}; \quad i = 1,2,..n \tag{6}$$

as multiplication factor on the right member of equation (1). In this case we write

$$-\frac{1}{RT}\frac{d\mu_i}{dz} = \sum_{\substack{j=1 \\ j\neq i}}^{n} \frac{\theta_j}{Đ_{ij}^{\theta}}\left(u_i - u_j\right) + \frac{1}{Đ_i}\left(u_i\right); \quad i = 1,2..n \tag{7}$$

The superscript θ on the exchange coefficients $Đ_{ij}^{\theta}$ serves as a reminder that these coefficients are distinct from those defined in equation (2).

Expressing the velocities u_j in terms of the intra-crystalline diffusion fluxes $u_i = N_i/\rho q_i$ we get

$$-\frac{1}{RT}\frac{d\mu_i}{dz} = \sum_{\substack{j=1 \\ j\neq i}}^{n} \frac{\theta_j}{Đ_{ij}^{\theta}}\left(\frac{N_i}{\rho q_i} - \frac{N_j}{\rho q_j}\right) + \frac{1}{Đ_i}\left(\frac{N_i}{\rho q_i}\right); \quad i = 1,2..n \tag{8}$$

Multiplying both sides of equation (8) by θ_i and re-arranging we get

$$-\rho\frac{\theta_i}{RT}\frac{d\mu_i}{dz} = \sum_{\substack{j=1 \\ j\neq i}}^{n} \frac{\theta_i\theta_j}{Đ_{ij}^{\theta}}\left(\frac{N_i}{q_i} - \frac{N_j}{q_j}\right) + \frac{\theta_i}{Đ_i}\left(\frac{N_i}{q_i}\right); \quad i = 1,2..n \tag{9}$$

In view of equation (6), equation (9) can be re-arranged to

$$-\rho\frac{\theta_i}{RT}\frac{d\mu_i}{dz} = \sum_{\substack{j=1 \\ j\neq i}}^{n} \left(\frac{q_j N_i - q_i N_j}{q_{i,sat} q_{j,sat} Đ_{ij}^{\theta}}\right) + \frac{N_i}{q_{i,sat} Đ_i}; \quad i = 1,2..n \tag{10}$$

The Onsager reciprocal relations demand the symmetry

$$q_{j,sat} Đ_{ij}^{\theta} = q_{i,sat} Đ_{ji}^{\theta}; \quad i = 1,2..n \tag{11}$$

The two sets of exchange coefficients defined in equations (2) and (7) are inter-related

$$q_{j,sat}Đ_{ij}^{\theta}/q_t = Đ_{ij} = Đ_{ji} = q_{i,sat}Đ_{ji}^{\theta}/q_t \tag{12}$$

The exchange coefficients $Đ_{ij}^{\theta}$ cannot be simply related to the fluid phase M-S diffusivity, $Đ_{12,fl}$. It is for this reason that we prefer the formulation in equations (2).

If the saturation capacities of all of the individual species are (nearly) equal to one another, equation (10) can be simplified to yield

$$-\rho\frac{1_i}{RT}\frac{d\mu_i}{dz} = \sum_{\substack{j=1\\ j\neq i}}^{n}\left(\frac{\theta_j N_i - \theta_i N_j}{Đ_{ij}^{\theta}}\right) + \frac{N_i}{Đ_i}; \quad i = 1,2..n \tag{13}$$

At thermodynamic equilibrium, the chemical potential of component *i* in the bulk gas mixture equals the chemical potential of that component in the adsorbed phase within the membrane at both upstream and downstream faces. For the bulk gas phase mixture we have

$$\frac{1}{RT}\frac{d\mu_i}{dz} = \frac{d\ln p_i}{dz} = \frac{1}{p_i}\frac{dp_i}{dz}; \quad i = 1,2 \tag{14}$$

The chemical potential gradients $d\mu_i/dz$ can be related to the gradients of the molar loadings, q_i, by defining thermodynamic correction factors Γ_{ij}

$$\frac{q_i}{RT}\frac{d\mu_i}{dz} = \sum_{j=1}^{n}\Gamma_{ij}\frac{dq_j}{dz}; \quad \Gamma_{ij} = \frac{q_i}{p_i}\frac{\partial p_i}{\partial q_j}; \quad i,j = 1,....n \tag{15}$$

The thermodynamic correction factors Γ_{ij} can be calculated by differentiation of the model describing mixture adsorption equilibrium. Generally speaking, the Ideal Adsorbed Solution Theory (IAST) of Myers and Prausnitz[18] is the preferred method for estimation of mixture adsorption equilibrium. In some special case, the mixed-gas Langmuir model

$$\frac{q_i}{q_{i,sat}} = \theta_i = \frac{b_i p_i}{1 + \sum_{i=1}^{n} b_i p_i}; \quad i = 1,2,...n \tag{16}$$

may be of adequate accuracy. Analytic differentiation of equation (16) yields

$$\Gamma_{ij} = \delta_{ij} + \left(\frac{q_{i,sat}}{q_{j,sat}}\right)\left(\frac{\theta_i}{\theta_V}\right); \quad i, j = 1,2 \ldots n \tag{17}$$

where the fractional vacancy θ_V is defined as

$$\theta_V = 1 - \theta_t = 1 - \sum_{i=1}^{n} \theta_i = \frac{1}{1 + \pi_1 + \pi_2 + ..\pi_n}; \quad \left(1 + \pi_1 + \pi_2 + ..\pi_n\right) = \frac{1}{\theta_V} \tag{18}$$

The dimensionless partial pressures are defined as

$$\pi_i \equiv b_i p_i \tag{19}$$

The elements of the matrix of thermodynamic factors Γ_{ij} can be calculated explicitly from information on the component loadings q_i in the adsorbed phase; this is the persuasive advantage of the use of the mixed-gas Langmuir model. By contrast, the IAST does not allow the calculation of Γ_{ij} explicitly from knowledge on the component loadings q_i in the adsorbed phase; an numerical procedure is required.

Specifically for binary mixtures, the mixed-gas Langmuir model is

$$\theta_i = \frac{q_i}{q_{i,sat}} = \frac{b_i p_i}{1 + b_1 p_1 + b_2 p_2} \equiv \frac{\pi_i}{1 + \pi_1 + \pi_2}; \quad i = 1,2 \tag{20}$$

and the four elements of the matrix of thermodynamic factors are:[15]

$$\begin{bmatrix} \Gamma_{11} & \Gamma_{12} \\ \Gamma_{21} & \Gamma_{22} \end{bmatrix} = \frac{1}{1-\theta_1-\theta_2} \begin{bmatrix} 1-\theta_2 & \frac{q_{1,sat}}{q_{2,sat}}\theta_1 \\ \frac{q_{2,sat}}{q_{1,sat}}\theta_2 & 1-\theta_1 \end{bmatrix} \quad (21)$$

4. Loading dependence of unary M-S diffusivities $Đ_i$ in zeolites

Figure 23a presents Molecular Dynamics (MD) data on unary M-S diffusivities $Đ_i$ of H_2, Ne, Ar, N_2, CH_4 and Kr in all-silica MFI zeolite at 300 K; the MD data are culled from our earlier publications.[4-11] For molar loadings < 4 mol kg^{-1}, the M-S diffusivity is practically independent of loading. Figures 23b, and 23c, and 23d present the data for "small" guest molecules such as H_2 and Ne in FAU, LTA, and CHA. The M-S diffusivities, $Đ_i$, are practically loading independent. This scenario has been termed the "weak confinement" scenario by Krishna and Baur:[15]

$$Đ_i = Đ_i(0) \quad (22)$$

where $Đ_i(0)$ is the M-S diffusivity at "zero-loading". It must be emphasized that the use of the weak confinement scenario is a simplified, idealized, picture of reality.

Generally speaking, unary M-S diffusivities $Đ_i$ show strong dependence on the molar loadings. See the publications of Krishna and van Baten[7, 9] for the theoretical background to the variety of loading dependencies that are encountered. For certain guest/host combinations, the M-S diffusivities $Đ_i$ decrease with loadings, approaching near-zero values at pore saturation. This characteristic is demonstrated in Figure 24 for a variety of guests in MFI, and FAU. The simplest model to describe this loading dependence is

$$Đ_i = Đ_i(0)\left(1-\theta_t\right) = Đ_i(0)\theta_V \quad (23)$$

where $\theta_V = (1-\theta_t)$ is the fractional vacancy. Equation (23) is essentially based on a simple hopping model in which a molecule can jump from one adsorption site to an adjacent one, provided it is not already occupied. The loading dependence portrayed in equation (23) has been termed the "strong confinement" scenario by Krishna and Baur.[15]

Zeolite structures such as LTA, CHA, DDR, and ERI consist of cages separated by 8-ring windows in the 3.2 -4.2 Å size range. In such structures, guest molecules jump one-at-a-time across the windows. As a first approximation, the inter-cage hopping of molecules can be considered to be uncorrelated. The constraining window regions offer significant free energy barriers for inter-cage hopping of molecules. An important consequence is that the free energy of the molecules within the cage increases with increasing cage occupancy. The net result is that there is a reduction in the free energy barrier for inter-cage hopping; this results in an increase in the M-S diffusivity; as illustration, Figure 25 presents MD data[4-11] on the loading dependence of the M-S diffusivities of various guest molecules in LTA and CHA. The increase of $Đ_i$ with q_i is not monotonic because the cage capacity is limited and there are fewer intra-cage vacant sites to occupy. As the saturation loading is approached, progressively fewer vacant sites become available, $\theta_V \to 0$; the net result is that $Đ_i$ displays a maximum.

5. The Maxwell-Stefan description of binary mixture permeation across zeolite membranes

For binary mixture diffusion inside porous crystalline materials, the Maxwell-Stefan equations (5) are written as

$$\begin{aligned} -\rho\frac{q_1}{RT}\frac{d\mu_1}{dz} &= \frac{x_2N_1 - x_1N_2}{Đ_{12}} + \frac{N_1}{Đ_1} \\ -\rho\frac{q_2}{RT}\frac{d\mu_2}{\partial z} &= \frac{x_1N_2 - x_2N_1}{Đ_{12}} + \frac{N_2}{Đ_2} \end{aligned} \qquad (24)$$

The first members on the right hand side of Equation (24) are required to quantify slowing-down effects that characterize binary mixture diffusion.[4, 6, 8] There is no experimental technique for direct determination of the exchange coefficients $Đ_{12}$, that quantify molecule-molecule interactions.

Let us define the square matrix $[B]$

$$[B] = \begin{bmatrix} \frac{1}{Đ_1} + \frac{x_2}{Đ_{12}} & -\frac{x_1}{Đ_{12}} \\ -\frac{x_2}{Đ_{12}} & \frac{1}{Đ_2} + \frac{x_1}{Đ_{12}} \end{bmatrix} \tag{25}$$

Equation (24) can be re-cast into 2-dimensional matrix notation

$$-\rho \begin{pmatrix} \frac{q_1}{RT}\frac{d\mu_1}{dz} \\ \frac{q_2}{RT}\frac{d\mu_2}{dz} \end{pmatrix} = [B] \begin{pmatrix} N_1 \\ N_2 \end{pmatrix}; \quad \begin{pmatrix} N_1 \\ N_2 \end{pmatrix} = -\rho [B]^{-1} \begin{pmatrix} \frac{q_1}{RT}\frac{d\mu_1}{dz} \\ \frac{q_2}{RT}\frac{d\mu_2}{dz} \end{pmatrix} \tag{26}$$

We define the square matrix $[\Lambda] \equiv [B]^{-1}$; The inverse of the square matrix $[B]$ can be obtained explicitly

$$[\Lambda] \equiv [B]^{-1} = \frac{1}{1 + \frac{x_1 Đ_2}{Đ_{12}} + \frac{x_2 Đ_1}{Đ_{12}}} \begin{bmatrix} Đ_1\left(1 + \frac{x_1 Đ_2}{Đ_{12}}\right) & \frac{x_1 Đ_1 Đ_2}{Đ_{12}} \\ \frac{x_2 Đ_1 Đ_2}{Đ_{12}} & Đ_2\left(1 + \frac{x_2 Đ_1}{Đ_{12}}\right) \end{bmatrix} \tag{27}$$

Combining equations (24), (26), and (27) we obtain

$$\begin{pmatrix} N_1 \\ N_2 \end{pmatrix} = -\rho \left[\Lambda\right]\left[\Gamma\right]\begin{pmatrix} \dfrac{dq_1}{dz} \\ \dfrac{dq_2}{dz} \end{pmatrix};$$

$$\begin{pmatrix} N_1 \\ N_2 \end{pmatrix} = -\frac{\rho}{1+\dfrac{x_1Đ_2}{Đ_{12}}+\dfrac{x_2Đ_1}{Đ_{12}}}\begin{bmatrix} Đ_1\left(1+\dfrac{x_1Đ_2}{Đ_{12}}\right) & \dfrac{x_1Đ_1Đ_2}{Đ_{12}} \\ \dfrac{x_2Đ_1Đ_2}{Đ_{12}} & Đ_2\left(1+\dfrac{x_2Đ_1}{Đ_{12}}\right) \end{bmatrix}\begin{bmatrix} \Gamma_{11} & \Gamma_{12} \\ \Gamma_{21} & \Gamma_{22} \end{bmatrix}\begin{pmatrix} \dfrac{dq_1}{dz} \\ \dfrac{dq_2}{dz} \end{pmatrix} \quad (28)$$

6. Negligible correlations scenario for diffusion in zeolites

Extensive Molecular Dynamics (MD) simulations have shown that correlation effects are of negligible importance for mixture diffusion across materials such as LTA, ZIF-8, CHA, DDR, ERI that consist of cages separated by windows in the 3.4 Å – 4.2 Å size range.[4, 6, 8, 19] Molecules jump one-at-a-time across the narrow windows, and the assumption of negligible correlations is justified.

In the limiting scenario in which correlations effects are of negligible importance:

$$\frac{Đ_i}{Đ_{ij}} \to 0; \quad \text{correlations negligible}$$

In cases in which correlations are negligible, Equation (28) simplifies to yield

$$N_i = -\rho\, Đ_i \frac{q_i}{RT}\frac{d\mu_i}{dz}; \quad i = 1,2$$

$$\left[\Lambda\right] \to \begin{bmatrix} Đ_1 & 0 \\ 0 & Đ_2 \end{bmatrix}; \quad \begin{pmatrix} N_1 \\ N_2 \end{pmatrix} = -\rho \begin{bmatrix} Đ_1 & 0 \\ 0 & Đ_2 \end{bmatrix}\begin{bmatrix} \Gamma_{11} & \Gamma_{12} \\ \Gamma_{21} & \Gamma_{22} \end{bmatrix}\begin{pmatrix} \dfrac{dq_1}{dz} \\ \dfrac{dq_2}{dz} \end{pmatrix} \quad (29)$$

7. Correlations dominant scenario for binary mixture diffusion in zeolites

For the case in which correlation effects are dominant

$\frac{Đ_1}{Đ_{12}} >> 1; \quad \frac{Đ_2}{Đ_{12}} >> 1;$ correlations dominant . This also implies

$$\frac{x_1 Đ_2 + x_2 Đ_1}{Đ_{12}} >> 1 \tag{30}$$

because the sum of the adsorbed phase mole fractions add to unity, i.e. x_1+x_2 = 1. Equation (30) implies that the term $1 + \frac{x_1 Đ_2}{Đ_{12}} + \frac{x_2 Đ_1}{Đ_{12}}$ in equation (28) can be simplified as follows

$$1 + \frac{x_1 Đ_2 + x_2 Đ_1}{Đ_{12}} \rightarrow \frac{x_1 Đ_2 + x_2 Đ_1}{Đ_{12}} \tag{31}$$

With the simplification given by eq.(31), the matrix $[\Lambda]$ reduces to

$$[\Lambda] = \frac{1}{\frac{x_1 Đ_2 + x_2 Đ_1}{Đ_{12}}} \begin{bmatrix} Đ_1\left(1 + \frac{x_1 Đ_2}{Đ_{12}}\right) & Đ_1 \frac{x_1 Đ_2}{Đ_{12}} \\ Đ_2 \frac{x_2 Đ_1}{Đ_{12}} & Đ_2\left(1 + \frac{x_2 Đ_1}{Đ_{12}}\right) \end{bmatrix} \tag{32}$$

The expressions for Λ_{12} and Λ_{21} can be further simplified

$$\Lambda_{12} = \frac{Đ_1\left(\frac{x_1 Đ_2}{Đ_{12}}\right)}{\frac{x_1 Đ_2}{Đ_{12}} + \frac{x_2 Đ_1}{Đ_{12}}} = \frac{Đ_1}{1 + \frac{x_2}{x_1}\frac{Đ_1}{Đ_2}} = \frac{x_1}{\frac{x_1}{Đ_1} + \frac{x_2}{Đ_2}};$$

$$\Lambda_{21} = \frac{Đ_2\left(\frac{x_2 Đ_1}{Đ_{12}}\right)}{\frac{x_1 Đ_2}{Đ_{12}} + \frac{x_2 Đ_1}{Đ_{12}}} = \frac{Đ_2}{1 + \frac{x_1}{x_2}\frac{Đ_2}{Đ_1}} = \frac{x_2}{\frac{x_1}{Đ_1} + \frac{x_2}{Đ_2}}$$

The expressions for Λ_{11} and Λ_{22} for the correlations dominant scenario must be derived with more care. The diagonal elements must degenerate to the corresponding pure component $Đ_i$ values at either ends of the composition range, i.e.

$$\Lambda_{11} \to Đ_1; \quad x_1 \to 1; \quad x_2 \to 0 \tag{33}$$

$$\Lambda_{22} \to Đ_2; \quad x_2 \to 1; \quad x_1 \to 0 \tag{34}$$

Equations (33) and (34) must be satisfied for *any* degree of correlations, not just in the Correlations Dominant scenario.

Consider Λ_{11}. For equation (32) to satisfy eq. (33) for $\frac{Đ_1}{Đ_{12}} >> 1; \quad \frac{Đ_2}{Đ_{12}} >> 1$ we must *also* satisfy the conditions

$$\frac{x_1 Đ_2}{Đ_{12}} >> 1; \quad \frac{x_2 Đ_1}{Đ_{12}} >> 1 \tag{35}$$

because, otherwise, eq. (33) will be violated. Imposing eq. (35) we obtain from equation (32)

$$\Lambda_{11} = \frac{Đ_1}{1 + \frac{x_2}{x_1}\frac{Đ_1}{Đ_2}} = \frac{x_1}{\frac{x_1}{Đ_1} + \frac{x_2}{Đ_2}}; \quad \Lambda_{22} = \frac{Đ_2}{1 + \frac{x_1}{x_2}\frac{Đ_2}{Đ_1}} = \frac{x_{21}}{\frac{x_1}{Đ_1} + \frac{x_2}{Đ_2}} \tag{36}$$

The M-S diffusivity matrix $[\Lambda]$ for the correlations dominant scenario yields the remarkably simple result

$$[\Lambda] = \frac{1}{\frac{x_1}{Đ_1} + \frac{x_2}{Đ_2}} \begin{bmatrix} x_1 & x_1 \\ x_2 & x_2 \end{bmatrix} \tag{37}$$

8. Models for calculation of steady-state permeation fluxes across zeolite membranes

Figure 26 provides a schematic of binary mixture permeation of components 1, and 2 across a zeolite membrane of thickness, δ. We define a dimensionless distance coordinate along the

membrane $\eta = \frac{z}{\delta}$. The first objective is to develop appropriate models to determine the steady-state permeation fluxes for the following set of boundary conditions

$$\text{upstream face}: z = 0; \quad p_i = p_{i0}; \quad q_i = q_{i0}; \quad \theta_i = \theta_{i0}; \quad \pi_i = \pi_{i0}; \quad \theta_V = \theta_{V0} \tag{38}$$

$$\text{downstream face}: z = \delta; \quad p_i = p_{i\delta}; \quad q_i = q_{i\delta}; \quad \theta_i = \theta_{i\delta}; \quad \pi_i = \pi_{i\delta}; \quad \theta_V = \theta_{V\delta} \tag{39}$$

For the case in which the mixture adsorption thermodynamics is adequately described by the mixed-gas Langmuir model, given by equation (20), Krishna and Baur[15] have developed explicit analytic expressions for calculation of the steady-state permeation fluxes for binary mixture permeation. Four different scenarios for the loading dependence and correlations are distinguished in their analytic expressions:

Weak confinement: equation (22), and assuming negligible correlations: equation (29)

Weak confinement: equation (22), and finite correlations: equation (28)

Strong confinement: equation (23), and assuming negligible correlations: equation (29)

Strong confinement: equation (23), and finite correlations: equation (28)

For the scenario in which the correlation effects are dominant, equation (37) is used in place equation (28).

For the convenience of the readers, the analytic expressions for the four different scenarios are summarized in the following sections.

9. Analytic solutions for steady-state permeation fluxes: Weak confinement, and negligible correlations

Combining equations (14), (18), (19), (20), and (29) we obtain

$$N_i = -\frac{\rho Đ_i q_{i,sat}}{\delta}\theta_V \frac{d\pi_i}{d\eta}; \quad i = 1,2 \tag{40}$$

It is convenient to define dimensionless component fluxes

$$\phi_i \equiv \frac{N_i \delta}{\rho \mathcal{D}_i q_{i,sat}} = -\theta_V \frac{d\pi_i}{d\eta}; \quad i = 1,2 \tag{41}$$

Equation (41) cannot be directly integrated because the vacancy profile (i.e. θ_V as function of η) in the membrane layer is, as yet, undetermined. The steady-state permeation fluxes N_i are η-invariant, and the dimensionless component fluxes are also η-invariant, i.e.

$$\phi_i \equiv \frac{N_i \delta}{\rho \mathcal{D}_i q_{i,sat}} = -\theta_{V0} \left.\frac{d\pi_i}{d\eta}\right|_{\eta=0} = -\theta_{V\delta} \left.\frac{d\pi_i}{d\eta}\right|_{\eta=1}; \quad i = 1,2 \tag{42}$$

The dimensionless total flux ϕ_t is defined as

$$\phi_t \equiv \frac{N_1 \delta}{\rho \mathcal{D}_1 q_{1,sat}} + \frac{N_2 \delta}{\rho \mathcal{D}_2 q_{2,sat}} \tag{43}$$

The dimensionless flux ϕ_t is obtained by summing equations (41) over the two species

$$\phi_t = \phi_1 + \phi_2 = -\theta_V \frac{d(\pi_1 + \pi_2)}{d\eta} \tag{44}$$

The total dimensionless flux is also η-invariant.

From equation (18) we have $\frac{d(\pi_1 + \pi_2)}{d\eta} = \frac{d(1/\theta_V)}{d\eta}$, and so we can re-write equation (44) as

$$\frac{d(1/\theta_V)}{d\eta} = -(1/\theta_V)\phi_t \tag{45}$$

The linear differential equation (45) can be solved for the boundary conditions (**38**) and (**39**) by separation of variables to give the vacancy profile (i.e. θ_V as function of η) within the membrane:

$$\left(\frac{\frac{1}{\theta_V}-\frac{1}{\theta_{V0}}}{\frac{1}{\theta_{V\delta}}-\frac{1}{\theta_{V0}}}\right)=\frac{\exp(-\phi_t\eta)-1}{\exp(-\phi_t)-1} \tag{46}$$

where the term ϕ_t can be evaluated explicitly from

$$\phi_t \equiv \frac{N_1\delta}{\rho q_{1,sat}Đ_1}+\frac{N_2\delta}{\rho q_{2,sat}Đ_2}=\ln\left(\frac{\theta_{V\delta}}{\theta_{V0}}\right) \tag{47}$$

It remains to solve eq. (41) to obtain the π-profiles within the membrane. Since the vacancy profile, θ_V as function of η, is now available from equation (46), this profile can be substituted back into equation (41). The resulting ordinary differential equation can be solved easily to obtain the component π-profiles

$$\left(\pi_{i\eta}-\pi_{i0}\right)=\frac{\exp(-\phi_t\eta)-1}{\exp(-\phi_t)-1}\left(\pi_{i\delta}-\pi_{i0}\right);\quad i=1,2 \tag{48}$$

The corresponding loading profiles are obtained from

$$\theta_{i\eta}=\theta_{V\eta}\pi_{i\eta};\quad q_{i,\eta}=\theta_{i\eta}\,q_{i,sat};\quad i=1,2 \tag{49}$$

Differentiating eq. (48) and evaluating at the upstream face, we obtain after substituting into eq. (42)

$$N_i=\frac{\rho}{\delta}\theta_{V0}\frac{-\phi_t}{\exp(-\phi_t)-1}q_{i,sat}\,Đ_i\left(\pi_{i0}-\pi_{i\delta}\right);\quad i=1,2 \tag{50}$$

where the subscript 0 and δ emphasize the fact that the relevant parameters are evaluated at the upstream and downstream conditions, respectively. Substituting the expression (47) for ϕ_t we get after re-arrangement

$$N_i = \frac{\rho}{\delta} \frac{\ln\left(\frac{\theta_{V\delta}}{\theta_{V0}}\right)}{\frac{1}{\theta_{V0}} - \frac{1}{\theta_{V\delta}}} q_{i,sat}\ Đ_i(\pi_{i0} - \pi_{i\delta}); \quad i = 1,2 \tag{51}$$

which allows explicit evaluation of the fluxes.

The component permeances are defined by

$$\Pi_i \equiv \frac{N_i}{p_{i0} - p_{i\delta}} \tag{52}$$

Therefore, the permeances can be calculated from

$$\Pi_i = \frac{\rho}{\delta} \frac{\ln\left(\frac{\theta_{V\delta}}{\theta_{V0}}\right)}{\frac{1}{\theta_{V0}} - \frac{1}{\theta_{V\delta}}} q_{i,sat}\ Đ_i \frac{(\pi_{i0} - \pi_{i\delta})}{(p_{i0} - p_{i\delta})} \tag{53}$$

The M-S diffusivities can be calculated from the experimental data on permeances using

$$Đ_i = \frac{\Pi_i \delta}{\rho q_{i,sat}} \frac{\frac{1}{\theta_{V0}} - \frac{1}{\theta_{V\delta}}}{\ln\left(\frac{\theta_{V\delta}}{\theta_{V0}}\right)} \frac{(p_{i0} - p_{i\delta})}{(\pi_{i0} - \pi_{i\delta})} \tag{54}$$

For unary permeation, the corresponding equations for fluxes, permeances, and M-S diffusivities are

$$N_i = \frac{\rho}{\delta} q_{i,sat}\ Đ_i \ln\left(\frac{1+\pi_{i0}}{1+\pi_{i\delta}}\right); \quad \Pi_i = \frac{\rho}{\delta} q_{i,sat}\ Đ_i \frac{\ln\left(\frac{1+\pi_{i0}}{1+\pi_{i\delta}}\right)}{(p_{i0} - p_{i\delta})}; \quad Đ_i = \frac{\Pi_i \delta}{\rho q_{i,sat}} \frac{(p_{i0} - p_{i\delta})}{\ln\left(\frac{1+\pi_{i0}}{1+\pi_{i\delta}}\right)} \tag{55}$$

10. Analytic solutions for steady-state permeation fluxes: Weak confinement and finite correlations

For the scenario in which the correlation effects are finite, the expression for the permeation fluxes is

$$(N) = \frac{\rho}{\delta} \frac{\ln\left(\frac{\theta_{V\delta}}{\theta_{V0}}\right)}{\frac{1}{\theta_{V0}} - \frac{1}{\theta_{V\delta}}} [q_{sat}][\Lambda](\pi_0 - \pi_\delta) \tag{56}$$

In equation (56), the matrix of M-S diffusivities $[\Lambda]$ is evaluated using equation (27) and the adsorbed phase mole fractions, x_{i0}, at the upstream face of the membrane. It is also to be noted that in the weak confinement scenario $[\Lambda]$ has the same values at both faces of the membrane.

The component loading profiles within the membrane are given by equations (48), and (49) using the same definition $\phi_t \equiv \frac{N_1\delta}{\rho q_{1,sat} Đ_1} + \frac{N_2\delta}{\rho q_{2,sat} Đ_2} = \ln\left(\frac{\theta_{V\delta}}{\theta_{V0}}\right)$ as in the foregoing section.

11. Analytic solutions for steady-state permeation fluxes for the strong confinement scenario

Exact analytic expressions can also be derived for the strong confinement scenario in which the M-S diffusivities follow the loading dependence described by equation (23): $Đ_i = Đ_i(0)\theta_V$.

For the strong confinement scenario in which the correlation effects are finite, the expression for the permeation fluxes is

$$(N) = \frac{\rho}{\delta} \begin{bmatrix} q_{1,sat} & 0 \\ 0 & q_{2,sat} \end{bmatrix} [\Lambda]\theta_{V\delta}\theta_{V0}(\pi_0 - \pi_\delta) \tag{57}$$

In equation (57), the matrix of M-S diffusivities $[\Lambda]$ is evaluated using equation (27) and the adsorbed phase mole fractions, x_{i0}, at the upstream face of the membrane. The component loading profiles within the membrane are given by

$$\theta_{i\eta} = \theta_{i0} + \eta\left(\theta_{i\delta} - \theta_{i0}\right); \quad \pi_{i\eta} = \pi_{i0} + \eta\left(\pi_{i\delta} - \pi_{i0}\right); \quad q_{i,\eta} = \theta_{i\eta}\, q_{i,sat}; \quad i = 1,2,...n \tag{58}$$

The component permeances can be calculated

$$\Pi_i = \frac{N_i}{\left(p_{i0} - p_{i\delta}\right)} \tag{59}$$

For unary permeation, equation (57) reduces to a scalar equation

$$N_i = \frac{\rho}{\delta} q_{i,sat}\, Đ_i(0)\theta_{V\delta}\theta_{V0}\left(\pi_{i0} - \pi_{i\delta}\right) \tag{60}$$

The component unary permeances can be determined from

$$\Pi_i = \frac{N_i}{\left(p_{i0} - p_{i\delta}\right)} = \frac{\rho}{\delta} Đ_i(0) q_{i,sat} \frac{\theta_{V\delta}\theta_{V0}\left(\pi_{i0} - \pi_{i\delta}\right)}{\left(p_{i0} - p_{i\delta}\right)} \tag{61}$$

The zero-loading M-S diffusivities can be calculated from the experimental data on permeances using

$$Đ_i(0) = \frac{\Pi_i \delta}{\rho q_{i,sat}} \frac{1}{\theta_{V\delta}\theta_{V0}} \frac{\left(p_{i0} - p_{i\delta}\right)}{\left(\pi_{i0} - \pi_{i\delta}\right)} \tag{62}$$

If correlation effects are assumed to be negligible, equation (57) further simplifies to yield

$$N_i = \frac{\rho}{\delta} q_{i,sat}\, Đ_i(0)\theta_{V0}\theta_{V\delta}\left(\pi_{i0} - \pi_{i\delta}\right); \quad i = 1,2 \tag{63}$$

If the component loadings at the downstream membrane face as vanishingly small, $\theta_{V\delta} \to 1$, and equation (63) further simplifies to yield

$$N_i = \frac{\rho}{\delta} q_{i,sat}\, Đ_i(0)\theta_{V0}\left(\pi_{i0} - \pi_{i\delta}\right) = \frac{\rho}{\delta} Đ_i(0)\left(q_{i0} - q_{i\delta}\right); \quad i = 1,2 \tag{64}$$

12. Analysis of the experimental data for steady-state permeation of Kr/Xe mixtures across SAPO-34 membrane

The application of the analytic solutions developed in the foregoing sections will be demonstrated by re-analysis of the experimental data for Kr/Xe permeation across SAPO-34 membranes as reported by two different research groups in the publications of Feng et al.[20] and Kwon et al.[3] Both groups report experimental data on adsorption isotherms and mixture permeation.

We first develop isotherm fits for the two sets of isotherm data.

The pure component isotherm data for Kr and Xe in SAPO-34 were measured by Feng et al.[20] at two different temperatures 278 K, and 298 K. The total pressures used in the experiments ranged to 140 kPa. The data were fitted with either the single-site Langmuir model

$$q = q_{sat}\frac{bp}{1+bp} \tag{65}$$

The Langmuir parameters is temperature-dependent

$$b = b_0 \exp\left(\frac{E}{RT}\right) \tag{66}$$

The Langmuir fit parameters are provided in Table 1. Particularly noteworthy is the fact that the saturation capacities, q_{sat}, of Kr and Xe are equal to 2.5 mol kg^{-1}. The equality of saturation capacities implies that the mixed-gas Langmuir model for mixture adsorption is precisely valid.

Figures 27 presents comparisons of experimental data of Feng et al.[20] on component loadings for Kr and Xe at 278 K, and 298 K in SAPO-34 with the isotherm fits. The agreement between the Langmuir fits and the experimental data is good at both temperatures.

Kwon et al.[3] have reported unary isotherms for Kr and Xe temperatures of 308 K, 323 K and 343 K. The total pressures used in the experiments ranged to 380 kPa. Their data, scanned from their paper, were fitted with the equations (65) and (66). The Langmuir fit parameters are specified in Table **2**. For the Kwon data, the saturation capacities, q_{sat}, of Kr and Xe are both equal to 3.1 mol kg^{-1}. The equality of saturation capacities implies that the mixed-gas Langmuir model for mixture adsorption is precisely valid. It is also appropriate to mention here that the Langmuir fits in Table **2** do not correspond to those reported in their Table 1 of Kwon et al;[3] there appears to be typographical errors in the parameter values cited by these authors. Furthermore, we find that their isotherm data can be fitted with good accuracy assuming equal saturation capacities of 3.1 mol kg^{-1}; this is important because it allows the mixed gas Langmuir model to be used for accurate calculations of the mixture adsorption equilibrium.

Figure 29a presents calculations of elements of the matrix of thermodynamic correction factors Γ_{ij} as a function of total pressure, $p_1 + p_2 = p_t$, using the mixed-gas Langmuir model for binary Kr(1)/Xe(2) mixture adsorption in SAPO-34 at 298 K. The ratio of partial pressures in the gas phase is 10:90. In these calculations the total gas pressure, p_t, was varied from 0 to 1 MPa. The off-diagonal elements Γ_{12}, and Γ_{21} become increasingly important with increased pressure. In particular, it is noteworthy that the off-diagonal element Γ_{21} get progressively closer to diagonal element Γ_{22} with increased pressure. This implies that the flux of Xe is strongly influenced by the driving force of Kr.

Figure 29b presents calculations of the elements of the matrix of thermodynamic correction factors Γ_{ij} as function of the mole fraction of Kr(1) in the bulk gas phase for total pressure $p_1 + p_2 = p_t = 0.2$ MPa. We note that the off-diagonal element Γ_{21} is of the same order of magnitude as the diagonal element Γ_{22}. In Figure 29c, the ratios of the elements of thermodynamic correction factors, $\frac{\Gamma_{12}}{\Gamma_{11}}, \frac{\Gamma_{21}}{\Gamma_{22}}$ as function of the mole fraction of Kr(1) in the bulk gas phase for total pressure $p_1 + p_2 = p_t = 0.2$ MPa. The off-diagonal elements are significant fractions of the corresponding diagonal elements, signaling strong thermodynamic coupling.

Feng et al.[20] have reported data on the component permeances for Kr(1)/Xe(2) mixture permeation across SAPO-34 membranes of varying thicknesses. The upstream total pressure was kept constant at 140 kPa. The downstream total pressure is 2 kPa, and the total pressure drop across the membrane was 138 kPa. Two different upstream compositions of Kr(1)/Xe(2) were used in the experiments: 90/10, and 9/91. The experimental data on component permeances are plotted in Figure 30a. We note that the component permeances are not constant, but show a decreasing trend with increasing membrane thickness.

The Maxwell-Stefan diffusivities of Kr and Xe, calculated using Equation (54), are shown in Figure 30b. We note that the M-S diffusivity of Xe is practically independent of the mixture composition and the membrane thickness. The M-S diffusivity of Kr is independent of composition and is only weakly dependent on the membrane thickness. From the experiments, the backed-out diffusivity values are $Đ_1 = 6\times10^{-11}$ m^2 s^{-1}, $Đ_2 = 4\times10^{-13}$ m^2 s^{-1}.

Figure 31 presents data on Maxwell-Stefan diffusivities, $Đ_i$, of Kr (1) and Xe (2) across a SAPO-34 tubular membrane of thickness δ = 4.9 μm thickness, backed out from data on unary and binary mixture permeances as reported by Kwon et al.[3] For unary permeance data, the $Đ_i$ are

backed out using Equation (55). For 10/90 mixture permeance data, the $Đ_i$ are backed out using Equation (54). The M-S diffusivities, backed out from unary and mixture permeances are practically the same; this underscores the advantage of the M-S formulation. The straight lines are Arrhenius fits of the $Đ_i$; the fit constants are provided in Table 3. It is also appropriate to mention here that the Arrhenius fits of the $Đ_i$ in Table 3 do not correspond to those reported in their Table 1 by Kwon et al.[3] because of two reasons (a) Kwon et al.[3] have used the wrong value of the framework density (= 1800 kg m^{-3}) for SAPO-34 zeolite for backing-out the M-S diffusivities, and (2) there are typographical errors in their Table 1 on Kwon et al.[3] on the Langmuir isotherm parameters.[3]

13. Analysis of the experimental data of Li et al. for mixture permeation across SAPO-34 membrane

Li et al.[21, 22] provide comparisons of transport coefficients, $\rho Đ_i/\delta$, backed out from unary permeation and binary mixtures permeation across SAPO-34 membrane for several mixtures. Figure 32 presents their data for four different mixtures: CO_2/CH_4, N_2/CH_4, CH_4/H_2, and CO/H_2. Broadly speaking, the $\rho Đ_i/\delta$ values backed out either from unary or mixture permeation experiments exhibit similar loading dependences and correspond reasonably closely to each other. This validates the advantage of the M-S formulation.

14. Linearized solution for steady-state permeation across zeolite membranes

There are many instances in which mixture adsorption equilibrium cannot be adequately described by the mixed-gas Langmuir model given by equation (20); this situation arises for permeation of linear and branched alkanes across MFI membranes for which the dual-site Langmuir model need to be used to take account of isotherm inflections. Exact analytic

solutions for steady-state fluxes cannot be derived in this case. Numerical solutions of the set of coupled ordinary differential equations (ODEs) is required; shooting methods are required for the determination of the steady-state fluxes. An alternative, practical, approach is to determine the two matrices $[\Lambda]$, and $[\Gamma]$ at the averaged adsorbed phase loadings, mole fractions, and occupancies within the membrane. In other words, $[\Lambda]$ and $[\Gamma]$ are evaluated at $q_{i,av} = \frac{q_{i0} + q_{i\delta}}{2}$; $x_{i,av} = \frac{x_{i0} + x_{i\delta}}{2}$; $\theta_{i,av} = \frac{\theta_{i0} + \theta_{i\delta}}{2}$. It is definitely not correct to determine $[\Lambda]$, and $[\Gamma]$ by determining the corresponding averages of their respective values at the two membrane faces.

In the linearized model, the fluxes are given by

$$\begin{pmatrix} N_1 \\ N_2 \end{pmatrix} = \frac{\rho}{\delta}[\Lambda][\Gamma]\begin{pmatrix} q_{10} - q_{1\delta} \\ q_{20} - q_{2\delta} \end{pmatrix} \tag{67}$$

The component permeances can be calculated using equation (59).

The linearized model essentially assumes that the component loading profiles within the membrane layer are linear. This assumption is always a good one for the strong confinement scenario for which the loading profiles are linear according to equation (58). For the weak confinement model, the loading profiles are non-linear (see equation (48)) and we should expect some deviations between the exact analytic solution and the estimations using the linearized model.

In order to test the accuracy of the linearized solution for steady state fluxes, described by equation (67), Figure 33a shows calculations of the component fluxes for 40/60 Kr (1)/Xe (2) mixture across SAPO-34 membrane of thickness δ = 4.9 μm at T = 298 K, with varying upstream total pressures. The continuous solid lines are the flux calculations using the exact

analytic solution given by Equation (51); the dashed lines are the linearized model described by equation (67). There is good agreement between the two sets of calculations. The exact analytic solution predicts slightly higher fluxes because the component loading profiles within the membrane layer are not linear; see Figure 33b. The linearized model, that essentially assumes linear loading profiles, underestimates the fluxes to a small extent.

15. Transient Kr/Xe permeation across SAPO-34 membrane

Diffusional coupling effects often lead to unusual phenomena such as overshoots in the flux of the more mobile partners during transient mixture permeation across nanoporous membranes. Geus et al.[23] report experimental data on transient permeation CH_4/nC_4H_{10} mixture across MFI; the flux of the more mobile CH_4 exhibits a pronounced maximum. The origin of this overshoot can be traced to thermodynamic coupling effects, embodied in the thermodynamic correction factors.[14] We now demonstrate the possibility of transient overshoots for Kr(1)/Xe(2) mixture permeation across SAPO-34 membrane.

For modeling purposes, the transient permeation fluxes are obtained by solving the set of partial differential equations

$$\frac{\partial q_i(z,t)}{\partial t} = -\frac{1}{\rho}\frac{\partial}{\partial z}\left(N_i\right) \tag{68}$$

where z is the distance coordinate along the direction of membrane thickness. The boundary conditions are the partial pressures and component molar loadings at the upstream ($z = 0$) and downstream ($z = \delta$) faces of the membrane; see schematic in Figure 26.

$$\begin{aligned} z &= 0; \quad p_i = p_{i0}; \quad q_i = q_{i0} \\ z &= \delta; \quad p_i = p_{i\delta}; \quad q_i = q_{i\delta} \end{aligned} \tag{69}$$

Figure 34 shows the fluxes for transient permeation of 10/90 Kr (1)/Xe (2) across SAPO-34 membrane of thickness δ = 8.7 μm at upstream total pressure of 140 kPa, and temperature T = 298 K; The input data of isotherms and diffusivities are based on Feng et al.[20] The transient overshoot of the more mobile component Kr is evident. Analogous overshoots are realized using the inputs from Kwon et al;[3] see the transient permeation fluxes at T = 254 K, and (b) T = 298 K in Figures 35a,b. The important advantage of transient operation is that the Kr/Xe selectivity exceeds the steady-state value by about three orders of magnitude; see Figure 35c.

16. Analysis of experimental data for CO_2/ H_2 mixture permeation across MFI membrane

Two sets of experimental data, emanating from the same group in Sweden, for steady-state $CO_2(1)/H_2(2)$ mixture permeation across MFI (silicalite-1) zeolite membrane are reported by Sandström et al.[24] and Sjöberg et al.[25] In both sets of data measured in the same laboratory set-up, equal partial pressures p_{10}=p_{20} are maintained in the upstream compartment; the total upstream pressure was varied. The downstream partial pressures are kept constant at $p_{1\delta}$ = 95 kPa, $p_{2\delta}$ = 5 kPa. The temperatures in the Sandström et al.[24] and Sjöberg et al.[25] experiments are maintained, respectively, at 296 K, and 273 K. The Langmuir isotherm data fits for 273 K and 296 K used in the calculations below are provided in Table 4.

The influence of correlations on mixture permeation is best illustrated by considering the experimental data of Sandström et al.[24] for permeances of $CO_2(1)$ and $H_2(2)$ in MFI membrane, determined both from unary and binary mixture permeation data; see Figure 36a. We note that the permeance of the tardier CO_2 in the mixture is only slightly lower than the values for unary permeation for the entire range of upstream (feed) partial pressures. For H_2, the permeance in the mixture is about an order of magnitude lower than from unary experiments. This implies that

mixture permeation is CO_2-selective, whereas the data based on unary permeation demonstrates H_2-selective performance. For a proper modeling of the permeation experiments we need to have an appropriate quantitative description of (a) the loading dependence of the M-S diffusivities, $Đ_1$, and $Đ_2$, and (b) estimates of the degrees of correlations, $Đ_1/Đ_{12}$, and $Đ_2/Đ_{12}$. This information is provided by the MD simulation data of Krishna and van Baten.[4, 6, 8, 13, 26]

Figure 37a shows snapshot showing the location of H_2 and CO_2 adsorbates within the intersecting channels. The presence of strongly adsorbed CO_2 serves to hinder the motion of H_2. Indeed, Sandström et al.[24] consider the reduction in the H_2 permeance to be a result of "blocking" by the partner CO_2 molecules. Figure 37b shows the MD simulation data on the unary M-S diffusivities of CO_2, and H_2 as a function of the component loadings. At first sight, the M-S diffusivity of CO_2 appears to follow the strong confinement scenario described by equation (23). The M-S diffusivity of H_2 also decreases with increased loading, but to a lower extent. Figure 37c shows the MD simulation data on the M-S diffusivities of CO_2, and H_2 determined for equimolar binary $CO_2(1)/H_2(2)$ mixtures a function of the total mixture loading, q_t. The loading dependences of both components in the binary mixture decrease with total mixture loading, and the trends are similar to that of the unary diffusivities in Figure 37b. Based on the MD simulation data, we shall adopt the strong confinement scenario described by equation (23), to model the Sandström experiments for unary permeation. Using equation (61), along with the values of the transport coefficients $\rho Đ_1(0)/\delta = 3.2$, and $\rho Đ_2(0)/\delta = 100$ kg m^{-2} s^{-1}, the experimental data on unary permeances can be reproduced with good accuracy; see the continuous solid lines in Figure 36b.

Figure 37d shows the MD simulation data for the degree of correlations, $Đ_2/Đ_{12}$, for diffusion of equimolar binary $CO_2(1)/H_2(2)$ mixtures in MFI zeolite at 300 K, as a function of the total

mixture loading, q_t. There is a sharp increase in the degree of correlations with increased loadings. In the Sandström et al.[24] experiments, the values of the total mixture loadings, q_t, are in the range 1 – 3 mol kg^{-1}, and $Đ_2/Đ_{12}$ values are in the range of 2 – 10 for this range of mixture loadings. From the data in Figure 37 we must conclude that correlation effects will have an important bearing on the mixture permeation characteristics, as is evidenced by the experimental data on mixture permeances shown in Figure 36.

With the estimates $\rho Đ_1(0)/\delta = 3.2$, and $\rho Đ_2(0)/\delta = 100$ kg m^{-2} s^{-1}, Equations (59) and (67) can be used to estimate the component permeances for $CO_2(1)/H_2(2)$ mixtures. An excellent match with the experimental permeances can be achieved with the choice $Đ_2/Đ_{12}$ = 8; see the continuous solid lines in Figure 38a. The choice of the precise value of the degree of correlations does not have a significant influence on the CO_2 permeance, but the value of H_2 permeance is severely affected. Generally speaking, correlation effects have a strong *retarding* influence of the permeation of more-mobile-less-strongly-adsorbed molecules. Conversely, correlation effects are of lesser importance for tardier-more-strongly-adsorbed species. In order to demonstrate this, Figure 38b compares the experimental data on permeances of H_2 with the estimations based on different values for the degree of correlations, $Đ_2/Đ_{12}$ = 2, 8, 20, and 40. Also shown are the estimates of the permeances using the limiting scenarios of negligible correlations (equation (29)), and dominant correlations (37). The experimental data on H_2 permeance lies about midway between the values of the limiting scenarios for degrees of corelations. The results in Figure 38 highlight the importance of using proper estimates of correlation effects to predict the permeances of H_2.

Figure 39a shows the experimental data of Sjöberg et al.[25] on the permeation fluxes of CO_2 and H_2 as a function of the upstream total pressure, p_{t0}; these data were measured at a slightly lower

temperature of 273 K. The continuous solid lines in Figure 39a are the flux estimations using equation (67), along with the same values of $\rho Đ_1(0)/\delta = 3.2$, and $\rho Đ_2(0)/\delta = 100$ kg m^{-2} s^{-1} and $Đ_2/Đ_{12} = 8$, as used to model the Sandström experiments. The only differences in the flux estimations are that the Langmuir isotherm data fits are for the lower temperature of 273 K; see Table 4. The estimations are in excellent agreement with the experimental data Sjöberg et al.[25] The strong influence of the choice of the degree of correlations $Đ_2/Đ_{12}$ is highlighted in the calculations in Figure 39b. For H_2, invoking the negligible correlations scenario, leads to larger fluxes than observed experimentally. For CO_2/H_2 separations, this implies that neglecting correlations leads to most pessimistic estimates of permeation selectivities. Conversely, the adoption of the correlations dominant scenario, leads to overly optimistic estimates of the permeation selectivities.

17. The Flory-Huggins description of phase equilibrium thermodynamics for polymeric systems

Polymer membranes are widely used for mixture separations; for an introduction to this topic see Wesselingh and Krishna.[27] The upstream compartment contains fluid mixtures that are in the gaseous state at elevated pressures, or in the liquid state; see schematic in Figure 40. The pressure in the downstream compartment corresponds to ambient pressures or vacuum. Thermodynamic equilibrium is assumed to prevail between the bulk fluid mixture in the upstream compartment and the sorbed mixture in the upstream face of the membrane. An analogous situation prevails in the downstream compartment; there is sorption equilibrium between the bulk fluid mixture in the downstream compartment and the downstream face of the membrane.

The thermodynamics of sorption equilibrium of penetrants and polymer is most commonly described by the Flory-Huggins relations.[27-29] The Flory-Huggins equation in its simplest form deals with molecules that are similar chemically, but differ greatly in length. An example might be cross-linked polyethylene with the penetrant propane (C_3H_8). The Flory-Huggins model is based on the idea that the chain elements of the polymer arrange themselves randomly (but with the molecules remaining connected) on a three-dimensional lattice; see Figure 40.

The Flory-Huggins model does not take effects of crystallization or other inhomogeneities into account. The resulting equation for the activity of the penetrant is a simple function of the volume fraction of the penetrant in the membrane. We use ϕ_i to denote the volume fraction of the penetrant species *i*; the volume fraction of species *i* is $\phi_i = c_i \overline{V_i}$. The volume fractions are related to the mass fractions, ω_i

$$\omega_i = \frac{\rho_i}{\rho_t} = \frac{\phi_i \rho_{i0}}{\sum_{i=1}^{n} \phi_i \rho_{i0}}; \quad \phi_i = c_i \overline{V_i} = \frac{\frac{\omega_i}{\rho_{i0}}}{\sum_{i=1}^{n} \frac{\omega_i}{\rho_{i0}}} \tag{70}$$

In equation (70), the ρ_{i0} are the pure component mass densities. The use of mole fractions is not convenient for description of the mixture equilibrium in polymers, because the molar mass of the polymer chains are ill defined.[27]

The Flory-Huggins model for binary mixture of penetrant (1) and polymer (indicated by subscript m) is

$$\begin{aligned} \ln a_1 &= \ln(\phi_1) + (1-\phi_1) - \phi_m \frac{\overline{V_1}}{\overline{V_m}} + \chi_{1m} \phi_m^2 \\ \phi_m &= 1 - \phi_1 \end{aligned} \tag{71}$$

Equation (71) contains a non-ideality, or interaction parameter χ_{1m} that is assumed to be independent of the volume fraction.

If the interaction parameter χ_{1m} in equation (71) is composition dependent, the F-H model for the activity needs to be extended as follows

$$\ln a_1 = \ln(\phi_1) + (1-\phi_1) - (1-\phi_1)\frac{\overline{V_1}}{\overline{V_m}} + \chi_{1m}(1-\phi_1)^2 + \phi_1(1-\phi_1)^2\frac{\partial \chi_{1m}}{\partial \phi_1} \tag{72}$$

The Flory-Huggins model for binary mixture of penetrants (Components 1, and 2) in a polymer (indicated by subscript m) is[30, 31]

$$\begin{aligned}
\ln a_1 &= \ln(\phi_1) + (1-\phi_1) - \phi_2\frac{\overline{V_1}}{\overline{V_2}} - \phi_m\frac{\overline{V_1}}{\overline{V_m}} + (\chi_{12}\phi_2 + \chi_{1m}\phi_m)(\phi_2+\phi_m) - \chi_{2m}\frac{\overline{V_1}}{\overline{V_2}}\phi_2\phi_m \\
\ln a_2 &= \ln(\phi_2) + (1-\phi_2) - \phi_1\frac{\overline{V_2}}{\overline{V_1}} - \phi_m\frac{\overline{V_2}}{\overline{V_m}} + \left(\chi_{12}\phi_1\frac{\overline{V_2}}{\overline{V_1}} + \chi_{2m}\phi_m\right)(\phi_1+\phi_m) - \chi_{1m}\frac{\overline{V_2}}{\overline{V_1}}\phi_1\phi_m \\
\phi_m &= 1-\phi_1-\phi_2
\end{aligned} \tag{73}$$

In the Flory-Huggins formulations presented in Equation (71) and Equation (73), the interaction parameters $\chi_{12}, \chi_{1m}, \chi_{2m}$ are assumed to be constant, i.e. independent of the volume fractions.

In the scenario in which the interaction parameter χ_{12} exhibits a composition dependence following equation (80) in the membrane phase, the Flory-Huggins equation (73) needs to be extended as follows (these equations correspond to equations (6) and (7) of Mulder et al.[32])

$$\begin{aligned}
\ln a_1 &= \ln(\phi_1) + (1-\phi_1) - \phi_2\frac{\overline{V_1}}{\overline{V_2}} - \phi_m\frac{\overline{V_1}}{\overline{V_m}} + (\chi_{12}\phi_2 + \chi_{1m}\phi_m)(\phi_2+\phi_m) - \chi_{2m}\frac{\overline{V_1}}{\overline{V_2}}\phi_2\phi_m - u_1u_2\phi_2\frac{\partial \chi_{12}}{\partial u_2} \\
\ln a_2 &= \ln(\phi_2) + (1-\phi_2) - \phi_1\frac{\overline{V_2}}{\overline{V_1}} - \phi_m\frac{\overline{V_2}}{\overline{V_m}} + \left(\chi_{12}\phi_1\frac{\overline{V_2}}{\overline{V_1}} + \chi_{2m}\phi_m\right)(\phi_1+\phi_m) - \chi_{1m}\frac{\overline{V_2}}{\overline{V_1}}\phi_1\phi_m + \frac{\overline{V_2}}{\overline{V_1}}u_1^2\phi_2\frac{\partial \chi_{12}}{\partial u_2}
\end{aligned}$$

(74)

In equation (74), we have defined $u_2 = \dfrac{\phi_2}{\phi_1 + \phi_2}$; $\quad u_1 = 1 - u_2 = \dfrac{\phi_1}{\phi_1 + \phi_2}$.

When all three interaction parameters $\chi_{12}, \chi_{1m}, \chi_{2m}$ are dependent on the volume fractions of the penetrants, equation (74) needs to be further extended; these equations are provided in equations (6) and (7) of Mulder et al.[32] The same set of extended equations are given by Yang and Lue;[33] see also Varady et al.[34] For readers' convenience, the extended F-H model equations are given below:

$$\ln a_1 = \ln(\phi_1) + (1-\phi_1) - \phi_2 \frac{\overline{V_1}}{\overline{V_2}} - \phi_m \frac{\overline{V_1}}{\overline{V_m}} + \left(\chi_{12}\phi_2 + \chi_{1m}\phi_m\right)\left(\phi_2 + \phi_m\right) - \chi_{2m} \frac{\overline{V_1}}{\overline{V_2}} \phi_2\phi_m - u_1 u_2 \phi_2 \frac{\partial \chi_{12}}{\partial u_2}$$
$$- u_1 u_2 \phi_m \frac{\partial \chi_{1m}}{\partial u_2} - \phi_1 \phi_m^2 \frac{\partial \chi_{1m}}{\partial \phi_m} + \frac{\overline{V_1}}{\overline{V_2}} u_2^2 \phi_m \frac{\partial \chi_{2m}}{\partial u_1} - \frac{\overline{V_1}}{\overline{V_2}} \phi_2 \phi_m^2 \frac{\partial \chi_{2m}}{\partial \phi_m}$$
$$\ln a_2 = \ln(\phi_2) + (1-\phi_2) - \phi_1 \frac{\overline{V_2}}{\overline{V_1}} - \phi_m \frac{\overline{V_2}}{\overline{V_m}} + \left(\chi_{12}\phi_1 \frac{\overline{V_2}}{\overline{V_1}} + \chi_{2m}\phi_m\right)\left(\phi_1 + \phi_m\right) - \chi_{1m} \frac{\overline{V_2}}{\overline{V_1}} \phi_1\phi_m + \frac{\overline{V_2}}{\overline{V_1}} u_1^2 \phi_2 \frac{\partial \chi_{12}}{\partial u_2}$$
$$+ \frac{\overline{V_2}}{\overline{V_1}} u_1^2 \phi_m \frac{\partial \chi_{1m}}{\partial u_2} - \frac{\overline{V_2}}{\overline{V_1}} \phi_1 \phi_m^2 \frac{\partial \chi_{1m}}{\partial \phi_m} - u_1 u_2 \phi_m \frac{\partial \chi_{2m}}{\partial u_1} - \phi_2 \phi_m^2 \frac{\partial \chi_{2m}}{\partial \phi_m}$$

(75)

18. F-H description of CO_2/C_2H_6/XLPEO phase equilibrium relevant to membrane gas separation

Let us first consider the scenario in which the upstream compartment contains a binary *gas* mixture. The equilibrium relation, for either upstream or downstream sides of the membrane, may be written as

$$\mu_i - \mu_{i0} = RT \ln\left(\frac{f_i}{f_{i,sat}}\right) = RT \ln\left(a_i\right) \tag{76}$$

where f_i is the partial fugacity of gaseous component *i* in the bulk fluid mixture, and $f_{i,sat}$ is the fugacity of pure component *i* at saturation, and a_i is the activity of component *i* in the sorbed

phase in the polymeric membrane; the activities within the membrane are described by Equation (73). For further discussions on fluid-polymer equilibrium and the interpretation of equation (76), see Ribeiro and Freeman.[28, 29]

For specified set of partial fugacities in the upstream compartment, the volume fractions of the penetrants in the polymer membrane may be calculated by solving equations (73) and (76) simultaneously, using an equation solver. All the calculations presented in this article were implemented in MathCad 15.[35] As illustration, Figures **41**a,b presents calculations of the volume fractions of penetrants CO_2 (1) and C_2H_6 (2) in a cross-linked polyethylene oxide (XLPEO) membrane (indicated by subscript m) at 298.15 K; at this temperature all interaction parameters $\chi_{12}, \chi_{1m}, \chi_{2m}$ are independent of the volume fractions in the membrane; the values are specified in Table 6. The upstream face of the membrane is in equilibrium with CO_2/C_2H_6 mixtures of five different compositions. The experimental data (indicated by symbols) on mixed-gas sorption are those presented in Figures 5 and 6 of Ribeiro and Freeman.[36] The simultaneous solution to equations (73) and (76), indicated by the continuous solid lines, are in excellent agreement with the experimental data of Ribeiro and Freeman.[36] This is to be expected because the three interaction parameters $\chi_{12}, \chi_{1m}, \chi_{2m}$ were determined by fitting the experimental data to Equation (73).

Figures **41**c,d presents the experimental data (indicated by symbols) for the volume fractions of penetrants CO_2 (1) and C_2H_6 (Compon2) in a cross-linked polyethylene oxide (XLPEO) membrane (indicated by subscript m) at 263.15 K with the F-H model calculations. At this lower temperature, all three interaction parameters $\chi_{12}, \chi_{1m}, \chi_{2m}$ were determined to be dependent on the volume fractions of the penetrants and empirical fits are provided by Ribeiro et al.[31] For convenience to readers, the data fits at 263.15 K are provided in Table 5. It is to be noted that

the fitted expressions obtained by Ribeiro et al.[31] are based on the use of Equations (73), and *not* on the extended equations provided by Yang and Lue,[33] Mulder et al.[32] and Varady et al.[34]

The simultaneous solution to equations (73) and (76), indicated by the continuous solid lines, are in excellent agreement with the experimental data of Ribeiro and Freeman.[36]

In a subsequent section, we will compare model calculations of mixture permeation fluxes with experimental data at 298.15 K and at 263.15 K.

19. F-H description of alcohol/water/polymer phase equilibria relevant to membrane pervaporation processes

Let us now turn our attention to a scenario in which the upstream compartment contains a binary liquid mixture; this scenario is relevant to membrane pervaporation processes. A detailed analysis of the equilibrium between the binary liquid mixture (Components 1, and 2) and the polymer membrane (Penetrants 1, 2, and polymer membrane (m)) is available in the works of Yang and Lue,[33] and Mulder et al.[32]

Let ϕ_1^L, ϕ_2^L represent the volume fractions of components 1 and 2 in the bulk liquid mixture. These volume fractions are related to the mass fractions in the bulk liquid mixture $\phi_i^L = \dfrac{\dfrac{\omega_i^L}{\rho_{i0}}}{\sum_{i=1}^{n} \dfrac{\omega_i^L}{\rho_{i0}}}$.

We also have the constraint $\phi_1^L + \phi_2^L = 1$. The component activities in the liquid mixture are described by the F-H model

$$\begin{aligned} \ln a_1^L &= \ln(\phi_1^L) + (1 - \frac{\overline{V_1}}{\overline{V_2}})\phi_2^L + \chi_{12}\left(\phi_2^L\right)^2 - \phi_1^L\left(\phi_2^L\right)^2 \frac{\partial \chi_{12}}{\partial \phi_2^L} \\ \ln a_2^L &= \ln(\phi_2^L) + (1 - \frac{\overline{V_2}}{\overline{V_1}})\phi_1^L + \frac{\overline{V_2}}{\overline{V_1}}\chi_{12}\left(\phi_1^L\right)^2 + \frac{\overline{V_2}}{\overline{V_1}}\phi_2^L\left(\phi_1^L\right)^2 \frac{\partial \chi_{12}}{\partial \phi_2^L} \end{aligned} \tag{77}$$

Equation (77) corresponds precisely with equations (9), and (10) of Mulder et al.[32] The χ_{12} is related to the excess Gibbs free energy

$$\chi_{12} = \frac{1}{x_1 \phi_2^L}\left[x_1 \ln(\frac{x_1}{\phi_1^L}) + x_2 \ln(\frac{x_2}{\phi_2^L}) + \frac{G^{excess}}{RT} \right]$$
$$\frac{G^{excess}}{RT} = x_1 \ln(\gamma_1) + x_2 \ln(\gamma_2) \qquad (78)$$

In equation (78), x_1, x_2 are liquid phase mole fractions $x_i = \frac{c_i}{c_t} = \frac{\frac{\omega_i^L}{M_i}}{\sum_{i=1}^{n} \frac{\omega_i^L}{M_i}} = \frac{\omega_i}{M_i}\overline{M}$. The interaction parameter χ_{12} for mixtures such as water/ethanol are strongly dependent on the liquid mixture composition. The excess Gibbs free energy $\frac{G^{excess}}{RT} = x_1 \ln(\gamma_1) + x_2 \ln(\gamma_2)$ can be calculated from activity coefficient models such as that of Wilson, NRTL, and UNIQUAC.[32, 33] Mulder et al.[32] have also shown that the dependence of χ_{12} on the volume fractions of components in the bulk liquid mixture can be expressed as a fourth-order polynomial in

$$u_2^L = \frac{\phi_2^L}{\phi_1^L + \phi_2^L} = \phi_2^L$$

$$\chi_{12} = a + b\left(u_2^L\right) + c\left(u_2^L\right)^2 + d\left(u_2^L\right)^3 + e\left(u_2^L\right)^4; \quad \text{bulk liquid mixture}$$
$$u_2^L = \frac{\phi_2^L}{\phi_1^L + \phi_2^L} = \phi_2^L; u_1^L = \frac{\phi_1^L}{\phi_1^L + \phi_2^L} = \phi_1^L = 1 - u_2^L = 1 - \phi_2^L \qquad (79)$$

In all the Flory-Huggins calculations presented in this article, the 4th order polynomial expressions are used to describe the volume fraction dependence of χ_{12}.

A significant contribution of Mulder et al.[32] is to demonstrate that the interaction parameter χ_{12} for the same two penetrants in the polymer membrane phase shows the same composition

dependence on the normalized volume fraction of component 2 within the membrane $u_2 = \frac{\phi_2}{\phi_1 + \phi_2}$, i.e.

$$\chi_{12} = a + b(u_2) + c(u_2)^2 + d(u_2)^3 + e(u_2)^4; \quad \text{polymer membrane phase}$$
$$u_2 = \frac{\phi_2}{\phi_1 + \phi_2}; u_1 = \frac{\phi_1}{\phi_1 + \phi_2} = 1 - u_2 \tag{80}$$

It is important to note that in the above equation (80), for convenience, we use the same nomenclature as Mulder et al.[32] However, in the Maxwell-Stefan formulation for diffusion, the quantities u_1 and u_2 refer to the diffusion velocities of the penetrants as they diffuse across the membrane.

In the scenario in which the interaction parameter χ_{12} exhibits a composition dependence following equation (80) in the membrane phase, the Flory-Huggins equation (73) needs to be extended as follows (these equations correspond to equations (6) and (7) of Mulder et al.[32])

$$\ln a_1 = \ln(\phi_1) + (1-\phi_1) - \phi_2 \frac{\overline{V_1}}{\overline{V_2}} - \phi_m \frac{\overline{V_1}}{\overline{V_m}} + (\chi_{12}\phi_2 + \chi_{1m}\phi_m)(\phi_2 + \phi_m) - \chi_{2m} \frac{\overline{V_1}}{\overline{V_2}} \phi_2 \phi_m - u_1 u_2 \phi_2 \frac{\partial \chi_{12}}{\partial u_2}$$
$$\ln a_2 = \ln(\phi_2) + (1-\phi_2) - \phi_1 \frac{\overline{V_2}}{\overline{V_1}} - \phi_m \frac{\overline{V_2}}{\overline{V_m}} + \left(\chi_{12}\phi_1 \frac{\overline{V_2}}{\overline{V_1}} + \chi_{2m}\phi_m \right)(\phi_1 + \phi_m) - \chi_{1m} \frac{\overline{V_2}}{\overline{V_1}} \phi_1 \phi_m + \frac{\overline{V_2}}{\overline{V_1}} u_1^2 \phi_2 \frac{\partial \chi_{12}}{\partial u_2}$$

(81)

By equating the activities of the components in the bulk liquid mixture (a_i^L from equation (77)) to the corresponding component activities in the membrane mixture (a_i from equation (81)), we can calculate the volume fractions in the polymer phase, ϕ_i, that is in equilibrium with any specified liquid mixture composition in the upstream face, with volume fractions ϕ_i^L. The

determination of the volume fractions in the polymer requires the use of an equation solver, such as MathCad 15[35] that was employed in this work.

As illustration, Figure **42**a presents calculations of the volume fractions of penetrants water (1), ethanol (2) in a cellulose acetate (polymer, component m) at 293.15 K. The upstream face of the membrane is in equilibrium with water/ethanol liquid mixture of varying mass fractions. Water is adsorbed preferentially in hydrophilic cellulose acetate. Another point to note is that the volume fractions of the penetrants in the membrane phase are significantly higher than those for CO_2/C_2H_6/XLPEO system. Figure **42**b presents calculations of the elements of the matrix of thermodynamic factors, defined by equation (99), discussed in a later section. Figure **42**c presents calculations of the ratios $-\frac{\Gamma_{12}}{\Gamma_{11}}, -\frac{\Gamma_{21}}{\Gamma_{22}}$.

Figure **43** presents calculations of the compositions of penetrants water (component 1), ethanol (component 2) in polyimide membrane (polymer, component m) at 293.15 K. The upstream face of the membrane is in equilibrium with water/ethanol liquid mixture of varying mass fractions. In the calculations, χ_{1m}, χ_{2m} are composition independent, and χ_{12} follows the composition dependence described by equations (79) and (80). The Flory-Huggins model calculations are in good agreement with the experimental sorption data of Ni et al.[37], as presented in Figures 1, and 2 of their paper.

Figure **44** shows the experimental data (symbols) of Heintz and Stephan[38] for binary sorption of water/ethanol mixtures across a poly (vinyl alcohol) /poly (acrylonitrile) (PVA/PAN) composite membrane. The continuous solid lines are the F-H model calculations using the input data in Table 9. There is reasonable agreement of F-H model with experimental data. The modelling of pervaporation will be presented in a subsequent section.

20. The M-S formulation for diffusion in multicomponent polymer solutions

We develop the Maxwell-Stefan (M-S) equations to describe the diffusion of *n* penetrants, 1, 2, 3,..*n* in a polymer matrix (m). The M-S equations represent a balance between the force exerted per mole of species *i* with the drag, or friction, experienced with each of the partner species in the mixture. We may expect that the frictional drag to be proportional to differences in the velocities of the diffusing species $\left(u_i - u_j\right)$, where u_i is the velocity of motion of the penetrant *i*. For diffusion in multicomponent polymer solutions such as acetone/cellulose acetate, $u_{\rm m} \neq 0$, i.e. the polymer chains have a finite velocity of diffusion. For a mixture containing a total of *n* penetrants, 1, 2, 3,..*n* we write

$$
\begin{aligned}
-\frac{d\mu_1}{dz} &= \frac{RT}{Đ_{12}} X_2\left(u_1 - u_2\right) + \frac{RT}{Đ_{13}} X_3\left(u_1 - u_3\right) + \ldots + \frac{RT}{Đ_{1m}} X_m\left(u_1 - u_m\right) \\
-\frac{d\mu_2}{dz} &= \frac{RT}{Đ_{21}} X_1\left(u_2 - u_1\right) + \frac{RT}{Đ_{23}} X_3\left(u_2 - u_3\right) + \ldots + \frac{RT}{Đ_{2m}} X_m\left(u_2 - u_m\right) \\
&\cdots\cdots \\
-\frac{d\mu_n}{dz} &= \frac{RT}{Đ_{n1}} X_1\left(u_n - u_1\right) + \frac{RT}{Đ_{n2}} X_2\left(u_n - u_3\right) + \ldots + \frac{RT}{Đ_{nm}} X_m\left(u_n - u_m\right) \\
-\frac{d\mu_m}{dz} &= \frac{RT}{Đ_{m1}} X_1\left(u_m - u_1\right) + \frac{RT}{Đ_{m2}} X_2\left(u_m - u_3\right) + \ldots + \frac{RT}{Đ_{mn}} X_n\left(u_m - u_n\right)
\end{aligned}
\qquad (82)
$$

The left members of equation (82) are the negative of the gradients of the chemical potentials, with the units N mol^{-1}; it represents the driving force acting per mole of species 1, 2, 3,..*n*. The subscript m refers to the polymer chain, that is regarded as the (*n*+1)*th* component in the mixture. The term $RT/Đ_{im}$ is interpreted as the drag or friction coefficient between the penetrant *i* and the polymer. The term $RT/Đ_{ij}$ is interpreted as the friction coefficient for the *i-j* pair of penetrants. The multiplier $X_{\rm j}$ in each of the right members represents a measure of the composition of

component *j* in the mixture because we expect the friction to be dependent on the number of molecules of *j* relative to that of component *i*.

There are many possible choices for composition measures X_i:

Mole fractions, x_i

Molar concentrations, c_i

Mass fractions, ω_i

Partial mass densities, ρ_i

Volume fractions, ϕ_i

Let us denote the molar masses of the species are M_i, and the mean molar mass of the mixture is $\overline{M} = \sum_{i=1}^{m} x_i M_i = \frac{1}{\sum_{i=1}^{m} \frac{\omega_i}{M_i}}$. Note that the summation includes the penetrants 1,2,3..n, *and* the polymer m.

Let us denote the partial molar volumes as $\overline{V_i}$. The mean molar volume is $\overline{V} = \sum_{k=1}^{m} x_k \overline{V_k}$.

We use ϕ_i to denote the volume fraction of the penetrant species *i*: $\phi_i = c_i \overline{V_i}$.

The volume fractions are related to the mass fractions, $\omega_i = \frac{\rho_i}{\rho_t} = \frac{\phi_i \rho_i}{\sum_{i=1}^{m} \phi_i \rho_i}$; $\phi_i = c_i \overline{V_i} = \frac{\frac{\omega_i}{\rho_i}}{\sum_{i=1}^{m} \frac{\omega_i}{\rho_i}}$. As an approximation, the partial mass densities ρ_i may be taken to equal to densities of the pure components.

The mole fraction is related to the volume fraction by $x_i = \frac{c_i}{c_t} = c_i \overline{V} = \frac{\phi_i}{\overline{V_i}} \overline{V} = \frac{\phi_i}{\overline{V_i}} \frac{1}{c_t} = \frac{\phi_i}{\overline{V_i}} \sum_{k=1}^{m} x_k \overline{V_k}$.

The inter-relations between the mole fractions and mass fractions are:

$$x_i = \frac{c_i}{c_t} = \frac{\dfrac{\omega_i}{M_i}}{\sum_{i=1}^{m} \dfrac{\omega_i}{M_i}} = \frac{\omega_i}{M_i}\overline{M}\ ;\ \omega_i = \frac{\rho_i}{\rho_t} = \frac{x_i M_i}{\sum_{i=1}^{m} x_i M_i} = \frac{x_i M_i}{\overline{M}}\ ;$$

Written in terms of mole fractions, x_i, equations (1) are

$$\begin{aligned}
-\frac{d\mu_1}{dz} &= \frac{RT}{Đ_{12}} x_2(u_1 - u_2) + \frac{RT}{Đ_{13}} x_3(u_1 - u_3) + \ldots + \frac{RT}{Đ_{1m}} x_m(u_1 - u_m) \\
-\frac{d\mu_2}{dz} &= \frac{RT}{Đ_{21}} x_1(u_2 - u_1) + \frac{RT}{Đ_{23}} x_3(u_2 - u_3) + \ldots + \frac{RT}{Đ_{2m}} x_m(u_2 - u_m) \\
&\cdots\cdots \\
-\frac{d\mu_n}{dz} &= \frac{RT}{Đ_{n1}} x_1(u_n - u_1) + \frac{RT}{Đ_{n2}} x_2(u_n - u_3) + \ldots + \frac{RT}{Đ_{nm}} x_m(u_n - u_m) \\
-\frac{d\mu_m}{dz} &= \frac{RT}{Đ_{m1}} x_1(u_m - u_1) + \frac{RT}{Đ_{m2}} x_2(u_m - u_3) + \ldots + \frac{RT}{Đ_{mn}} x_n(u_m - u_n)
\end{aligned} \tag{83}$$

Only n of the chemical potential gradients $\dfrac{d\mu_i}{dz}$ are independent, because of the Gibbs-Duhem relationship

$$x_1 \frac{d\mu_1}{dz} + x_2 \frac{d\mu_2}{dz} + \cdots x_n \frac{d\mu_n}{dz} + x_m \frac{d\mu_m}{dz} = 0 \tag{84}$$

The Maxwell-Stefan diffusion formulation (83) is consistent with the theory of irreversible thermodynamics. The Onsager Reciprocal Relations imply that the M-S pair diffusivities are symmetric

$$Đ_{ij} = Đ_{ji} \tag{85}$$

Written in terms of volume fractions, the n independent chemical potential gradients are related to the velocity differences as follows

$$
\begin{aligned}
-\frac{1}{RT}\frac{d\mu_i}{dz} &= \sum_{\substack{j=1\\ j\neq i}}^{n}\frac{\phi_j\left(u_i-u_j\right)}{Đ_{ij}^{V}}+\frac{\phi_m\left(u_i-u_m\right)}{Đ_{im}^{V}};\quad i=1,2,...n\\
-\phi_i\frac{1}{RT}\frac{d\mu_i}{dz} &= \sum_{\substack{j=1\\ j\neq i}}^{n}\frac{\phi_i\phi_j\left(u_i-u_j\right)}{Đ_{ij}^{V}}+\frac{\phi_i\phi_m\left(u_i-u_m\right)}{Đ_{im}^{V}};\quad i=1,2,...n
\end{aligned}
\tag{86}
$$

The modified M-S diffusivities $Đ_{ij}^{V}$ are related to the M-S diffusivities $Đ_{ij}=Đ_{ji}$, defined in terms of mole fractions, by: $c_t Đ_{ij}\overline{V_j}=\frac{Đ_{ij}\overline{V_j}}{\overline{V}}=Đ_{ij}^{V}$, and $c_t Đ_{im}\overline{V_m}=\frac{Đ_{im}\overline{V_m}}{\overline{V}}=Đ_{im}^{V}$. The symmetry constraint imposed by the Onsager Reciprocal Relations is $Đ_{ij}=\frac{Đ_{ij}^{V}}{\overline{V_j}}\overline{V}=Đ_{ji}=\frac{Đ_{ji}^{V}}{\overline{V_i}}\overline{V};\quad \frac{Đ_{ji}^{V}}{\overline{V_i}}=\frac{Đ_{ij}^{V}}{\overline{V_j}}$. It is important to note that the M-S diffusivities $Đ_{ij}^{V}$ are *not* symmetric.

We define the *volumetric* flux of component *i* in a laboratory-fixed reference frame, expressed as $m^3\ m^{-2}\ s^{-1}$

$$
N_i^{V}=\phi_i u_i \tag{87}
$$

The corresponding *molar* flux of component *i*, in a laboratory-fixed reference frame, expressed as mol $m^{-2}\ s^{-1}$ is $N_i=c_i u_i=\frac{\phi_i}{\overline{V_i}}u_i=\frac{N_i^{V}}{\overline{V_i}}$.

Let us define the volumetric diffusion fluxes relative to the volume average velocity of the mixture,

$$
\begin{aligned}
&J_i^{V}=\phi_i\left(u_1-u^{V}\right);\quad J_m^{V}=\phi_m\left(u_m-u^{V}\right)=-J_1-J_2-...-J_n;\\
&u^{V}=\phi_1 u_1+\phi_2 u_2...+\phi_n u_n+\phi_m u_m
\end{aligned}
\tag{88}
$$

Equation (86) can be re-written in terms of the diffusion fluxes

$$-\phi_i \frac{1}{RT}\frac{d\mu_i}{dz} = \sum_{\substack{j=1 \\ j\neq i}}^{n} \frac{\left(\phi_j J_i^V - \phi_i J_j^V\right)}{Đ_{ij}^V} + \frac{\left(\phi_m J_i^V - \phi_i J_m^V\right)}{Đ_{im}^V}; \quad i = 1,2,...n \tag{89}$$

It is helpful to express the chemical potential gradients in terms of the volume fraction gradients by introducing an $n\times n$ dimensional matrix of thermodynamic factors $[\Gamma]$:

$$\frac{\phi_i}{RT}\frac{d\mu_i}{dz} = \phi_i \frac{d\ln a_i}{dz} = \sum_{j=1}^{j=n} \Gamma_{ij}\frac{d\phi_j}{dz}; \quad \Gamma_{ij} = \frac{\phi_i}{\phi_j}\frac{\partial \ln a_i}{\partial \ln \phi_j}; \quad i,j = 1,,..n$$

For diffusion in a ternary mixture consisting of two solvent species (1, 2) and polymer (m), a combination of equations (88) and (89) yields

$$\begin{aligned} -\phi_1 \frac{1}{RT}\frac{d\mu_1}{dz} &= \frac{\left(\phi_2 J_1^V - \phi_1 J_2^V\right)}{Đ_{12}^V} + \frac{\left(\phi_m J_1^V - \phi_1\left(-J_1^V - J_2^V\right)\right)}{Đ_{1m}^V} \\ -\phi_2 \frac{1}{RT}\frac{d\mu_2}{dz} &= \frac{\left(\phi_1 J_2^V - \phi_2 J_1^V\right)}{Đ_{21}^V} + \frac{\left(\phi_m J_2^V - \phi_2\left(-J_1^V - J_2^V\right)\right)}{Đ_{2m}^V} \end{aligned} \tag{90}$$

In proceeding further, it is convenient to define two 2×2 dimensional square matrices [B], and $[\Lambda]$:

$$[B] = \begin{bmatrix} \frac{\phi_1}{Đ_{1m}^V} + \frac{\phi_2}{Đ_{12}^V} + \frac{\phi_m}{Đ_{1m}^V} & -\phi_1\left(\frac{1}{Đ_{12}^V} - \frac{1}{Đ_{1m}^V}\right) \\ -\phi_2\left(\frac{1}{Đ_{21}^V} - \frac{1}{Đ_{2m}^V}\right) & \frac{\phi_1}{Đ_{21}^V} + \frac{\phi_2}{Đ_{2m}^V} + \frac{\phi_m}{Đ_{2m}^V} \end{bmatrix}; \quad [\Lambda] = [B]^{-1} \tag{91}$$

In 2-dimensional matrix notation, equation (90) takes the form

$$\left(J^V\right) = -[D]\frac{d(\phi)}{dz}; \quad [D] = [B]^{-1}[\Gamma] = [\Lambda][\Gamma] \tag{92}$$

21. The M-S formulation vs Bearman friction formulation for diffusion in multicomponent polymer solutions

In the vast literature on diffusion in polymer solutions,[39, 40] it is customary to use the friction formulation for multicomponent diffusion, normally credited to Bearman,[41] written in a manner such as in equation (1) of Price and Romdhane:[40]

$$-\frac{d\mu_i}{dz}=\sum_{\substack{j=1\\ j\neq i}}^{n}\frac{\rho_j}{M_j}\varsigma_{ij}\left(u_i-u_j\right)+\frac{\rho_m}{M_m}\varsigma_{im}\left(u_i-u_m\right) \tag{93}$$

or equivalently, as $-\frac{d\mu_i}{dz}=\sum_{\substack{j=1\\ j\neq i}}^{n}c_j\varsigma_{ij}\left(u_i-u_j\right)+c_m\varsigma_{im}\left(u_i-u_m\right)$.

In equation (93), the $\varsigma_{ij},\varsigma_{im}$ are friction coefficients that are related to the modified M-S diffusivities $Đ_{ij}^{V}$:

$$\frac{\rho_j}{M_j}\varsigma_{ij}=\frac{RT\phi_j}{Đ_{ij}^{V}};\frac{\rho_m}{M_m}\varsigma_{im}=\frac{RT\phi_m}{Đ_{im}^{V}} \tag{94}$$

22. Maxwell-Stefan formulation for permeation across polymer membranes

For diffusion across polymeric membranes, the velocity of the polymer, $u_m = 0$. For modelling mixture permeation across polymeric membranes, we need to reformulate the Maxwell-Stefan equations using volume fractions instead of mole fractions.[31, 34, 42] The use of volume fractions facilitates the application of the F-H thermodynamics to describe equilibrium between the membrane phase and the bulk fluid mixtures on either side of the membrane layer.

The mole fraction is related to the volume fraction by $x_i=\frac{c_i}{c_t}=c_i\overline{V}=\frac{\phi_i}{\overline{V}_i}\overline{V}=\frac{\phi_i}{\overline{V}_i}\frac{1}{c_t}=\frac{\phi_i}{\overline{V}_i}\sum_{k=1}^{m}x_k\overline{V_k}$. We re-write equation (**83**) in terms of volume fractions

by replacing the mole fractions by the volume fractions: $-\frac{\phi_i}{\overline{V_i}}\frac{1}{c_t RT}\frac{d\mu_i}{dz}=\sum_{\substack{j=1\\ j\neq i}}^{m}\frac{\left(u_i-u_j\right)}{Đ_{ij}}\frac{\phi_i}{\overline{V_i}}\frac{1}{c_t}\frac{\phi_j}{\overline{V_j}}\frac{1}{c_t}$, or $-\frac{\phi_i}{\overline{V_i}}\frac{1}{RT}\frac{d\mu_i}{dz}=\sum_{\substack{j=1\\ j\neq i}}^{m}\frac{\phi_i\phi_j\left(u_i-u_j\right)}{Đ_{ij}}\frac{1}{\overline{V_i}}\frac{1}{\overline{V_j}}\frac{1}{c_t}$. Let us define modified M-S diffusivities: $c_t Đ_{ij}\overline{V_j}=\frac{Đ_{ij}\overline{V_j}}{\overline{V}}=Đ_{ij}^V$, $c_t Đ_{12}\overline{V_2}=\frac{Đ_{12}\overline{V_2}}{\overline{V}}=Đ_{12}^V$, and $c_t Đ_{1m}\overline{V_m}=\frac{Đ_{1m}\overline{V_m}}{\overline{V}}=Đ_{1m}^V$ We have the symmetry constraint $Đ_{ij}=\frac{Đ_{ij}^V}{\overline{V_j}}\overline{V}=Đ_{ji}=\frac{Đ_{ji}^V}{\overline{V_i}}\overline{V}$; $\frac{Đ_{ji}^V}{\overline{V_i}}=\frac{Đ_{ij}^V}{\overline{V_j}}$ demanded by the Onsager Reciprocal Relations.

The M-S equations written in terms of volume fractions take the form

$$\begin{aligned}-\frac{1}{RT}\frac{d\mu_i}{dz}&=\sum_{\substack{j=1\\ j\neq i}}^{n}\frac{\phi_j\left(u_i-u_j\right)}{Đ_{ij}^V}+\frac{\phi_m\left(u_i\right)}{Đ_{im}^V};\quad i=1,2,...n\\ -\phi_i\frac{1}{RT}\frac{d\mu_i}{dz}&=\sum_{\substack{j=1\\ j\neq i}}^{n}\frac{\phi_i\phi_j\left(u_i-u_j\right)}{Đ_{ij}^V}+\frac{\phi_i\phi_m\left(u_i\right)}{Đ_{im}^V};\quad i=1,2,...n\end{aligned}\tag{95}$$

In contrast to diffusion across zeolite membrane, an important distinguishing feature of diffusion across polymer membranes, is that the polymer (m) is considered as part of the mixture. The zeolite framework, on the other hand, is not part of the mixture.

We re-write equation (95) as

$$-\phi_i\frac{1}{RT}\frac{d\mu_i}{dz}=\sum_{\substack{j=1\\ j\neq i}}^{n}\frac{\left(\phi_i\phi_j u_i-u_j\phi_i\phi_j\right)}{Đ_{ij}^V}+\frac{\left(\phi_i\phi_m u_i\right)}{Đ_{im}^V};\quad i=1,2,...n\tag{96}$$

Let us define the *volumetric* flux of component *i*, expressed as $m^3\ m^{-2}\ s^{-1}$ as $N_i^V=\phi_i u_i$. The molar flux of component *i*, expressed as mol $m^{-2}\ s^{-1}$ is $N_i=c_i u_i=\frac{\phi_i}{\overline{V_i}}u_i=\frac{N_i^V}{\overline{V_i}}$. In terms of the volumetric fluxes of components, equation (96) is

$$-\phi_i \frac{1}{RT}\frac{d\mu_i}{dz} = \sum_{\substack{j=1 \\ j\neq i}}^{n} \frac{\left(\phi_j N_i^V - \phi_i N_j^V\right)}{Đ_{ij}^V} + \frac{\left(\phi_m N_i^V\right)}{Đ_{im}^V}; \quad i = 1,2,...n \tag{97}$$

Let us define an $n\times n$ dimensional matrix of inverse diffusivities $[B]$ whose elements are given by

$$B_{ii} = \sum_{j=1; j\neq i}^{j=n} \frac{\phi_j}{Đ_{ij}^V} + \frac{\phi_m}{Đ_{1m}^V}; \quad B_{ij;i\neq j} = -\frac{\phi_i}{Đ_{ij}^V}; \quad i, j = 1,2,...n \tag{98}$$

The reader should note that the elements of $[B]$ are relevant for permeation across polymer membranes that is considered to be stagnant, i.e. $u_m = 0$. For diffusion in polymer solutions, with $u_m \neq 0$, the elements are given by equation (91).

It is helpful to express the left member of equation (96) in terms of the volume fraction gradients by introducing an $n\times n$ dimensional matrix of thermodynamic factors $[\Gamma]$:

$$\frac{\phi_i}{RT}\frac{d\mu_i}{dz} = \phi_i \frac{d\ln a_i}{dz} = \sum_{j=1}^{j=n} \Gamma_{ij} \frac{d\phi_j}{dz}; \quad \Gamma_{ij} = \frac{\phi_i}{\phi_j}\frac{\partial \ln a_i}{\partial \ln \phi_j}; \quad i, j = 1,,..n \tag{99}$$

Combining Equations (97), (98) and (99) and casting these in n-dimensional matrix notation we write

$$(N^V) = -[B]^{-1}[\Gamma]\frac{d(\phi)}{dz} \tag{100}$$

The corresponding expression for the molar fluxes is obtained from use of the $N_i = \frac{N_i^V}{\overline{V}_i}$; this results in the final expression given below

$$(N) = -\begin{bmatrix} 1/\overline{V_1} & 0 & 0 & 0 \\ 0 & 1/\overline{V_2} & 0 & 0 \\ 0 & 0 & \ddots & 0 \\ 0 & 0 & 0 & 1/\overline{V_n} \end{bmatrix} [B]^{-1}[\Gamma]\frac{d(\phi)}{dz} \tag{101}$$

We now consider the special cases of unary permeation and binary mixture permeation.

23. The Maxwell-Stefan description of unary permeation

For the special case of unary permeation through polymer membrane (indicated with subscript m), $N_m = N_m^V = 0$, we write

$$N_1^V = -\frac{Đ_{1m}^V}{\phi_m}\Gamma\frac{d\phi_1}{dz}; \quad \Gamma = \frac{\partial \ln a_1}{\partial \ln \phi_1}; \quad N_1 = \frac{N_1^V}{\overline{V_1}} = -\frac{1}{\overline{V_1}}\frac{1}{1-\phi_1}Đ_{1m}^V\frac{\partial \ln a_1}{\partial \ln \phi_1}\frac{d\phi_1}{dz}; \tag{102}$$

The thermodynamic correction factor, $\Gamma = \dfrac{\partial \ln a_1}{\partial \ln \phi_1}$ can be evaluated by analytic differentiation of the Flory-Huggins Equation (71).

The unary molar flux of penetrant 1 can be determined by integrating equation (102) over the membrane thickness, δ.

$$N_1\delta = -\frac{1}{\overline{V_1}}\int_{\phi_{10}}^{\phi_{1\delta}}\frac{1}{1-\phi_1}Đ_{1m}^V\frac{\partial \ln a_1}{\partial \ln \phi_1}d\phi_1 \tag{103}$$

In equation (103), ϕ_{10} and $\phi_{1\delta}$ are the volume fractions of the penetrant 1 at the upstream and downstream faces, respectively. Fornasiero et al.[43] use Equation (103) to describe the steady-state diffusion of water through soft-contact-lens materials. The integral in Equation (103) can be determined analytically.

In the membrane literature, the experimental data are commonly presented in terms of the permeability of component *i* that is defined as

$$\Pi_i = \frac{N_i}{\Delta f_i/\delta} == \frac{N_i^V/\overline{V_i}}{\Delta f_i/\delta} \tag{104}$$

In equation (104), $\Delta f_i = f_{i0} - f_{i\delta}$ is the difference in the fugacities in the upstream and downstream compartments. The SI units for the permeability is mol m m^{-2} s^{-1} Pa^{-1}. The more commonly used engineering unit for permeability is the Barrer expressed in cm^3 (STP) cm cm^{-2} s^{-1} $(cm\ Hg)^{-1}$. To convert to the commonly used engineering units of Barrers we divide the value in mol m m^{-2} s^{-1} Pa^{-1} by 3.348×10^{-16}.

Combining equation (103) and (104), we obtain

$$\Pi_1 = \frac{N_i}{\Delta f_i/\delta} == \frac{N_i^V/\overline{V_i}}{\Delta f_i/\delta} = -\frac{1}{\Delta f_1}\frac{1}{\overline{V_1}}\int_{\phi_{10}}^{\phi_{1\delta}} \frac{1}{1-\phi_1} Đ_{1m}^V \frac{\partial \ln a_1}{\partial \ln \phi_1} d\phi_1 \tag{105}$$

The membrane thickness does not appear in the permeability calculations presented in Equation (105). This equation can be used to back-out the M-S diffusivity $Đ_{im}^V$ from experimental data on permeabilities.

24. The Maxwell-Stefan description of binary mixture permeation

For binary mixture permeation across a polymeric membrane (indicated with subscript m), $N_m = N_m^V = 0$, we write

$$\begin{aligned} -\phi_1 \frac{1}{RT}\frac{d\mu_1}{dz} &= \frac{\left(\phi_2 N_1^V - \phi_1 N_2^V\right)}{Đ_{12}^V} + \frac{\left(\phi_m N_1^V\right)}{Đ_{1m}^V} \\ -\phi_2 \frac{1}{RT}\frac{d\mu_2}{dz} &= \frac{\left(\phi_1 N_2^V - \phi_2 N_1^V\right)}{Đ_{21}^V} + \frac{\left(\phi_m N_2^V\right)}{Đ_{2m}^V} \end{aligned} \tag{106}$$

Let us define a 2×2 dimensional matrix of inverse diffusivities $[B]$ whose elements are given by

$$B_{11} = \frac{\phi_2}{Đ_{12}^V} + \frac{\phi_m}{Đ_{1m}^V}; \quad B_{12} = -\frac{\phi_1}{Đ_{12}^V}$$
$$B_{21} = -\frac{\phi_2}{Đ_{21}^V}; \quad B_{22} = \frac{\phi_1}{Đ_{21}^V} + \frac{\phi_m}{Đ_{2m}^V} \tag{107}$$

It is helpful to express the left member of equation (96) in terms of the volume fraction gradients by introducing an 2×2 dimensional matrix of thermodynamic factors $[\Gamma]$:

$$\frac{\phi_i}{RT}\frac{d\mu_i}{dz} = \phi_i \frac{d\ln a_i}{dz} = \sum_{j=1}^{2} \Gamma_{ij} \frac{d\phi_j}{dz}; \quad \Gamma_{ij} = \frac{\phi_i}{\phi_j}\frac{\partial \ln a_i}{\partial \ln \phi_j}; \quad i,j = 1,2$$
$$\begin{bmatrix} \Gamma_{11} & \Gamma_{12} \\ \Gamma_{21} & \Gamma_{22} \end{bmatrix} = \begin{bmatrix} \phi_1 \dfrac{\partial \ln a_1}{\partial \phi_1} & \phi_1 \dfrac{\partial \ln a_1}{\partial \phi_2} \\ \phi_2 \dfrac{\partial \ln a_2}{\partial \phi_1} & \phi_2 \dfrac{\partial \ln a_2}{\partial \phi_2} \end{bmatrix} \tag{108}$$

The four elements $\Gamma_{11}, \Gamma_{12}, \Gamma_{21}, \Gamma_{22}$ can be determined by analytic differentiation of Equation (73). Explicit analytic expressions are provided by Ribeiro et al.[31] for the special scenario in which the interaction parameters $\chi_{12}, \chi_{1m}, \chi_{2m}$ are constant.

Combining Equations (106), (107) and (108) and casting these in 2-dimensional matrix notation we obtain

$$(N^V) = -[B]^{-1}[\Gamma]\frac{d(\phi)}{dz}; \quad \begin{pmatrix} N_1^V \\ N_2^V \end{pmatrix} = -\begin{bmatrix} B_{11} & B_{12} \\ B_{21} & B_{22} \end{bmatrix}^{-1}\begin{bmatrix} \Gamma_{11} & \Gamma_{12} \\ \Gamma_{21} & \Gamma_{22} \end{bmatrix}\frac{d}{dz}\begin{pmatrix} \phi_1 \\ \phi_2 \end{pmatrix} \tag{109}$$

The matrix inversion $\begin{bmatrix} \Lambda_{11} & \Lambda_{12} \\ \Lambda_{21} & \Lambda_{22} \end{bmatrix} = \begin{bmatrix} B_{11} & B_{12} \\ B_{21} & B_{22} \end{bmatrix}^{-1}$ can be performed explicitly:

$$\begin{bmatrix}\Lambda_{11} & \Lambda_{12}\\ \Lambda_{21} & \Lambda_{22}\end{bmatrix}=\frac{\begin{bmatrix}\dfrac{\phi_1}{Đ^V_{21}}+\dfrac{\phi_m}{Đ^V_{2m}} & \dfrac{\phi_1}{Đ^V_{12}}\\ \dfrac{\phi_2}{Đ^V_{21}} & \dfrac{\phi_2}{Đ^V_{12}}+\dfrac{\phi_m}{Đ^V_{1m}}\end{bmatrix}}{\phi_m\left(\dfrac{\phi_1}{Đ^V_{21}Đ^V_{1m}}+\dfrac{\phi_2}{Đ^V_{12}Đ^V_{2m}}+\dfrac{\phi_m}{Đ^V_{1m}Đ^V_{2m}}\right)}=\frac{Đ^V_{1m}Đ^V_{2m}\begin{bmatrix}\dfrac{\phi_1}{Đ^V_{21}}+\dfrac{\phi_m}{Đ^V_{2m}} & \dfrac{\phi_1}{Đ^V_{12}}\\ \dfrac{\phi_2}{Đ^V_{21}} & \dfrac{\phi_2}{Đ^V_{12}}+\dfrac{\phi_m}{Đ^V_{1m}}\end{bmatrix}}{\phi_m\left(\dfrac{\phi_1Đ^V_{2m}}{Đ^V_{21}}+\dfrac{\phi_2Đ^V_{1m}}{Đ^V_{12}}+\phi_m\right)}$$

$$=\frac{\begin{bmatrix}Đ^V_{1m}\left(\phi_m+\dfrac{\phi_1Đ^V_{2m}}{Đ^V_{21}}\right) & Đ^V_{1m}\dfrac{\phi_1Đ^V_{2m}}{Đ^V_{21}}\\ Đ^V_{2m}\dfrac{\phi_2Đ^V_{1m}}{Đ^V_{12}} & Đ^V_{2m}\left(\phi_m+\dfrac{\phi_2Đ^V_{1m}}{Đ^V_{12}}\right)\end{bmatrix}}{\phi_m\left(\dfrac{\phi_1Đ^V_{2m}}{Đ^V_{21}}+\dfrac{\phi_2Đ^V_{1m}}{Đ^V_{12}}+\phi_m\right)} \tag{110}$$

The reader should note that the elements of $\begin{bmatrix}\Lambda_{11} & \Lambda_{12}\\ \Lambda_{21} & \Lambda_{22}\end{bmatrix}=\begin{bmatrix}B_{11} & B_{12}\\ B_{21} & B_{22}\end{bmatrix}^{-1}$ are relevant for permeation across polymer membranes that is considered to be stagnant, i.e. $u_m=0$. For diffusion in polymer solutions, with $u_m\neq 0$, the elements of $\begin{bmatrix}\Lambda_{11} & \Lambda_{12}\\ \Lambda_{21} & \Lambda_{22}\end{bmatrix}=\begin{bmatrix}B_{11} & B_{12}\\ B_{21} & B_{22}\end{bmatrix}^{-1}$ are given by equation (91).

The corresponding expression for the molar fluxes are

$$\begin{pmatrix}N_1\\ N_2\end{pmatrix}=-\begin{bmatrix}1/\overline{V_1} & 0\\ 0 & 1/\overline{V_2}\end{bmatrix}\begin{bmatrix}\Lambda_{11} & \Lambda_{12}\\ \Lambda_{21} & \Lambda_{22}\end{bmatrix}\begin{bmatrix}\phi_1\dfrac{\partial \ln a_1}{\partial \phi_1} & \phi_1\dfrac{\partial \ln a_1}{\partial \phi_2}\\ \phi_2\dfrac{\partial \ln a_2}{\partial \phi_1} & \phi_2\dfrac{\partial \ln a_2}{\partial \phi_2}\end{bmatrix}\frac{d}{dz}\begin{pmatrix}\phi_1\\ \phi_2\end{pmatrix} \tag{111}$$

25. Limiting scenarios for 1-2 friction

The M-S diffusivities $Đ^V_{im}$ can be backed-out from experimental data on unary permeation, but there is no experimental techniques for direct determination of the M-S diffusivities describing

1-2 friction: $Đ_{12}^V = Đ_{21}^V \frac{\overline{V_2}}{\overline{V_1}}$. Ribeiro et al.[31] adopt the strategy of fitting the three parameters $Đ_1^V, Đ_2^V, Đ_{12}^V$ to match their experimental data on permeabilities of binary of CO_2/C_2H_6 mixtures, of varying compositions, across XLPEO membrane.

From a practical point of view it is useful to derive limiting scenarios for 1-2 friction that should serve as guidelines for estimations of mixture permeation fluxes and selectivities. Using the analysis of mixture permeation across zeolite membranes as guideline, we consider the two limiting scenarios of (a) negligible 1-2 friction, and (b) dominant 1-2 friction.

26. Scenario in which 1-2 friction is considered to be negligible

In the limiting scenario in which 1-2 friction is considered to be of negligible importance:

$$\frac{\phi_1 Đ_{2m}^V}{Đ_{21}^V} \to 0; \quad \frac{\phi_2 Đ_{1m}^V}{Đ_{12}^V} \to 0 \tag{112}$$

For this scenario, the matrix $\begin{bmatrix} \Lambda_{11} & \Lambda_{12} \\ \Lambda_{21} & \Lambda_{22} \end{bmatrix}$ simplifies to yield

$$\begin{bmatrix} \Lambda_{11} & \Lambda_{12} \\ \Lambda_{21} & \Lambda_{22} \end{bmatrix} = \frac{\begin{bmatrix} Đ_{1m}^V\left(\phi_m + \frac{\phi_1 Đ_{2m}^V}{Đ_{21}^V}\right) & Đ_{1m}^V \frac{\phi_1 Đ_{2m}^V}{Đ_{21}^V} \\ Đ_{2m}^V \frac{\phi_2 Đ_{1m}^V}{Đ_{12}^V} & Đ_{2m}^V\left(\phi_m + \frac{\phi_2 Đ_{1m}^V}{Đ_{12}^V}\right) \end{bmatrix}}{\phi_m\left(\frac{\phi_1 Đ_{2m}^V}{Đ_{21}^V} + \frac{\phi_2 Đ_{1m}^V}{Đ_{12}^V} + \phi_m\right)} = \frac{1}{\phi_m}\begin{bmatrix} Đ_{1m}^V & 0 \\ 0 & Đ_{2m}^V \end{bmatrix} \tag{113}$$

Broadly speaking, we should expect the negligible 1-2 friction scenario to hold when the volume fractions of both penetrants in the membrane are negligibly small.

Equation (113), in essence, is used by Mulder et al.[30, 44] for modelling pervaporation of water (component 1), and ethanol (component 2) using cellulose acetate (polymer, component m)

membrane. Mulder et al[30, 44] do not, however, provide any justification for making this assumption; we return to this point later in this article.

27. Dominant 1-2 friction scenario for binary mixture permeation

The other extreme scenario that should be considered is one in which the friction between penetrants 1-2 is dominant. To develop this scenario we re-arrange the elements of the matrix $\begin{bmatrix} \Lambda_{11} & \Lambda_{12} \\ \Lambda_{21} & \Lambda_{22} \end{bmatrix}$ as follows

$$\begin{bmatrix} \Lambda_{11} & \Lambda_{12} \\ \Lambda_{21} & \Lambda_{22} \end{bmatrix} = \frac{\begin{bmatrix} Đ_{1m}^{V}\left(1+\frac{\phi_1 Đ_{2m}^{V}}{\phi_m Đ_{21}^{V}}\right) & Đ_{1m}^{V}\frac{\phi_1 Đ_{2m}^{V}}{\phi_m Đ_{21}^{V}} \\ Đ_{2m}^{V}\frac{\phi_2 Đ_{1m}^{V}}{\phi_m Đ_{12}^{V}} & Đ_{2m}^{V}\left(1+\frac{\phi_2 Đ_{1m}^{V}}{\phi_m Đ_{12}^{V}}\right) \end{bmatrix}}{\phi_m\left(\frac{\phi_1 Đ_{2m}^{V}}{\phi_m Đ_{21}^{V}}+\frac{\phi_2 Đ_{1m}^{V}}{\phi_m Đ_{12}^{V}}+1\right)} \tag{114}$$

The friction between penetrants 1-2 is dominant will be dominant if the following conditions are satisified

$$\frac{\phi_2 Đ_{1m}^{V}}{\phi_m Đ_{12}^{V}} >> 1; \quad \frac{\phi_1 Đ_{2m}^{V}}{\phi_m Đ_{21}^{V}} >> 1 \tag{115}$$

Invoking equation (115), along with $Đ_{12}^{V} = Đ_{21}^{V}\frac{\overline{V_2}}{\overline{V_1}}$, we derive

$$\begin{bmatrix} \Lambda_{11} & \Lambda_{12} \\ \Lambda_{21} & \Lambda_{22} \end{bmatrix} = \frac{\begin{bmatrix} Đ_{1m}^{V}\left(\frac{\phi_1 Đ_{2m}^{V}}{Đ_{21}^{V}}\right) & Đ_{1m}^{V}\frac{\phi_1 Đ_{2m}^{V}}{Đ_{21}^{V}} \\ Đ_{2m}^{V}\frac{\phi_2 Đ_{1m}^{V}}{Đ_{12}^{V}} & Đ_{2m}^{V}\left(\frac{\phi_2 Đ_{1m}^{V}}{Đ_{12}^{V}}\right) \end{bmatrix}}{\phi_m\left(\frac{\phi_1 Đ_{2m}^{V}}{Đ_{21}^{V}}+\frac{\phi_2 Đ_{1m}^{V}}{Đ_{12}^{V}}\right)}$$

The expressions for Λ_{12} and Λ_{21} are simplified to yield

$$\Lambda_{12} = \frac{Đ_{1m}^{V} \dfrac{\phi_1 Đ_{2m}^{V}}{Đ_{21}^{V}}}{\phi_m \left(\dfrac{\phi_1 Đ_{2m}^{V}}{Đ_{21}^{V}} + \dfrac{\phi_2 Đ_{1m}^{V}}{Đ_{12}^{V}} \right)} = \frac{\phi_1}{\phi_m \left(\dfrac{\phi_1}{Đ_{1m}^{V}} + \dfrac{\phi_2 Đ_{21}^{V}}{Đ_{2m}^{V} Đ_{12}^{V}} \right)} = \frac{\phi_1}{\phi_m \left(\dfrac{\phi_1}{Đ_{1m}^{V}} + \dfrac{\phi_2}{Đ_{2m}^{V}} \dfrac{\overline{V_1}}{\overline{\overline{V_2}}} \right)} \tag{116}$$

$$\Lambda_{21} = \frac{Đ_{2m}^{V} \dfrac{\phi_2 Đ_{1m}^{V}}{Đ_{12}^{V}}}{\phi_m \left(\dfrac{\phi_1 Đ_{2m}^{V}}{Đ_{21}^{V}} + \dfrac{\phi_2 Đ_{1m}^{V}}{Đ_{12}^{V}} \right)} = \frac{\phi_2}{\phi_m \left(\dfrac{\phi_1}{Đ_{1m}^{V}} \dfrac{Đ_{12}^{V}}{Đ_{21}^{V}} + \dfrac{\phi_2}{Đ_{2m}^{V}} \right)} = \frac{\phi_2}{\phi_m \left(\dfrac{\phi_1}{Đ_{1m}^{V}} \dfrac{\overline{V_2}}{\overline{\overline{V_1}}} + \dfrac{\phi_2}{Đ_{2m}^{V}} \right)} \tag{117}$$

The expressions for Λ_{11} and Λ_{22} for the dominant 1-2 friction scenario must be derived with more care. The diagonal elements must degenerate to the corresponding pure component $Đ_{im}^{V}$ values at either ends of the composition range, i.e. $\Lambda_{11} \to Đ_{1m}^{V}$; $\dfrac{\phi_1}{\phi_m} \to 1$; $\dfrac{\phi_2}{\phi_m} \to 0$, $\Lambda_{22} \to Đ_{2m}^{V}$; $\dfrac{\phi_1}{\phi_m} \to 0$; $\dfrac{\phi_2}{\phi_m} \to 1$

Imposing these conditions we obtain

$$\Lambda_{11} = \frac{Đ_{1m}^{V} \left(\dfrac{\phi_1 Đ_{2m}^{V}}{Đ_{21}^{V}} \right)}{\phi_m \left(\dfrac{\phi_1 Đ_{2m}^{V}}{Đ_{21}^{V}} + \dfrac{\phi_2 Đ_{1m}^{V}}{Đ_{12}^{V}} \right)} = \frac{\phi_1}{\phi_m \left(\dfrac{\phi_1}{Đ_{1m}^{V}} + \dfrac{\phi_2}{Đ_{2m}^{V}} \dfrac{\overline{V_1}}{\overline{\overline{V_2}}} \right)} \tag{118}$$

and

$$\Lambda_{22} = \frac{Đ_{2m}^{V} \left(\phi_m + \dfrac{\phi_2 Đ_{1m}^{V}}{Đ_{12}^{V}} \right)}{\phi_m \left(\dfrac{\phi_1 Đ_{2m}^{V}}{Đ_{21}^{V}} + \dfrac{\phi_2 Đ_{1m}^{V}}{Đ_{12}^{V}} \right)} = \frac{\phi_2}{\phi_m \left(\dfrac{\phi_1}{Đ_{1m}^{V}} \dfrac{\overline{V_2}}{\overline{\overline{V_1}}} + \dfrac{\phi_2}{Đ_{2m}^{V}} \right)} \tag{119}$$

Combining equation (116), (117), (118), and (119) we obtain the remarkably simple result

$$\begin{bmatrix} \Lambda_{11} & \Lambda_{12} \\ \Lambda_{21} & \Lambda_{22} \end{bmatrix} = \frac{1}{\phi_m \left(\frac{\phi_1}{\overline{\overline{V}}_1 \mathcal{D}_{1m}^V} + \frac{\phi_2}{\overline{\overline{V}}_2 \mathcal{D}_{2m}^V} \right)} \begin{bmatrix} \frac{\phi_1}{\overline{\overline{V}}_1} & \frac{\phi_1}{\overline{\overline{V}}_1} \\ \frac{\phi_2}{\overline{\overline{V}}_2} & \frac{\phi_2}{\overline{\overline{V}}_2} \end{bmatrix} \tag{120}$$

28. Determination of steady-state fluxes for binary mixture permeation across polymer membranes

Combining Equations (106), (107) and (108) and casting these in 2-dimensional matrix notation we obtain

$$\frac{d(\phi)}{dz} = -[\Gamma]^{-1}[B](N^V); \quad \frac{d}{dz}\begin{pmatrix} \phi_1 \\ \phi_2 \end{pmatrix} = -\begin{bmatrix} \Gamma_{11} & \Gamma_{12} \\ \Gamma_{21} & \Gamma_{22} \end{bmatrix}^{-1} \begin{bmatrix} B_{11} & B_{12} \\ B_{21} & B_{22} \end{bmatrix} \begin{pmatrix} N_1^V \\ N_2^V \end{pmatrix} \tag{121}$$

At steady-state, the volumetric fluxes N_i^V are z-invariant. Equations (121) represent a set of two coupled ordinary differential equations (ODEs) that are subject to the following set of boundary conditions (see schematic in Figure 40)

$$\text{upstream face}: \; z = 0; \quad f_i = f_{i0}; \quad \phi_i = \phi_{i0}$$

$$\text{downstream face}: \; z = \delta; \quad f_i = f_{i\delta}; \quad \phi_i = \phi_{i\delta}$$

The elements of the 2-dimensional square matrix $\begin{bmatrix} \Gamma_{11} & \Gamma_{12} \\ \Gamma_{21} & \Gamma_{22} \end{bmatrix}^{-1} \begin{bmatrix} B_{11} & B_{12} \\ B_{21} & B_{22} \end{bmatrix}$ are strongly composition dependent and, therefore, the set of coupled ODEs need to be solved numerically, as was done in the work reported by Ribeiro et al.[31] Since the fluxes are not known in advance, shooting methods are required for their determination. Consequently, the interpretation of experimental data is not an easy task. For this reason, it is helpful to derive a simplified, linearized, approach for calculation of the permeation fluxes.

29. Linearized model for binary mixture permeation across polymer membrane

In the linearized approach, we essentially assume that the composition profiles for both penetrants across the membrane layer is linear. The elements of each of the two matrices $\begin{bmatrix} \Lambda_{11} & \Lambda_{12} \\ \Lambda_{21} & \Lambda_{22} \end{bmatrix}$, and $\begin{bmatrix} \Gamma_{11} & \Gamma_{12} \\ \Gamma_{21} & \Gamma_{22} \end{bmatrix}$ is evaluated by calculating the elements $Đ^V_{im}\left(\phi_{1,av},\phi_{2,av}\right)$, $Đ^V_{ij}\left(\phi_{1,av},\phi_{2,av}\right)$and $\Gamma_{ij}\left(\phi_{1,av},\phi_{2,av}\right)$ at the arithmetic averaged volume fractions $\phi_{i,av}=\frac{\left(\phi_{i0}+\phi_{i\delta}\right)}{2}$. With this assumption the volumetric fluxes are calculated explicitly using

$$(N^V)=\frac{[\Lambda]}{\delta}[\Gamma](\phi_0-\phi_\delta) \tag{122}$$

The permeabilities can then be calculated using

$$\Pi_i=\frac{N_i^V/\overline{V_i}}{\Delta f_i/\delta} \tag{123}$$

For the scenario in which the 1-2 friction is considered to be negligible, equations (122) and (123) simplify to yield

$$\begin{aligned} N_i^V &= \frac{Đ^V_{im}\left(\phi_{1,av},\phi_{2,av}\right)}{\delta}\sum_{j=1}^{2}\Gamma_{ij}\left(\phi_{1,av},\phi_{2,av}\right)\left(\phi_{j0}-\phi_{j\delta}\right); \quad i=1,2 \\ \Pi_i &= \frac{N_i^V/\overline{V_i}}{\Delta f_i/\delta}=\frac{Đ^V_{im}\left(\phi_{1,av},\phi_{2,av}\right)}{\overline{V_i}}\sum_{j=1}^{2}\Gamma_{ij}\left(\phi_{1,av},\phi_{2,av}\right)\left(\phi_{j0}-\phi_{j\delta}\right); \quad i=1,2 \end{aligned} \tag{124}$$

Experimental data on the penetrant permeabilities $\Pi_i=\frac{N_i^V/\overline{V_i}}{\Delta f_i/\delta}$ can be used to back-out the *averaged* Maxwell-Stefan diffusivities $Đ^V_{im}\left(\phi_{1,av},\phi_{2,av}\right)$, determined at the compositions, $\phi_{i,av}=\frac{\left(\phi_{i0}+\phi_{i\delta}\right)}{2}$.

The accuracy of the linearized model, described by equations (122), is demonstrated by analysis of pervaporation of water(1)/ethanol(2) liquid phase feed mixtures across two different polymeric membranes.

Figure 45 shows the volume fractions within cellulose acetate (CA) membrane layer for a liquid phase water(1)/ethanol(2) feed mixture with mass fraction $\omega_1^L = 0.40563$. From the F-H phase equilibrium relations, the volume fractions at the upstream face are $\phi_1 = 0.16187 \quad \phi_2 = 0.26327$. The continuous solid lines are the profiles obtained from an exact numerical solution to the set of two coupled ODEs, resulting in the flux values $N_1^V = 2.4\times10^{-7}$, and $N_2^V = 2.2\times10^{-7}$ m^3 m^{-2} s^{-1}. The dashed lines are the linear profiles resulting from the linearized model, using equations (122), that result in the permeation flux values of $N_1^V = 2.33\times10^{-7}$, and $N_2^V = 1.98\times10^{-7}$ m^3 m^{-2} s^{-1}. The input data on F-H thermodynamics and diffusivities are provided in Table 7. The linearized model yields fluxes that are within 5% of those obtained from exact numerical solutions of the set of two coupled ODEs.

Figure 46 shows calculations of the volume fractions within the polyimide membrane layer for a liquid phase water(1)/ethanol(2) feed mixture with mass fraction $\omega_1^L = 0.7473$. From the F-H phase equilibrium relations, the volume fractions at the upstream face are $\phi_1 = 0.1424; \quad \phi_2 = 0.0226$. The volumetric fluxes calculated using equations (122) are $N_1^V = 15.78\times10^{-9}$, and $N_2^V = 0.448\times10^{-9}$ m^3 m^{-2} s^{-1}. The corresponding volume fraction profiles within the membrane layer are linear; see dashed lines in Figure 46. An exact numerical solution to the set of two coupled ODEs, results in the flux values $N_1^V = 15.5\times10^{-9}$, and $N_2^V = 0.487\times10^{-9}$ m^3 m^{-2} s^{-1}, that about 5% different from the calculations using the linearized

model. The corresponding volume fraction profiles within show slight deviations from linearity; see the continuous solid lines in Figure 46.

30. Water/ethanol pervaporation across polyimide membrane

Thermodynamic coupling effects are significant for water/ethanol pervaporation across polyimide membrane. Figure 47a shows calculations of the elements of $[\Gamma]$ as function of the mass fraction of water in the liquid feed mixture in the upstream compartment. ω_1^L. The negative values of the off-diagonal elements are noteworthy. Figure 47b plots the ratios of the elements of thermodynamic correction factors, $-\frac{\Gamma_{12}}{\Gamma_{11}}, -\frac{\Gamma_{21}}{\Gamma_{22}}$ as function of the mass fraction of water(1) in the liquid feed mixture in the upstream compartment ω_1^L. The off-diagonal elements are significant fractions of the corresponding diagonal elements. Clearly, thermodynamic coupling has a significant influence on the permeation fluxes. The experimental data of Ni et al.[37] on the volumetric fluxes of water, and ethanol are plotted in Figures 47c, and 47d, along with the estimates of the permeation fluxes using the linearized equations (122). The M-S diffusivities at zero vacancies for penetrant-membrane interactions used in the calculations are the same as reported in Table 1 of Ni et al.[37] $Đ_{1m}^V = 25.5\times10^{-13}$ m^2 s^{-1}; $Đ_{2m}^V = 2.1\times10^{-13}$ m^2 s^{-1}. Three different scenarios for 1-2 friction are assumed: (a) negligible 1-2 friction, (b) dominant 1-2 friction, along with an intermediate value $\frac{Đ_{2m}^V}{Đ_{21}^V} = 2$; the fluxes of both penetrants, mobile water and tardy ethanol, are strongly influenced by the chosen scenario for 1-2 friction. Increasing 1-2 friction, reduces the flux of the more mobile water, but decreases the flux of the tardier ethanol; this influence is precisely the same as witnessed earlier for CO_2/C_2H_6/XLPEO permeation. The experimentally observed maximum in the ethanol flux, observed at a feed mixture mass fraction

$\omega_1^L \approx 0.2$, can only be captured if 1-2 friction is taken to be sufficiently large in magnitude. If 1-2 friction is ignored, there is no discernible maximum in the ethanol flux. Ni et al.[37] have also concluded that 1-2 friction cannot be ignored.

31. Water/ethanol pervaporation across PVA/PAN membrane

Heintz and Stephan[45] have also underscored the importance of diffusional coupling effects for pervaporation of water/ethanol mixtures across a poly (vinyl alcohol) /poly (acrylonitrile) (PVA/PAN) composite membrane (m). Interestingly, their experimental data (see Figure 48) also show a maximum in the ethanol fluxes. For tracing the origins of the observed maximum in the ethanol flux, simulations of the molar permeation fluxes with the linearized equations (122) are attempted.

Figure 49a shows calculations of the elements of $[\Gamma]$ as function of the mass fraction of water in the liquid feed mixture in the upstream compartment. ω_1^L. The negative values of the off-diagonal elements are noteworthy. Figure 49b plots the ratios of the elements of thermodynamic correction factors, $-\frac{\Gamma_{12}}{\Gamma_{11}}, -\frac{\Gamma_{21}}{\Gamma_{22}}$ as function of the mass fraction of water(1) in the liquid feed mixture in the upstream compartment ω_1^L. The off-diagonal elements are significant in magnitude in comparison with the corresponding diagonal elements. Clearly, thermodynamic coupling has a significant influence on the permeation fluxes. The experimental data of Heintz and Stephan[45] on the permeation fluxes of water and ethanol are compared in Figures 49c,d with the estimates using the linearized equations (122). Three different scenarios are chosen to describe the magnitude of 1-2 friction: $\frac{Đ_{2m}^V}{Đ_{21}^V} = 0.2, \frac{Đ_{2m}^V}{Đ_{21}^V} = 4; \frac{Đ_{2m}^V}{Đ_{21}^V} = 20$. It is noteworthy that the maximum in the ethanol flux, observed in the experiments at a feed mixture mass fraction

$\omega_1^L \approx 0.7$, is adequately captured by the model taking $\frac{Đ_{2m}^V}{Đ_{21}^V} = 4$. If the relative magnitude of 1-2 friction is reduced and $\frac{Đ_{2m}^V}{Đ_{21}^V} = 0.2$, the ethanol flux maximum practically vanishes; however, for this choice there is a maximum in the water flux that is not observed experimentally.

32. Analysis of Ribeiro experiments for CO_2/C_2H_6 permeation across XLPEO membrane

In Figure 2 of Ribeiro et al.,[46] the permeabilities for unary permeation of CO_2 and C_2H_6 across a cross-linked polyethylene oxide (XLPEO) membrane at 298.15 K, and 263.15 are reported. Figures 50a,b show the backed-out, averaged, M-S diffusivities $Đ_{im}^V$ for CO_2 and C_2H_6 at the two temperatures $Đ_{1m}^V = \dfrac{\Pi_i}{-\dfrac{1}{\Delta f_1}\dfrac{1}{\overline{V}_1}\displaystyle\int_{\phi_{10}}^{\phi_{1\delta}} \frac{1}{1-\phi_1}\frac{\partial \ln a_1}{\partial \ln \phi_1} d\phi_1}$. The backed-out diffusivities demonstrate the validity of the exponential model $Đ_{im}^V = Đ_{im,0}^V \exp\left[A_i \phi_i\right]$ commonly used to describe the composition dependence of M-S diffusivities.

In Figures 50c, and 50d, the published experimental data of Ribeiro et al.[46] for CO_2/C_2H_6 mixture permeation across XLPEO membrane, measured at temperatures of 263.15 K, and 298.15 K, and varying upstream compositions and partial pressures, are used to back-out the $Đ_{im}^V$ using equations (124). At both temperatures, there is qualitative agreement between the M-S diffusivity in the mixture with the corresponding composition dependence of unary diffusivities. For the more mobile CO_2, the diffusivity in the mixture is somewhat lower than the corresponding unary diffusivity values, when compared at the same *total* volume fraction of penetrants, $\phi_1 + \phi_2$. Conversely, for the tardier C_2H_6, the diffusivity in the mixture is slightly

higher than the corresponding unary diffusivity values. For both penetrants, the deviations are higher at the lower temperature; this is to be expected because of the larger compositions of penetrants within the membrane. The lack of perfect match between the data on M-S diffusivities backed out from unary and mixture permeation experiments indicates that the assumption of negligible 1-2 friction, implicit in the use of equations (124), does not hold.

For a quantitative analysis of the Ribeiro experiments, we need to include the 1-2 friction contributions and use equations (122) and (123). Good match between the experimental data of Ribeiro et al.[46] with obtained with the choice $\frac{Đ_{2m}^{V}}{Đ_{21}^{V}} = 4$, at either temperature; see comparisons in Figure 51. The *x*-axis represents the partial fugacity of the permeants in the bulk gas phase in the upstream compartment. Five different mixture compositions are considered. We note that the permeability of C_2H_6 is strongly influenced (increased) by increasing proportion of CO_2 in the bulk gas phase mixture in the upstream compartment. On the other hand, the permeability of CO_2 is influenced to a much reduced extent by the feed mixture composition. The linearized solution to the M-S equations, shown by the continuous solid lines captures, quantitatively, all the essential features of the composition dependence of the permeabilities of CO_2 and C_2H_6, for all feed mixtures.

In order to gain further insights into the influence of 1-2 friction on the component permeabilities, Figure 52 compares the model predictions with experiments for the limiting scenarios of negligible and dominant friction, along with the "fitted' value of $\frac{Đ_{2m}^{V}}{Đ_{21}^{V}} = 4$. Neglecting 1-2 friction leads to over-prediction of the CO_2 permeability, while under-predicting that of the tardier C_2H_6. In the other extreme, adoption of the dominant friction scenario has the effect of slowing-down the more mobile CO_2 while speeding-up the transport of C_2H_6. The

Maxwell-Stefan formulation serves to provide insights into how 1-2 friction affects the separation selectivity, and how improvements can be attempted by perhaps altering the degree of polymer cross-linking to adjust the 1-2 friction to the desired level.

33. Immersion precipitation process for preparation of cellulose acetate membrane

The influence of the thermodynamic correction factors is particularly strong in composition regions close to demixing regions. Diffusion close to demixing regions is of importance in membrane preparation by immersion precipitation.[47, 48] In order to illustrate this, let us consider diffusion in the ternary mixture consisting of water (non-solvent, component 1), acetone (solvent, component 2) and cellulose acetate (polymer, component m). The binodal and spinodal curves for this ternary mixture are shown in Figure 53a. The binodal and spinodal curves for this system were determined using the numerical procedures outlined in Altena and Smolders.[49] The spinodal curve defines the limit of phase stability, and along the spinodal curve, the condition $|\Gamma|$ = 0 must be satisfied, i.e. we must have $\Gamma_{11}\Gamma_{22} = \Gamma_{12}\Gamma_{21}$, the product of the off-diagonal elements is equal in magnitude to the product of the diagonal elements.[50, 51] This situation implies a significant degree of thermodynamic coupling.

Figure 53b shows calculations of the thermodynamic correction factors $-\frac{\Gamma_{12}}{\Gamma_{11}}, -\frac{\Gamma_{21}}{\Gamma_{22}}$ as a function of the volume fraction of acetone, ϕ_2, keeping the ratio $\frac{\phi_1}{\phi_3} = \frac{25}{75}$. We note the sharp increase in the value of $-\frac{\Gamma_{21}}{\Gamma_{22}}$ as the binodal curve is approached. This implies that the flux of acetone is strongly coupled with the flux of water. Strong thermodynamic coupling will induce strong diffusional coupling.

In order to demonstrate the influence of thermodynamic coupling, let us consider transient inter-diffusion between two compartments for the mixture water/acetone/CA.

The right compartment (R) contains the polymer solution with initial volume fractions $\phi_{1R} = 0.25; \phi_{2R} = 0.6; \phi_{mR} = 0.15$; the matrix of thermodynamic correction factors at this composition is $[\Gamma] = \begin{bmatrix} 0.44884 & -0.10945 \\ -0.09748 & 1.03539 \end{bmatrix}$.

The left compartment (L) is has the initial volume fractions $\phi_{1L} = 0.16609; \phi_{2L} = 0.02356; \phi_{mL} = 0.81035$, that lie on the binodal curve; the matrix of thermodynamic correction factors at this composition is $[\Gamma] = \begin{bmatrix} 0.1621 & -0.06745 \\ -0.5692 & 0.39739 \end{bmatrix}$. Note the large negative value of Γ_{21} in relation to Γ_{22}; this implies that the flux of acetone is strongly influenced by the driving force for water.

The transient equilibration process is described by the coupled two-dimensional matrix equation

$$\begin{pmatrix} \phi_1 \\ \phi_2 \end{pmatrix} = \frac{1}{2}\begin{pmatrix} \phi_{1L} + \phi_{1R} \\ \phi_{2L} + \phi_{2R} \end{pmatrix} + \frac{1}{2} erf\left[\frac{z}{\sqrt{4t}} [D]^{-1/2} \right] \begin{pmatrix} \phi_{1R} - \phi_{1L} \\ \phi_{2R} - \phi_{2L} \end{pmatrix} \tag{125}$$

The Sylvester theorem, detailed in Appendix A of Taylor and Krishna,[52] is required for explicit determination of the 2-dimensional square matrix $[Q] = erf\left[\frac{z}{\sqrt{4t}} [D]^{-1/2} \right]$. The matrix of Fick diffusivities $[D] = [\Lambda][\Gamma] = [B]^{-1}[\Gamma]$ are calculated from equation (91) at the average compositions $\frac{1}{2}\begin{pmatrix} \phi_{1L} + \phi_{1R} \\ \phi_{2L} + \phi_{2R} \end{pmatrix}$. The magnitude of 1-2 friction is assumed to bedescribed by $\frac{Đ_{2m}^V}{Đ_{21}^V} = 1$. At the average volume fractions, the values of the elements of the Fick diffusivity matrix are

$[D] = \begin{bmatrix} 1.81121 & -0.72445 \\ -1.71947 & 1.96922 \end{bmatrix} \times 10^{-10}$ m^2 s^{-1}. The large off-diagonal elements are particularly noteworthy.

For the case of two distinct eigenvalues, λ_1, and λ_2 of the 2-dimensional Fick matrix $[D]$, the Sylvester theorem yields

$$[Q] = \frac{f(\lambda_1)[[D] - \lambda_2[I]]}{(\lambda_1 - \lambda_2)} + \frac{f(\lambda_2)[[D] - \lambda_1[I]]}{(\lambda_2 - \lambda_1)} \tag{126}$$

In equation (126), $[I]$ is the identity matrix with elements δ_{ik}. The functions $f(\lambda_i)$ are calculated from

$$f(\lambda_i) = erf\left[\frac{z}{\sqrt{4t}}\lambda_i^{-1/2}\right] \tag{127}$$

The calculations of the transient equilibration trajectories can be easily implemented in MathCad 15.[35]

Figure 54a shows the transient equilibration trajectories followed in the two compartments, plotted as a function of the dimensionless distance coordinate $\frac{z}{\sqrt{4D_{ref}t}}$ with the choice of the reference diffusivity value of $D_{ref} = 1 \times 10^{-10}$ m^2 s^{-1}. The equilibration of water is seen to exhibit an undershoot (left compartment) and overshoot (right compartment). This is indicative of uphill diffusion.[14, 53]

Figure 54b shows the equilibration trajectory plotted in volume fraction space. We note that equilibration trajectory follows a strongly curvilinear path. Also significant is the incursion into the meta-stable region that lies between the binodal and spinodal curves. Curvilinear

equilibration trajectories for water/acetone/CA, and forays into metstable regions, have been reported in the immersion precipitation process for membrane preparation.[47, 48]

34. Notation

a_i	activity of species *i*, dimensionless
b_i	parameter in the pure component Langmuir adsorption isotherm, Pa^{-1}
$[B]$	M-S matrix, m^{-2} s
c_i	molar concentration of species *i*, mol m^{-3}
c_t	total molar concentration in mixture, mol m^{-3}
$Đ_i$	M-S diffusivity of component *i* for molecule-pore interactions, m^2 s^{-1}
$Đ_i(0)$	M-S diffusivity at zero-loading, m^2 s^{-1}
$Đ_{ij}^V$	modified M-S diffusivity for binary penetrant pair *i*-*j*, m^2 s^{-1}
$Đ_{im}^V$	modified M-S diffusivity for penetrant *i* in polymer m, m^2 s^{-1}
$Đ_{ij}$	M-S exchange coefficient, m^2 s^{-1}
$Đ_{12}$	M-S exchange coefficient for binary mixture, m^2 s^{-1}
E	energy parameter, J mol^{-1}
f_i	partial fugacity of species *i*, Pa
$f_{i,sat}$	saturation fugacity of species *i*, Pa
$[I]$	Identity matrix with elements δ_{ij}, dimensionless
m	refers to polymer membrane (= species *n*+1), dimensionless
M_i	molar mass of species *i*, kg mol^{-1}
$\overline{M}$	mean molar mass of mixture, kg mol^{-1}
N_i	molar flux of species *i* defined in terms of the membrane area, mol m^{-2} s^{-1}
N_i^V	volumetric flux of species *i*, m^3 m^{-2} s^{-1}
n	number of penetrants, dimensionless
p_i	partial pressure of species *i*, Pa
p_t	total system pressure, Pa

q_i molar loading of species *i*, mol kg^{-1}

$q_{i,sat}$ molar loading of species *i* at saturation, mol kg^{-1}

q_t total molar loading of mixture, mol kg^{-1}

R gas constant, 8.314 J mol^{-1} K^{-1}

T absolute temperature, K

$u_2^L = \dfrac{\phi_2^L}{\phi_1^L + \phi_2^L}$ relative volume fractions in bulk liquid mixture, dimensionless

$u_2 = \dfrac{\phi_2}{\phi_1 + \phi_2}$ relative volume fractions in polymer phase, dimensionless

u_i velocity of motion of *i*, m s^{-1}

$\overline{V_i}$ partial molar volume of species *i,* m^3 mol^{-1}

$\overline{V}$ molar volume of mixture, m^3 mol^{-1}

V_p pore volume, m^3 kg^{-1}

x_i mole fraction of species *i* in adsorbed phase, dimensionless

V_p pore volume, m^3 kg^{-1}

z distance coordinate, m

Greek letters

Γ_{ij} thermodynamic factors, dimensionless

$[\Gamma]$ matrix of thermodynamic factors, dimensionless

δ thickness of membrane, m

δ_{ij} Kronecker delta, dimensionless

ζ Bearman friction coefficient

η dimensionless distance, dimensionless

θ_i fractional occupancy of component *i*, dimensionless

θ_t fractional occupancy of adsorbed mixture, dimensionless

θ_V fractional vacancy, dimensionless

$[\Lambda]$	matrix of Maxwell-Stefan diffusivities, $m^2\ s^{-1}$
μ_i	molar chemical potential, J mol^{-1}
π_i	dimensionless partial pressures, $b_i p_i$, dimensionless
Π_i	permeability of species *i* for polymer membrane, mol m m^{-2} s^{-1} Pa^{-1}
Π_i	permeance of species *i* for zeolite membrane, mol m^{-2} s^{-1} Pa^{-1}
ρ	framework density, kg m^{-3}
ρ_i	mass density of component *i*, kg m^{-3}
ρ_{i0}	mass density of pure component *i*, kg m^{-3}
ρ_t	mass density of mixture, kg m^{-3}
ϕ_i	non-dimensional flux of component *i*, dimensionless
ϕ_t	non-dimensional mixture flux, dimensionless
χ	interaction parameter in Flory-Huggins model, dimensionless
ω_i	mass fraction of component *i*, dimensionless
ω_i^L	mass fraction of component *i* in liquid phase feed mixture, dimensionless

Subscripts

0	upstream face of membrane
1	referring to species 1
2	referring to species 2
i,j	components in mixture
η	position along membrane
δ	downstream face of membrane
i	referring to component *i*
t	referring to total mixture
s	referring to surface at position $\xi = 1$.

sat	referring to saturation conditions
V	vacancy

Vector and Matrix Notation

( )	component vector
[ ]	square matrix

35. References

(1) Baerlocher, C.; Meier, W. M.; Olson, D. H. *Atlas of Zeolite Framework Types*; 5th Edition, Elsevier: Amsterdam, 2002.

(2) Baerlocher, C.; McCusker, L. B. Database of Zeolite Structures. http://www.iza-structure.org/databases/, International Zeolite Association, 10 January 2002.

(3) Kwon, Y. H.; Kiang, C.; Benjamin, E.; Crawford, P. r.; Nair, S.; Bhave, R. Krypton-Xenon Separation Properties of SAPO-34 Zeolite Materials and Membranes. *A.I.Ch.E.J.* **2017**, *63*, 761-769.

(4) Krishna, R. Diffusion in Porous Crystalline Materials. *Chem. Soc. Rev.* **2012**, *41*, 3099-3118.

(5) Krishna, R. The Maxwell-Stefan Description of Mixture Diffusion in Nanoporous Crystalline Materials. *Microporous Mesoporous Mater.* **2014**, *185*, 30-50.

(6) Krishna, R. Describing the Diffusion of Guest Molecules inside Porous Structures. *J. Phys. Chem. C* **2009**, *113*, 19756-19781.

(7) Krishna, R.; van Baten, J. M. Investigating the Relative Influences of Molecular Dimensions and Binding Energies on Diffusivities of Guest Species Inside Nanoporous Crystalline Materials *J. Phys. Chem. C* **2012**, *116*, 23556-23568.

(8) Krishna, R.; van Baten, J. M. Investigating the Influence of Diffusional Coupling on Mixture Permeation across Porous Membranes *J. Membr. Sci.* **2013**, *430*, 113-128.

(9) Krishna, R.; van Baten, J. M. Influence of Adsorption Thermodynamics on Guest Diffusivities in Nanoporous Crystalline Materials. *Phys. Chem. Chem. Phys.* **2013**, *15*, 7994-8016.

(10) Krishna, R.; van Baten, J. M. Insights into diffusion of gases in zeolites gained from molecular dynamics simulations. *Microporous Mesoporous Mater.* **2008**, *109*, 91-108.

(11) Krishna, R.; van Baten, J. M. Diffusion of alkane mixtures in MFI zeolite. *Microporous Mesoporous Mater.* **2008**, *107*, 296-298.

(12) Krishna, R.; van Baten, J. M. Unified Maxwell-Stefan Description of Binary Mixture Diffusion in Micro- and Meso- Porous Materials. *Chem. Eng. Sci.* **2009**, *64*, 3159-3178.

(13) Krishna, R.; van Baten, J. M. Maxwell-Stefan modeling of slowing-down effects in mixed gas permeation across porous membranes. *J. Membr. Sci.* **2011**, *383*, 289-300.

(14) Krishna, R. Tracing the Origins of Transient Overshoots for Binary Mixture Diffusion in Microporous Crystalline Materials. *Phys. Chem. Chem. Phys.* **2016**, *18*, 15482-15495.

(15) Krishna, R.; Baur, R. Modelling Issues in Zeolite Based Separation Processes. *Sep. Purif. Technol.* **2003**, *33*, 213-254.

(16) Kapteijn, F.; Moulijn, J. A.; Krishna, R. The generalized Maxwell-Stefan model for diffusion in zeolites: sorbate molecules with different saturation loadings. *Chem. Eng. Sci.* **2000**, *55*, 2923-2930.

(17) Skoulidas, A. I.; Sholl, D. S.; Krishna, R. Correlation effects in diffusion of CH_4/CF_4 mixtures in MFI zeolite. A study linking MD simulations with the Maxwell-Stefan formulation. *Langmuir* **2003**, *19*, 7977-7988.

(18) Myers, A. L.; Prausnitz, J. M. Thermodynamics of Mixed Gas Adsorption. *A.I.Ch.E.J.* **1965**, *11*, 121-130.

(19) Krishna, R.; van Baten, J. M. A molecular dynamics investigation of the diffusion characteristics of cavity-type zeolites with 8-ring windows. *Microporous Mesoporous Mater.* **2011**, *137*, 83-91.

(20) Feng, X.; Zong, Z.; Elsaidi, S.; Jasinski, J. B.; Krishna, R.; Thallapally, P. K.; Carreon, M. A. Kr/Xe Separation over a Chabazite Zeolite Membrane *J. Am. Chem. Soc.* **2016**, *138*, 9791-9794.

(21) Krishna, R.; Li, S.; van Baten, J. M.; Falconer, J. L.; Noble, R. D. Investigation of slowing-down and speeding-up effects in binary mixture permeation across SAPO-34 and MFI membranes. *Sep. Purif. Technol.* **2008**, *60*, 230-236.

(22) Li, S.; Falconer, J. L.; Noble, R. D.; Krishna, R. Interpreting unary, binary and ternary mixture permeation across a SAPO-34 membrane with loading-dependent Maxwell-Stefan diffusivities. *J. Phys. Chem. C* **2007**, *111*, 5075-5082.

(23) Geus, E. R.; van Bekkum, H.; Bakker, W. J. W.; Moulijn, J. A. High-temperature Stainless Steel Supported Zeolite (MFI) Membranes: Preparation, Module Construction, and Permeation Experiments. *Microporous Mater.* **1993**, *1*, 131-147.

(24) Sandström, L.; Sjöberg, E.; Hedlund, J. Very high flux MFI membrane for CO_2 separation. *J. Membr. Sci.* **2011**, *380*, 232-240.

(25) Sjöberg, E.; Barnes, S.; Korelskiy, D.; Hedlund, J. MFI membranes for separation of carbon dioxide from synthesis gas at high pressures. *J. Membr. Sci.* **2015**, *486*, 132-137.

(26) Krishna, R.; van Baten, J. M. Investigating the potential of MgMOF-74 membranes for CO_2 capture. *J. Membr. Sci.* **2011**, *377*, 249-260.

(27) Wesselingh, J. A.; Krishna, R. *Mass transfer in multicomponent mixtures*; VSSD: Delft, 2000.

(28) Ribeiro, C. P.; Freeman, B. D. Sorption, Dilation, and Partial Molar Volumes of Carbon Dioxide and Ethane in Cross-Linked Poly(ethylene oxide). *Macromolecules* **2008**, *41*, 9458-9468.

(29) Ribeiro, C. P.; Freeman, B. D. Solubility and Partial Molar Volume of Carbon Dioxide and Ethane in Crosslinked Poly(ethylene oxide) Copolymer. *J. Polym. Sci.: Part B: Polym. Phys.* **2010**, *41*, 9458-9468.

(30) Mulder, M. H. V.; Franken, A. C. M.; Smolders, C. A. On the Mechanism of Separation of Ethanol/Water Mixtures by Pervaporation. II. Experimental Concentration Profiles *J. Membr. Sci.* **1985**, *22*, 41-58.

(31) Ribeiro, C. P.; Freeman, B. D.; Paul, D. R. Modeling of Multicomponent Mass Transfer across Polymer Films using a Thermodynamically Consistent Formulation of the Maxwell-Stefan Equations in terms of Volume Fractions. *Polymer* **2011**, *52*, 3970-3983.

(32) Mulder, M. H. V.; Franken, A. C. M.; Smolders, C. A. Preferential Sorpton versus Preferential Permeability in Pervaporation. *J. Membr. Sci.* **1985**, *22*, 155-178.

(33) Yang, T.-H.; Lue, J. Modeling Sorption Behavior for Ethanol/Water Mixtures in a Cross-linked Polydimethylsiloxane Membrane Using the Flory-Huggins Equation. *J. Macromol. Sci., Part B: Phys* **2013**, *52*, 1009-1029.

(34) Varady, M. J.; Pearl, T. P.; Stevenson, S. M.; Mantooth, B. A. Decontamination of VX from Silicone: Characterization of Multicomponent Diffusion Effects. *Ind. Eng. Chem. Res.* **2016**, *55*, 3139-3149.

(35) PTC MathCad 15.0. http://www.ptc.com/, PTC Corporate Headquarters, Needham, 3 November 2015.

(36) Ribeiro, C. P.; Freeman, B. D. Carbon Dioxide/ethane Mixed-gas Sorption and Dilation in a Cross-linked Poly(ethylene oxide) Copolymer. *Polymer* **2010**, *51*, 1156-1158.

(37) Ni, X.; Sun, X.; Ceng, D. Coupled Diffusion of Water and Ethanol in a Polyimide Membrane. *Polymer Eng. Sci.* **2001**, *41*, 1440-1447.

(38) Heintz, A.; Stephan, W. A generalized solution-diffusion model of the pervaporation process through composite membranes Part I. Prediction of mixture solubilities in the dense active layer using the UNIQUAC model. *J. Membr. Sci.* **1994**, *89*, 143-151.

(39) Vrentas, J. S.; Duda, J. L. Molecular diffusion in polymer solutions. *A.I.Ch.E.J.* **1979**, *25*, 1-24.

(40) Price, P. E.; Romdhane, I. H. Multicomponent Diffusion Theory and Its Applications to Polymer-Solvent Systems. *A.I.Ch.E.J.* **2003**, *49*, 309-322.

(41) Bearman, R. J. On the Molecular Basis of some Current Theories of Diffusion. *J. Phys. Chem.* **1961**, *65*, 1961-1968.

(42) Fornasiero, F.; Prausnitz, J. M.; Radke, C. J. Multicomponent Diffusion in Highly Asymmetric Systems. An Extended Maxwell-Stefan Model for Starkly Different-Sized, Segment-Accessible Chain Molecules. *Macromolecules* **2005**, *38*, 1364-1370.

(43) Fornasiero, F.; Krull, F.; Prausnitz, J. M.; Radke, C. J. Steady-state Diffusion of Water through Soft-contact-lens Materials. *Biomaterials* **2005**, *26*, 5704-5716.

(44) Mulder, M. H. V.; Smolders, C. A. On the Mechanism of Separation of Ethanol/Water Mixtures by Pervaporation. I. Calculation of Concentration Profiles *J. Membr. Sci.* **1984**, *17*, 289-307.

(45) Heintz, A.; Stephan, W. A generalized solution-diffusion model of the pervaporation process through composite membranes Part II. Concentration polarization, coupled diffusion and the influence of the porous support layer. *J. Membr. Sci.* **1994**, *89*, 153-169.

(46) Ribeiro, C. P.; Freeman, B. D.; Paul, D. R. Pure- and Mixed-Gas Carbon Dioxide/Ethane Permeability and Diffusivity in a Cross-linked Poly(ethylene oxide) Copolymer. *J. Membr. Sci.* **2011**, *377*, 110-123.

(47) van den Berg, G. B.; Smolders, C. A. Diffusional phenomena in membrane separation processes. *J. Membr. Sci.* **1992**, *73*, 103-118.

(48) Reuvers, A. J.; Smolders, C. A. Formation of membranes by means of immersion precipitation Part II. The mechanism of formation of membranes prepared from the system cellulose acetate - acetone - water. *J. Membr. Sci.* **1987**, *34*, 67-86.

(49) Altena, F. W.; Smolders, C. A. Calculation of Liquid-Liquid Phase Separation in a Ternary System of a Polymer in a Mixture of a Solvent and a Nonsolvent. *Macromolecules* **1982**, *15*, 1491-1497.

(50) Krishna, R. Serpentine Diffusion Trajectories and the Ouzo Effect in Partially Miscible Ternary Liquid Mixtures. *Phys. Chem. Chem. Phys.* **2015**, *17*, 27428-27436.

(51) Krishna, R. Highlighting Diffusional Coupling Effects in Ternary Liquid Extraction and Comparisons with Distillation. *Ind. Eng. Chem. Res.* **2016**, *55*, 1053-1063.

(52) Taylor, R.; Krishna, R. *Multicomponent mass transfer*; John Wiley: New York, 1993.

(53) Krishna, R. Uphill Diffusion in Multicomponent Mixtures. *Chem. Soc. Rev.* **2015**, *44*, 2812-2836.

(54) Golden, T. C.; Sircar, S. Gas Adsorption on Silicalite. *J. Colloid Interface Sci.* **1994**, *162*, 182-188.

(55) Krishna, R. Describing Mixture Permeation across Polymeric Membranes by a Combination of Maxwell-Stefan and Flory-Huggins Models. *Polymer* **2016**, *103*, 124-131.

(56) Altinkaya, S. A.; Ozbas, B. Modeling of Asymmetric Membrane Formation by Dry-casting Method. *J. Membr. Sci.* **2004**, *230*, 71-89.

Table 1. *T*-dependent Langmuir parameters for Kr and Xe in SAPO-34. The fit parameters were determined from the unary isotherm data of Feng et al.[20] measured at temperatures of 278 K and 298 K.

	q_{sat} mol kg^{-1}	b_0 Pa^{-1}	E kJ mol^{-1}
Kr	2.5	5.75×10^{-10}	20.7
Xe	2.5	1.32×10^{-9}	23.6

Table 2. *T*-dependent Langmuir parameters for Kr and Xe in SAPO-34. The fit parameters were determined from the unary isotherm data of Kwon et al.[3] measured at temperatures of 308 K, 323 K and 343 K.

	q_{sat} mol kg^{-1}	b_0 Pa^{-1}	E kJ mol^{-1}
Kr	3.1	3.13×10^{-9}	16.3
Xe	3.1	5.52×10^{-9}	19

Table 3. Arrhenius temperature dependence of the M-S diffusivities for Kr and Xe in SAPO-34. The fit parameters were determined the backed-out data for unary and binary permeances as shown in Figure 31.

$$Đ_i = Đ_{i,0} \exp\left(\frac{-E}{RT}\right)$$

	$Đ_{i,0}$ m^2 s-1	E kJ mol^{-1}
Kr	2.12×10^{-10}	11.14
Xe	4.1×10^{-11}	17.88

Table 4. Langmuir parameter fits for CO_2 and H_2 in MFI (silicalite-1) zeolite. The CO_2 isotherm fits are based on CBMC simulation data at three different temperatures, 200 K, 253 K, and 300 K. The H_2 fits are based on CBMC simulation data at 300 K, combined with experimental data of Golden and Sircar [54] at 305.15 K, and 353.25 K. The *T*-dependent isotherm fits from the sets of data were interpolated, or extrapolated, to 273 K and 296 K. The single-site Langmuir parameters at these two temperatures are provided below.

T = 273 K:

$q = \frac{q_{sat} bp}{1 + bp}$	q_{sat} mol kg^{-1}	b Pa^{-1}
CO_2	3.7	1.447×10^{-5}
H_2	3.7	7.70×10^{-8}

T = 296 K:

$q = \frac{q_{sat} bp}{1 + bp}$	q_{sat} mol kg^{-1}	b Pa^{-1}
CO_2	3.7	5.94×10^{-6}
H_2	3.7	5.50×10^{-8}

Table 5. Flory-Huggins parameters for permeation of penetrants CO_2 (1) and C_2H_6 (2) across a cross-linked polyethylene oxide (XLPEO) membrane (indicated by subscript m) at $T = 263.15$ K. The input parameters are based on calculations using the information presented in Appendix A of Ribeiro et al.[31] In the Supplementary material of the paper by Krishna,[55] detailed comparison of experimental phase equilibrium data with predictions of the F-H equations are provided.

$$f_{1,sat} = 21\times10^5 \text{ Pa}; \quad f_{2,sat} = 14.5\times10^5 \text{ Pa}$$

$$\chi_{12} = -28.2 - \frac{44.3}{\ln(\phi_1)}; \quad \chi_{1m} = 1.0421 + 12.3\phi_2; \quad \chi_{2m} = 2.421 + 4.76\sqrt{\phi_1}$$

$$\overline{V_1} = 3.31\times10^{-5} \text{ m}^3 \text{ mol}^{-1}; \quad \overline{V_2} = 4.14\times10^{-5} \text{ m}^3 \text{ mol}^{-1}$$

Modified Maxwell-Stefan diffusivities for permeation of penetrants CO_2 (component 1) and C_2H_6 (Component 2) across a cross-linked polyethylene oxide (XLPEO) membrane (indicated by subscript m) at $T = 263.15$ K.

Unary fits of M-S diffusivities

$$Đ_{1m}^V = 7.8\times10^{-12}\exp(22\phi_1) \quad \text{m}^2 \text{ s}^{-1}$$
$$Đ_{2m}^V = 1.6\times10^{-12}\exp(33\phi_2) \quad \text{m}^2 \text{ s}^{-1}$$

Input data for diffusivities used in the mixture permeability calculations:

$$Đ_{1m}^V = 100\times10^{-12}\exp(8(\phi_1+\phi_2)) \quad \text{m}^2 \text{ s}^{-1}$$
$$Đ_{2m}^V = 38\times10^{-12}\exp(9(\phi_1+\phi_2)) \quad \text{m}^2 \text{ s}^{-1}$$

Three different scenarios are chosen to describe the magnitude of 1-2 friction:

$$\frac{Đ_{2m}^V}{Đ_{21}^V} = 4, \frac{Đ_{2m}^V}{Đ_{21}^V} \to 0; \quad \frac{Đ_{1m}^V}{Đ_{12}^V} \to 0; \frac{\phi_2 Đ_{1m}^V}{\phi_m Đ_{12}^V} >> 1; \quad \frac{\phi_1 Đ_{2m}^V}{\phi_m Đ_{21}^V} >> 1.$$

Table 6. Flory-Huggins parameters for permeation of penetrants CO_2 (1) and C_2H_6 (2) across a cross-linked polyethylene oxide (XLPEO) membrane (indicated by subscript m) at $T = 298.15$ K. The input parameters are based on calculations using the information presented in Appendix A of Ribeiro et al.[31] In the Supplementary material of the paper by Krishna,[55] detailed comparison of experimental phase equilibrium data with predictions of the F-H equations are provided.

$f_{1,sat} = 43\times10^5$ Pa; $f_{2,sat} = 28\times10^5$ Pa

$\chi_{12} = 1.52$; $\chi_{1m} = 0.9085$; $\chi_{2m} = 2.0804$

$\overline{V_1} = 4.174\times10^{-5}$ m^3 mol^{-1}; $\overline{V_2} = 6.04\times10^{-5}$ m^3 mol^{-1}

Modified Maxwell-Stefan diffusivities for permeation of penetrants CO_2 (component 1) and C_2H_6 (Component 2) across a cross-linked polyethylene oxide (XLPEO) membrane (indicated by subscript m) at $T = 298.15$ K.

Unary fits of M-S diffusivities

$$Đ_{1m}^V = 100\times10^{-12}\exp(8\phi_1) \quad \text{m}^2\ \text{s}^{-1}$$
$$Đ_{2m}^V = 38\times10^{-12}\exp(9\phi_2) \quad \text{m}^2\ \text{s}^{-1}$$

Input data for diffusivities used in the mixture permeability calculations:

$$Đ_{1m}^V = 100\times10^{-12}\exp(8(\phi_1+\phi_2)) \quad \text{m}^2\ \text{s}^{-1}$$
$$Đ_{2m}^V = 38\times10^{-12}\exp(9(\phi_1+\phi_2)) \quad \text{m}^2\ \text{s}^{-1}$$

Three different scenarios are chosen to describe the magnitude of 1-2 friction:

$$\frac{Đ_{2m}^V}{Đ_{21}^V} = 4\,,\ \frac{Đ_{2m}^V}{Đ_{21}^V}\to 0;\quad \frac{Đ_{1m}^V}{Đ_{12}^V}\to 0\,;\ \frac{\phi_2 Đ_{1m}^V}{\phi_m Đ_{12}^V} >> 1;\quad \frac{\phi_1 Đ_{2m}^V}{\phi_m Đ_{21}^V} >> 1\,.$$

Table 7. The Flory-Huggins parameters for penetrants water (1) and ethanol (2) in cellulose acetate (CA) membrane (indicated by subscript m) at T = 293.15 K. The data are taken from Mulder et al.:[30, 32, 44]

$$\chi_{12} = a + b(u_2) + c(u_2)^2 + d(u_2)^3 + e(u_2)^4; \quad u_2 = \frac{\phi_2}{\phi_1 + \phi_2}$$
$$a = 0.9820; b = -1.3483; c = 4.15; d = -3.3116; e = 0.8897;$$
$$\chi_{1m} = 1.4; \chi_{2m} = 1.1;$$
$$\overline{V_1} = 18 \times 10^{-6} \text{ m}^3 \text{ mol}^{-1}$$
$$\frac{\overline{V_1}}{\overline{V_2}} = 0.309; \frac{\overline{V_1}}{\overline{V_m}} = 0.002; \frac{\overline{V_2}}{\overline{V_m}} = 0.00647;$$

Modified Maxwell-Stefan diffusivities for permeation of penetrants water (component 1) and ethanol (Component 2) across a cellulose acetate (CA) membrane (indicated by subscript m) at T = 293.15 K. The data are taken from the legend to Figure 5 of Mulder and Smolders.[44]

$$Đ_{1m}^V = 8.8 \times 10^{-12} \exp(7.3\phi_1 + 7.3\phi_2) \quad \text{m}^2 \text{ s}^{-1}$$
$$Đ_{2m}^V = 6 \times 10^{-12} \exp(7.3\phi_1 + 7.3\phi_2) \quad \text{m}^2 \text{ s}^{-1}$$
$$\delta = 20 \times 10^{-6} \quad \text{m}$$

For simulations of water(1)/ethanol(2) pervaporation across CA membrane, the magnitude of 1-2 friction is chosen as $\frac{Đ_{2m}^V}{Đ_{21}^V} = 2$.

Table 8. The Flory-Huggins parameters for penetrants water (1) and ethanol (2) in Polyimide membrane (indicated by subscript m) at T = 293.15 K. The data are based on the information provided from Ni et al.[37] The χ_{12} parameters were taken to be the same as for water/ethanol/CA.

$$\chi_{12} = a + b(u_2) + c(u_2)^2 + d(u_2)^3 + e(u_2)^4; \quad u_2 = \frac{\phi_2}{\phi_1 + \phi_2}$$

$$a = 0.9820; b = -1.3483; c = 4.15; d = -3.3116; e = 0.8897;$$

$$\chi_{1m} = 1.4; \chi_{2m} = 2.2 + 0.7\left(\frac{\phi_1}{\phi_1 + \phi_2}\right);$$

$$\overline{V_1} = 18 \times 10^{-6} \text{ m}^3 \text{ mol}^{-1}$$

$$\frac{\overline{V_1}}{\overline{V_2}} = 0.309; \frac{\overline{V_1}}{\overline{V_m}} \approx 0.002; \frac{\overline{V_2}}{\overline{V_m}} = 0.00649;$$

Modified Maxwell-Stefan diffusivities for permeation of penetrants water (component 1) and ethanol (Component 2) across the polyimide membrane (indicated by subscript m) at T = 293.15 K. The data on modified M-S diffusivities are zero volume fractions are taken from Table 1 of Ni et al.[37]. $Đ_{1m}^V = 25.5 \times 10^{-13} \exp(2\phi_1 + 2\phi_2)$ m^2 s^{-1} $Đ_{2m}^V = 2.1 \times 10^{-13} \exp(2\phi_1 + 2\phi_2)$ m^2 s^{-1} . The exponential model is used to describe $\delta = 20 \times 10^{-6}$ m the variation of the modified M-S diffusivities on the volume fractions.

Three different scenarios are chosen to describe the magnitude of 1-2 friction:

$$\frac{Đ_{2m}^V}{Đ_{21}^V} = 2, \frac{Đ_{2m}^V}{Đ_{21}^V} \to 0; \quad \frac{Đ_{1m}^V}{Đ_{12}^V} \to 0; \frac{\phi_2 Đ_{1m}^V}{\phi_m Đ_{12}^V} >> 1; \quad \frac{\phi_1 Đ_{2m}^V}{\phi_m Đ_{21}^V} >> 1.$$

Table 9. Flory-Huggins parameters for permeation of penetrants water (1) and ethanol (2) across a poly (vinyl alcohol) /poly (acrylonitrile) (PVA/PAN) composite membrane (indicated by subscript m) at T = 333 K. The χ_{12} parameters were taken to be the same as for water/ethanol/CA. The values of χ_{1m}, χ_{2m} were chosen to match the experimental sorption data presented in Figure 2 of Heintz and Stephan.[38]

$$\chi_{12} = a + b(u_2) + c(u_2)^2 + d(u_2)^3 + e(u_2)^4; \quad u_2 = \frac{\phi_2}{\phi_1 + \phi_2}$$

$$a = 0.9820; b = -1.3483; c = 4.15; d = -3.3116; e = 0.8897;$$

$$\chi_{1m} = 0.65 + 0.5\left(\frac{\phi_2}{\phi_1 + \phi_2}\right); \chi_{2m} = 1.75 - 1.5\left(\frac{\phi_1}{\phi_1 + \phi_2}\right)$$

$$\overline{V_1} = 18 \times 10^{-6} \text{ m}^3 \text{ mol}^{-1}; \overline{V_2} = 58.4 \times 10^{-6} \text{ m}^3 \text{ mol}^{-1}$$

$$\frac{\overline{V_1}}{V_m} \approx 0; \frac{\overline{V_2}}{V_m} \approx 0; \rho_{1L} = 1000; \rho_{2L} = 789; \rho_m = 1200 \quad \text{kg m}^{-3}$$

Membrane thickness: $\delta = 1.3 \times 10^{-7}$ m. Modified Maxwell-Stefan diffusivities for permeation of penetrants water (1) and ethanol (2) across the PVA/PAN (indicated by subscript m) at T = 333 K. The M-S diffusivities for water and ethanol penetrants are assumed to follow an exponential dependence on the volume fractions $\begin{matrix} Đ_{1m}^V = 7 \times 10^{-14} \exp(5\phi_1 + 5\phi_2) & \text{m}^2 \text{ s}^{-1} \\ Đ_{2m}^V = 5 \times 10^{-13} \exp(5\phi_1 + 5\phi_2) & \text{m}^2 \text{ s}^{-1} \end{matrix}$.

Three different scenarios are chosen to describe the magnitude of 1-2 friction:

$$\frac{Đ_{2m}^V}{Đ_{21}^V} = 0.2, \frac{Đ_{2m}^V}{Đ_{21}^V} = 4; \frac{Đ_{2m}^V}{Đ_{21}^V} = 20.$$

Table 10. The Flory-Huggins parameters for penetrants water (anti-solvent, component 1) and acetone (solvent, Component 2) in cellulose acetate (CA) (polymer, indicated by subscript m) at T = 298.15 K. The Flory-Huggins parameters are taken from Altena and Smolders[49] and Altinkaya and Ozbas.[56]

$$\chi_{12} = a + b(u_2) + c(u_2)^2 + d(u_2)^3 + e(u_2)^4; \quad u_2 = \frac{\phi_2}{\phi_1 + \phi_2}$$

$a = 1.1; b = -0.42; c = 4.09; d = -6.7; e = 4.28;$

$\chi_{1m} = 1.4; \chi_{2m} = 0.45;$

$\overline{V_1} = 18 \times 10^{-6}$ m^3 mol^{-1}

$\overline{V_2} = 73.92 \times 10^{-6}$ m^3 mol^{-1}

$\overline{V_m} = 0.030532$ m^3 mol^{-1}

Modified Maxwell-Stefan diffusivities for permeation of penetrants water (component 1) and acetone (Component 2) are taken to be the same as for water/ethanol/CA system.[44]

$$Đ_{1m}^V = 8.8 \times 10^{-12} \exp(7.3\phi_1 + 7.3\phi_2) \quad \text{m}^2\ \text{s}^{-1}$$

$$Đ_{2m}^V = 6 \times 10^{-12} \exp(7.3\phi_1 + 7.3\phi_2) \quad \text{m}^2\ \text{s}^{-1}$$

For simulations of water(1)/acetone(2)/CA(m) diffusion in polymer solutions, the magnitude of 1-2 friction is described by $\frac{Đ_{2m}^V}{Đ_{21}^V} = 1$.

36. Captions for Figures

Figure 1. Pore landscape of all-silica BEA zeolite.

Figure 2. Structural details for BEA zeolite.

Figure 3. Pore landscape of all-silica CHA zeolite.

Figure 4. Structural details for CHA zeolite.

Figure 5. Pore landscape of all-silica DDR zeolite.

Figure 6. Structural details for DDR zeolite.

Figure 7. Pore landscape of all-silica ERI zeolite.

Figure 8. Structural details for ERI zeolite.

Figure 9. Pore landscape of all-silica FAU zeolite.

Figure 10. Structural details for FAU zeolite.

Figure 11. Pore landscape of all-silica ISV zeolite.

Figure 12. Structural details for ISV zeolite.

Figure 13. Pore landscape of all-silica LTA zeolite.

Figure 14. Structural details for LTAzeolite.

Figure 15. Pore landscape for MFI zeolite.

Figure 16. Structural details for MFI zeolite.

Figure 17. Pore landscape of IRMOF-1.

Figure 18. Structural details for IRMOF-1.

Figure 19. Pore landscape of MgMOF-74.

Figure 20. Structural details of MgMOF-74.

Figure 21. Pore landscape of ZIF-8.

Figure 22. Structural details of ZIF-8.

Figure 23. MD data[4-11] on the loading dependence of the M-S diffusivities of various guest molecules in all-silica (a) MFI, (b) FAU, and (c) LTA zeolites at 300 K. The data demonstrate "weak confinement".

Figure 24. MD data[4-11] on the loading dependence of the M-S diffusivities of various guest molecules in all-silica (a) MFI, and (b) FAU zeolites at 300 K. The data demonstrate "strong confinement".

Figure 25. MD data[4-11] on the loading dependence of the M-S diffusivities of various guest molecules in all-silica (a) LTA, and (b) CHA zeolites at 300 K. The data demonstrate an increase in the diffusivity with loading for initial increase in the loading.

Figure 26. Schematic of zeolite membrane permeation device.

Figure 27. Comparison of experimental data of Feng et al.[20] on component loadings for Kr and Xe at 278 K, and 298 K with Langmuir fits, with parameters specified in Table 1.

Figure 28. Comparison of experimental data of Kwon et al.[3] on component loadings for Kr and Xe at 308 K, 323 K and 343 K with Langmuir fits, with parameters specified in Table 2.

Figure 29. (a) Elements of the matrix of thermodynamic correction factors Γ_{ij} as a function of total pressure, $p_1 + p_2 = p_t$, calculated using the mixed-gas Langmuir model for binary

Kr(1)/Xe(2) mixture adsorption in SAPO-34 at 298 K. The ratio of partial pressures in the gas phase is 10:90. In these calculations the total gas pressure, p_t, was varied from 0 to 1 MPa. (b) Elements of the matrix of thermodynamic correction factors Γ_{ij} as function of the mole fraction of Kr(1) in the bulk gas phase for total pressure $p_1 + p_2 = p_t = 0.2$ MPa. (c) Ratios of the elements of thermodynamic correction factors, $\frac{\Gamma_{12}}{\Gamma_{11}}, \frac{\Gamma_{21}}{\Gamma_{22}}$ as function of the mole fraction of Kr(1) in the bulk gas phase for total pressure $p_1 + p_2 = p_t = 0.2$ MPa. The calculations are based on the Langmuir isotherm fit parameters specified in Table 2.

Figure 30. (a) Component permeances of Kr (1) and Xe (2) across SAPO-34 membranes of varying thicknesses, δ, as reported by Feng et al.[20] The upstream total pressure was kept constant at 140 kPa. The downstream total pressure is 2 kPa, and the total pressure drop across the membrane was 138 kPa. Two different upstream compositions of Kr/Xe were used in the experiments: 90/10, and 9/91. (b) Calculations of the Maxwell-Stefan diffusivities, $Đ_i$, using Equation (54).

Figure 31. Maxwell-Stefan diffusivities, $Đ_i$, of Kr (1) and Xe (2) across SAPO-34 tubular membrane of thickness δ = 4.9 μm thickness, backed out from data on unary and binary 10/90 Kr/Xe mixture permeances as reported by Kwon et al.[3]; the data were scanned from Figure 6 and Figure 7 of their paper. For unary permeance data, the $Đ_i$ are backed out using Equation (55). For

10/90 mixture permeance data, the $Đ_i$ are backed out using Equation (54). The straight lines are Arrhenius fits of the $Đ_i$ with parameters as specified in Table 3.

Figure 32. Comparison of transport coefficients, $\rho Đ_i/\delta$, backed out from unary permeation and binary mixtures permeation across SAPO-34 membrane; data culled from Li et al.[22] The four different mixtures considered are (a) CO_2/CH_4, (b) N_2/CH_4, (c) CH_4/H_2, and (d) CO/H_2.

Figure 33. (a) Component fluxes for steady-state permeation of 40/60 Kr (1)/Xe (2) across SAPO-34 membrane of thickness δ = 4.9 μm at T = 298 K, with varying upstream total pressures. (b) Loading profiles in the membrane for operation at upstream pressure of 5 bar. The continuous solid lines are the flux calculations using the exact analytic solution given by Equation (51). The dashed lines are the linearized model described by equation (67). The isotherm data are based on Kwon et al.[3]; see Table 2. The M-S diffusivity values are based on the Arrhenius fits of the $Đ_i$; the fit constants are provided in Table 3.

Figure 34. Transient permeation of 10/90 Kr (1)/Xe (2) across SAPO-34 membrane of thickness δ = 8.7 μm at upstream total pressure of 140 kPa, and temperature T = 298 K. The isotherm data are based on Feng et al.[20]; see Table 1. The M-S diffusivity values are $Đ_1 = 6\times10^{-11}$ m^2 s^{-1}, $Đ_2 = 4\times10^{-13}$ m^2 s^{-1}.

Figure 35. Transient permeation 10/90 Kr (1)/Xe (2) across SAPO-34 membrane of thickness δ = 4.9 μm at upstream total pressure of 400 kPa, and temperatures (a) T = 254 K, and (b) T = 298 K. The isotherm data are based on Kwon et al.[3]; see Table 2. The M-S diffusivity values are based on the Arrhenius fits of the $Đ_i$; the fit constants are provided in Table 3.

Figure 36. (a) Permeances CO_2 (1) and H_2 (2) determined for unary and binary mixture permeation across MFI membrane; data of Sandström et al.[24] (b) Comparison of experimental data on unary permeances of H_2 and CO_2 with the model predictions using equation (61), along with the values of the transport coefficients $\rho Đ_1(0)/\delta = 3.2$, and $\rho Đ_2(0)/\delta = 100$ kg m^{-2} s^{-1}. The Langmuir isotherm data fits used in the calculations are provided in Table 4.

Figure 37. (a) Snapshot showing the location of CO_2 (1) and H_2 (2) adsorbates within the intersecting channel structures of MFI. (b) MD simulation data on the unary M-S diffusivities, $Đ_1$, and $Đ_2$, of CO_2, and H_2 as a function of the component loadings. (c) MD simulation data on the M-S diffusivities, $Đ_1$, and $Đ_2$, of CO_2, and H_2 determined for equimolar binary CO_2(1)/H_2(2) mixtures a function of the total mixture loading. (d) MD simulation data for the degree of correlations, $Đ_2/Đ_{12}$, for diffusion of equimolar binary CO_2(1)/H_2(2) mixtures in MFI

zeolite at 300 K, as a function of the total mixture loading, q_t. The Langmuir isotherm data fits used in the calculations are provided in Table 4.

Figure 38. (a) Experimental data of Sandström et al.[24] on permeances of CO_2(1) and H_2(2) compared with the estimations using equations (59) and (67), along with the values of $\rho Đ_1(0)/\delta = 3.2$, and $\rho Đ_2(0)/\delta = 100$ kg m^{-2} s^{-1}. The degree of correlations is chosen to be $Đ_2/Đ_{12} = 8$. (b) Experimental data on permeances of H_2 and compared with the estimations based on varying degrees of correlations, $Đ_2/Đ_{12}$. The Langmuir isotherm data fits used in the calculations are provided in Table 4.

Figure 39. (a) Experimental data of Sjöberg et al.[25] on permeation fluxes of CO_2(1) and H_2(2) compared with the estimations using equation (67), along with the values of $\rho Đ_1(0)/\delta = 3.2$, and $\rho Đ_2(0)/\delta = 100$ kg m^{-2} s^{-1}. The degree of correlations is chosen to be $Đ_2/Đ_{12} = 8$. (b) Experimental data on permeances of H_2 and compared with the estimations based on varying degrees of correlations, $Đ_2/Đ_{12}$. The Langmuir isotherm data fits used in the calculations are provided in Table 4.

Figure 40. Schematic showing mixture permeation across polymeric membrane. Also shown is the schematic of the Flory-Huggins lattice model.

Figure 41. Calculations of the volume fractions of penetrants (a) CO_2 (1) and (b) C_2H_6 (2) in a cross-linked polyethylene oxide (XLPEO) membrane (m) at (a, b) 298.15 K, and (c, d). The upstream face of the membrane is in equilibrium with CO_2/C_2H_6 mixtures of five different compositions. The experimental data (symbols) on mixed-gas sorption are those presented in Figures 5 and 6 of Ribeiro and Freeman.[36] Note that the experimental component solubility data are converted to volume fractions of penetrants, using the molar volumes. The continuous solid lines are the the simultaneous solutions to equations (73) and (76). The input data are summarized in Table 5 and Table 6. In these calculations, the ratio $\frac{\overline{V_1}}{V_m} = 0$, i.e. the molar volume of the penetrant is negligible in comparison to the molar volume of the polymer.

Figure 42. (a) Calculations of the volume fractions of penetrants water (1), ethanol (2) in a cellulose acetate membrane (m) at 293.15 K, plotted as function of the mass fraction of water(1) in the liquid feed mixture in the upstream compartment ω_1^L. (b) Thermodynamic correction factors. (c) Ratios of the elements of thermodynamic correction factors, $-\frac{\Gamma_{12}}{\Gamma_{11}}, -\frac{\Gamma_{21}}{\Gamma_{22}}$. The upstream face of the membrane is in equilibrium with water/ethanol liquid mixture of varying mass fractions. In the calculations, χ_{1m}, χ_{2m} are composition independent, and χ_{12} follows the composition dependence described by equations (79) and (80). The Flory-Huggins parameters are specified in Table 7.

Figure 43. (a, b) Flory-Huggins calculations (continuous solid lines) of the compositions of penetrants (a) water (1), (b) ethanol (2) in polyimide membrane (m) at 293.15 K as a function of the composition of the liquid feed mixture in the upstream compartment. The experimental data (shown by the symbols) are taken from Figure 1 (for ethanol) and Figure 2 (for water) of Ni et al.[37]. The Flory-Huggins parameters are specified in Table 8.

Figure 44. Experimental data (symbols) of Heintz and Stephan[38] for binary sorption of water(1)/ethanol(2) mixtures in poly (vinyl alcohol) /poly (acrylonitrile) (PVA/PAN) composite membrane. The continuous solid lines are the F-H model calculations using the input data in Table 9.

Figure 45. Volume fractions within cellulose acetate (CA) membrane layer for a liquid phase water(1)/ethanol(2) feed mixture with volume fraction $\phi_1^L = 0.35$, or mass fraction $\omega_1^L = 0.40563$. From the F-H phase equilibrium relations, the volume fractions at the upstream face are $\phi_1 = 0.16187 \quad \phi_2 = 0.26327$. The continuous solid lines are the profiles obtained from an exact numerical solution to the set of two coupled ODEs, resulting in the flux values $N_1^V = 2.4 \times 10^{-7}$, and $N_2^V = 2.2 \times 10^{-7}$ m^3 m^{-2} s^{-1}. The dashed lines are the linear profiles resulting from the linearized model, using equations (122), that result in the permeation flux

values of $N_1^V = 2.33\times10^{-7}$, and $N_2^V = 1.98\times10^{-7}$ m^3 m^{-2} s^{-1}. The input data on F-H thermodynamics and diffusivities are provided in Table 7.

Figure 46. Volume fractions within the polyimide membrane layer for a bulk liquid phase water(1)/ethanol(2) feed mixture with volume fraction $\phi_1^L = 0.7$, or mass fraction $\omega_1^L = 0.7473$. From the F-H phase equilibrium relations, the volume fractions at the upstream face are $\phi_1 = 0.1549;\quad \phi_2 = 0.0639$. The continuous solid lines are the profiles obtained from an exact numerical solution to the set of two coupled ODEs, resulting in the flux values $N_1^V = 14.25\times10^{-9}$, and $N_2^V = 0.585\times10^{-9}$ m^3 m^{-2} s^{-1}. The dashed lines are the linear profiles resulting from the linearized model, using equations (122), that result in the permeation flux values of $N_1^V = 14.1\times10^{-9}$, and $N_2^V = 0.603\times10^{-9}$ m^3 m^{-2} s^{-1}. The Flory-Huggins parameters, and diffusivity input data are provided in Table 8.

Figure 47. (a) Thermodynamic correction factors for the ternary mixture consisting of water(1), ethanol(2) and polyimide (m), plotted as function of the mass fraction of water(1) in the liquid feedcmixture in the upstream compartment ω_1^L. (b) Ratios of the elements of thermodynamic correction factors, $-\frac{\Gamma_{12}}{\Gamma_{11}}, -\frac{\Gamma_{21}}{\Gamma_{22}}$ as function of the mass fraction of water(1) in the liquid feed mixture in the upstream compartment ω_1^L. (c, d) Volumetric fluxes of water, and ethanol across

polyimide membrane calculated using the linearized equations (122), plotted as function of the mass fraction of water(1) in the liquid mixture in the upstream compartment ω_1^L. Three different scenarios are chosen to describe the magnitude of 1-2 friction:

$$\frac{Đ_{2m}^V}{Đ_{21}^V}=2\,,\frac{Đ_{2m}^V}{Đ_{21}^V}\to 0;\quad \frac{Đ_{1m}^V}{Đ_{12}^V}\to 0\,;\frac{\phi_2 Đ_{1m}^V}{\phi_m Đ_{12}^V}>>1;\quad \frac{\phi_1 Đ_{2m}^V}{\phi_m Đ_{21}^V}>>1\,.$$

The symbols represent the experimental data as presented in Figure 3 and Figure 4 of Ni et al.[37]. The Flory-Huggins parameters, and diffusivity input data are provided in Table 8.

Figure 48. Experimental data (symbols) of Heintz and Stephan[45] for permeation of water(1)/ethanol(2) mixtures across a poly (vinyl alcohol) /poly (acrylonitrile) (PVA/PAN) composite membrane (m) at 333 K, plotted as function of the mass fraction of water(1) in the liquid feed mixture in the upstream compartment ω_1^L.

Figure 49. (a) Thermodynamic correction factors for the ternary mixture consisting of water(1), ethanol(2), and poly (vinyl alcohol) /poly (acrylonitrile) (PVA/PAN) composite membrane (m) at 333 K, plotted as function of the mass fraction of water(1) in the liquid feed mixture in the upstream compartment ω_1^L. (b) Ratios of the elements of thermodynamic correction factors, $-\frac{\Gamma_{12}}{\Gamma_{11}},-\frac{\Gamma_{21}}{\Gamma_{22}}$ as function of the mass fraction of water(1) in the liquid feed mixture in the upstream compartment ω_1^L. (c, d) Calculations of the pervaporation fluxes for permeation of

water(1)/ethanol(2) mixtures across PVA/PAN composite membrane (m) at 333 K. Three different scenarios are chosen to describe the magnitude of 1-2 friction: $\frac{Đ_{2m}^{V}}{Đ_{21}^{V}} = 0.2$, $\frac{Đ_{2m}^{V}}{Đ_{21}^{V}} = 4$; $\frac{Đ_{2m}^{V}}{Đ_{21}^{V}} = 20$. The experimental data are shown by the symbols. The input data on F-H thermodynamics and diffusivities are provided in Table 9.

Figure 50. Averaged values of the Maxwell-Stefan diffusivities $Đ_{im}^{V}$ for CO_2(1) and C_2H_6(2) in cross-linked polyethylene oxide (XLPEO) membrane at (a, c) 263.15 K, and (b, d) 298.15 K. The *x*-axis represents the average volume fraction in the membrane, calculated from $\phi_{i,av} = \frac{\left(\phi_{i0} + \phi_{i\delta}\right)}{2}$, assuming $\phi_{i\delta} \approx 0$. The diffusivities are backed out from the (a, b) unary permeabilities, and (c,d) mixture permeabilities (expressed in Barrers), as reported in Figures 2, 4, and 5 of Ribeiro et al.[46] The continuous solid lines are the exponential fits using $Đ_{im}^{V} = Đ_{im,0}^{V} \exp\left[A_i \phi_i\right]$; these are *not* the fits using the parameters provided by Ribeiro et al.[31] The input data on Flory-Huggins parameters, and molar volumes, and diffusivities used in the calculations are summarized in Tables 5, and 6. Furthermore, in these calculations, the ratio $\frac{\overline{V_1}}{V_m} = 0$, i.e. the molar volume of the penetrant is negligible in comparison to the molar volume of the polymer.

Figure 51. Membrane permeabilities, expressed in Barrers, of (a, c) $CO_2(1)$, and (b, d) $C_2H_6(2)$ for binary $CO_2(1)/C_2H_6(2)$ mixture permeation across a cross-linked polyethylene oxide (XLPEO) membrane at (a, b) 263.15 K, (c, d) 298.15 K. The *x*-axis represents the partial fugacity of (a, c) $CO_2(1)$, and (b, d) $C_2H_6(2)$ in the bulk gas phase in the upstream compartment. The experimental data (symbols) on component permeabilities are those presented in Figures 2, 4, and 5 of Ribeiro et al.[46] The continuous solid lines are the calculations using the linearized equations (122), and (123). The input data on Flory-Huggins parameters, and molar volumes, and diffusivities used in the calculations are summarized in Tables 5, and 6. Furthermore, in these calculations, the ratio $\frac{\overline{V_1}}{V_m} = 0$, i.e. the molar volume of the penetrant is negligible in comparison to the molar volume of the polymer.

Figure 52. Comparison of the experimental data on membrane permeabilities reported by Ribeiro et al.[46] of (a, c) CO_2, and (b, d) C_2H_6 for binary CO_2/C_2H_6 mixture permeation across cross-linked polyethylene oxide (XLPEO) membrane at (a, b) 263.15 K, (c, d) 298.15 K with the model predictions using the linearized equations (122). The model calculations use three different scenarios for estimation of 1-2 friction. The input data on Flory-Huggins parameters, and molar volumes, and diffusivities used in the calculations are summarized in Tables 5, and 6. Furthermore, in these calculations, the ratio $\frac{\overline{V_1}}{V_m} = 0$, i.e. the molar volume of the penetrant is negligible in comparison to the molar volume of the polymer.

Figure 53. (a) The binodal and spinodal curves, plotted in volume fraction space, for the ternary mixture consisting of water (non-solvent, component 1), acetone (solvent, component 2) and cellulose acetate (polymer, component m). (b) Calculations of the thermodynamic correction factors $-\frac{\Gamma_{12}}{\Gamma_{11}}, -\frac{\Gamma_{21}}{\Gamma_{22}}$ at compositions that lie along the dotted line indicated in the phase diagram. The Flory-Huggins parameters are provided in Table 10.

Figure 54. Diffusional equilibration trajectory in a ternary system consisting of water (non-solvent, component 1), acetone (solvent, component 2) and cellulose acetate (polymer, component m). The plotted data in ternary composition space are in terms of volume fractions. The equilibration trajectory is indicated by the blue line in ternary composition space. The inset shows the volume fraction profiles in the coagulation bath (left compartment) and in the polymer solution (right compartment) at time t = 1 s after the start. The Flory-Huggins parameters and diffusivity data are provided in Table 10.

BEA pore landscape

Fig. S1

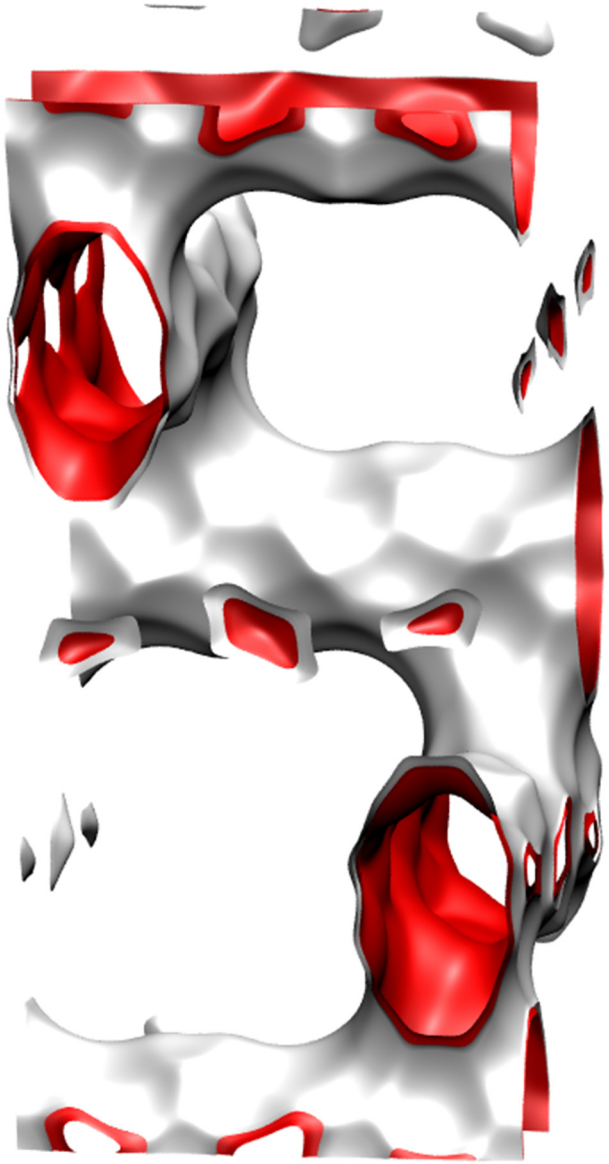

	BEA
a /Å	12.661
b /Å	12.661
c /Å	26.406
Cell volume / Å^3	4232.906
conversion factor for [molec/uc] to [mol per kg Framework]	0.2600
conversion factor for [molec/uc] to [kmol/m^3]	0.9609
ρ [kg/m3]	1508.558
MW unit cell [g/mol(framework)]	3845.427
ϕ, fractional pore volume	0.408
open space / Å^3/uc	1728.1
Pore volume / cm^3/g	0.271
Surface area /m^2/g	923.0
DeLaunay diameter /Å	5.87

BEA pore dimensions

This plot of surface area versus pore dimension is determined using a combination of the DeLaunay triangulation method for pore dimension determination, and the procedure of Düren for determination of the surface area.

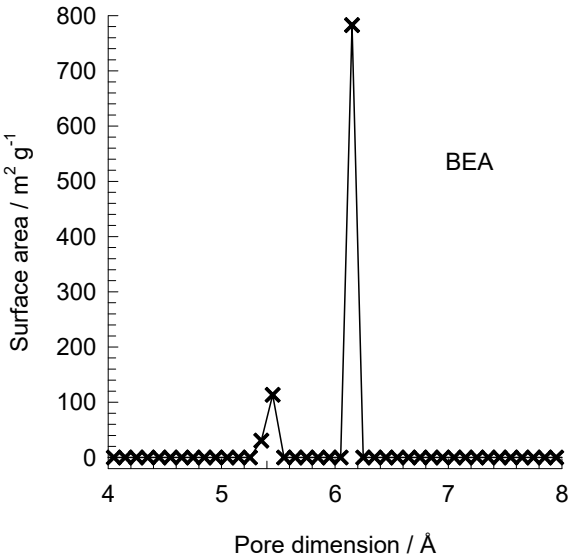

Intersecting channels of two sizes: 12-ring of 6.8 Å - 6.2 Å and 10-ring of 5.6 – 5.6 Å

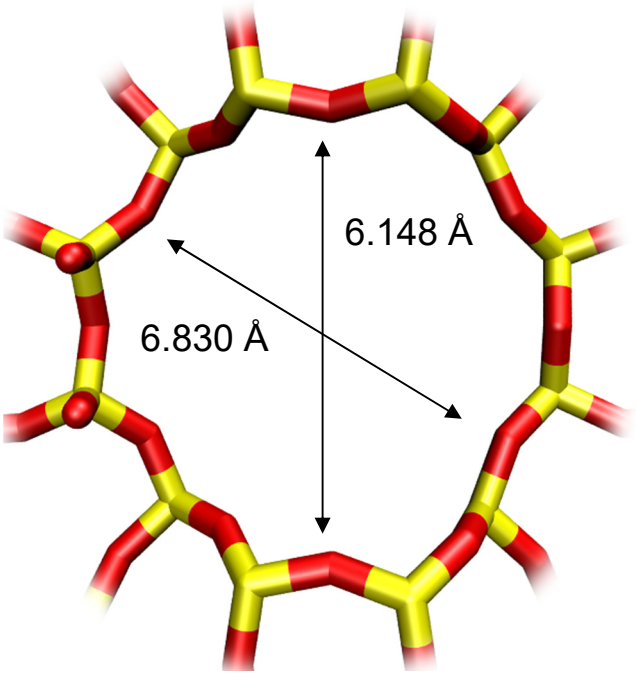

BEA [1 0 0]

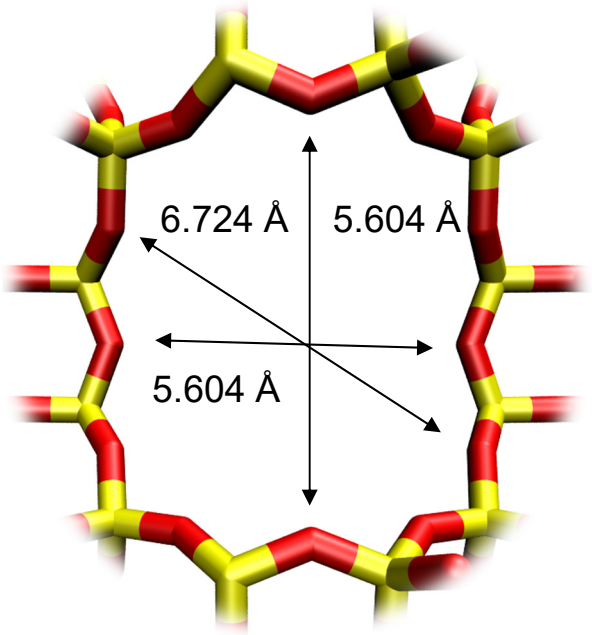

BEA [0 0 1]

Fig. S3

CHA landscape

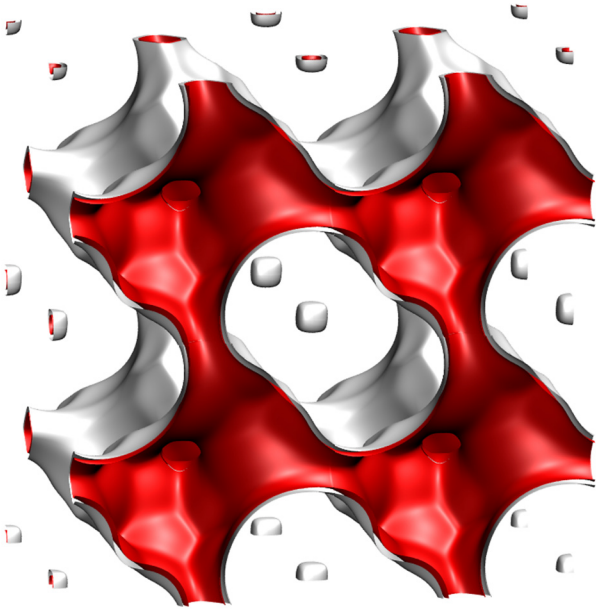

There are 6 cages per unit cell. The volume of one CHA cage is 316.4 Å^3, slightly larger than that of a single cage of DDR (278 Å^3), but significantly lower than FAU (786 Å^3).

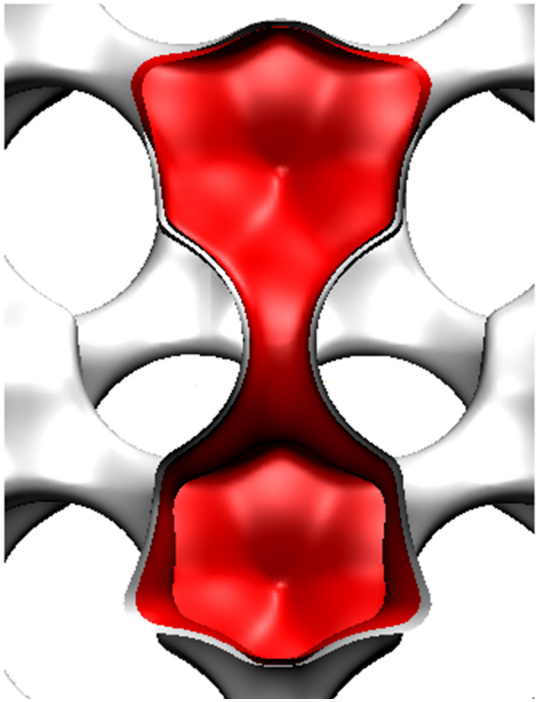

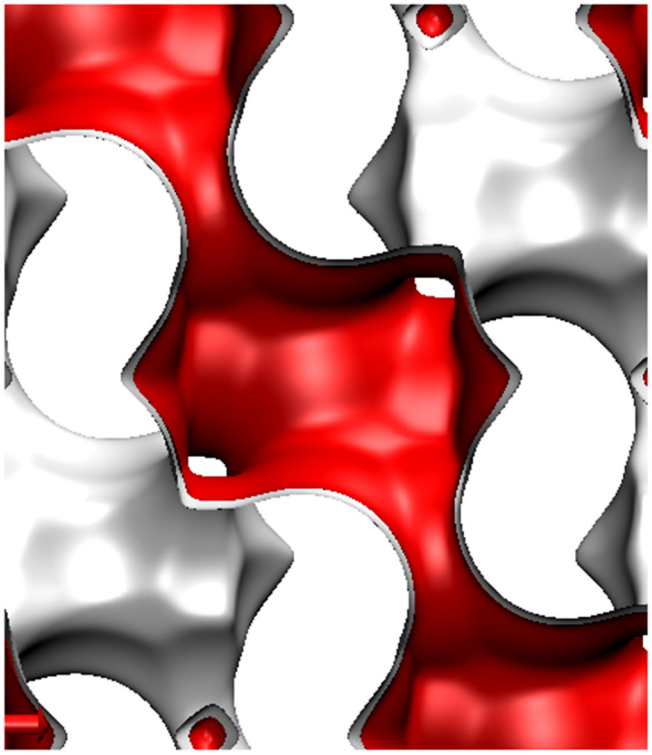

Snapshots showing location of CH_4

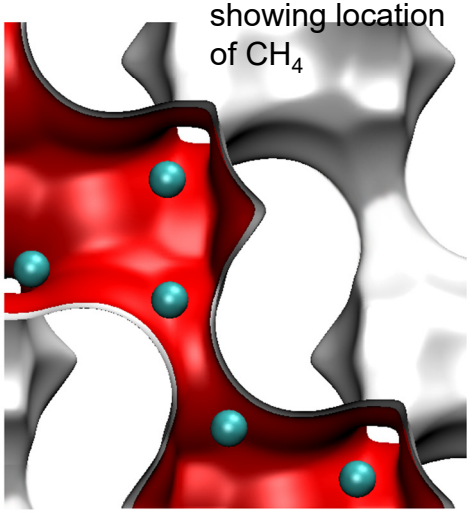

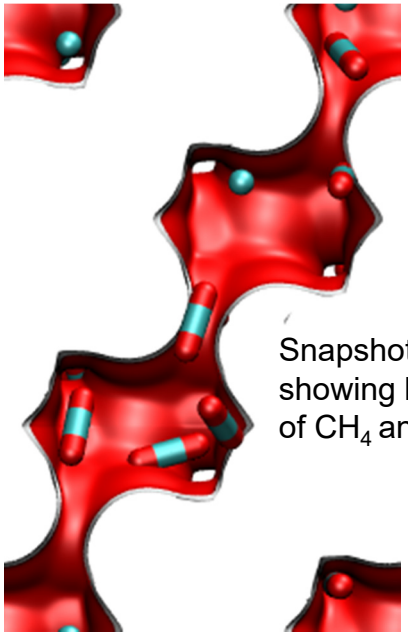

Snapshots showing location of CH_4 and CO_2

Structural information from: C. Baerlocher, L.B. McCusker, Database of Zeolite Structures, International Zeolite Association, http://www.iza-structure.org/databases/

CHA window and pore dimensions

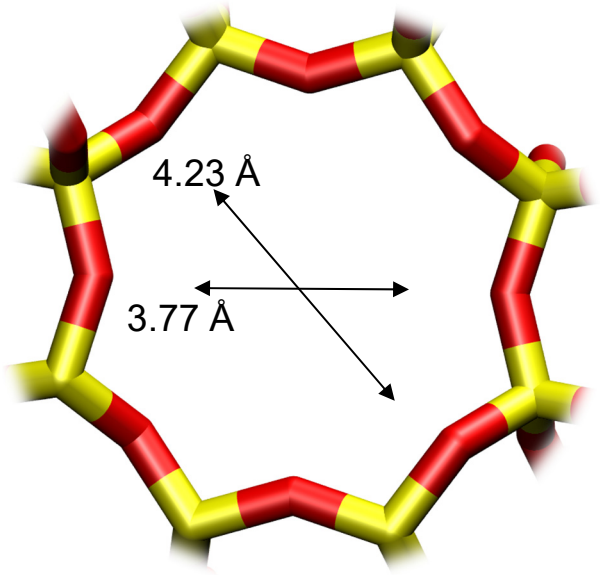

CHA

The window dimensions calculated using the van der Waals diameter of framework atoms = 2.7 Å are indicated above by the arrows.

This plot of surface area versus pore dimension is determined using a combination of the DeLaunay triangulation method for pore dimension determination, and the procedure of Düren for determination of the surface area.

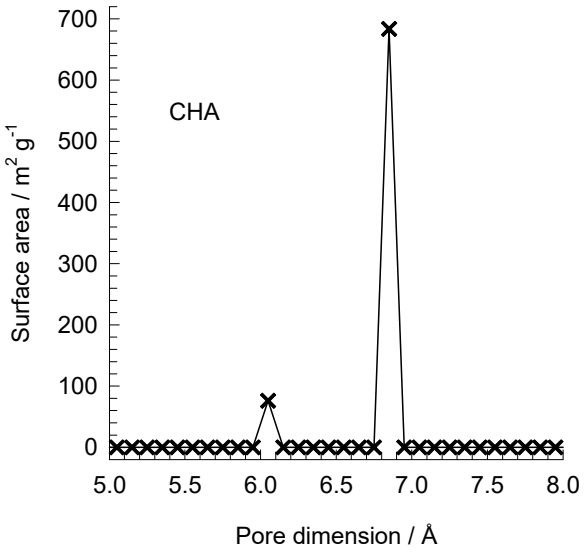

	CHA
a /Å	15.075
b /Å	23.907
c /Å	13.803
Cell volume / Å^3	4974.574
conversion factor for [molec/uc] to [mol per kg Framework]	0.2312
conversion factor for [molec/uc] to [kmol/m^3]	0.8747
ρ [kg/m3]	1444.1
MW unit cell [g/mol(framework)]	4326.106
ϕ, fractional pore volume	0.382
open space / Å^3/uc	1898.4
Pore volume / cm^3/g	0.264
Surface area /m^2/g	758.0
DeLaunay diameter /Å	3.77

Fig. S5

DDR landscape

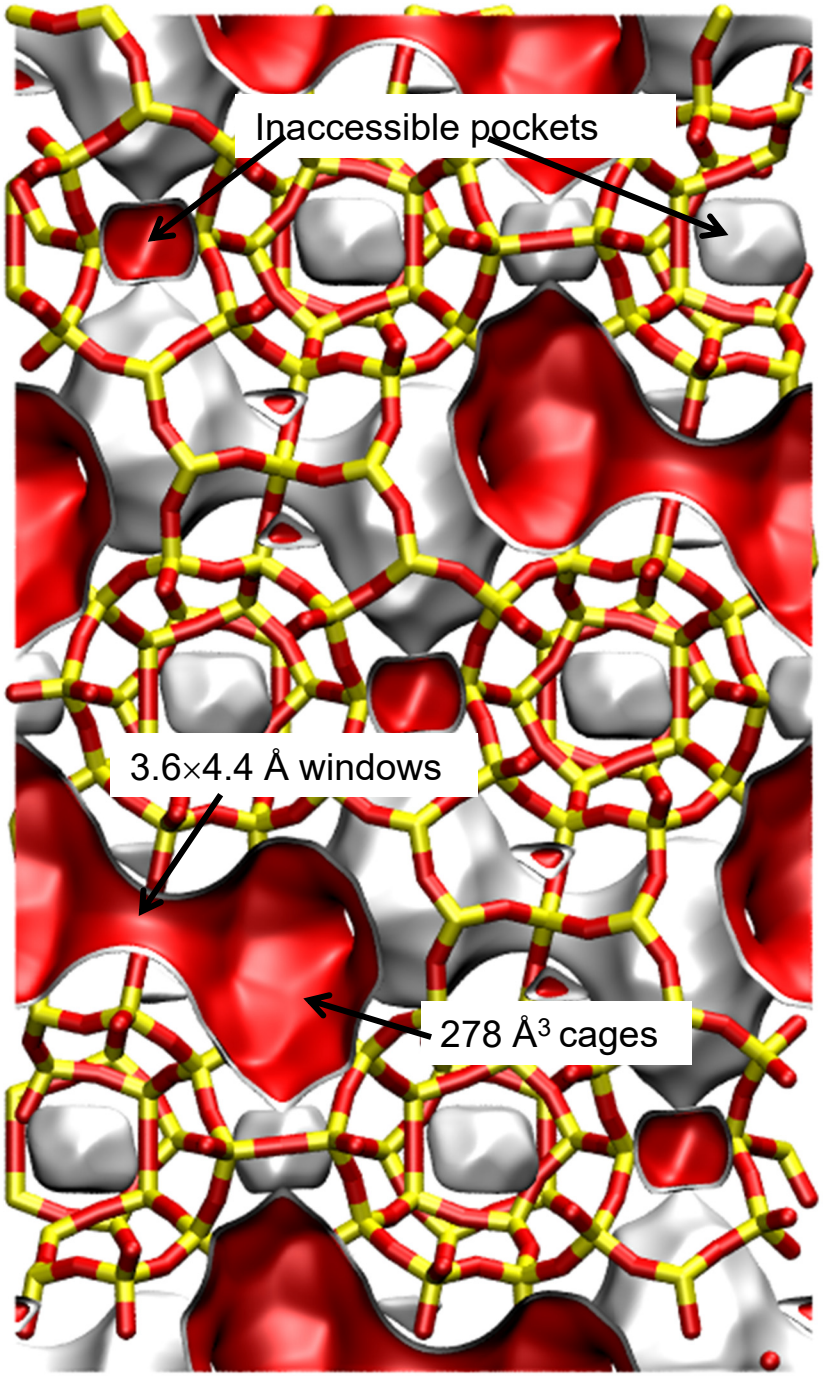

To convert from molecules per unit cell to mol kg^{-1}, multiply by 0.06936.
The pore volume is 0.182 cm^3/g.

There are 12 cages per unit cell. The volume of one DDR cage is 278 Å^3, significantly smaller than that of a single cage of FAU (786 Å^3), or ZIF-8 (1168 Å^3).

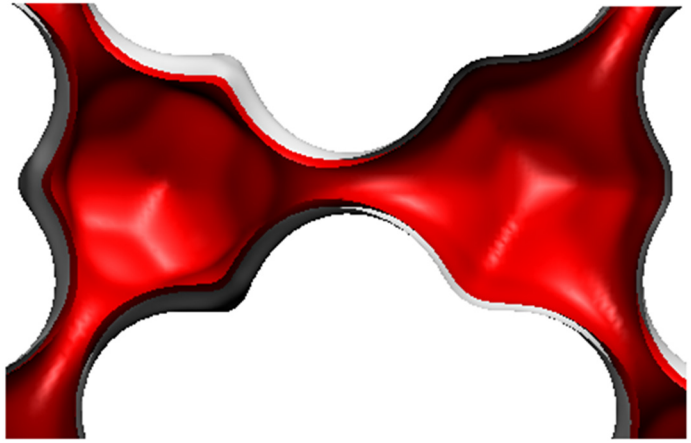

Structural information from: C. Baerlocher, L.B. McCusker, Database of Zeolite Structures, International Zeolite Association, http://www.iza-structure.org/databases/

DDR window and pore dimensions

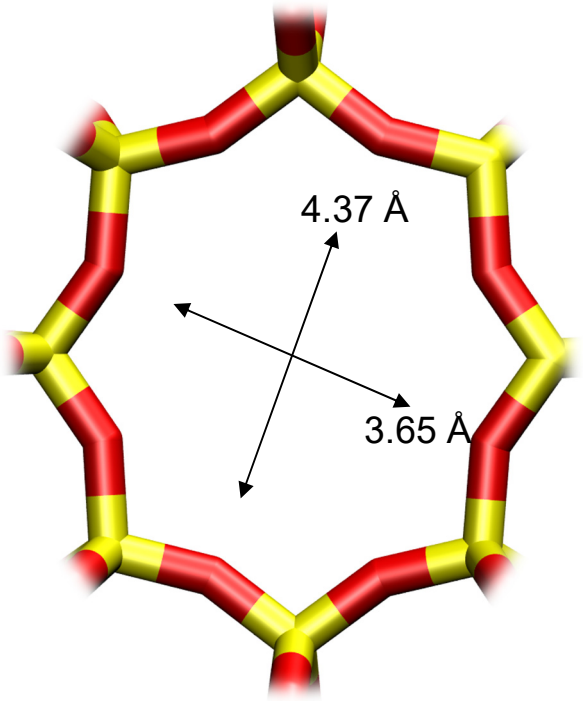

DDR

The window dimensions calculated using the van der Waals diameter of framework atoms = 2.7 Å are indicated above by the arrows.

This plot of surface area versus pore dimension is determined using a combination of the DeLaunay triangulation method for pore dimension determination, and the procedure of Düren for determination of the surface area.

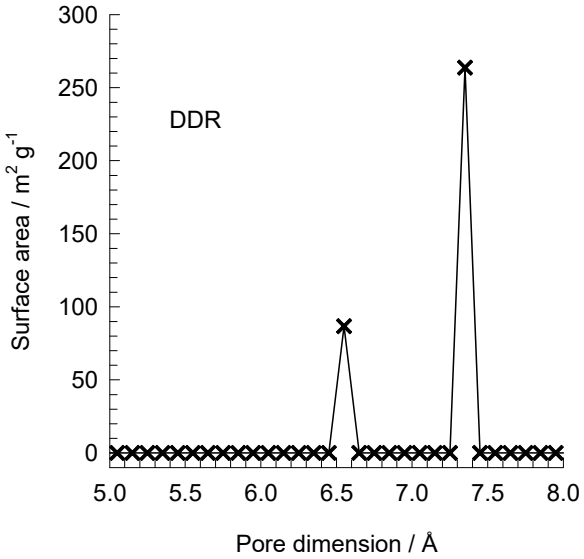

	DDR
a /Å	24.006
b /Å	13.86
c /Å	40.892
Cell volume / Å^3	13605.72
conversion factor for [molec/uc] to [mol per kg Framework]	0.0693
conversion factor for [molec/uc] to [kmol/m^3]	0.4981
ρ [kg/m3]	1759.991
MW unit cell [g/mol(framework)]	14420.35
ϕ, fractional pore volume	0.245
open space / Å^3/uc	3333.5
Pore volume / cm^3/g	0.139
Surface area /m^2/g	350.0
DeLaunay diameter /Å	3.65

Fig. S7

ERI pore landscape

There are 4 cages per unit cell.
The volume of one ERI cage is 408.7 Å^3, significantly smaller than that of a single cage of FAU-Si (786 Å^3), or ZIF-8 (1168 Å^3).

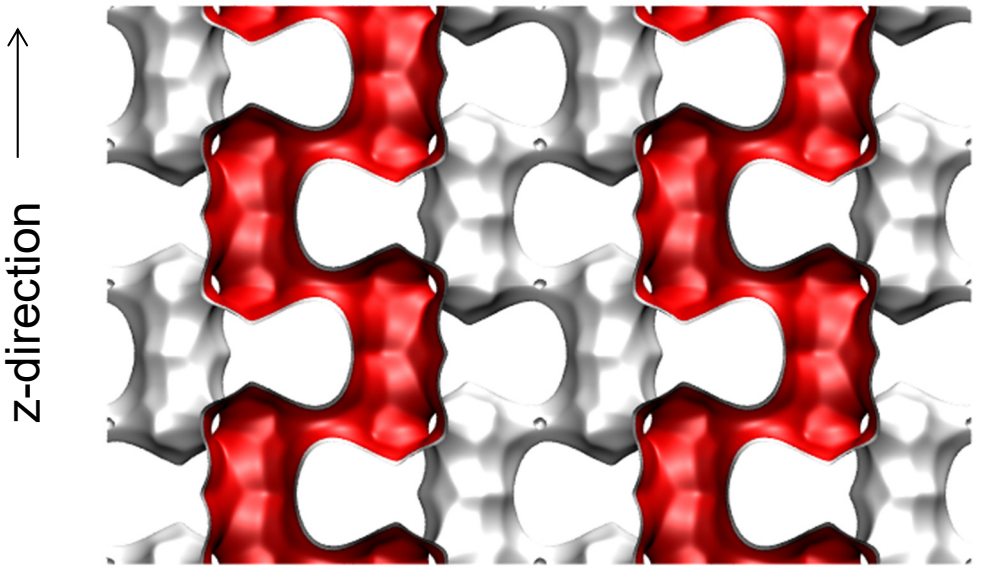

x-y projection

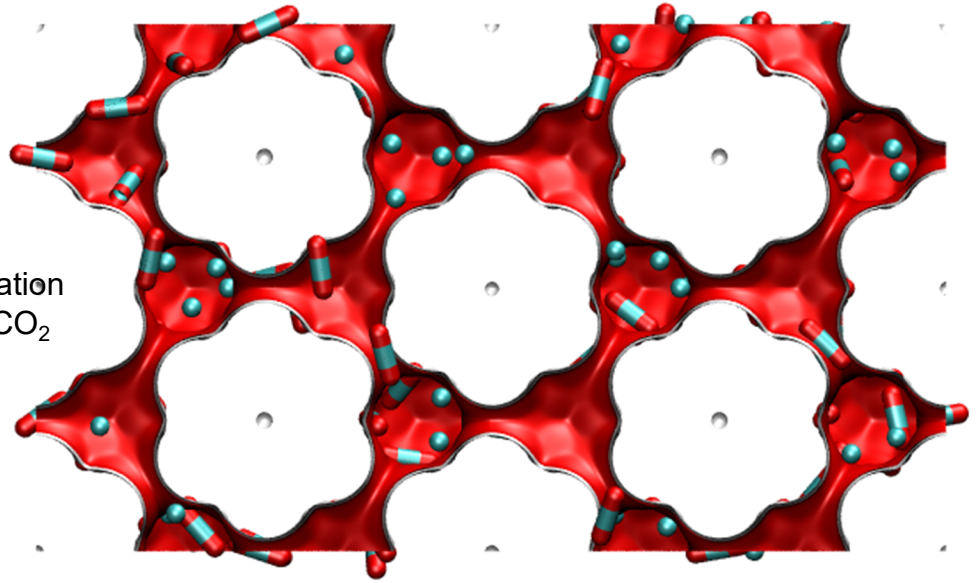

Snapshots showing location of CH_4 and CO_2

Structural information from: C. Baerlocher, L.B. McCusker, Database of Zeolite Structures, International Zeolite Association, http://www.iza-structure.org/databases/

ERI window and pore dimensions

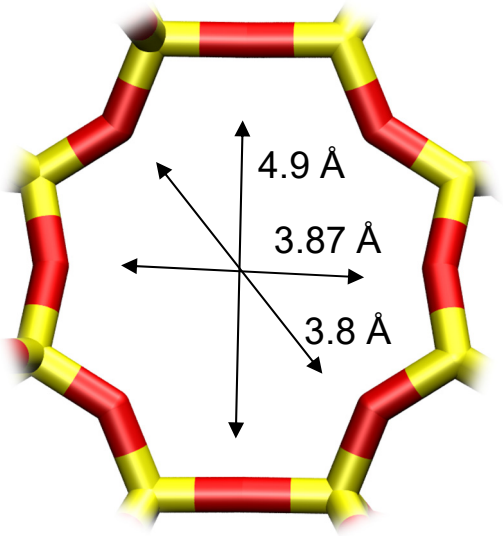

ERI

The window dimensions calculated using the van der Waals diameter of framework atoms = 2.7 Å are indicated above by the arrows.

This plot of surface area versus pore dimension is determined using a combination of the DeLaunay triangulation method for pore dimension determination, and the procedure of Düren for determination of the surface area.

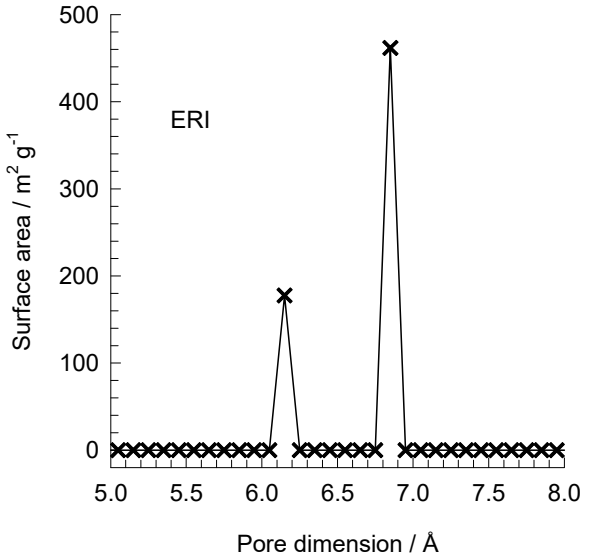

	ERI
a /Å	22.953
b /Å	13.252
c /Å	14.81
Cell volume / Å^3	4504.804
conversion factor for [molec/uc] to [mol per kg Framework]	0.2312
conversion factor for [molec/uc] to [kmol/m^3]	1.0156
ρ [kg/m3]	1594.693
MW unit cell [g/mol(framework)]	4326.106
ϕ, fractional pore volume	0.363
open space / Å^3/uc	1635.0
Pore volume / cm^3/g	0.228
Surface area /m^2/g	635.0
DeLaunay diameter /Å	3.81

FAU-Si pore landscape

Fig. S9

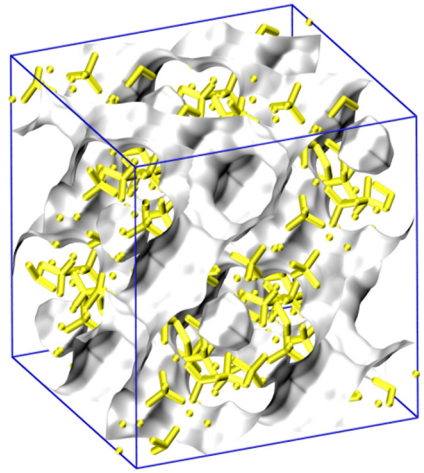

12-ring
window of FAU

There are 8 cages per unit cell. The volume of one FAU cage is 786 Å^3, larger in size than that of LTA (743 Å^3) and DDR (278 Å^3).

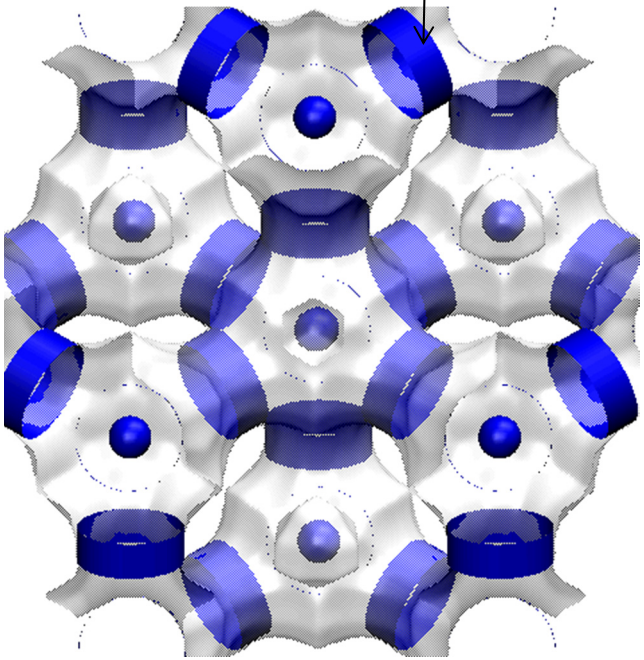

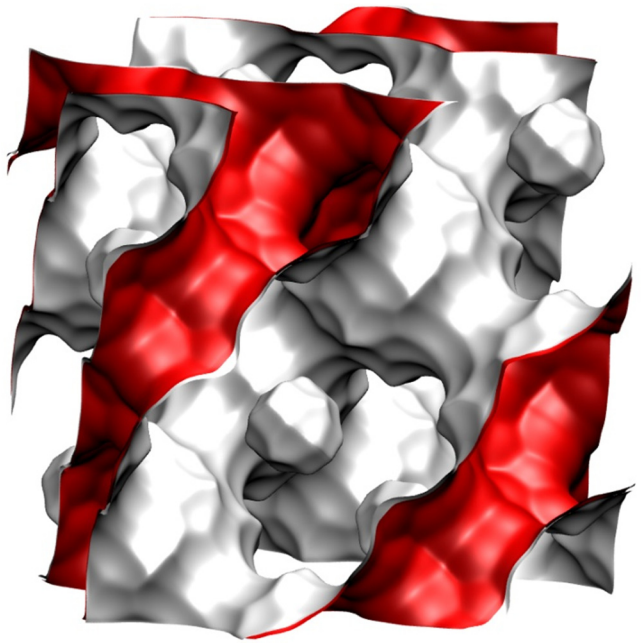

Structural information from: C. Baerlocher, L.B. McCusker, Database of Zeolite Structures, International Zeolite Association, http://www.iza-structure.org/databases/

FAU-Si window and pore dimensions

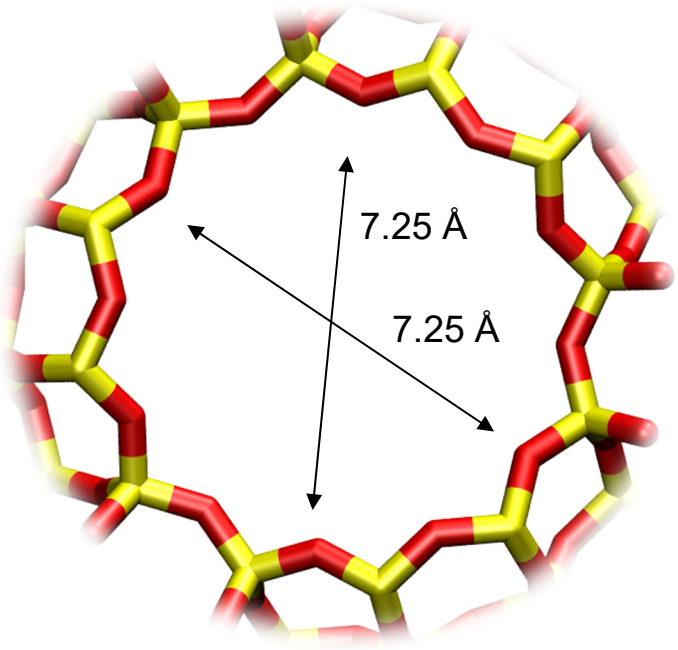

This plot of surface area versus pore dimension is determined using a combination of the DeLaunay triangulation method for pore dimension determination, and the procedure of Düren for determination of the surface area.

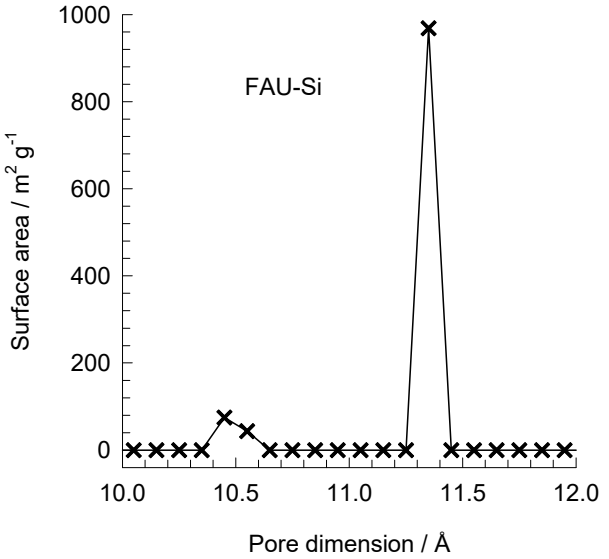

	FAU-Si
a /Å	24.28
b /Å	24.28
c /Å	24.28
Cell volume / Å^3	14313.51
conversion factor for [molec/uc] to [mol per kg Framework]	0.0867
conversion factor for [molec/uc] to [kmol/m^3]	0.2642
ρ [kg/m3]	1338.369
MW unit cell [g/mol (framework)]	11536.28
ϕ, fractional pore volume	0.439
open space / Å^3/uc	6285.6
Pore volume / cm^3/g	0.328
Surface area /m^2/g	1086.0
DeLaunay diameter /Å	7.37

ISV pore landscape

Fig. S11

Intersecting 12-ring channels structure

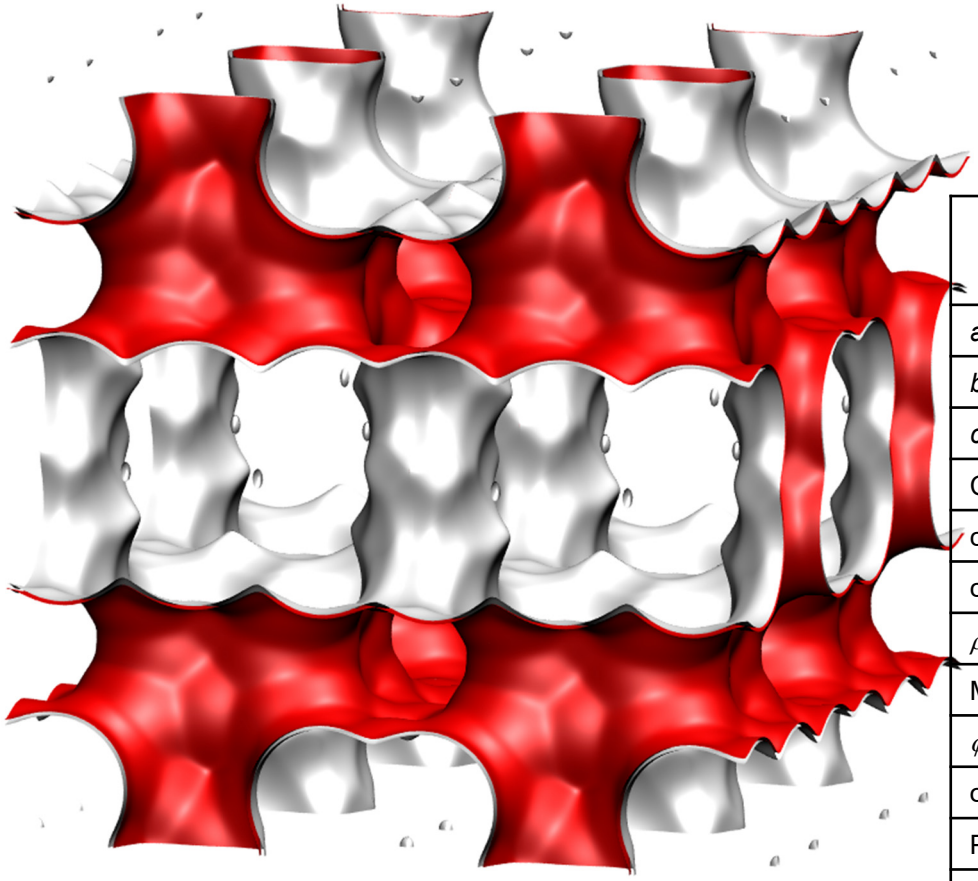

	ISV
a /Å	12.853
b /Å	12.853
c /Å	25.214
Cell volume / Å^3	4165.343
conversion factor for [molec/uc] to [mol per kg Framework]	0.2600
conversion factor for [molec/uc] to [kmol/m^3]	0.9361
ρ [kg/m3]	1533.027
MW unit cell [g/mol(framework)]	3845.427
ϕ, fractional pore volume	0.426
open space / Å^3/uc	1773.9
Pore volume / cm^3/g	0.278
Surface area /m^2/g	911.0
DeLaunay diameter /Å	5.96

Structural information from: C. Baerlocher, L.B. McCusker, Database of Zeolite Structures, International Zeolite Association, http://www.iza-structure.org/databases/

ISV pore dimensions

This plot of surface area versus pore dimension is determined using a combination of the DeLaunay triangulation method for pore dimension determination, and the procedure of Düren for determination of the surface area.

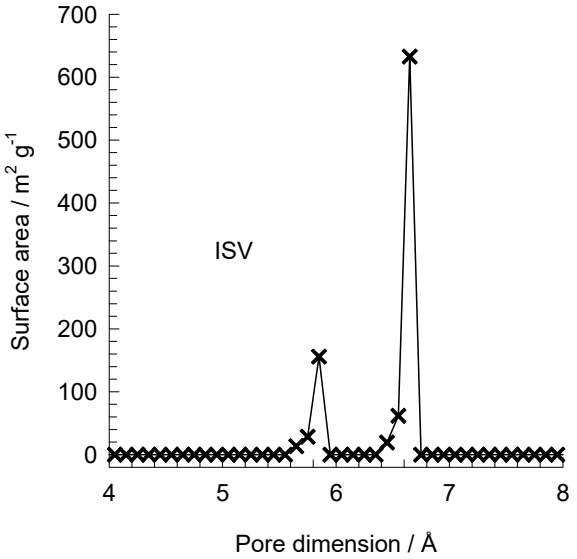

Intersecting 12-ring channels structure

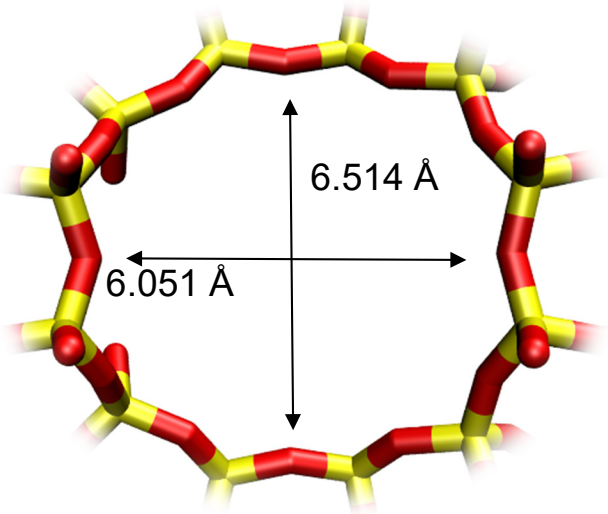

ISV [1 0 0]

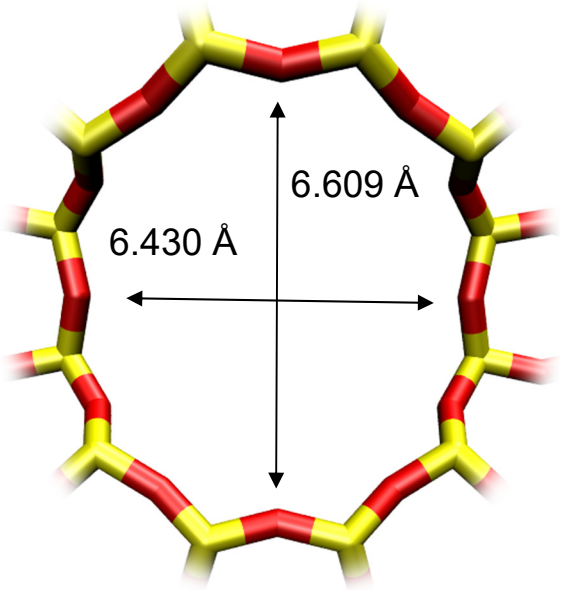

ISV [0 0 1]

Fig. S13

LTA-Si landscapes

This is a *hypothetical* structure constructed from dealuminized LTA-5A structure

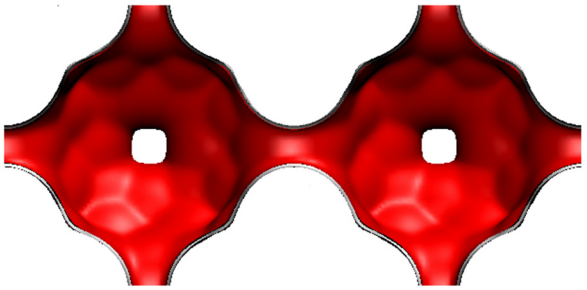

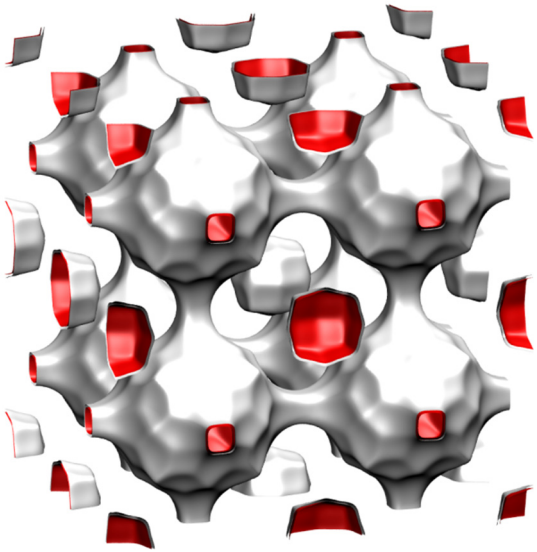

There are 8 cages per unit cell.
The volume of one LTA cage is 743 Å^3, intermediate in size between a single cage of ZIF-8 (1168 Å^3) and of DDR (278 Å^3).

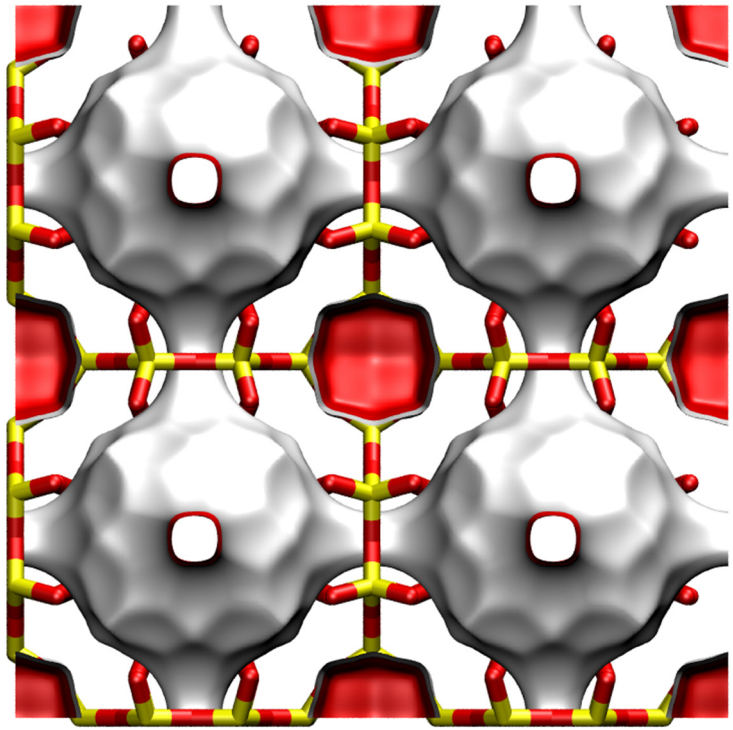

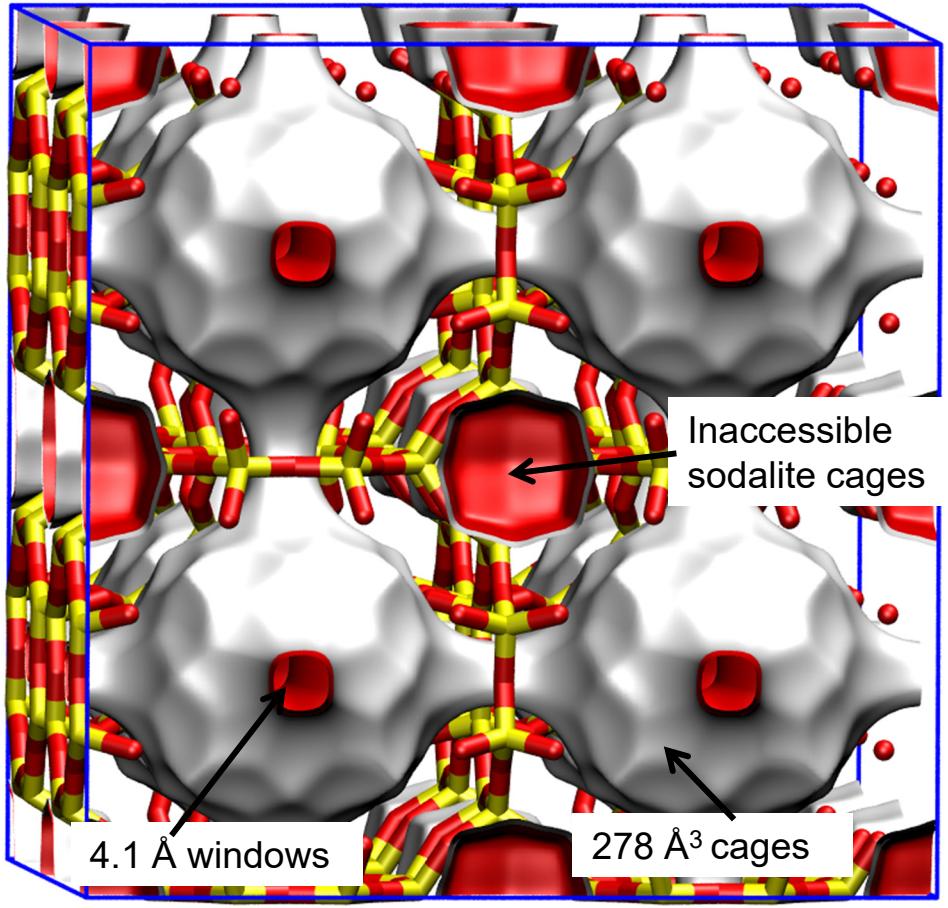

LTA-Si window and pore dimensions

8-ring window of LTA

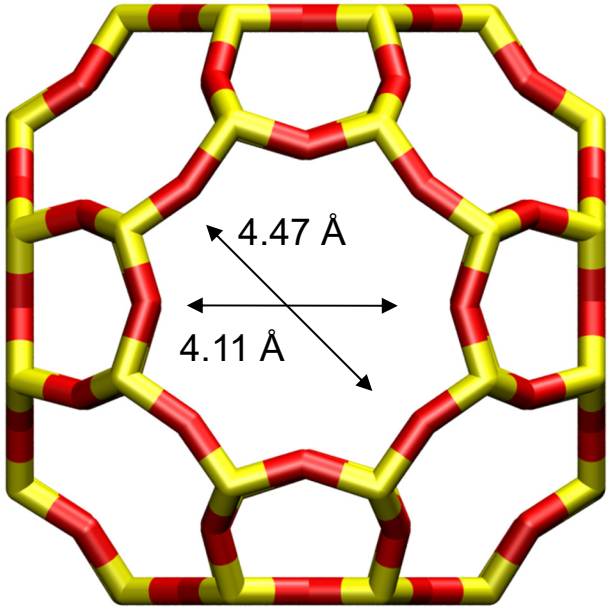

The window dimension calculated using the van der Waals diameter of framework atoms = 2.7 Å is indicated above by the arrows.

This plot of surface area versus pore dimension is determined using a combination of the DeLaunay triangulation method for pore dimension determination, and the procedure of Düren for determination of the surface area.

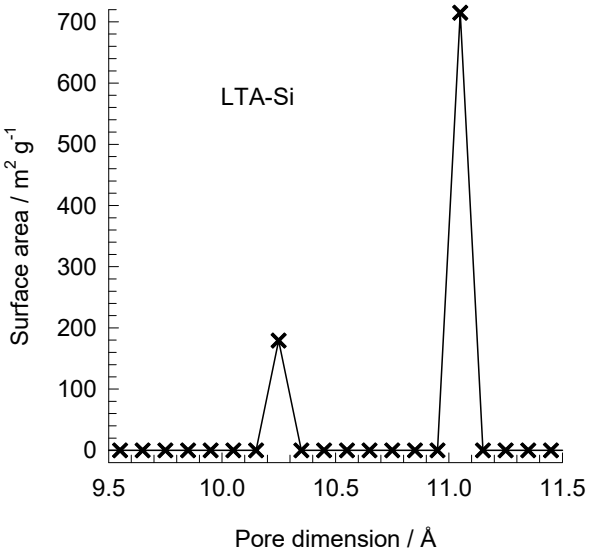

	LTA-Si
a /Å	24.61
b /Å	24.61
c /Å	24.61
Cell volume / Å^3	14905.1
conversion factor for [molec/uc] to [mol per kg Framework]	0.0867
conversion factor for [molec/uc] to [kmol/m^3]	0.2794
ρ [kg/m3]	1285.248
MW unit cell [g/mol(framework)]	11536.28
ϕ, fractional pore volume	0.399
open space / Å^3/uc	5944.4
Pore volume / cm^3/g	0.310
Surface area /m^2/g	896.0
DeLaunay diameter /Å	4.10

MFI pore landscape

Fig. S15

	MFI
a /Å	20.022
b /Å	19.899
c /Å	13.383
Cell volume / Å^3	5332.025
conversion factor for [molec/uc] to [mol per kg Framework]	0.1734
conversion factor for [molec/uc] to [kmol/m^3]	1.0477
ρ [kg/m3]	1796.386
MW unit cell [g/mol(framework)]	5768.141
ϕ, fractional pore volume	0.297
open space / Å^3/uc	1584.9
Pore volume / cm^3/g	0.165
Surface area /m^2/g	487.0
DeLaunay diameter /Å	5.16

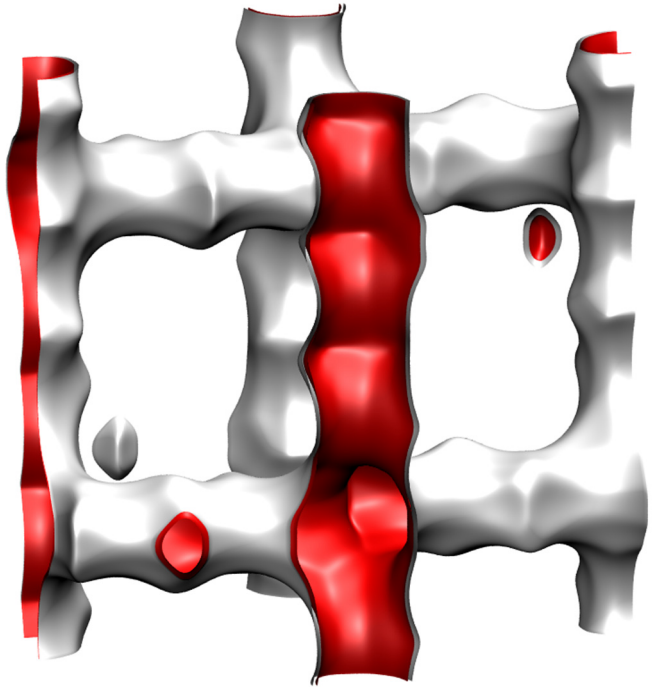

Structural information from: C. Baerlocher, L.B. McCusker, Database of Zeolite Structures, International Zeolite Association, http://www.iza-structure.org/databases/

MFI pore dimensions

10 ring channel of MFI viewed along [100]

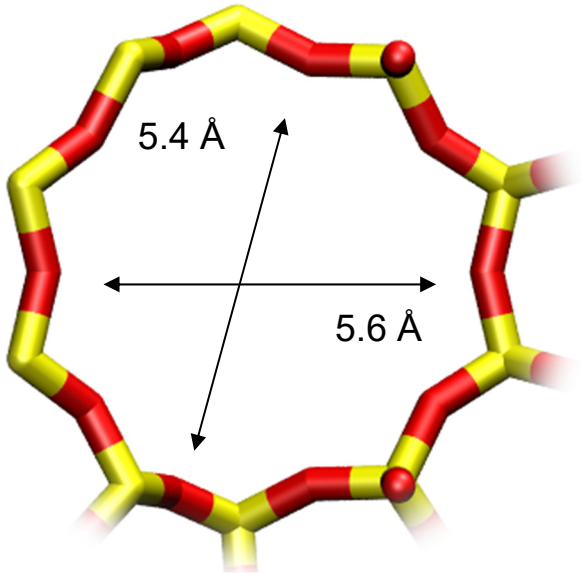

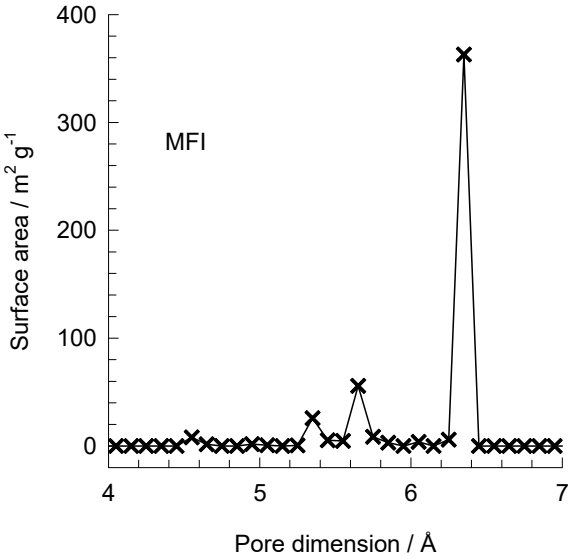

10 ring channel of MFI viewed along [010]

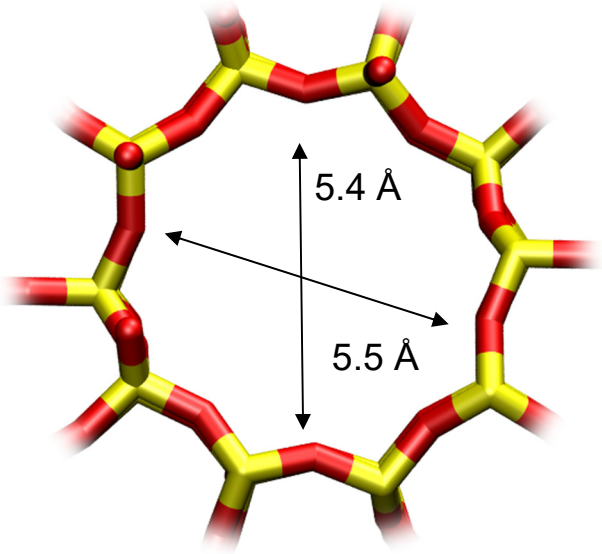

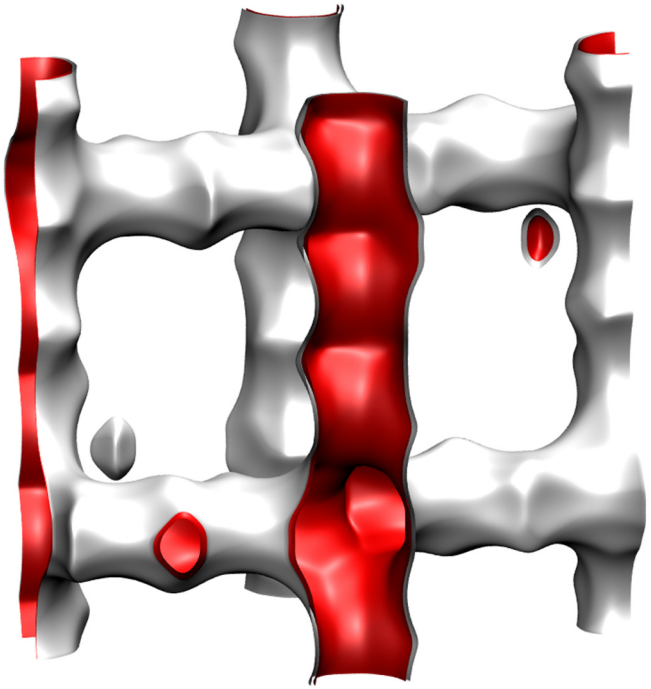

IRMOF-1 pore landscape

For IRMOF-1 (= MOF 5 = $Zn_4O(BDC)_3$ with BDC^{2-} = 1-4 benzenedicarboxylate) the structural information was obtained from

D. Dubbeldam, K.S. Walton, D.E. Ellis, R.Q. Snurr, Exceptional Negative Thermal Expansion in Isoreticular Metal–Organic Frameworks, Angew. Chem. Int. Ed. 46 (2007) 4496-4499.

D. Dubbeldam, H. Frost, K.S. Walton, R.Q. Snurr, Molecular simulation of adsorption sites of light gases in the metal-organic framework IRMOF-1, Fluid Phase Equilib. 261 (2007) 152-161.

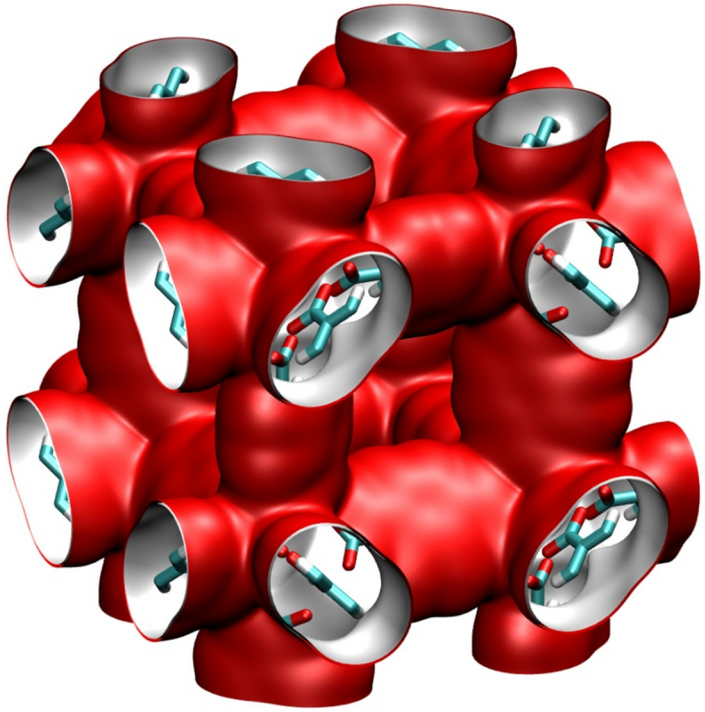

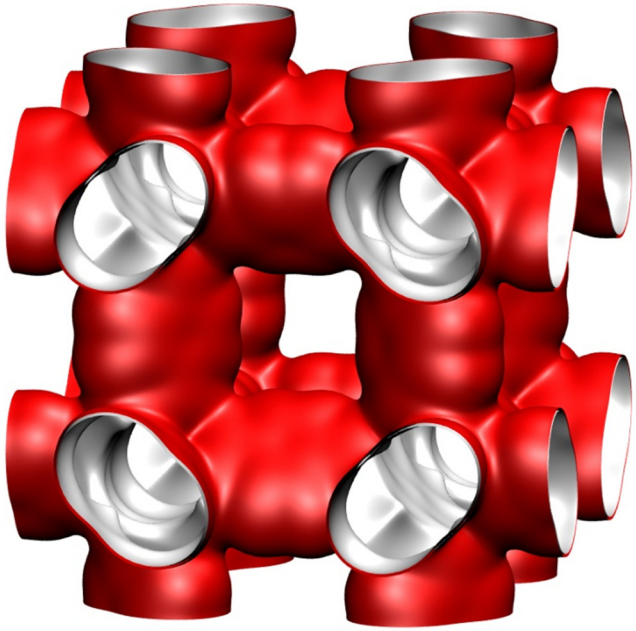

Snapshot of CO_2/CH_4 mixture

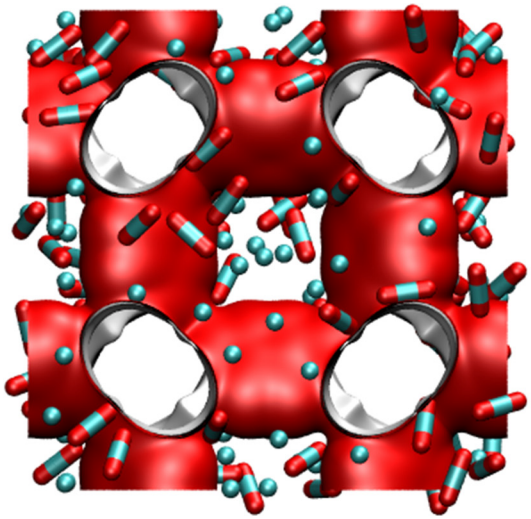

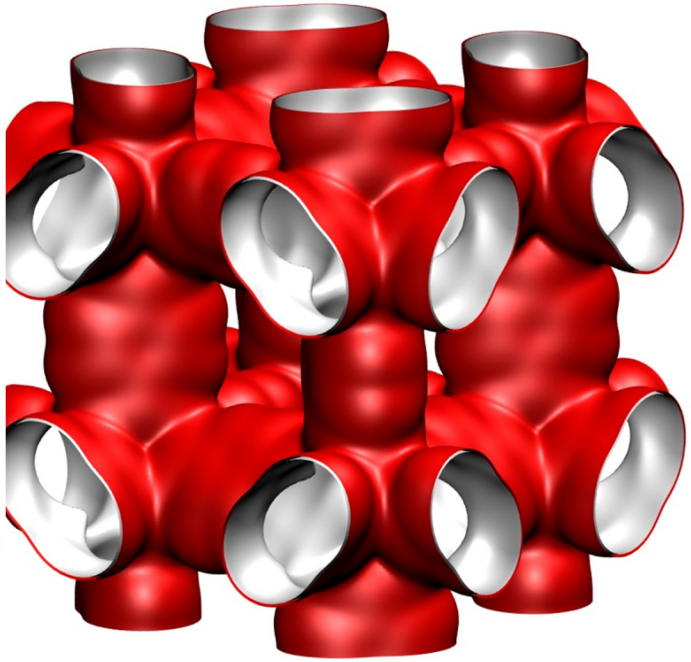

IRMOF-1 pore dimensions

Fig. S18

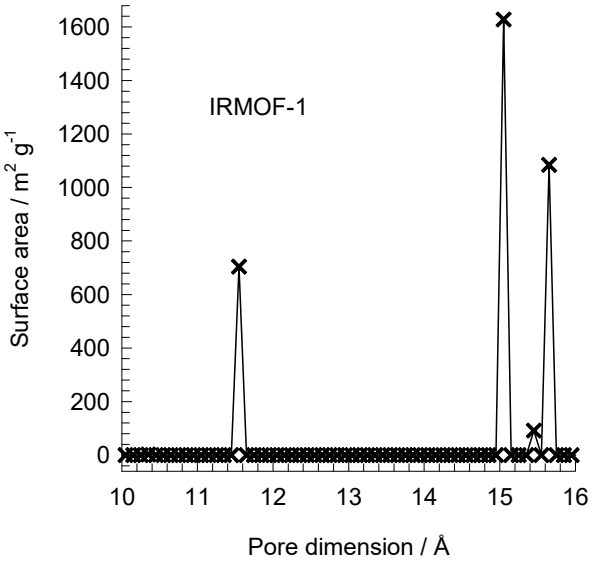

This plot of surface area versus pore dimension is determined using a combination of the DeLaunay triangulation method for pore dimension determination, and the procedure of Düren for determination of the surface area.

	IRMOF-1
a /Å	25.832
b /Å	25.832
c /Å	25.832
Cell volume / Å^3	17237.49
conversion factor for [molec/uc] to [mol per kg Framework]	0.1624
conversion factor for [molec/uc] to [kmol/m^3]	0.1186
ρ [kg/m3]	593.2075
MW unit cell [g/mol(framework)]	6157.788
ϕ, fractional pore volume	0.812
open space / Å^3/uc	13996.3
Pore volume / cm^3/g	1.369
Surface area /m^2/g	3522.2
DeLaunay diameter /Å	7.38

Two alternating, inter-connected, cavities of 11 Å and 15 Å with window size of 8 Å.

Fig. S19

MgMOF-74 pore landscapes

The structural information on MgMOF-74 (= Mg_2(dobdc) = Mg\(dobdc = CPO-27-Mg) with dobdc = ($dobdc^{4-}$ = 2,5-dioxido-1,4-benzenedicarboxylate)) were obtained from

A.Ö. Yazaydın, R.Q. Snurr, T.H. Park, K. Koh, J. Liu, M.D. LeVan, A.I. Benin, P. Jakubczak, M. Lanuza, D.B. Galloway, J.J. Low, R.R. Willis, Screening of Metal-Organic Frameworks for Carbon Dioxide Capture from Flue Gas using a Combined Experimental and Modeling Approach, J. Am. Chem. Soc. 131 (2009) 18198-18199.

D. Britt, H. Furukawa, B. Wang, T.G. Glover, O.M. Yaghi, Highly efficient separation of carbon dioxide by a metal-organic framework replete with open metal sites, Proc. Natl. Acad. Sci. U.S.A. 106 (2009) 20637-20640.

N.L. Rosi, J. Kim, M. Eddaoudi, B. Chen, M. O'Keeffe, O.M. Yaghi, Rod Packings and Metal-Organic Frameworks Constructed from Rod-Shaped Secondary Building Units, J. Am. Chem. Soc. 127 (2005) 1504-1518.

P.D.C. Dietzel, B. Panella, M. Hirscher, R. Blom, H. Fjellvåg, Hydrogen adsorption in a nickel based coordination polymer with open metal sites in the cylindrical cavities of the desolvated framework, Chem. Commun. (2006) 959-961.

P.D.C. Dietzel, V. Besikiotis, R. Blom, Application of metal–organic frameworks with coordinatively unsaturated metal sites in storage and separation of methane and carbon dioxide, J. Mater. Chem. 19 (2009) 7362-7370.

S.R. Caskey, A.G. Wong-Foy, A.J. Matzger, Dramatic Tuning of Carbon Dioxide Uptake via Metal Substitution in a Coordination Polymer with Cylindrical Pores, J. Am. Chem. Soc. 130 (2008) 10870-10871.

One-dimensional hexagonal-shaped channels with free internal diameter of ca. 11 Å

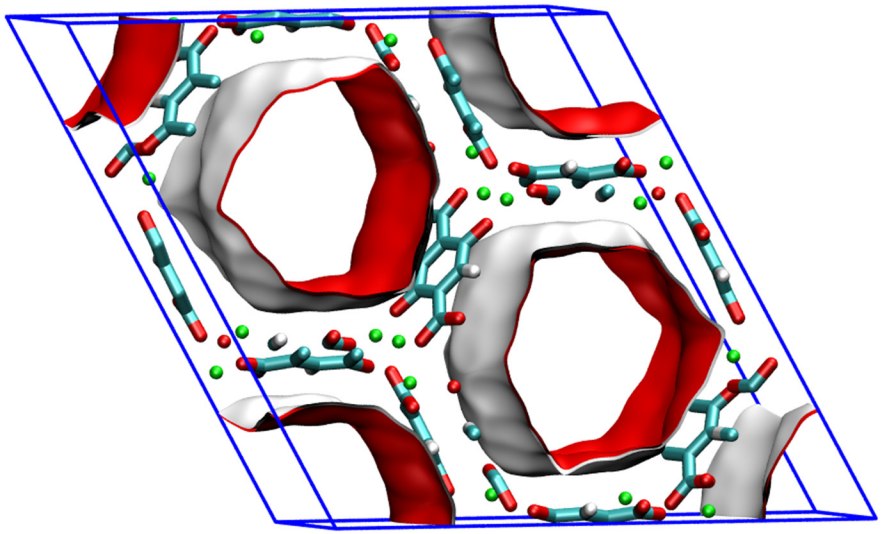

MgMOF-74 pore dimensions

Fig. S20

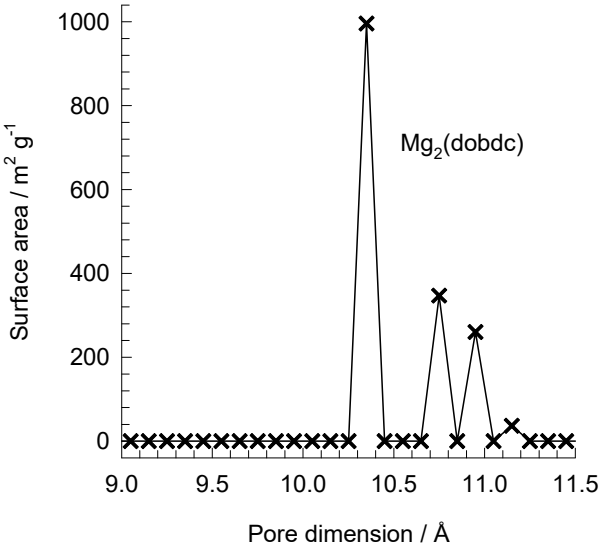

This plot of surface area versus pore dimension is determined using a combination of the DeLaunay triangulation method for pore dimension determination, and the procedure of Düren for determination of the surface area.

	MgMOF-74
a /Å	25.8621
b /Å	25.8621
c /Å	6.91427
Cell volume / Å^3	4005.019
conversion factor for [molec/uc] to [mol per kg Framework]	0.4580
conversion factor for [molec/uc] to [kmol/m^3]	0.5856
ρ [kg/m3]	905.367
MW unit cell [g/mol(framework)]	2183.601
ϕ, fractional pore volume	0.708
open space / Å^3/uc	2835.6
Pore volume / cm^3/g	0.782
Surface area /m^2/g	1640.0
DeLaunay diameter /Å	10.66

ZIF-8 pore landscapes

The ZIF-8 = Zn(methylimidazole)$_2$ structure was taken from
R. Banerjee, A. Phan, B. Wang, C. Knobler, H. Furukawa, M. O'Keeffe, O.M. Yaghi, High-Throughput Synthesis of Zeolitic Imidazolate Frameworks and Application to CO_2 Capture, Science 319 (2008) 939-943.
The original structural data (cif file) contains solvent molecules; these were removed and the solvent-free structures were simulated.

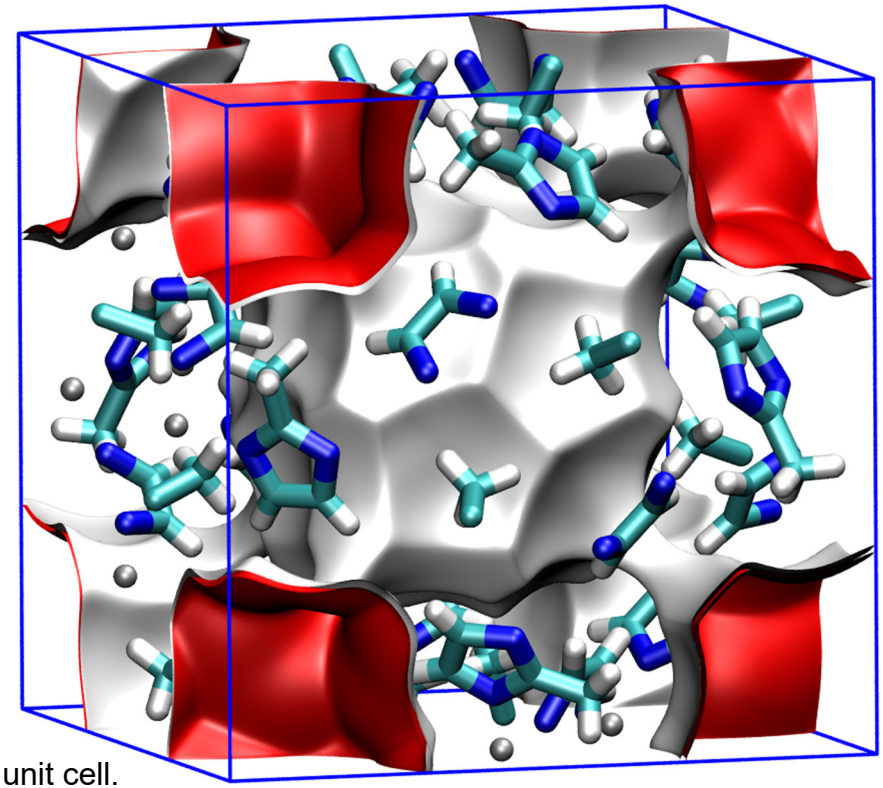

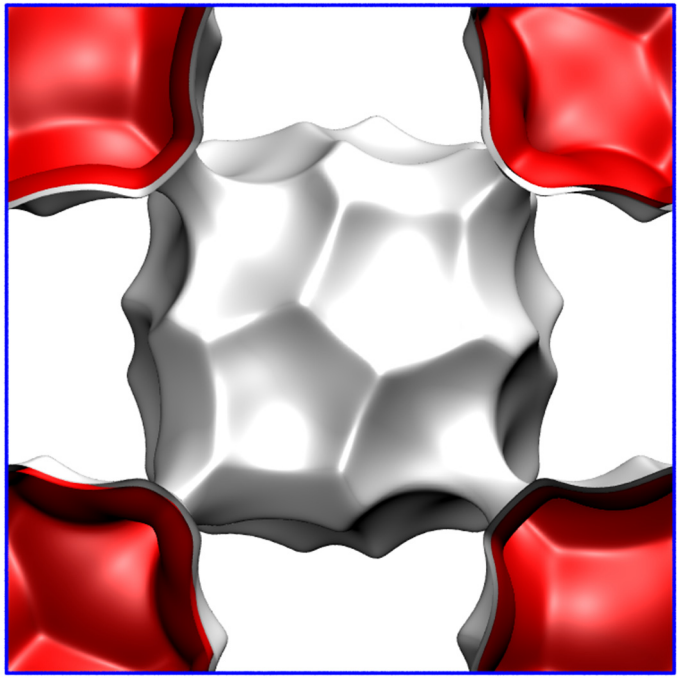

There are 2 cages per unit cell. The volume of one ZIF-8 cage is 1168 Å^3, significantly larger than that of a single cage of DDR (278 Å^3), or FAU (786 Å^3).

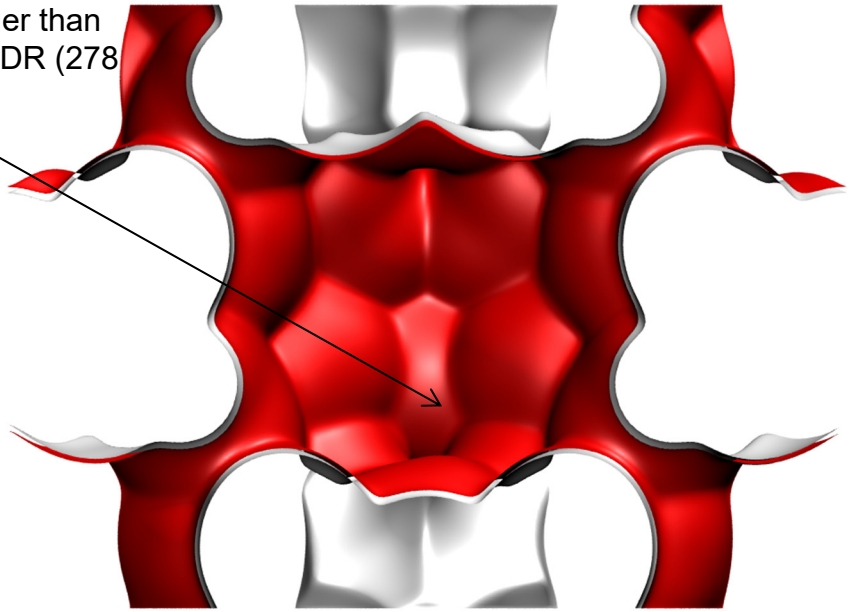

ZIF-8 dimensions

Fig. S22

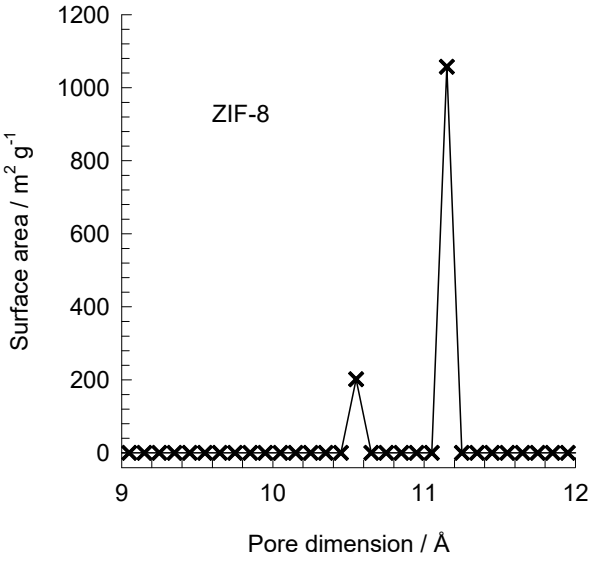

This plot of surface area versus pore dimension is determined using a combination of the DeLaunay triangulation method for pore dimension determination, and the procedure of Düren for determination of the surface area.

	ZIF-8
a /Å	16.991
b /Å	16.991
c /Å	16.991
Cell volume / Å^3	4905.201
conversion factor for [molec/uc] to [mol per kg Framework]	0.3663
conversion factor for [molec/uc] to [kmol/m^3]	0.7106
ρ [kg/m3]	924.253
MW unit cell [g/mol(framework)]	2730.182
ϕ, fractional pore volume	0.476
open space / Å^3/uc	2337.0
Pore volume / cm^3/g	0.515
Surface area /m^2/g	1164.7
DeLaunay diameter /Å	3.26

Weak confinement in zeolites

Fig. S23

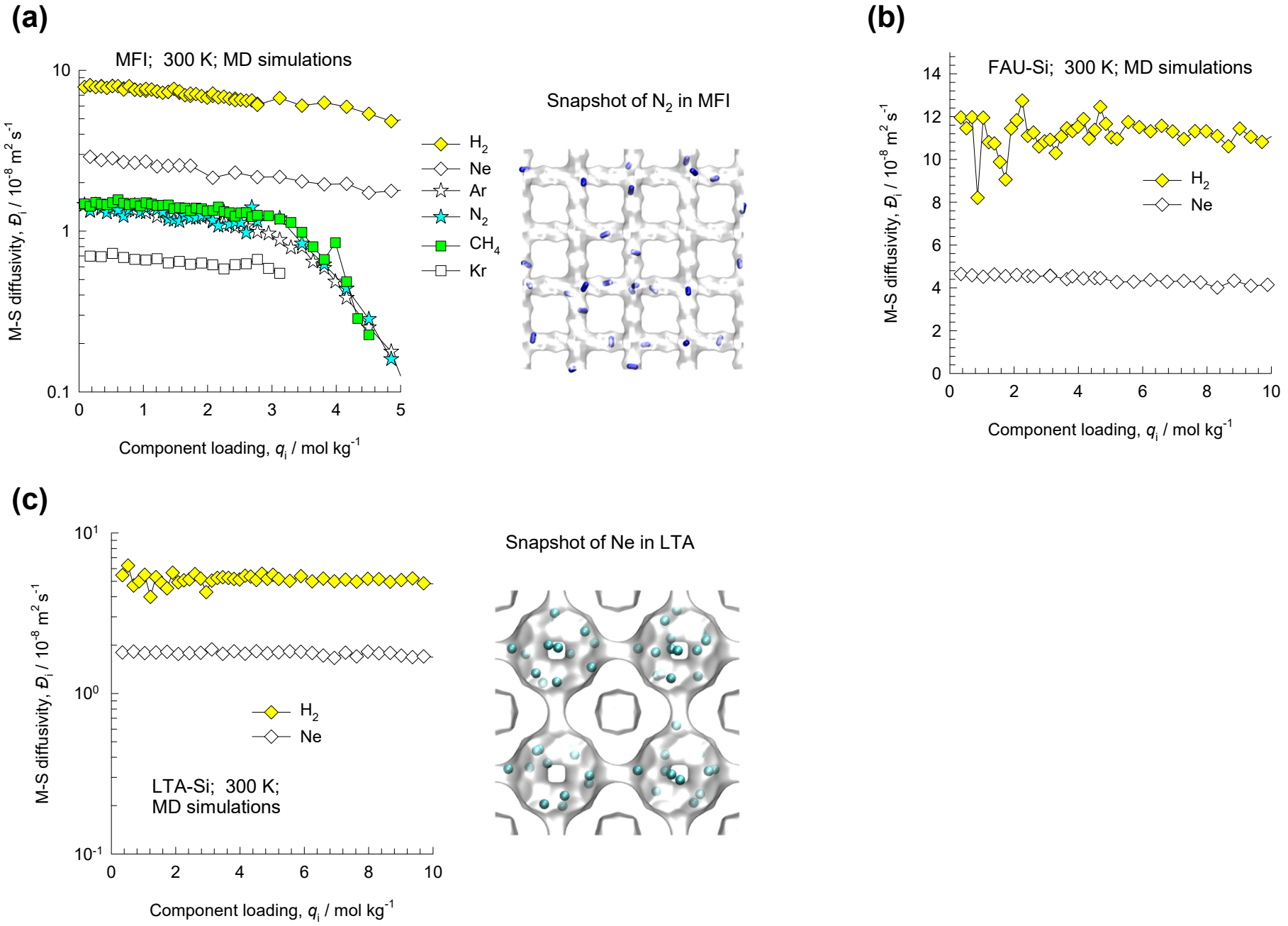

Strong confinement in zeolites

Fig. S24

(a)

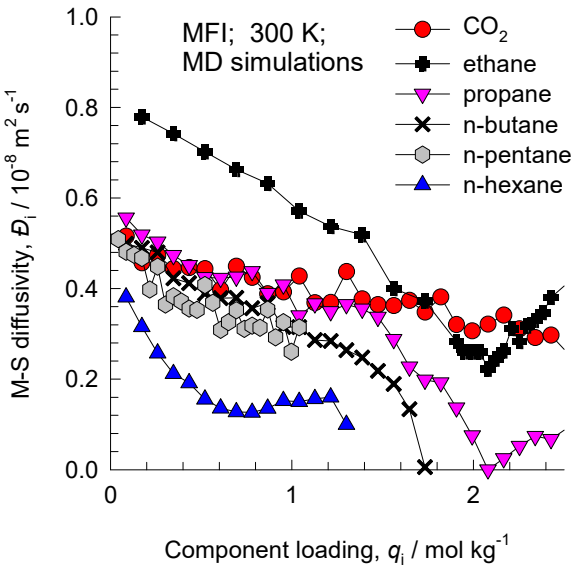

(b)

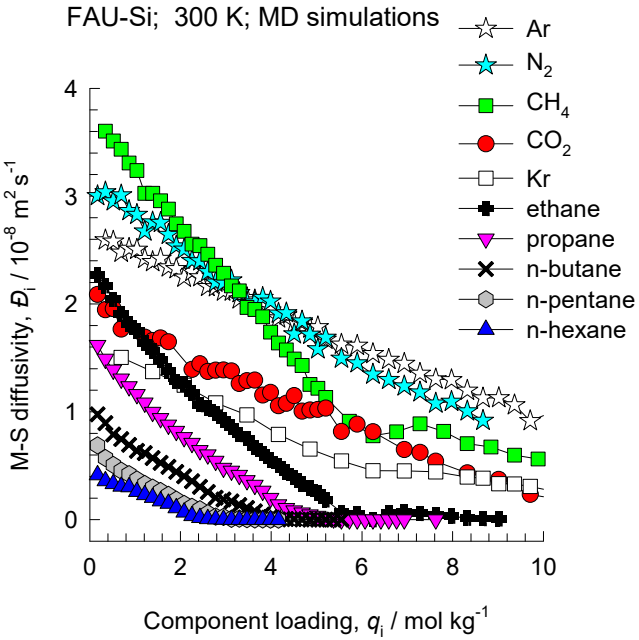

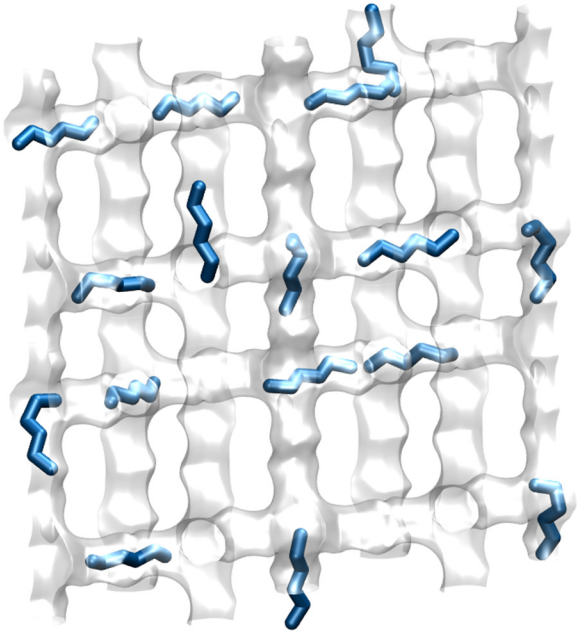

Snapshot of n-hexane in MFI

Inter-cage hopping in LTA and CHA

Fig. S25

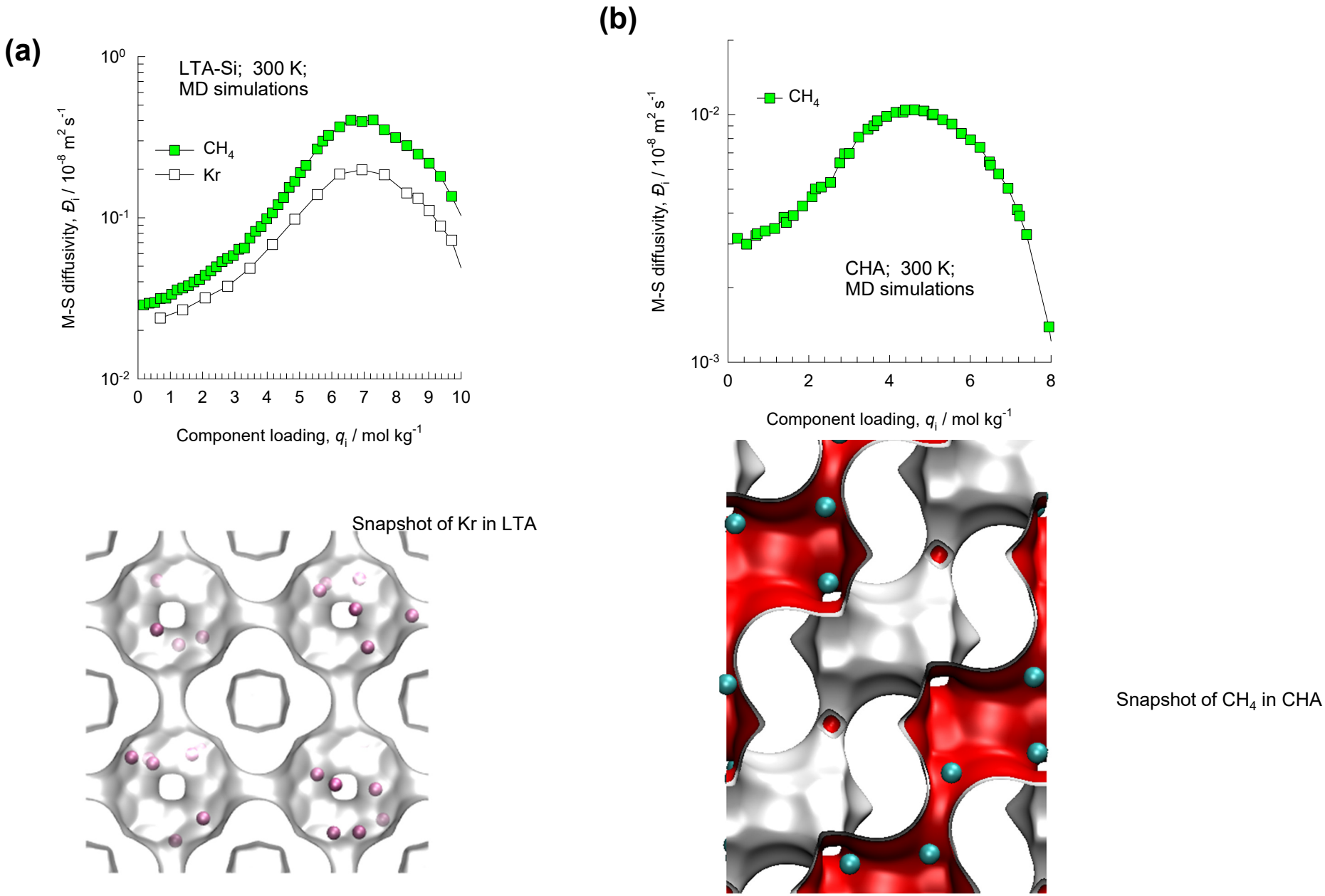

Fig. S26

Schematic for zeolite membrane permeation

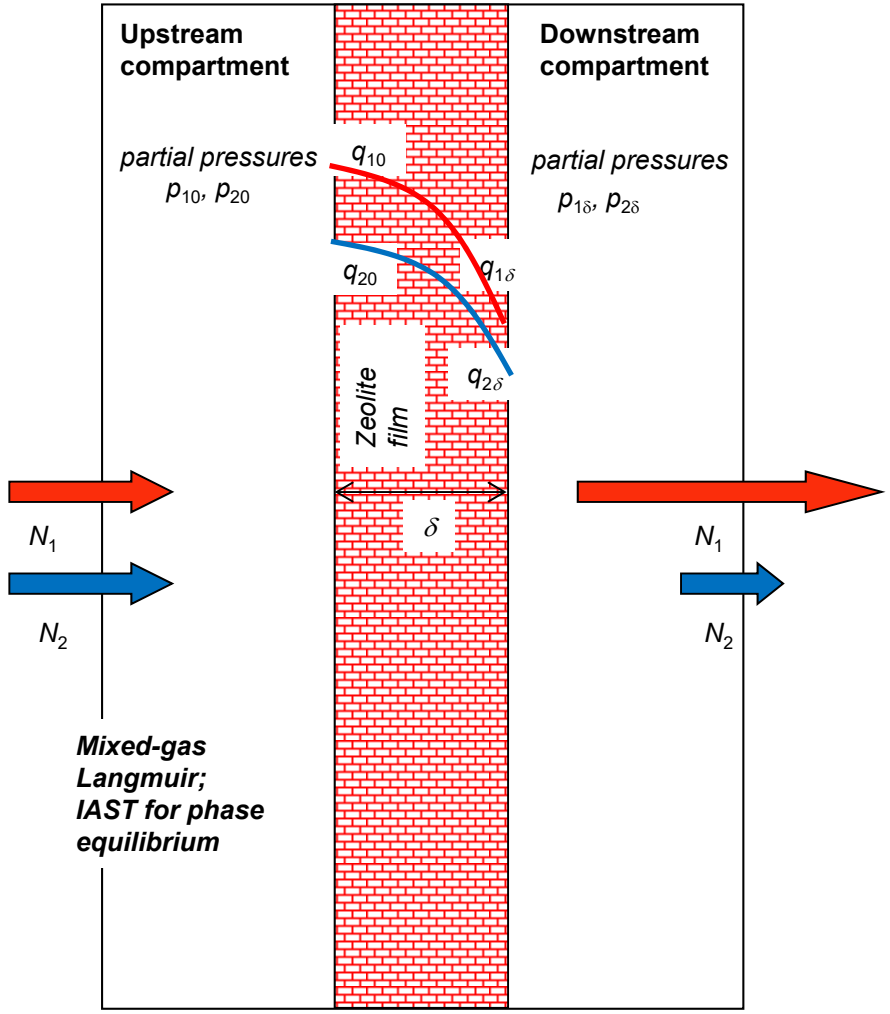

Fig. S27

Isotherm fits: Feng isotherm data

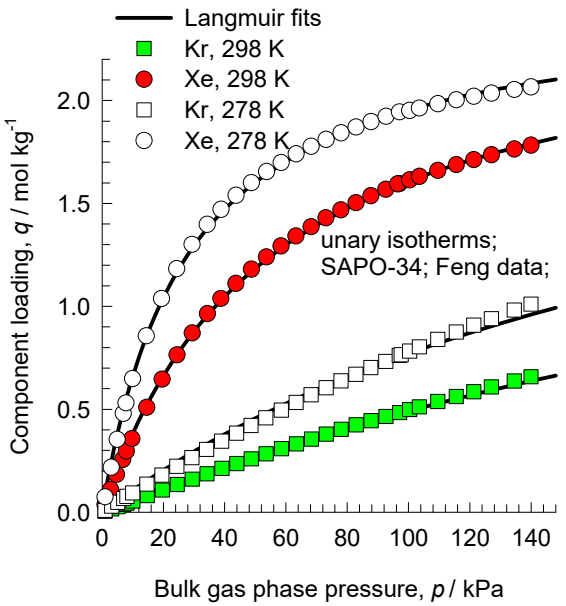

Fig. S28

Isotherm fits: Kwon isotherm data

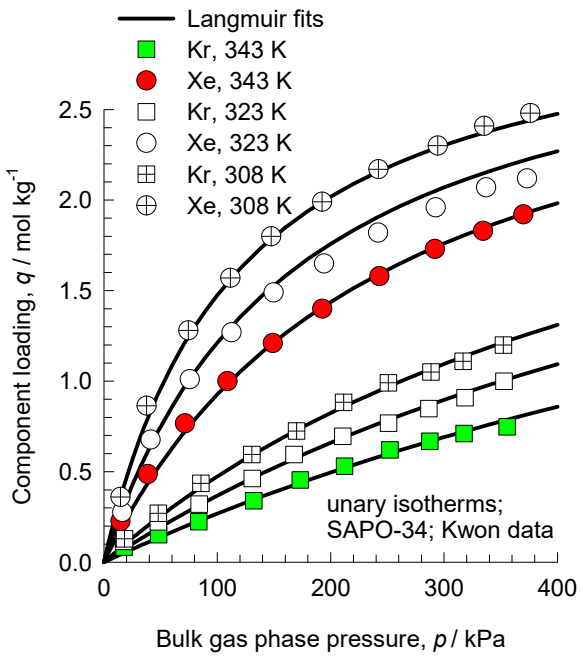

Fig. S29

Thermodynamic Correction Factors

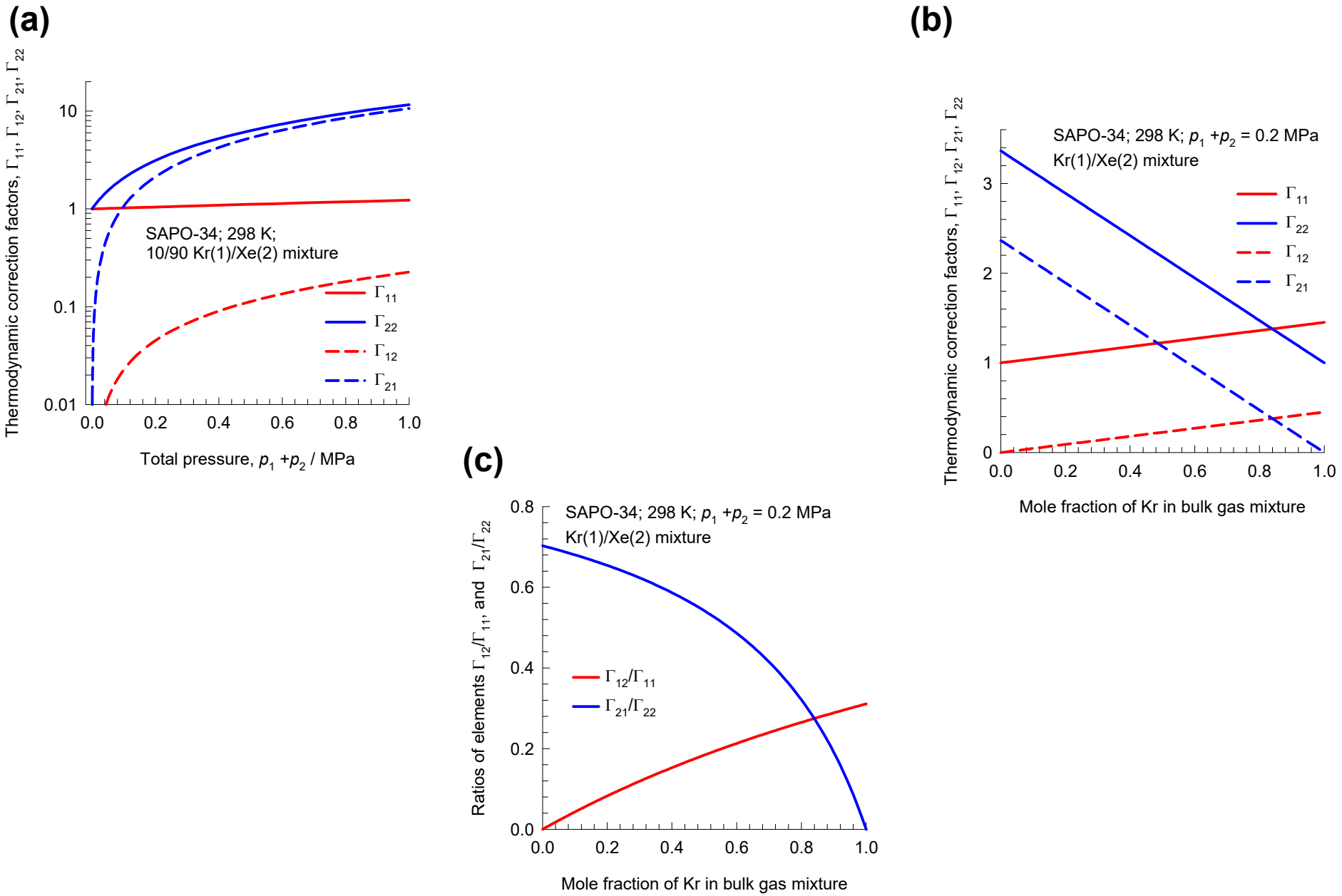

Fig. S30

Permeances and Diffusivities: Feng expt data

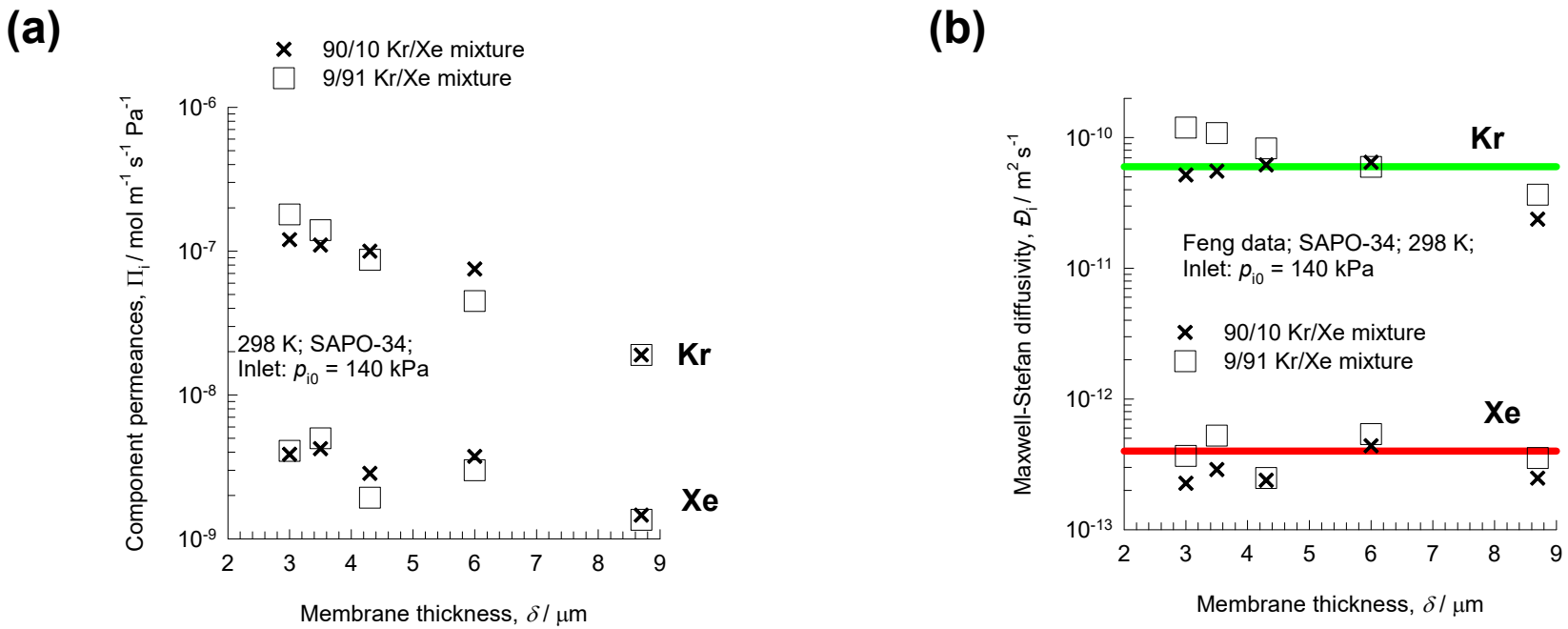

Fig. S31

Permeances and diffusivities: Kwon expt data

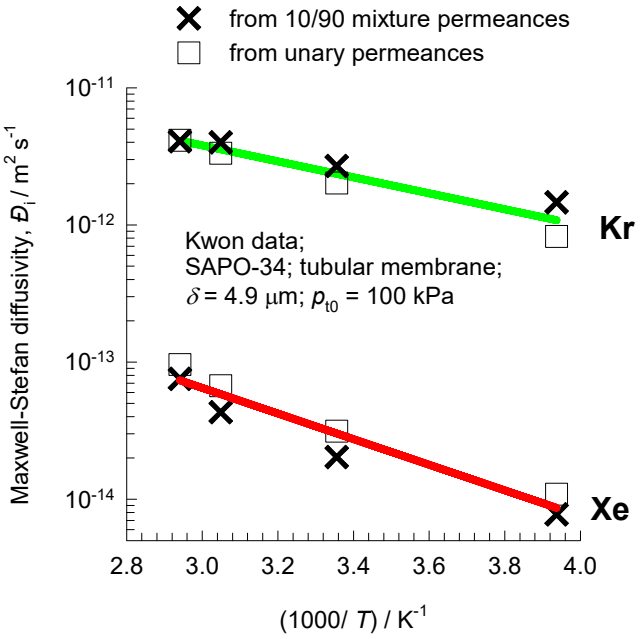

M-S diffusivities in SAPO-34 membrane

Fig. S32

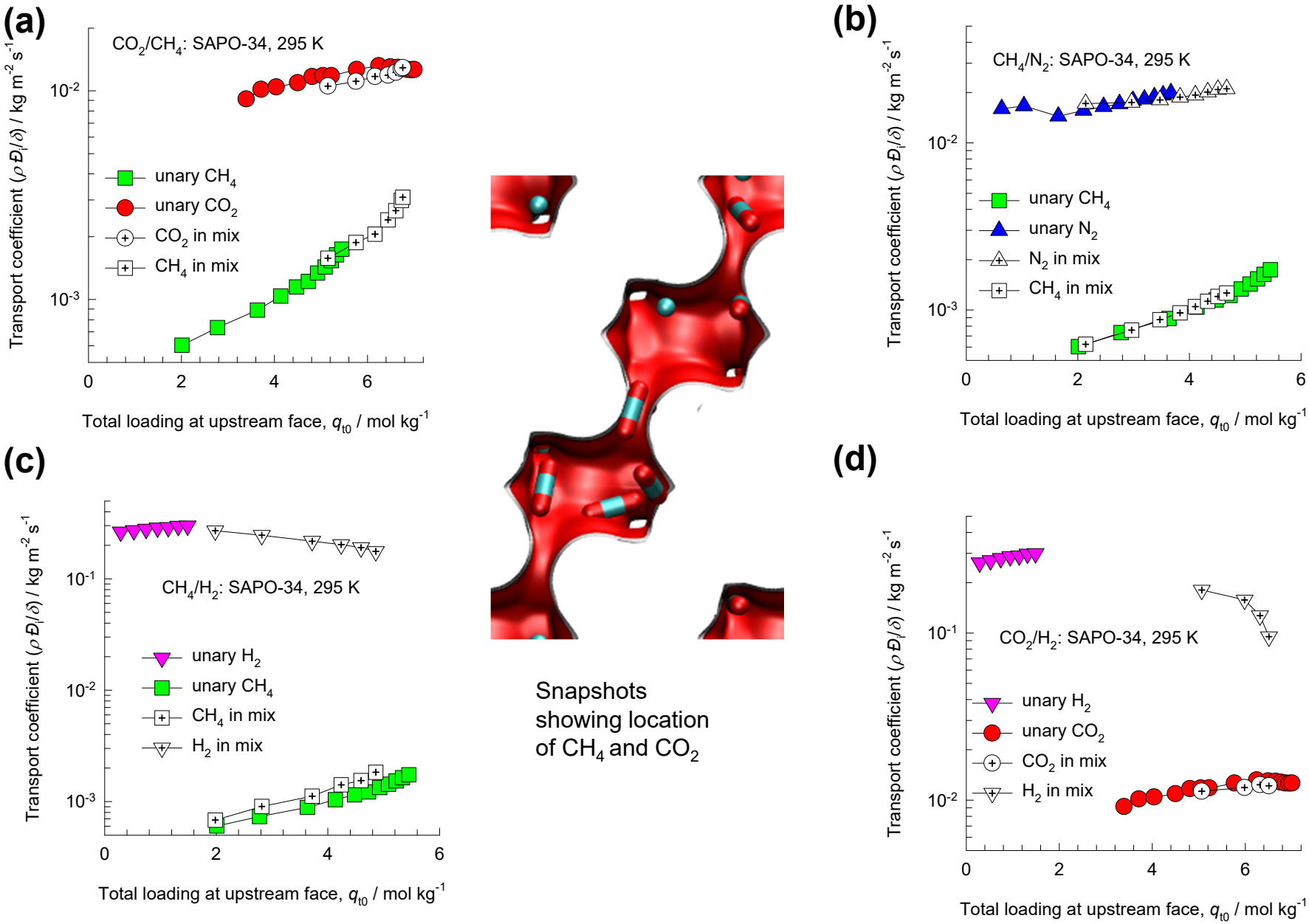

Fig. S33

Exact vs Linearized Model: Kwon isotherm data

(a)

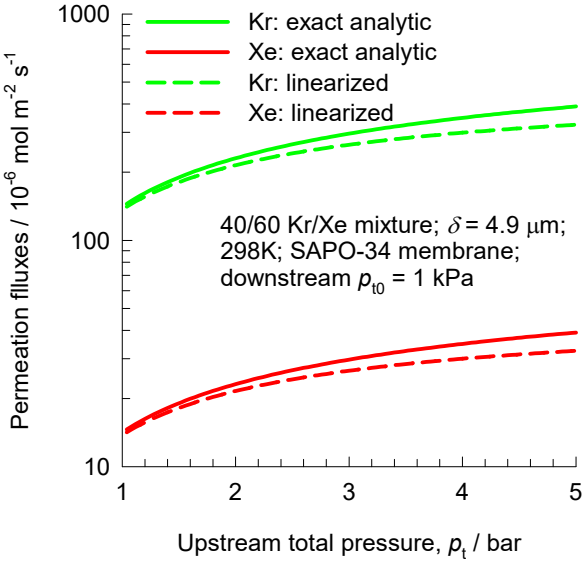

(b)

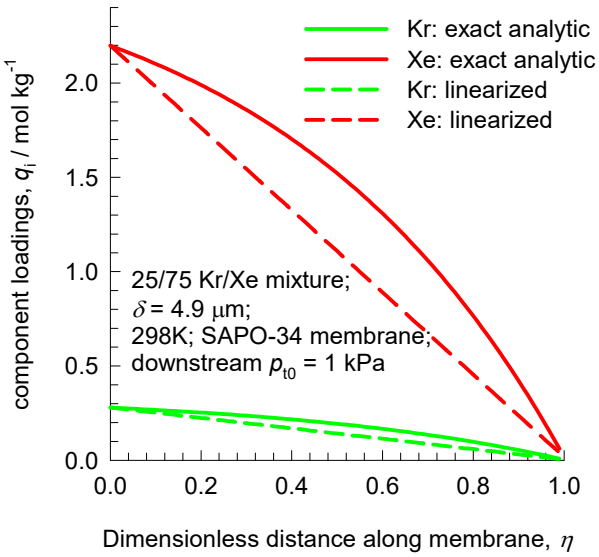

Fig. S34

Transient Overshoot: Feng isotherm data

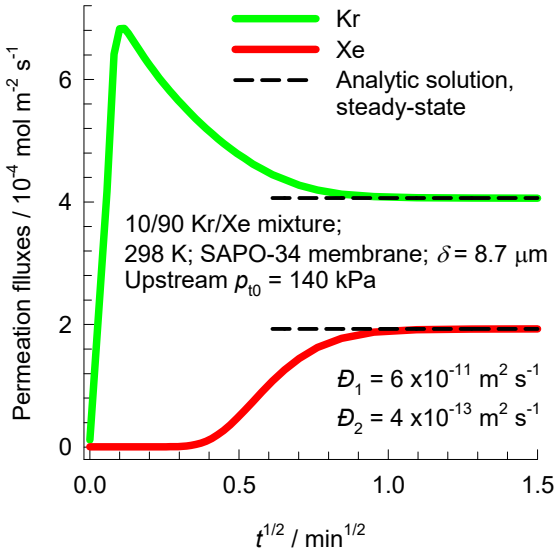

Fig. S35

Transient Overshoot: Kwon isotherm data

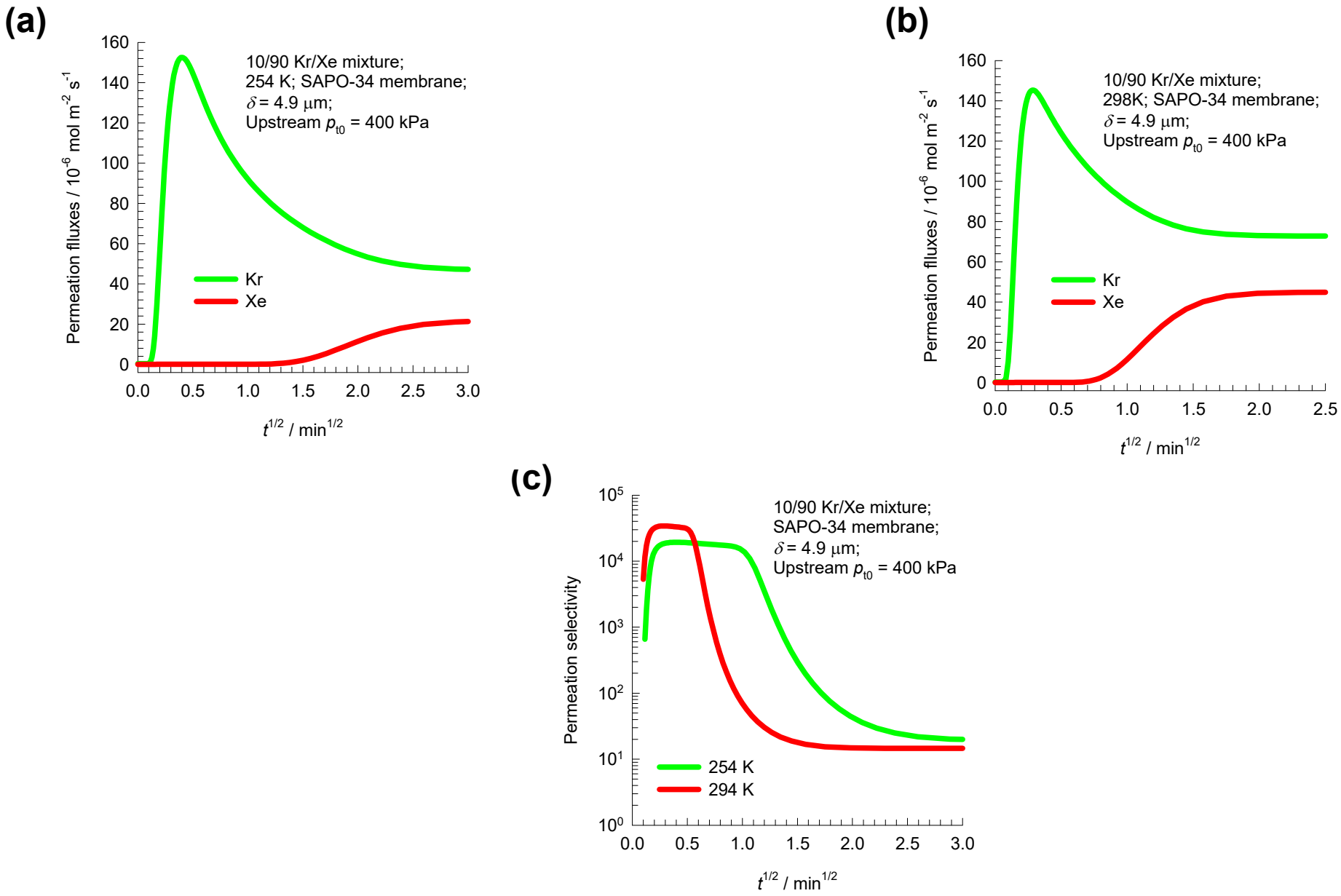

Fig. S36

Unary and mixture permeances in MFI zeolite

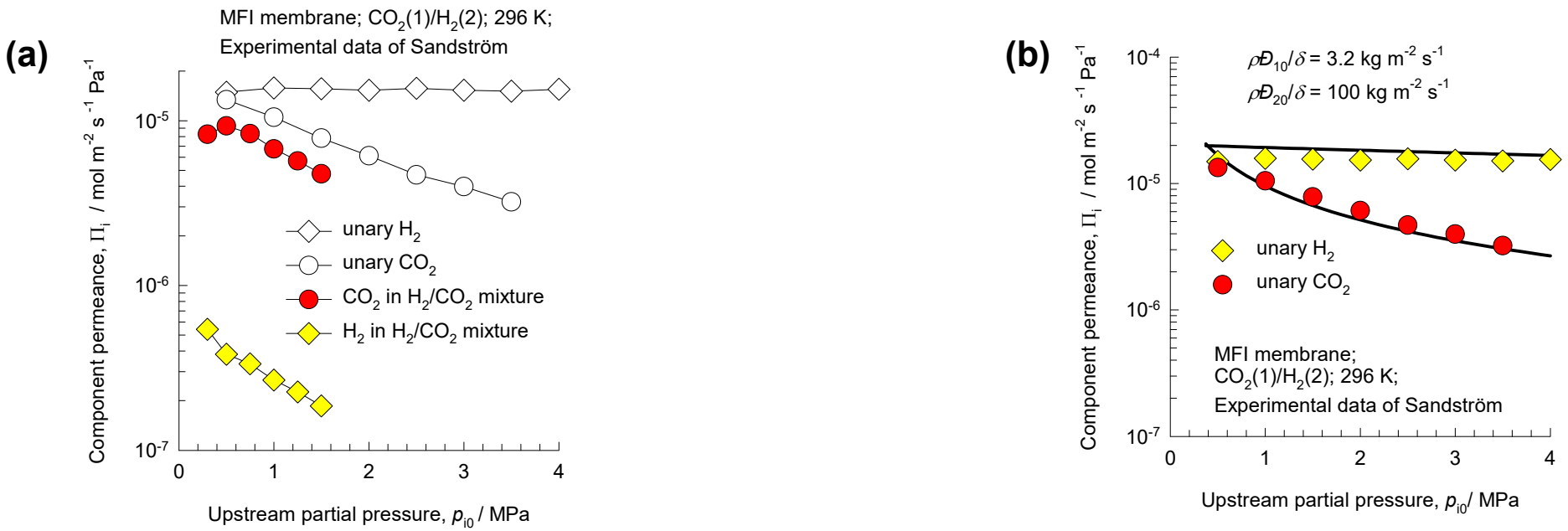

Fig. S37

MD simulations of M-S diffusivities

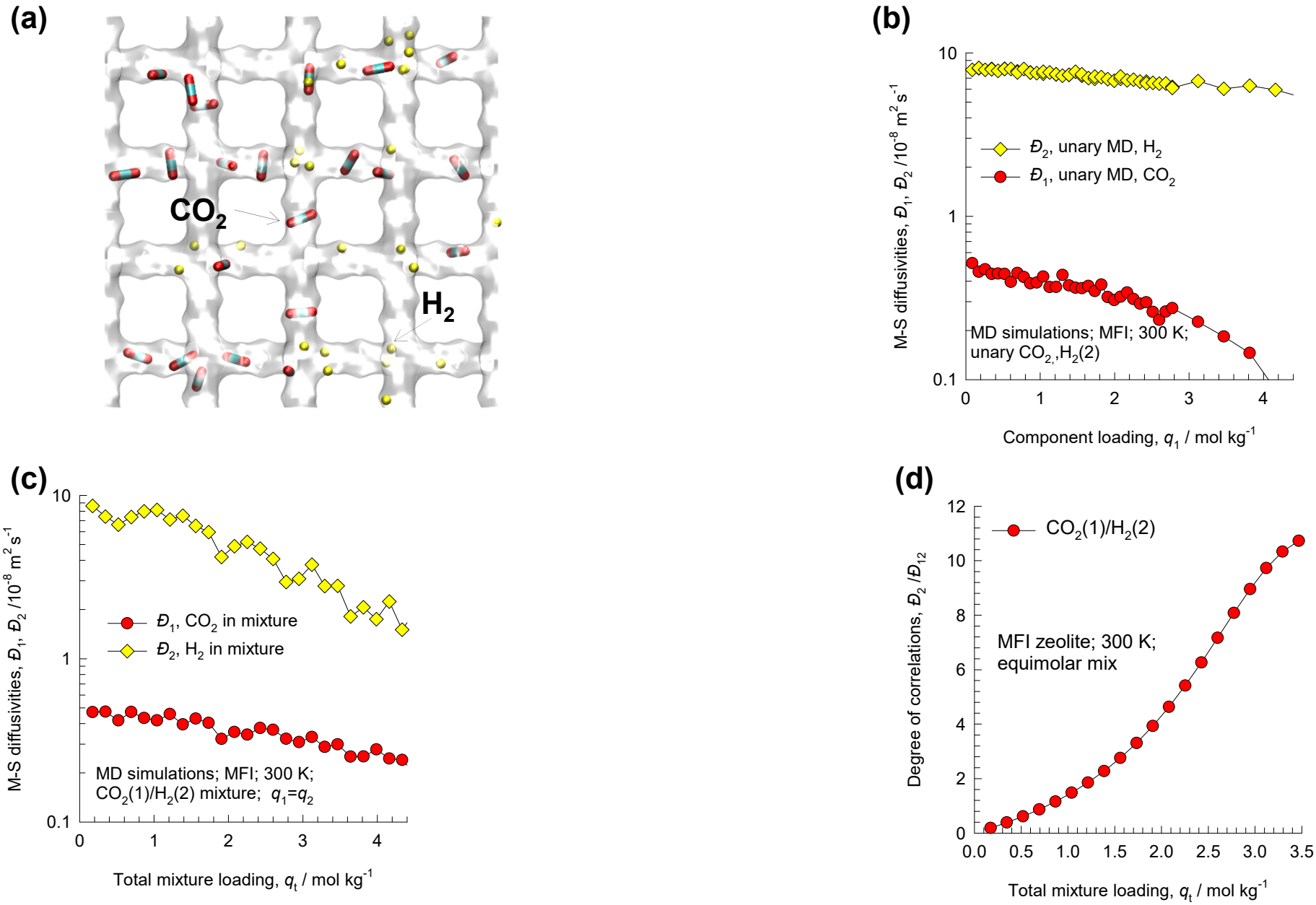

Fig. S38

CO_2/H_2 mixture permeances in MFI zeolite

(a)

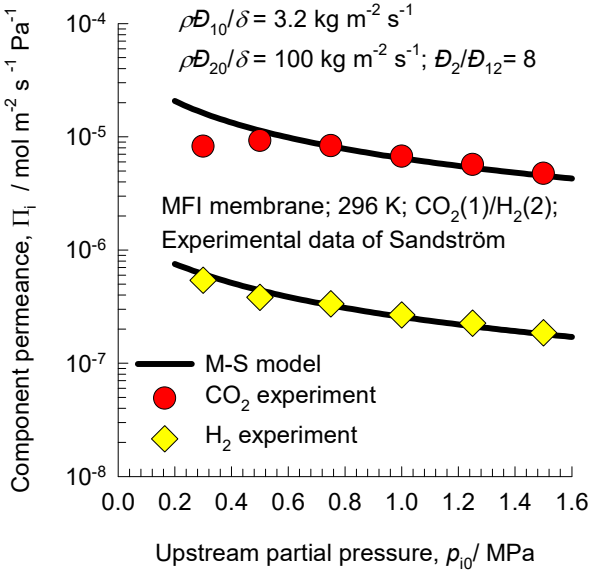

(b)

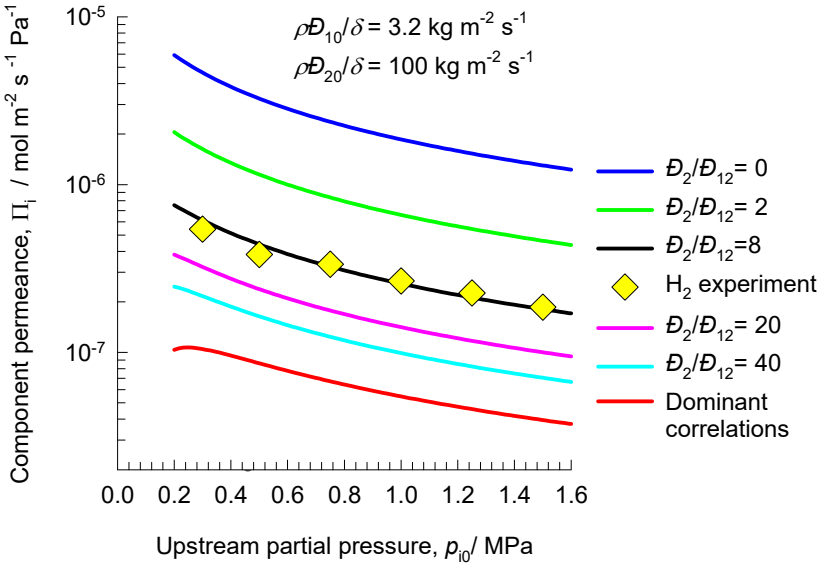

Fig. S39

CO_2/H_2 mixture fluxes in MFI zeolite

(a)

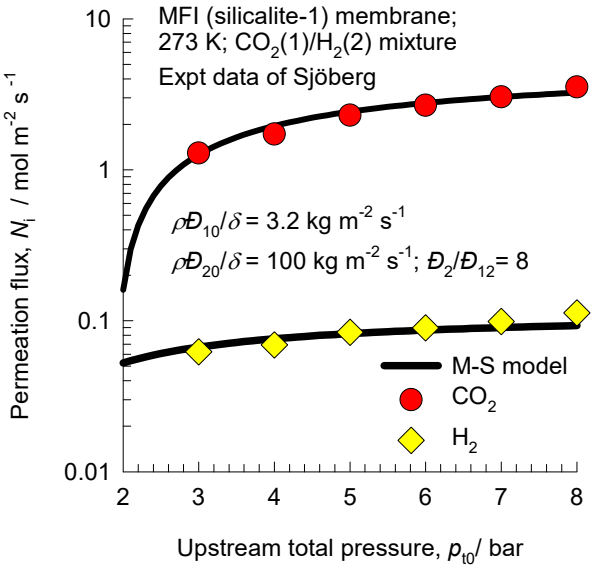

(b)

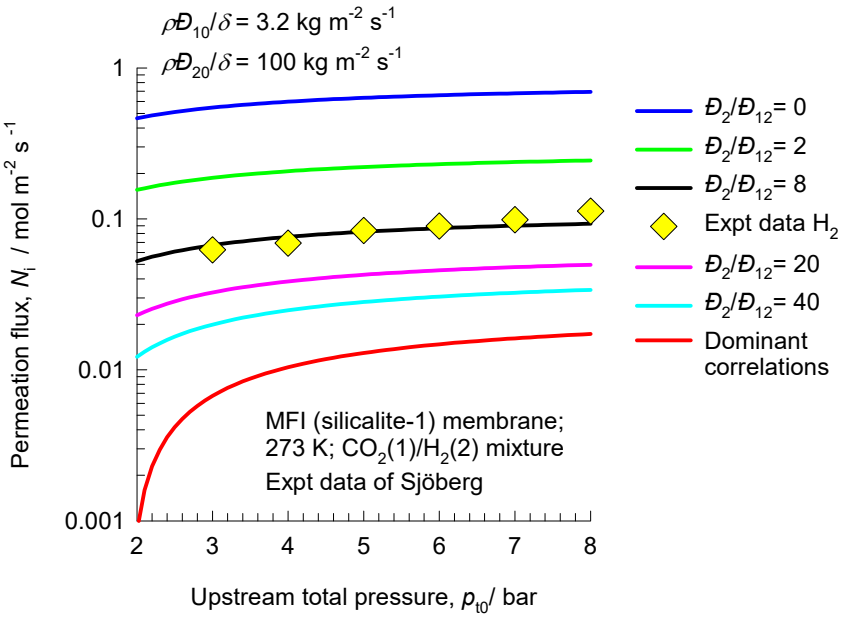

Permeation across polymeric membrane

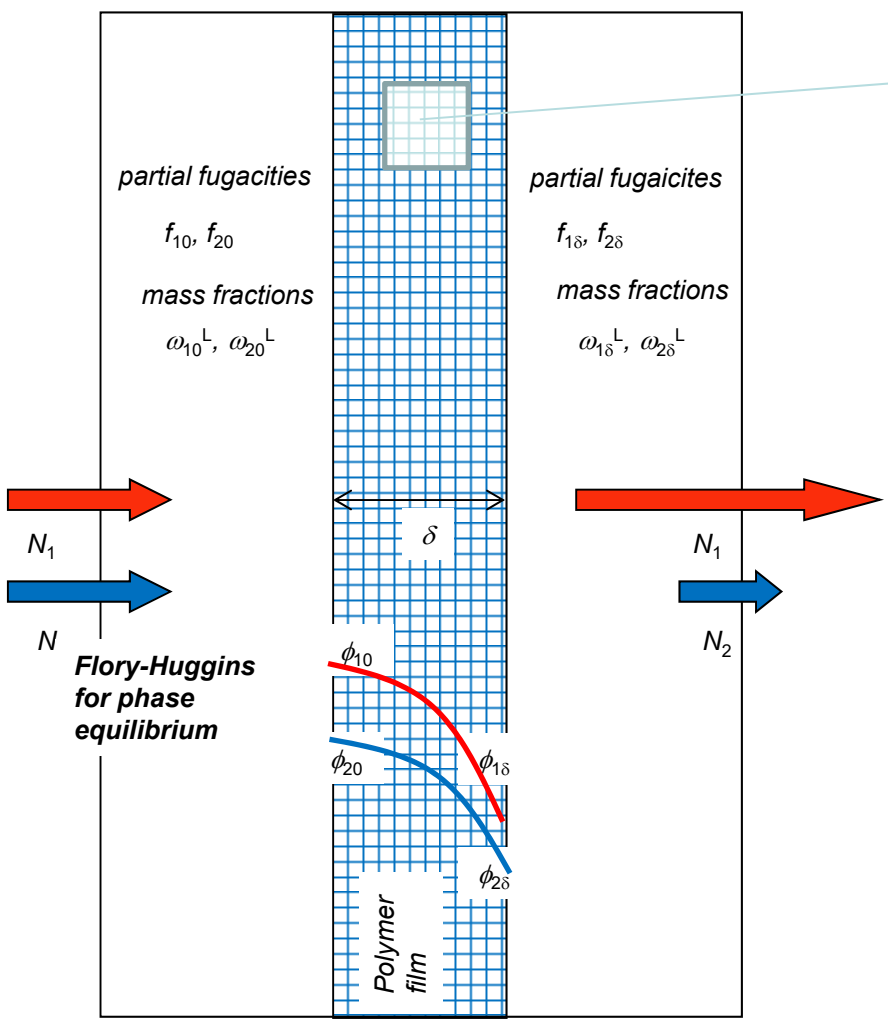

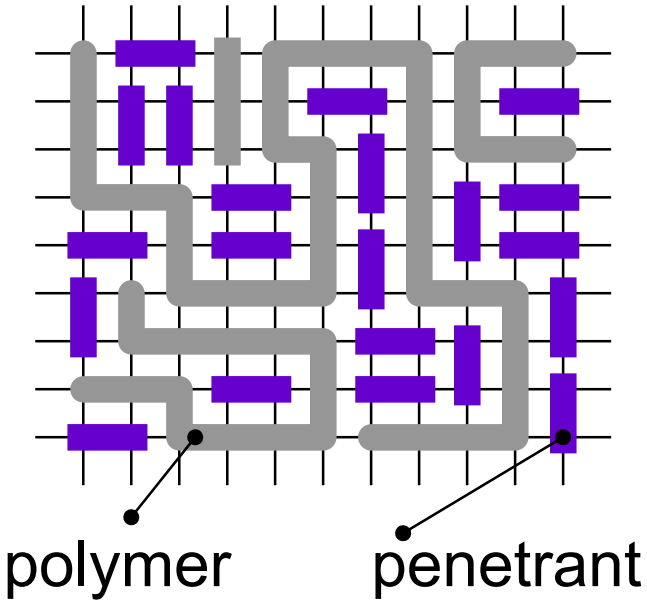

penetrant and polymer fit on a 3D lattice

Fig. S41

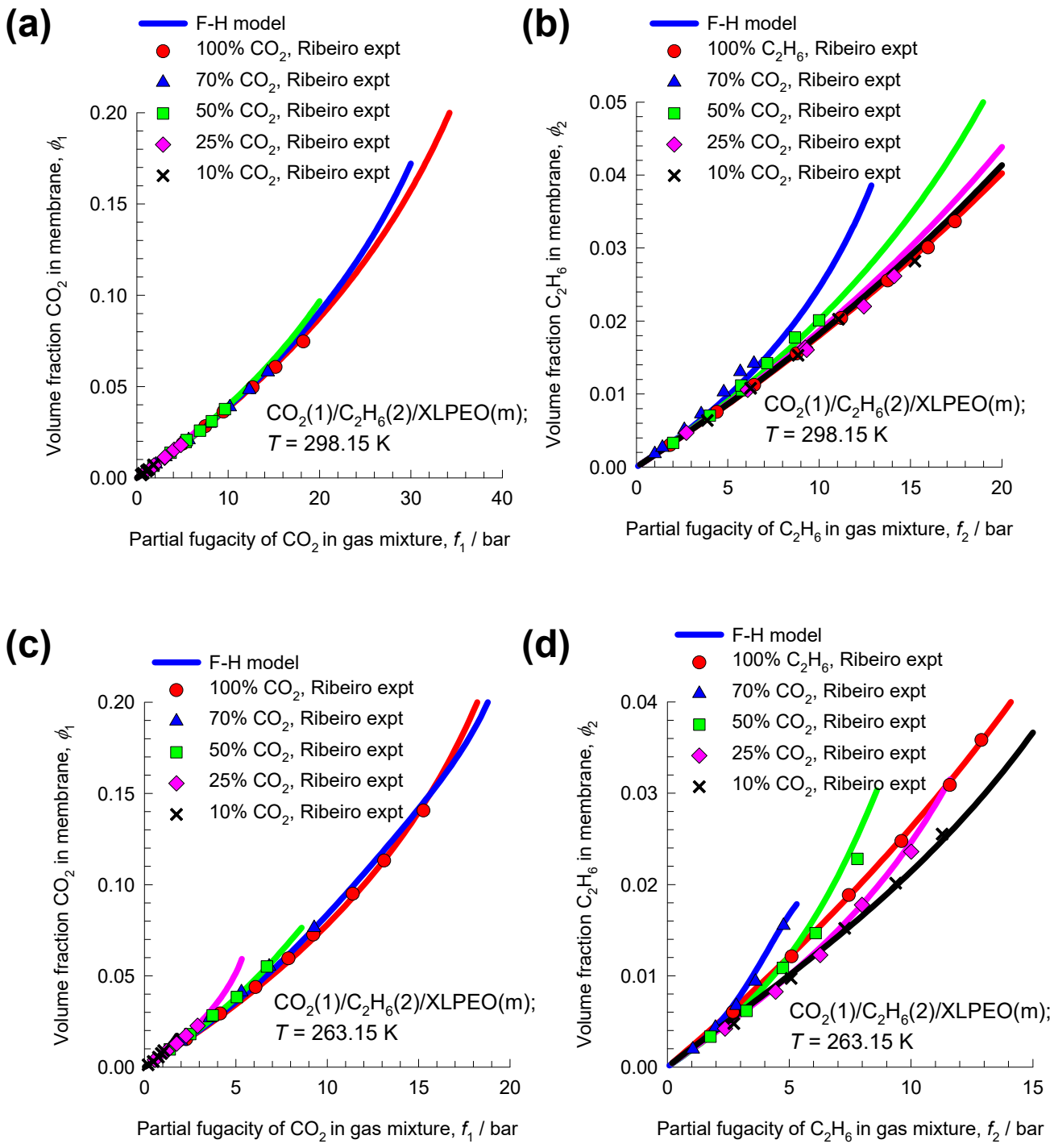

CO_2/ C_2H_6/ XLPEO equilibrium

Water/ethanol/CA equilibrium

Fig. S42

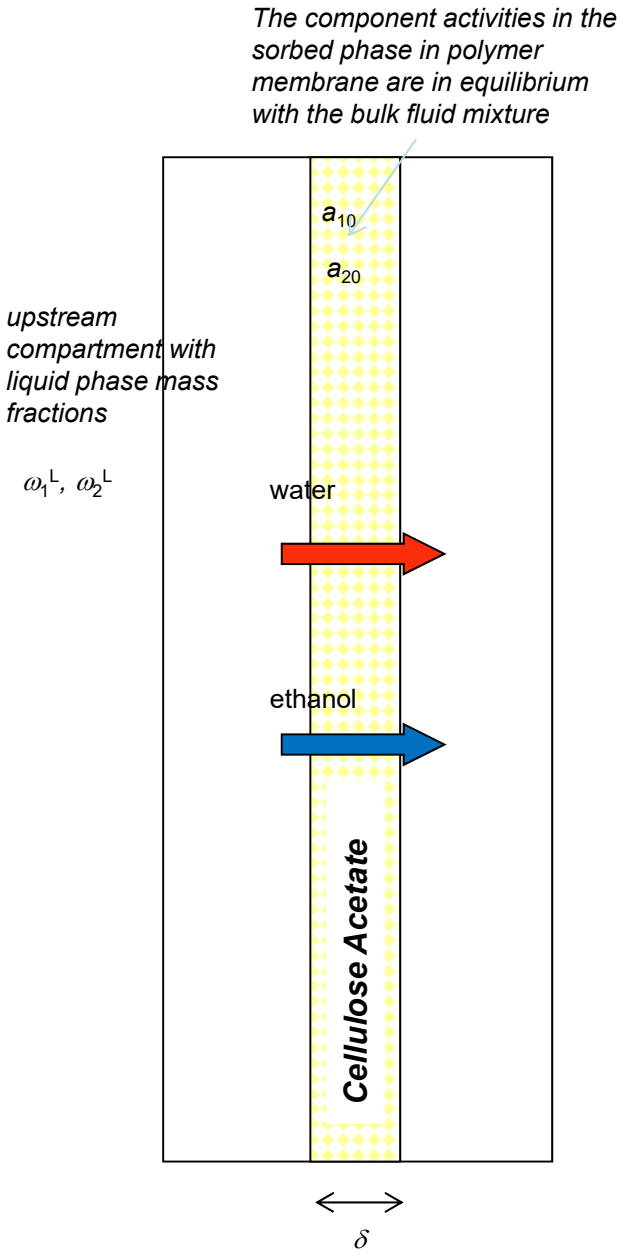

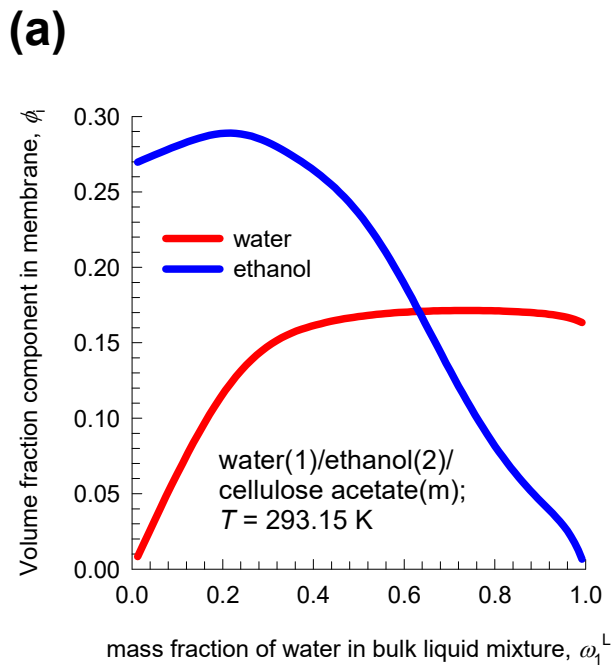

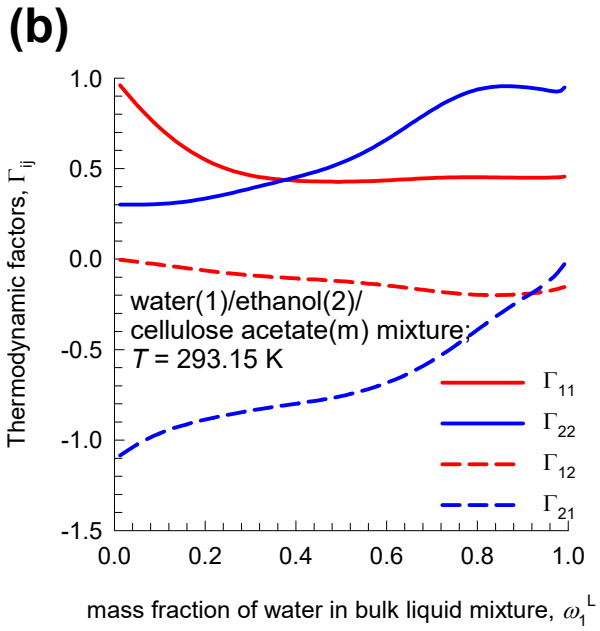

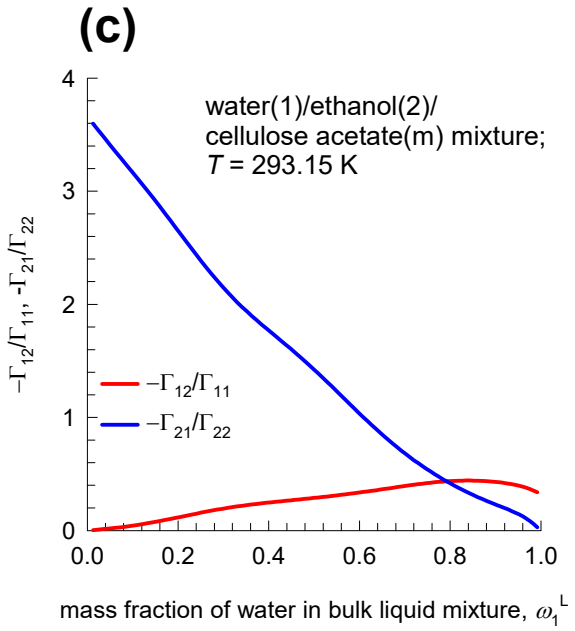

Water/ethanol/Polyimide equilibrium

Fig. S43

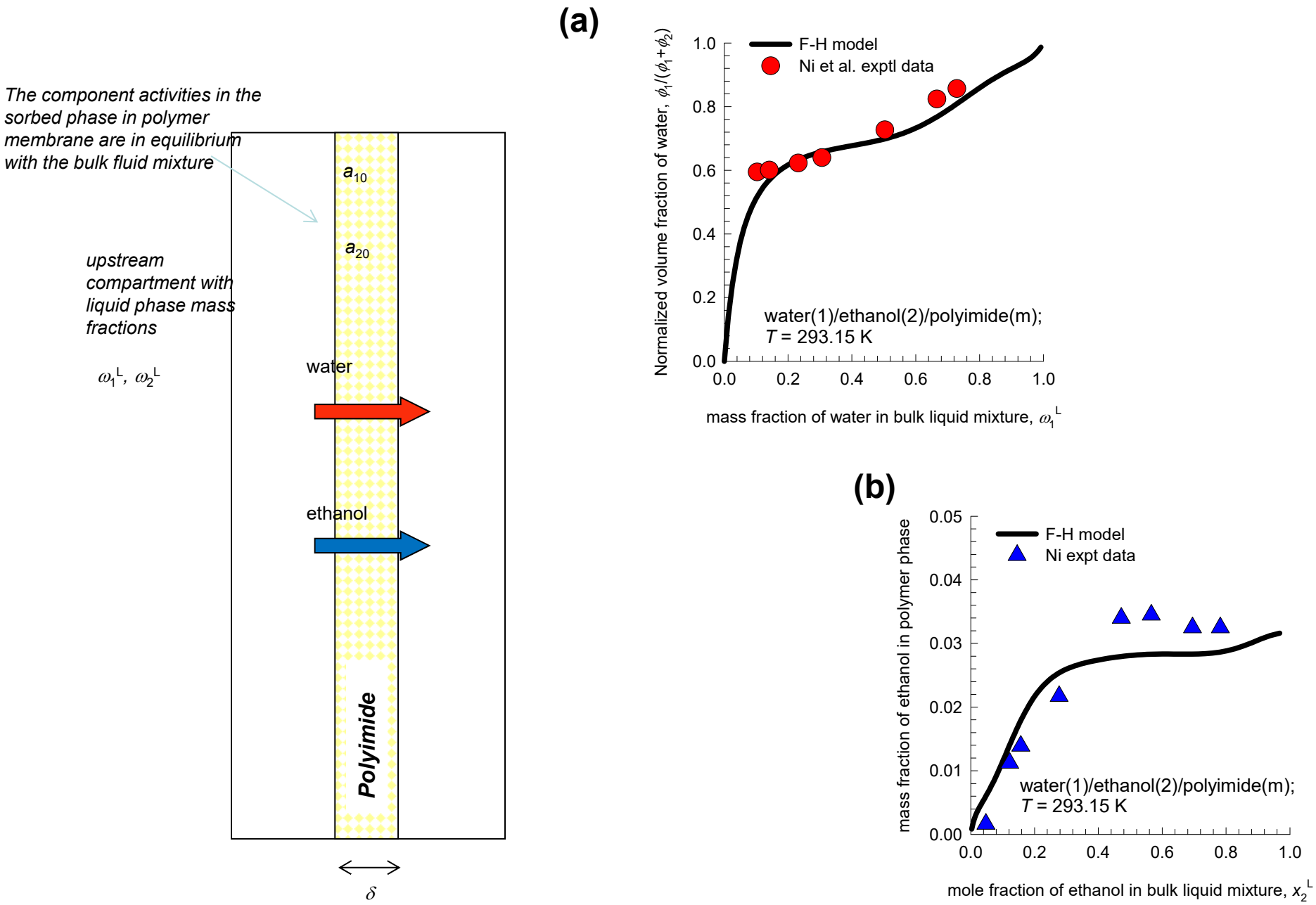

Water/ethanol/PVA/PAN equilibrium

Fig. S44

The component activities in the sorbed phase in polymer membrane are in equilibrium with the bulk fluid mixture

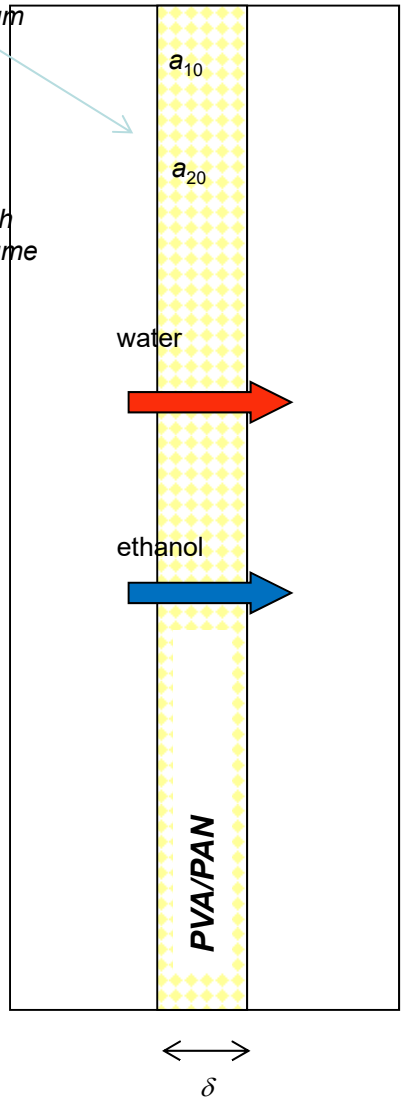

upstream compartment with liquid phase volume fractions

ϕ_1^L, ϕ_2^L

upstream compartment with liquid phase mass fractions

ω_1^L, ω_2^L

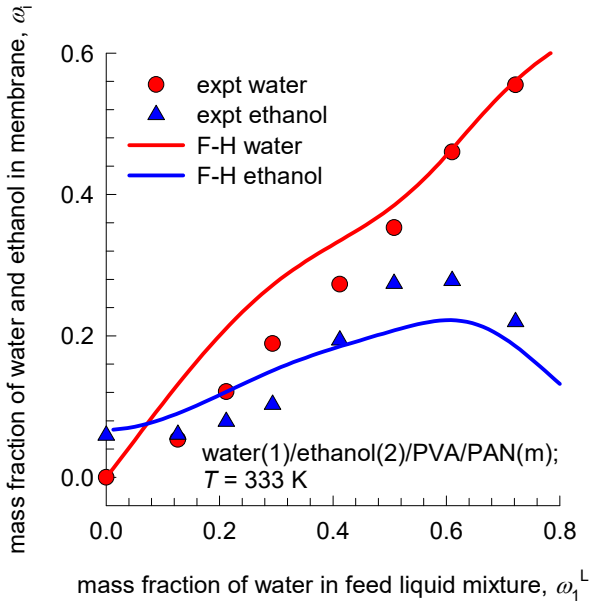

Water/ethanol/cellulose acetate pervaporation

Fig. S45

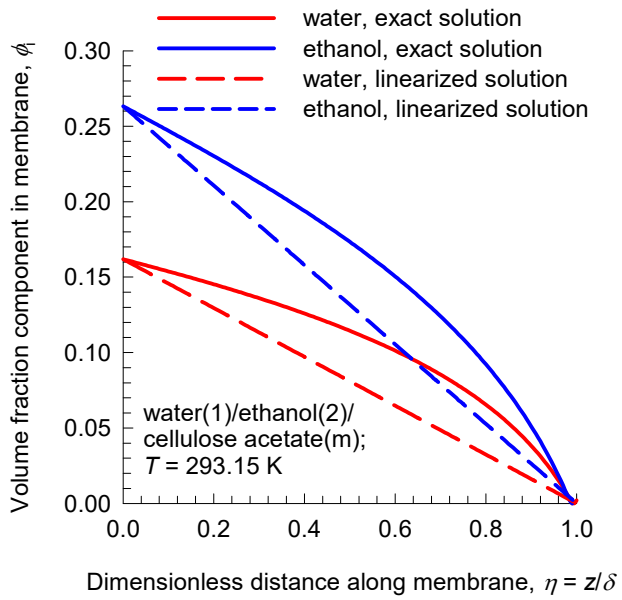

Fig. S46

Water/ethanol/polyimide pervaporation

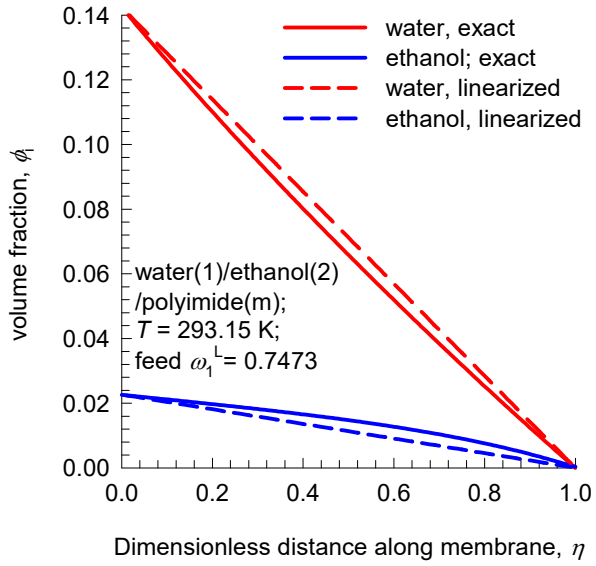

Water/ethanol/polyimide pervaporation

Fig. S47

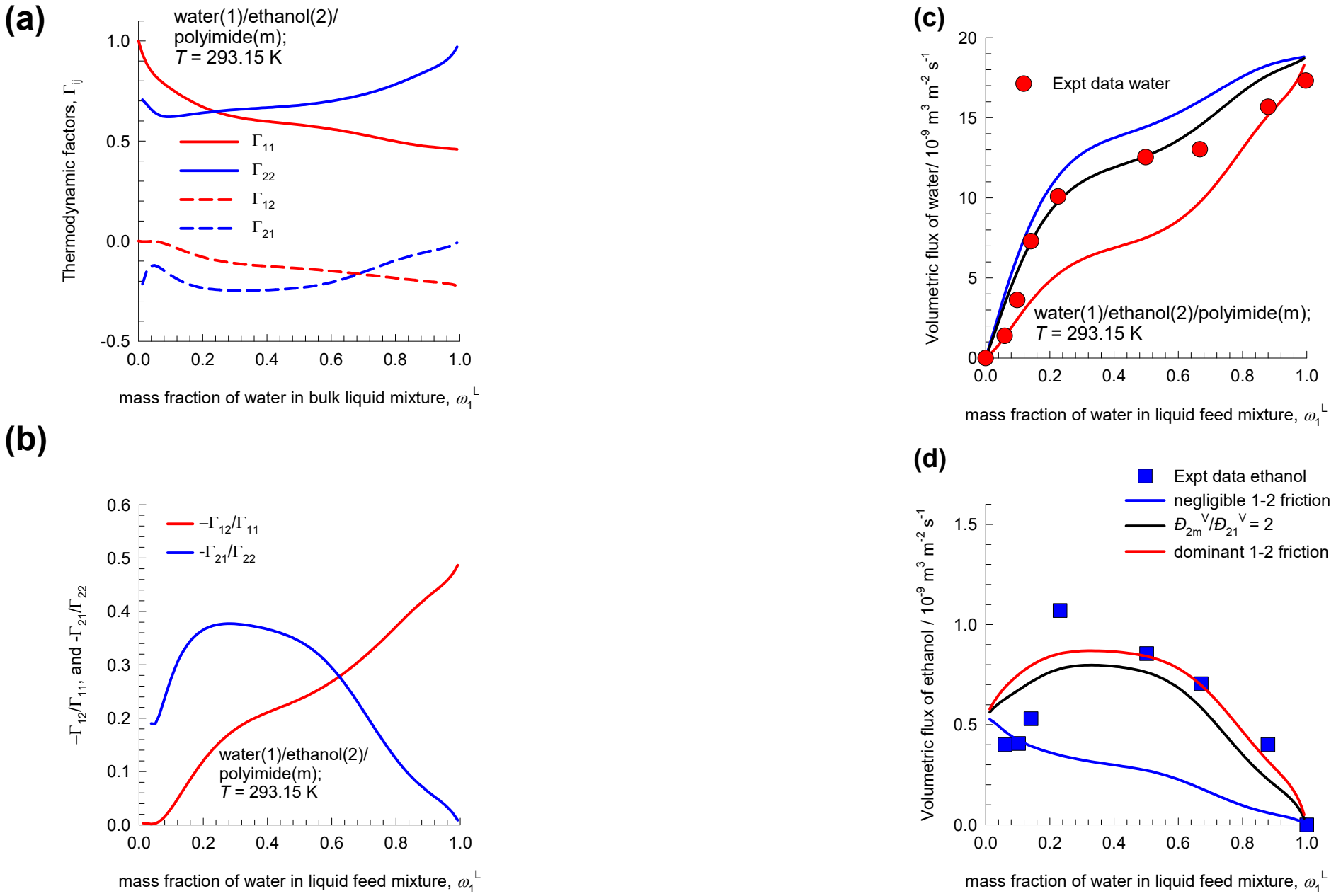

Water/ethanol/PVA/PAN pervaporation

Fig. S48

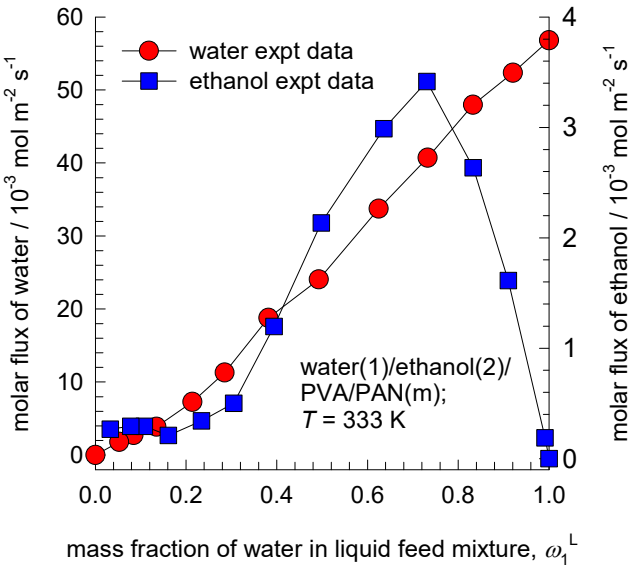

Water/ethanol/PVA/PAN pervaporation

Fig. S49

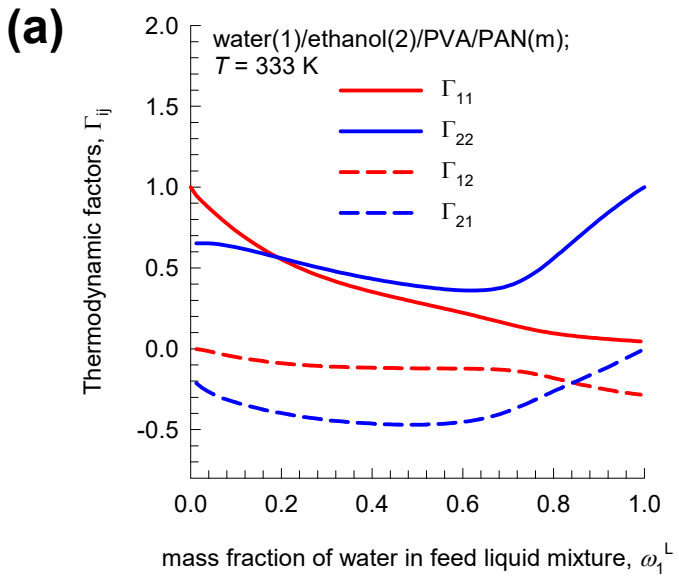

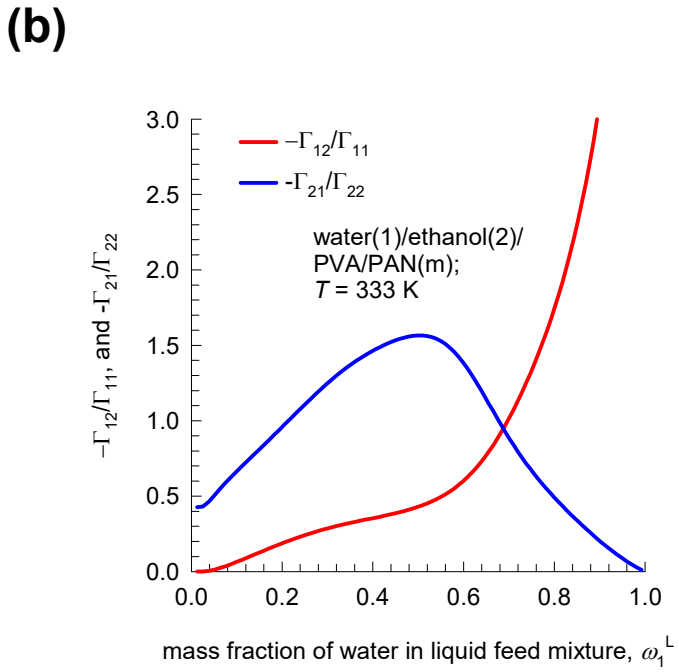

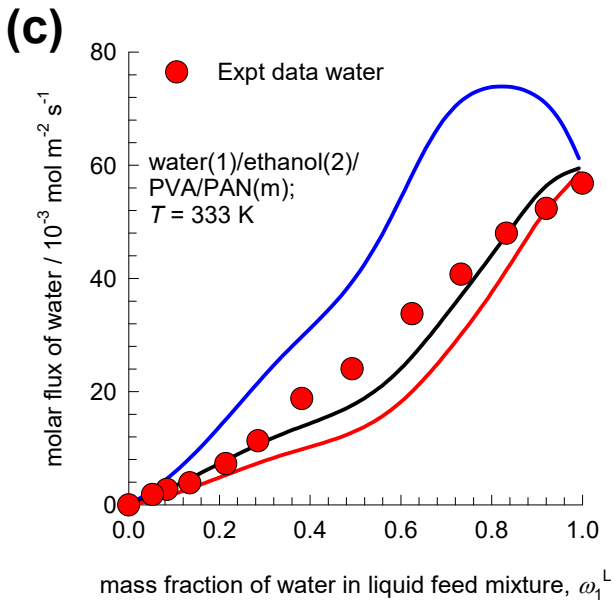

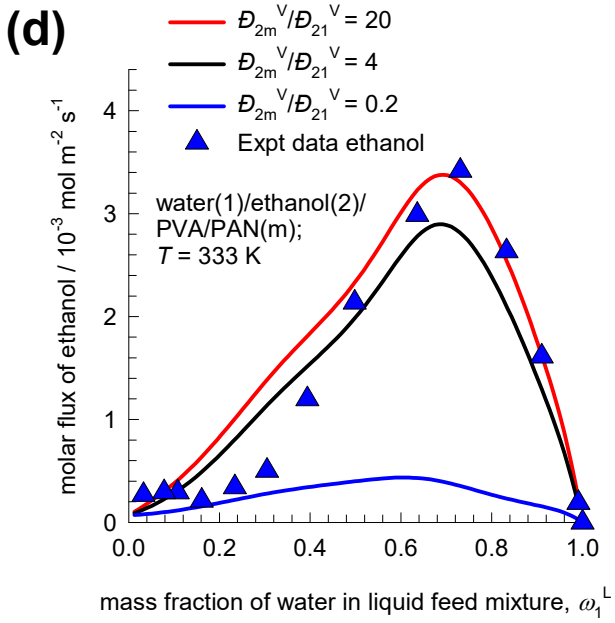

CO_2/C_2H_6 /XPLEO permeation

Fig. S50

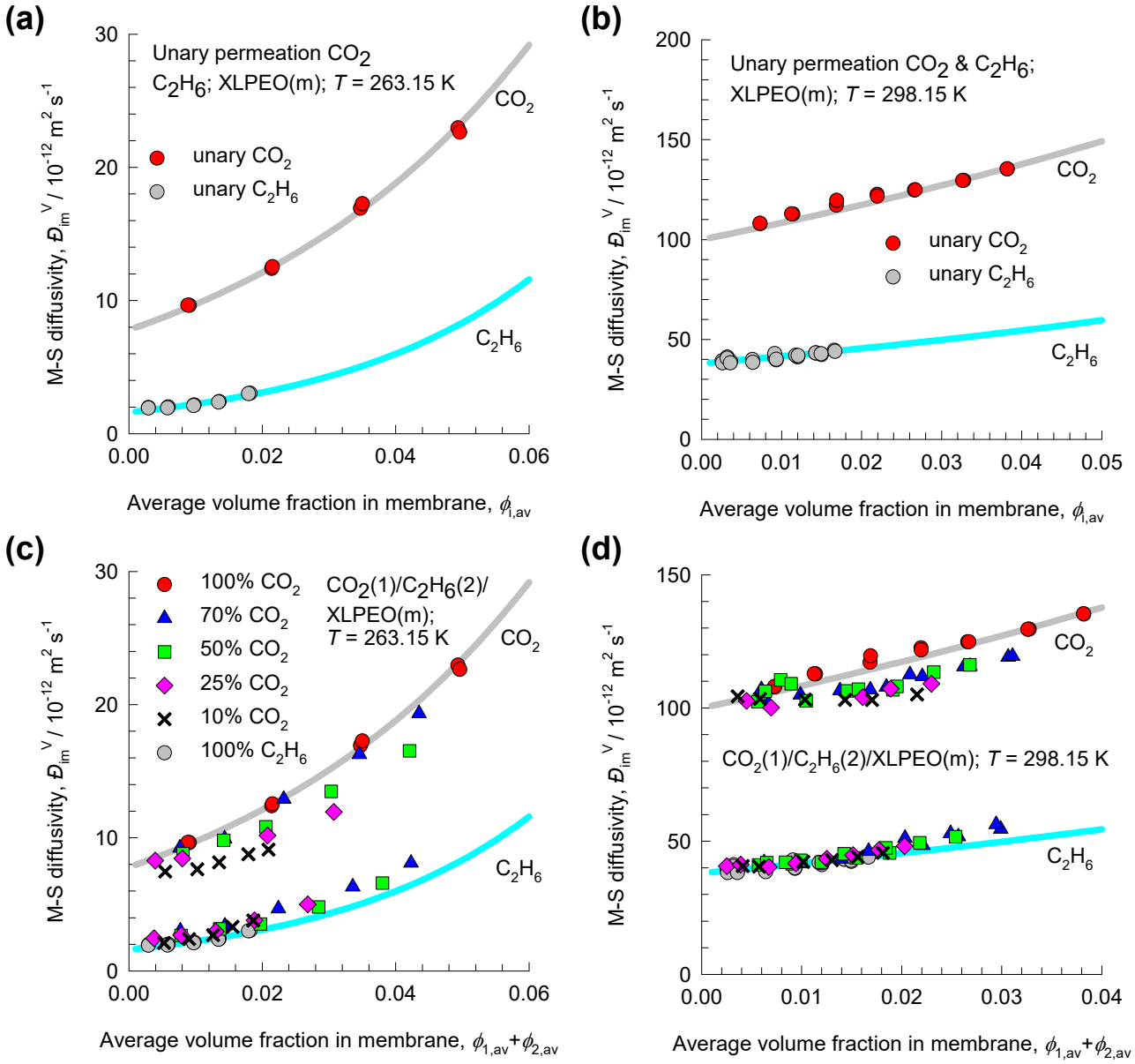

CO_2/C_2H_6 /XPLEO permeation

Fig. S51

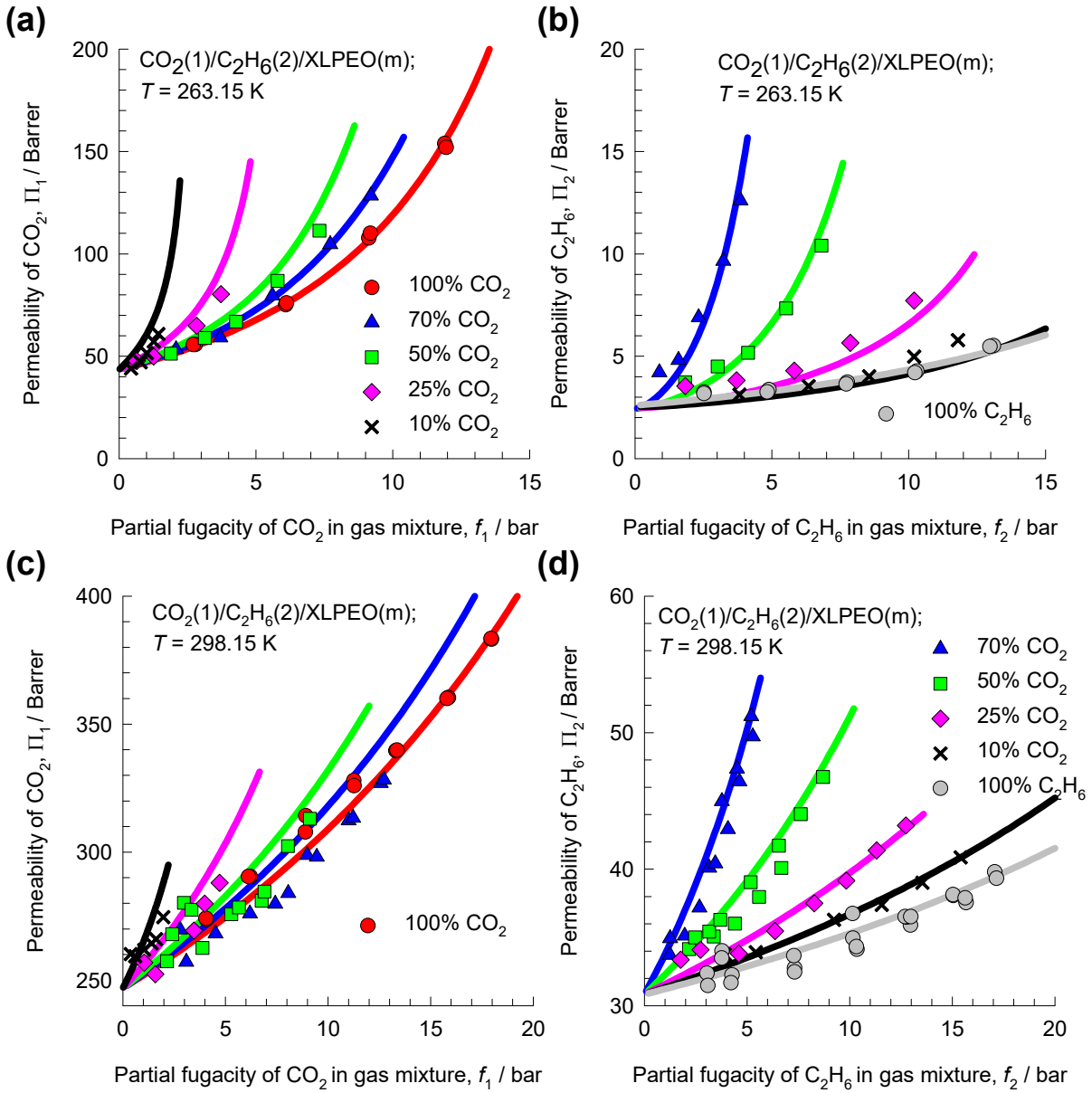

CO_2/C_2H_6 /XPLEO permeation

Fig. S52

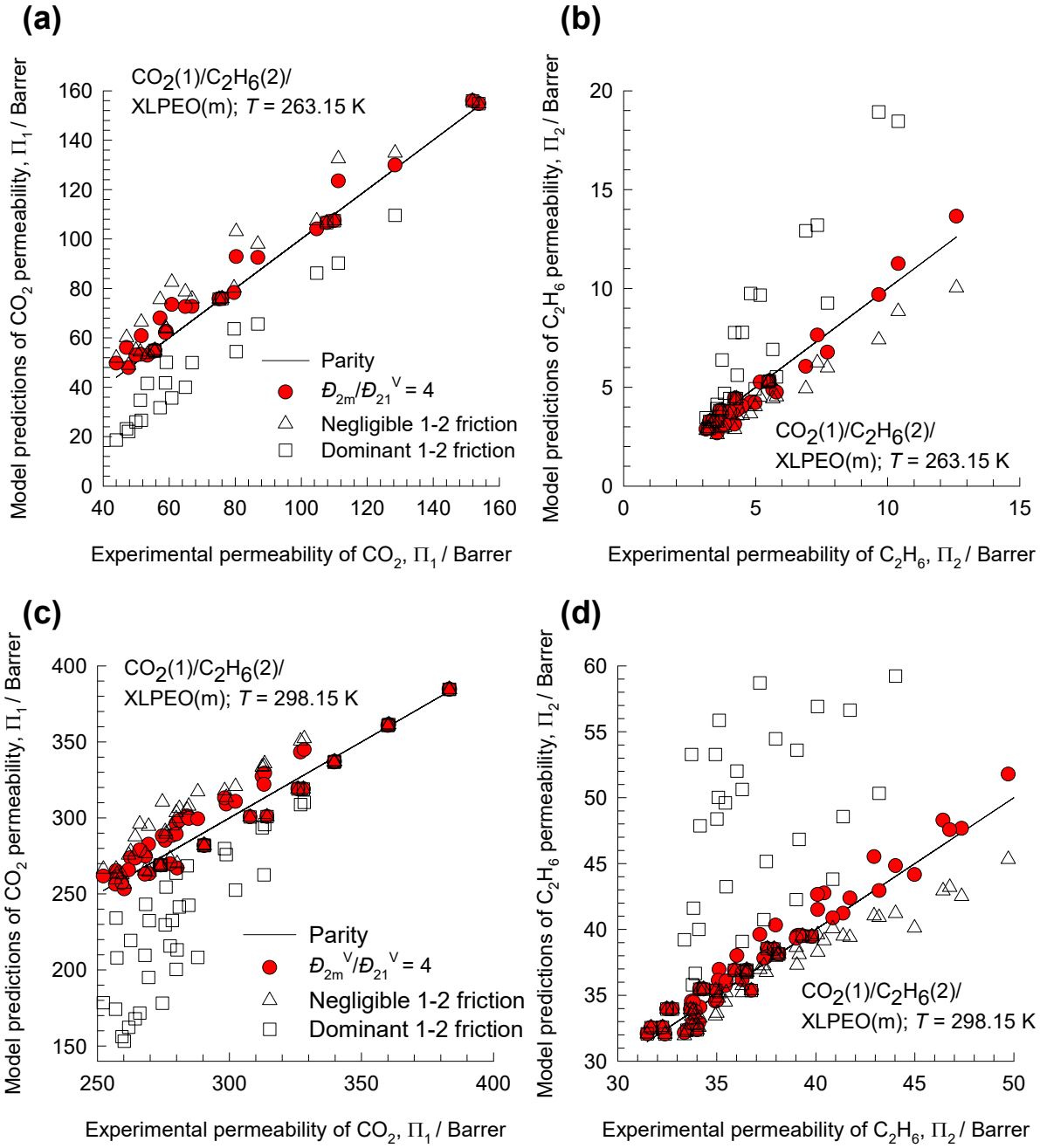

Phase equilibrium in water/acetone/cellulose acetate

(a)

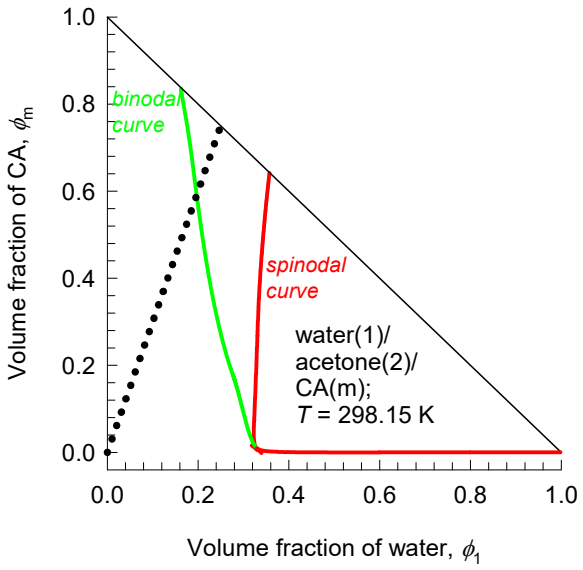

Calculations of the ratio of thermodynamic correction factors along the compositions on the dotted line

(b)

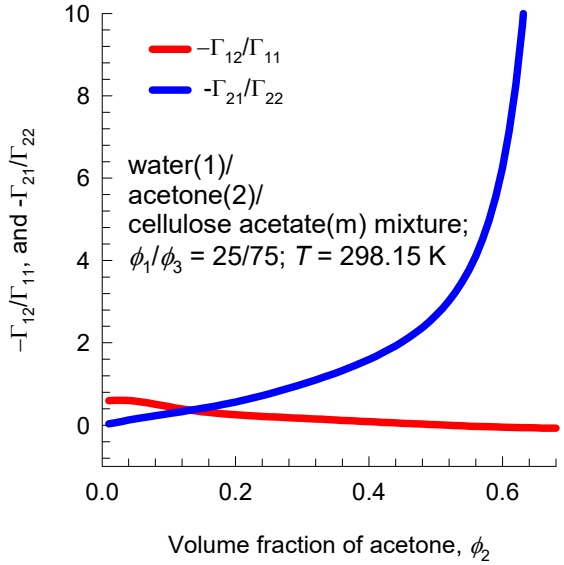

Foray into meta-stable region

Fig. S54

(a)

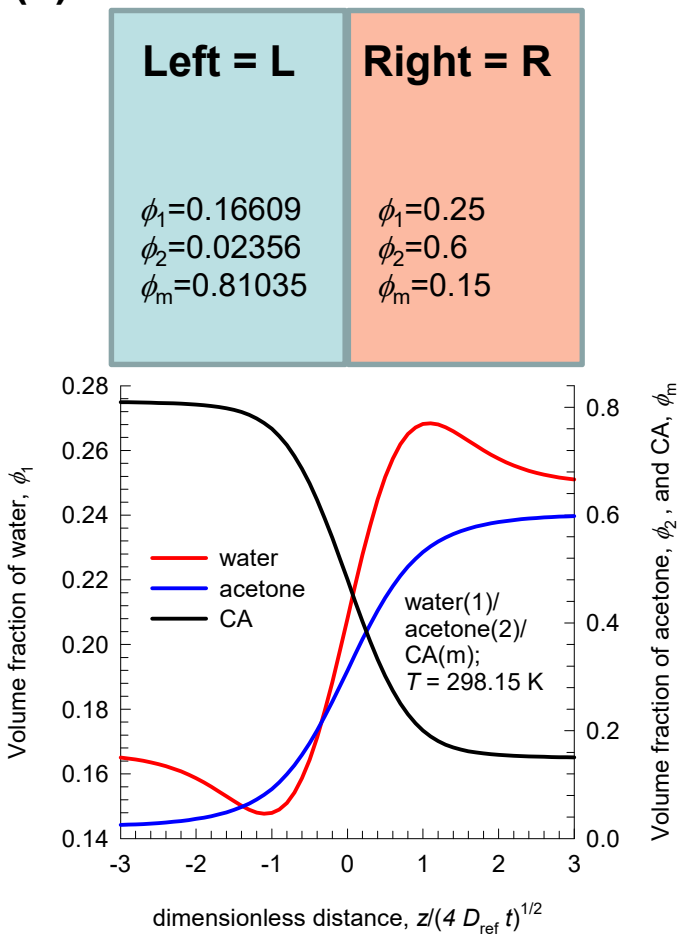

(b)